NASA Reference Publication 1221

1989

Nimbus-7 Stratospheric and Mesospheric Sounder (SAMS) Experiment Data User's Guide

F. W. Taylor
and C. D. Rodgers
University of Oxford
Oxford, England

S. T. Nutter
and N. Oslik
ST Systems Corporation (STX)
Lanham, Maryland

National Aeronautics and Space Administration
Office of Management
Scientific and Technical Information Division

FOREWORD

;-7 Stratospheric and Mesospheric Sounder (SAMS) Experiment Data User's Guide is intended to provide ımmunity with the background information necessary for understanding and using data products on SAMS ved Temperature Tapes (GRID-T), and Zonal Mean Methane and Nitrous Oxide Tapes (ZMT-G). The ɜnt was flown aboard the Nimbus-7 spacecraft and collected data from October 26, 1978 through June 9, ument provides users with information concerning the operational principles of the SAMS instrument and the retrieval of temperature and atmospheric constituents, and the scientific validity of SAMS data. nts that influence the quality of data are included along with the mission history. Data formats of the MT-G tape products and descriptions of SAMS data are also given.

al discussion in this document was prepared originally by the SAMS processing team at Oxford, England. nvestigator was Dr. F. W. Taylor and the NET chairman was Dr. C. D. Rodgers. All questions of a ɜ should be addressed to these individuals, at the address given in Section 1.5. The description of the tape ed upon the data tapes provided for conversion from the DEC format available from Oxford to the IBM l by the Nimbus project. The text provided by the SAMS processing team and the information gained from the data tapes were compiled into this document for NASA by S. T. Nutter and N. Oslik of ST Systems TX) under contract NAS5-28063.

PRECEDING PAGE BLANK NOT FILMED

TABLE OF CONTENTS

Section			Page
	FOREWORD		iii
1	PURPOSE, INTRODUCTION, AND OBJECTIVES		1
	1.1	Purpose of the Data User's Guide	1
	1.2	Introduction	1
	1.3	Objectives	2
	1.4	Data Products	2
	1.5	Principal Investigators	3
2	INSTRUMENT DESCRIPTION		5
3	DATA PROCESSING		7
	3.1	Calibration	7
	3.2	Retrieval of Temperature and Constituents	10
	3.3	SAMS Temperature Gridding	11
4	VALIDATION		13
5	MISSION HISTORY AND CHANNEL STATUS		15
6	DATA FORMATS		49
	6.1	Format of SAMS Gridded Retrieved Temperature Tapes (GRID-T)	49
	6.2	Format of SAMS Zonal Mean Methane and Nitrous Oxide Composition Tape (ZMT-G)	61

REFERENCES . . . 67

LIST OF ACRONYMS, INITIALS, AND ABBREVIATIONS . . . 69

Appendixes

A	SEQUENCE NUMBERS OF SAMS DATA TAPES	71
B	FORTRAN SOURCE LISTING OF SAMS TAPE DUMP	73
C	STRATOSPHERIC AND MESOSPHERIC SOUNDER ON NIMBUS-7	89
D	RETRIEVAL OF TEMPERATURE AND COMPOSITION FROM NIMBUS-7 SAMS MEASUREMENTS	113
E	TEMPERATURE COMPARISONS BETWEEN THE NIMBUS-7 SAMS, ROCKET/RADIOSONDES AND THE NOAA 6 SSU	121
F	OBSERVATIONS OF CH_4 AND N_2O BY THE NIMBUS-7 SAMS: A COMPARISON WITH IN SITU DATA AND TWO-DIMENSIONAL NUMERICAL MODEL CALCULATIONS	131
G	SOME ASPECTS OF THE DESIGN AND BEHAVIOR OF THE STRATOSPHERIC AND MESOSPHERIC SOUNDER	149

SECTION 1

PURPOSE, INTRODUCTION, AND OBJECTIVES

1.1 Purpose of the Data User's Guide

The SAMS Data User's Guide is intended to provide the scientific community with the background information needed to access data on SAMS GRID-T and ZMT-G tapes. The document describes the SAMS instrument, the method of temperature and constituent retrieval, data calibration, and data validation.

Section 1 of this document explains the scientific and technical objectives of the SAMS instrument. Section 2 briefly discusses the literature from which a description of the instrument can be obtained. Reprints of two relevant papers appear as Appendixes C and G to this User's Guide. Section 3 outlines the data processing system, explains instrument calibration, briefly describes the temperature and constituent retrieval process, and explains the temperature gridding procedure. Section 4, like Section 2, provides an introduction to literature that discusses the accuracy of the retrievals and compares the SAMS results with those of other measurements. Reprints of two relevant papers are included as Appendixes E and F of this User's Guide. Important dates in the history of the SAMS instrument and information concerning the status of SAMS channels are given in Section 5. The data formats of the SAMS GRID-T and ZMT-G tapes are described in detail in Section 6. A FORTRAN source listing of a SAMS tape dump program is included in Appendix B. This program enables users to access data on GRID-T and ZMT-G tapes.

1.2 Introduction

The Stratospheric and Mesospheric Sounder (SAMS) instrument flown on Nimbus-7 is the fourth in a series of multi-channel infrared radiometers designed to measure emission from the upper atmosphere, for which conventional spectral filtering techniques do not give adequate performance. The technique used in these radiometers is known as gas correlation spectroscopy and is based on the use of gas cells to select emission from chosen spectral lines or from particular parts of spectral lines.

In the Selective Chopper Radiometer (SCR) on Nimbus-4, a beam-chopping technique was employed to switch the scene (at 10 Hz) between the atmosphere and space view in a differential manner between two gas cells containing different amounts of CO_2. The "difference" signal was then detected by a thermistor bolometer. The chief limitation in performance of the Nimbus-4 SCR was the difficulty in maintaining a balance condition due to stray thermal emission from within the instrument.

Nimbus-5 employed a variation of this technique, in which cells containing different amounts of CO_2 were switched in sequence (one each second) into the optical path to a pyroelectric detector. The difference signals were then extracted on the ground. Performance in this case was limited by gas leakage with time, by uncertainties in the effects of degradation, and by contamination of the cell windows (which give spurious difference signals).

The Pressure Modulator Radiometer (PMR) on Nimbus-6 overcame earlier difficulties by employing a single gas cell and no moving parts in front of the detector. The gas (CO_2) amount in the cell is modulated at approximately 35 Hz by an oscillating piston, and the oscillatory component of the signal arriving at the detector is related directly to the radiance of the scene, but only at the frequencies corresponding to the variation in absorption of the spectral lines of the gas in the modulator cell.

The SAMS instrument views the limb of the atmosphere, rather than employing vertical sounding as in the earlier radiometers. The technique has been extended to gases other than CO_2.

1.3 Objectives

The SAMS is a 12-channel infrared radiometer observing thermal emission and solar resonance fluorescence from the atmospheric limb. Global measurements are made of radiation from the molecular species listed in Table 1-1. These measurements, when interpreted together with results from the LIMS and SBUV/TOMS instruments, provide extensive data for chemical and dynamical models of the stratosphere and mesosphere.

Specific objectives of the SAMS experiment were to derive the following quantities:

a) Temperature for altitudes from 15 km to 80 km, from emission in the 15 μm CO_2 band.

b) Vibrational temperature of CO_2 bands where they depart from local thermodynamic equilibrium (LTE), between 50 km and 140 km.

c) Distributions of CO, NO, CH_4, N_2O, and H_2O from 15 km to 60 km.

d) Distributions of CO_2 (4.3 μm) from 100 km to 140 km and H_2O from 60 km to 100 km, to study dissociation in the lower thermosphere.

The study of planetary waves that used data from the Nimbus-5 SCR and Nimbus-6 PMR can be continued and extended by making use of these new data. In addition, the measurements allow calculation of the transfer of momentum, energy, and trace gases by mean motions and eddies.

The SAMS instrument is designed to exploit the selectivity, energy grasp, and tuning capability of the pressure modulation technique proved earlier for CO_2 emission measurements in the Nimbus-6 PMR (Curtis *et al.*,1974). The main technical innovations in SAMS are as follows:

a) The extension of the pressure modulation technique to other gases.

b) The simultaneous use of conventional chopping and pressure modulation to

   1) Extend the range of heights that can be sounded

   2) Determine the pressure at the viewing level

   3) Enable some interfering radiance signals to be eliminated

   4) Provide additional calibration information and confidence checks

c) The use of a programmable scan system with two independent axes to optimize usage of the observing time and to accommodate uncertainties in spacecraft attitude.

1.4 Data Products

Retrieved temperature and constituent information from the SAMS instrument is stored on two data products, GRID-T and ZMT-G tapes, respectively, which are archived at the National Space Science Data Center (NSSDC). The temperature data on the GRID-T tapes cover the period December 24, 1978 to June 9, 1983. The ZMT-G tape consists of methane and nitrous oxide mixing ratios and covers the period January 1, 1979 to December 30, 1981.

The tapes are 9-track, 6250 bpi. Data records are of variable length. The data formats of the SAMS tapes are described in detail in Section 6.

Table 1-1

Molecular Species and Spectral Bands

Constituent	Spectral Band
Carbon dioxide	4.3 µm and 15 µm
Water vapor	2.7 µm, and 25 µm to 100 µm
Carbon monoxide	4.7 µm
Nitrous oxide	7.7 µm
Methane	7.7 µm
Nitric oxide	5.3 µm

1.5 Principal Investigators

The principal investigator for the Nimbus-7 SAMS experiment at the University of Oxford is F. W. Taylor. Clive D. Rodgers is the NET chairman. Users should contact these individuals if questions arise concerning SAMS data or scientific algorithms: Their address is

Department of Atmospheric Physics
Clarendon Laboratory
University of Oxford
Oxford OX1 3PU
Great Britain

Telephone: Oxford (0865) 272905
Telex 83650 ATMOXF G

The NASA contact regarding SAMS is

Nimbus-7 Manager
NASA/GSFC, Code 636
Greenbelt, MD 20771

Telephone: (301) 286-9846

SECTION 2

INSTRUMENT DESCRIPTION

A complete discussion of the instrument, its principles of operation, calibration, and measurement procedures is given by Drummond *et al.* (1980). For convenience, this article is reproduced in its entirety from the *Philosophical Transactions of the Royal Society of London* as Appendix C of this report. Sections 2-5 (pp. 220-237) of that paper present relevant information about the instrument's behavior. Additional material on the design and behavior of the SAMS is contained in a paper by Wale and Peskett (1984), which is reproduced from the Journal of Geophysical Research and presented here as Appendix G. The articles are reproduced here with the permission of the authors and the journals in which they were originally published.

A somewhat less detailed description of the SAMS instrument is found in Section 6 of the Nimbus-7 User's Guide (Drummond *et al.*, 1978).

SECTION 3

DATA PROCESSING

Continuous observations from all eight experiments were recorded aboard the spacecraft. In normal operation, one tape recorder was recording while another was playing back data to a receiving station, resulting in no loss of data. Initial processing of all data took place at Goddard Space Flight Center (GSFC), after which SAMS data were transmitted by data lines to Oxford for all further processing.

Approximately 13 orbits per day requiring about 2 hours of transmission time were received at Oxford for further processing. The data were received by a PDP 11/70 computer, where they were simultaneously written directly to 9-track, 1600 bpi phase-encoded magnetic tape in raw format and processed to a "quick-look" plotting stage. The processing was performed by a suite of programs that ran under a controlling program requiring operator intervention only when problems occurred. The data were quality checked and calibrated. A "quick-look" estimate of spacecraft attitude was calculated using data from two channels of the SAMS instrument. Various data products were plotted for each orbit. These plots were regularly checked to determine instrument health. When all data had been received, the software produced data products required on a daily basis rather than by orbit, as well as additional plots, e.g., retrieved temperature and listings of housekeeping functions. The temperature plots enabled a watch to be kept for sudden warmings and the housekeeping information assisted in defining operating modes and data quality of the instrument.

A stage of final processing took place when all the raw data had been sorted into time order. The same suite of programs was used but a better calibration and other data, e.g., ILT, were included.

Figure 3-1 provides a schematic overview of the data processing.

3.1 Calibration

The calibration of SAMS can be divided into two broad areas:

a) Conversion of signal channel telemetry counts into a radiance, expressed as a fraction of the signal obtained from a black body at a specified temperature, with sufficient additional information to define the spectral properties of the instrument and its field of view.

b) Calculation of the spectroscopic properties of each channel and the physical properties of the gases being investigated in the atmosphere, in order to retrieve useful quantities (temperature, composition) from the calibrated radiances.

This section deals with the first area only; the second area is discussed in Section 3.2. The Nimbus-7 User's Guide contains an outline of the various preflight calibration measurements made, including the following:

a) Measurement of the response of the instrument to black bodies at temperatures between 77 K and 320 K. The temperature variations experienced in orbit were simulated during this test, so that temperature coefficients could be determined dynamically and likely operating conditions estimated. The basic measurement verifies the linearity of the instrument response and that the spectral properties of each channel are known.

b) Measurements of the field of view of each channel, and calibration of the scan mirror telemetry system.

The response of each channel is linear with respect to the incoming radiance, and may, therefore, be characterized by a slope (the instrument gain) and an offset, corresponding to the signals observed when observing space (zero radiance input).

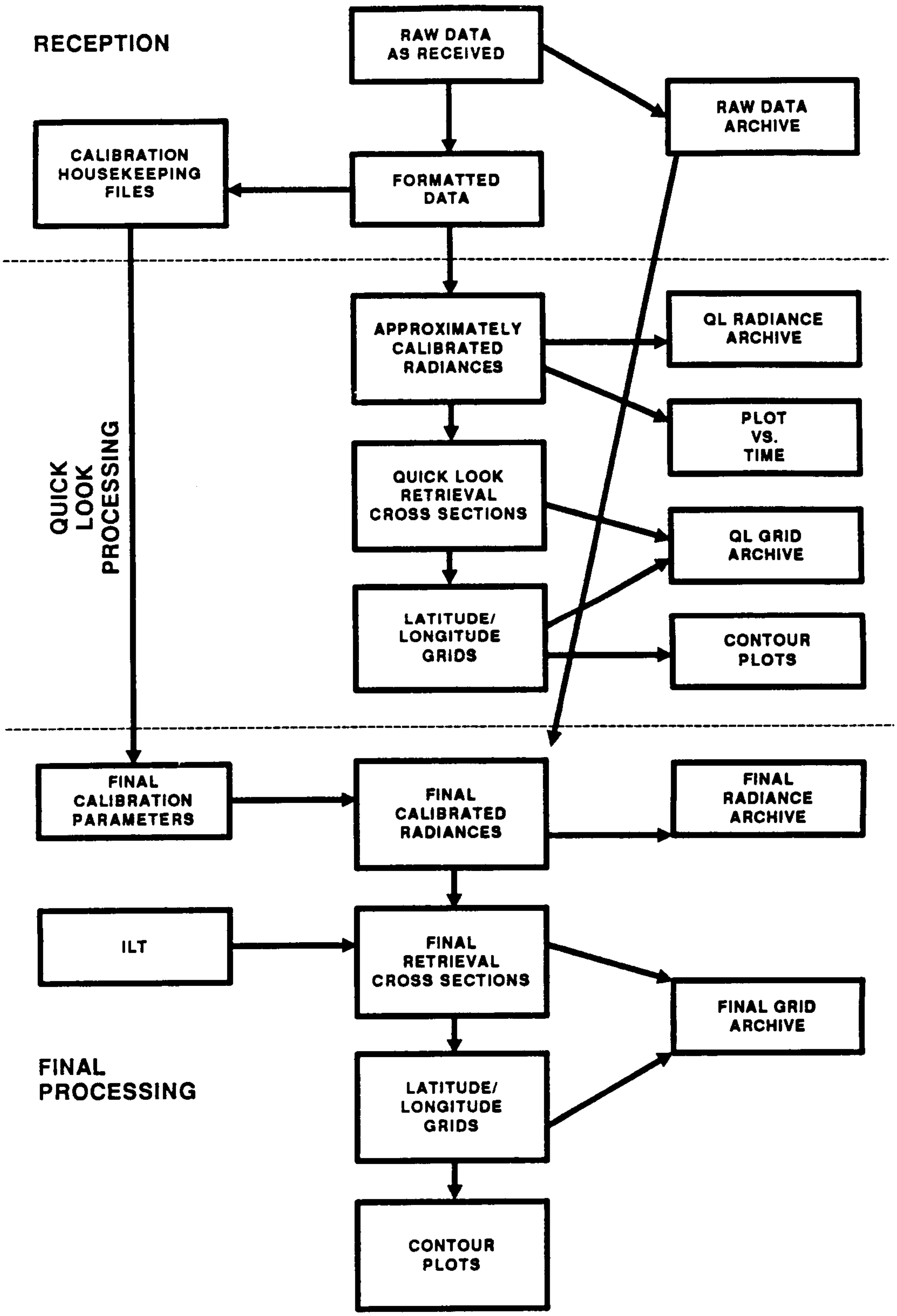

Figure 3-1. Overall view of data processing.

The following are some of the most important factors that affect the gain of a *narrow band* pressure-modulated channel (PMC):

a) Cell pressure

The equivalent width of the pressure modulation depends on the pressure in the cell, as a result of changes in the absorber amount and line shape. An additional influence is the variation of the frequency of the modulation with the mean cell pressure, as the response of the detector and signal channel is not uniform with frequency. There is also a phase difference between the cycling of the cell pressure and the piston position, which is used to derive the phase sensitive detector (PSD) reference wave forms. This results from the flow of gas to and from the PMC head and is also pressure dependent; it may be significant in some cases at low cell pressures.

b) Cell temperature

The molecular sieve gas containment system ensures that the mean pressure of gas in the PMC is held sensibly constant as the temperature T varies. The absorber amount, therefore, changes as 1/T, with a corresponding change in the equivalent width. This variation is quite distinct from the very small changes that result from variation of the line width and strength with temperature.

c) Detector temperature

The responsivity of all of the detectors varies with temperature; in the case of the PbS unit employed in the B1 channel, the phase shift is also temperature dependent.

d) PMC amplitude

There is a small variation in the amplitude of the oscillation of the pressure modulator with temperature; this is significant not only because of its direct effect on the gain, but also because it causes a small shift in resonant frequency.

For the *wideband channels*, the situation is very much simpler; the gain depends principally on the detector temperature and the chopper amplitude.

The *offset* is the sum of a large number of components, the principal contributions being from

a) The emission from the modulator or chopper against which the incoming radiation is being chopped.

b) Temperature cycling within the pressure modulator cell, which results in an additional emission signal, with amplitude and phase that are strong functions of cell pressure but not significantly dependent on temperature.

c) The emission from optical components in front of the modulator or chopper, including the system aperture stop (in the case of the PMR channels, the mask of the ellipsoid mirror M3) and the front optics components.

d) Stray radiation detected as a result of aberrations and imperfections in the optical system.

e) Synchronous pick-up. Pyroelectric detectors such as the triglycine sulfate (TGS) detectors employed in SAMS also display a piezoelectric effect and show a significant microphonic response. The pressure modulators and the chopper cause a small level of vibration in the instrument structure. This vibration is detected directly through the detector piezoelectric response. The level of vibration is, unfortunately, not very stable, and varies with operating modes; there is also variation around the orbit, which is of a constant form over a period of a day or so. Such a response is especially noticeable in the detector fitted to the C2/3 channel. This particular detector has been noted in other ways to exhibit an unusually high level of microphonic response. This problem is treated by fitting the residual space view variation to terms periodic in the orbital position, after normal calibration.

Most of the above factors depend on the instrument gain and are, therefore, subject to all the same variations with temperature, etc.

Because of the very large number of factors that contribute to the gain and offset of each channel, overall calibration of the instrument must be performed frequently during flight. The zero radiance signal is checked by moving the scan mirror so that the tangent height of the path viewed by the lowest of the three fields of view is at least 150 km (space view); a second calibration point is found by inserting a room temperature black body into the optical path at the focus of the paraboloid, M2. Since SAMS measures signals that are very close to zero, the zero offset of the system must be known extremely precisely. Every scan program, therefore, includes frequent space view calibration periods. One of the commonly used programs has two samples of space view data every 32 seconds. Black body calibrations are required less frequently.

It is not possible to find the magnitude of all the relevant factors by calibration in flight, as many of them show a high correlation, and the variations in operating conditions experienced in a typical period of operation in a given mode are not sufficiently wide. Taken in isolation, the calibration sequences do not have good enough signal to noise ratios to permit their direct use. Many of the factors (e.g., the effect of temperature on the PMR equivalent width, the emission from the cell or chopper and the emission from optical components) can be calculated explicitly; the remaining coefficients may then be found by regression analysis with respect to the temperatures, etc. involved. Normally, SAMS is kept in a given operating mode for one 24-hour period at a time, the first orbit of the day being used to allow the cell pressures to stabilize after the mode change. During this period, continuous black body and space view information is needed.

Calibration of the instrument is performed on a day-by-day basis, and the effects of the variations (e.g., cell pressure) are treated as perturbations from a nominal value. The cell pressures show long-term trends, however, and for this reason the calibration coefficients cannot be fixed in a single test, for instance as part of the preflight calibration tests. Various special tests have been run in orbit to provide additional calibration information, including one 3-day period of continuous calibration sequences. During this test, auxiliary heaters were employed to provide a wider variation in temperature than that found in normal operation. Tests have also been run to investigate the signal levels observed at all possible positions of the scan mirror. These tests have shown that the variation of the stray signal (including microphonic terms) with mirror position is negligible.

3.2 Retrieval of Temperature and Constituents

The retrieval problem has two aspects, temperature and composition. The temperature profile is determined from the two 15 μm CO_2 pressure-modulated (PM) channels and the two corresponding wideband (WB) channels in the A and C fields of view, which are separated by 0.56 degrees (about 35 km). The composition retrieval is determined from radiances in the other channels, but requires the temperature profile as input.

As with remote sounding in general, the problem is underdetermined and cannot be solved explicitly without recourse to *a priori* information. The temperature retrieval problem has some complications that make it less nearly linear than its nadir sounding counterpart. The most serious complication is that the attitude of the spacecraft is not adequately measured or controlled, so that the tangent height of the line of sight is not known accurately enough to compute the corresponding transmittance function. However, there is enough information in the radiances to determine both temperature profile and tangent height. The composition retrieval is nonlinear because the unknown enters the equation of transfer as an argument of the transmittance function.

Our approach to both retrieval problems is to linearize the direct equation about an *a priori* profile, and to use a statistically optimum estimator (Rodgers, 1976) to find the most likely solution. Iteration is avoided by ensuring that the *a priori* profile is sufficiently close to the solution that the linearization is adequate. In the case of temperatures this is achieved by using a sequential maximum-likelihood estimator, in which the retrieval corresponding to time t and its error covariance matrix are used to construct the *a priori* profile and its error covariance at time $t + \Delta t$, where Δt is the time interval between measurements. For composition retrieval, it has proved necessary to average the data, for example zonally, in order to improve the signal-to-noise ratio and to reduce computing time. In this case, the previous day's retrieval for the same averaging box is used to construct the *a priori* profile. Full details of the methods adopted have been described by Rodgers *et al.* (1984), reprinted as Appendix D of this user's guide.

3.3 SAMS Temperature Gridding

The sequential estimator used to retrieve temperature and attitude obtains estimated retrieval coefficients and the corresponding covariance matrix every 2 seconds around the orbit (about every 14 km). These values are ultimately interpolated onto a regular latitude-longitude grid at latitudes 50° S, 47.5° S, 45° S, ..., 67.5° N and longitude 0°, 10°, 20°, 30°, ..., 350° E. As a first step, the sequential estimator selects the 2-second retrieval nearest to each 2.5° latitude line (but no farther than 1.25° away), and arranges for a combined forward + backward estimate of the temperature retrieval and error information to be written to an output file.

These results are combined into two "orbit" grids per day, one for the northbound (ascending) portions of each orbit (all between about 1400 and 1800 hours local time) and one for the southbound (descending) portions (1800 to 2200 hours local time). Each grid has 48 rows (latitudes) and 14 columns (orbits). Some grid points will be empty because of missing orbits. For example, the first orbit each day is generally spent calibrating while the PMC pressure settles down, so no retrievals are obtained; other orbits or parts of orbits were never received. Note that the data here are divided into "orbits" starting and ending when the satellite is at 80° N or S; they bear no relation to an 'orbit' as received from NASA, which is normally one data dump of the satellite tape recorder. Note also that the orbit number has only approximate meaning, because those given by NASA can be the orbit on which the recorder was replayed, which may be several orbits after the observations were made.

Given a northbound and southbound grid for each day, gaps of up to two points along an orbit are filled by linear interpolation between values at the north and south ends of the gap for each grid. The values are then interpolated in longitude using linear interpolation, to obtain still separate northbound and southbound latitude/longitude grids. Where there is a missing orbit, no attempt is made to interpolate into the gap, except that the last good observation on either side of the gap is used for points up to a quarter of the orbital separation into the gap on that side. This procedure is carried out for the following quantities:

a) Eigenfunction coefficients of Planck deviation from the climatological first guess.

b) Standard deviations of (a).

c) Temperature at 10 special pressure levels.

d) Standard deviations of (c).

The off-diagonal elements of the eigenfunction covariance matrix are not gridded because there are so many of them; however, the standard deviations of temperature at the selected levels are obtained in the retrieval program using the full covariance matrix.

The northbound and southbound grids are now combined by taking both values where possible to form a combined daily average grid. In the case of temperatures and eigenfunction coefficients, the values are weighted inversely by the reciprocal of their variances, while standard deviations are combined by taking the square root of the sum of reciprocals of the variances. If data are available from only one of the grids (northbound or southbound, not both) the retrieved values from that grid are used unchanged in the final mean analysis.

The combined mean analyses are supplied on the data tape in a format where each field is given as a separate tape block, with eigenfunction coefficient or temperature fields followed by the corresponding error grid. In addition, the grids of eigenfunction coefficients are used to obtain temperature grids with a vertical resolution of 0.2 pressure scale heights (62 levels in all). These temperatures are stored on the tape in profiles together with the first guess climatological profile used and the zonal mean for each latitude.

SECTION 4

VALIDATION

Two papers concerning the accuracy of the retrieved SAMS temperatures and the methane and nitrous oxide distributions are reprinted from the *Journal of Geophysical Research* (Barnett and Corney, 1984; Jones and Pyle, 1984) as Appendixes E and F of this User's Guide. The articles are included with the permission of the authors and the Journal. Independent comparisons of several stratospheric data sources, including SAMS and LIMS, may be found in the Middle Atmosphere Program [MAP] Handbook, (Rodgers, 1984*a*; Grose and Rodgers, 1986), published by SCOSTEP, and available from the SCOSTEP secretariat, University of Illinois, 1406 W. Green Street, Urbana, IL 61801.

PRECEDING PAGE BLANK NOT FILMED

PAGE 12 INTENTIONALLY BLANK

SECTION 5

MISSION HISTORY AND CHANNEL STATUS

Table 5-1 lists the significant dates in the history of SAMS. The first 2 months of instrument operation were an experimental period, during which many changes were made to the scan pattern and sieve setting programs. Tables 5-2 and 5-3 provide full details of the settings used, along with comments on some problems.

The following points concerning the instrument have significant consequences for the quality of the data.

a) SAMS operated on a 3-day-on, 1-day-off duty cycle; atmospheric phenomena with a 4-day period will not be well represented in the data.

b) The first orbit of any day is almost always a calibration orbit.

c) The passive cooler did not reach the design temperature; as a result, the shortwave channels (NO, CO, and CO_2 4.3 microns) all had a poorer signal-to-noise ratio than expected.

d) A chemical problem with the NO molecular sieve rendered the channel unusable. The NO modulator failed by driving at too high an amplitude on day 91 of 1980.

e) PMC frequencies depend on cell pressure, and hence on sieve setting. For some combinations, there are "beats" between different modulators at similar frequencies. These occasions are noted in Table 5-2. One significant consequence of the possible beating is that the upper CO_2 15 micron channel (A1) is sometimes in a low pressure setting to avoid beats with the CO channel. There is a systematic difference between temperatures retrieved with A1 sieve 3 and those retrieved with other sieve settings, particularly in the mid and upper mesosphere. We suggest that temperatures from days with A1 settings other than sieve 3 be treated with caution.

f) A problem with the housekeeping analog/digital (A/D) converter caused some instrument temperature measurements to be made with low accuracy. This problem was largely circumvented in the processing.

g) Changes were made in the water PMC drive circuits after the final pressure calibration runs were made. Consequently, the water cell pressure measurements are uncertain.

h) The instrument failed partially during 1982 when the scan mechanism stuck. After a period of recovery, final failure occurred in June 1983.

i) The eruption of El Chichon in April 1982 injected a considerable amount of aerosol into the lower stratosphere. This event is reflected in significant changes to the temperature retrievals, but it is uncertain whether these changes are real or are the result of unmodeled emission from the aerosol affecting the retrieval process. Before September 1982, the effects were confined to the region equatorwards of about 30° N and below about 30 km but, after this date, the dust cloud quickly moved to higher latitudes but with lower concentration. We have not carried out nitrous oxide and methane retrievals for this period because of these uncertainties.

Table 5-1

Significant Dates in the History of SAMS

Day	Year	Event
297	1978	Launch.
299	1978	SAMS turned on.
317	1978	Cooler door opened.
358	1978	First usable data.
48	1979	Cooler decontamination heaters on.
91	1980	NO modulator failed.
100	1982	El Chichon effects first seen in data.
132	1982	Cooler decontamination heaters on.
277	1982	Scan problem - first appearance.
301	1982	Cooler decontamination heaters on.
44	1983	Scan problem - apparent recovery.
164	1983	Scan problem - final failure.

Following is the status of the channels:

a) A1 and C1; CO_2 15 micron temperature sounding channels.

Temperature retrievals have been carried out for the whole data set, except for a few occasions when the data quality was poor, or when the instrument was not scanning due to scan problem or azimuth scan tests.

b) A2; 4.3 micron CO_2 channel. Non LTE studies.

This channel suffered from the poor signal-to-noise (S/N) problem of all the shortwave channels.

c) A3; carbon monoxide.

The SAMS measured CO during the daytime using a pressure modulator to measure resonant fluorescent scattering of sunlight near 4.7 microns. The noise level was high, and it was necessary to average over time periods of 6 months and 35-50° wide latitude bands. Consequently, the total number of profiles obtained was small, and they are all given in Figure 5-1. It should be noted that,

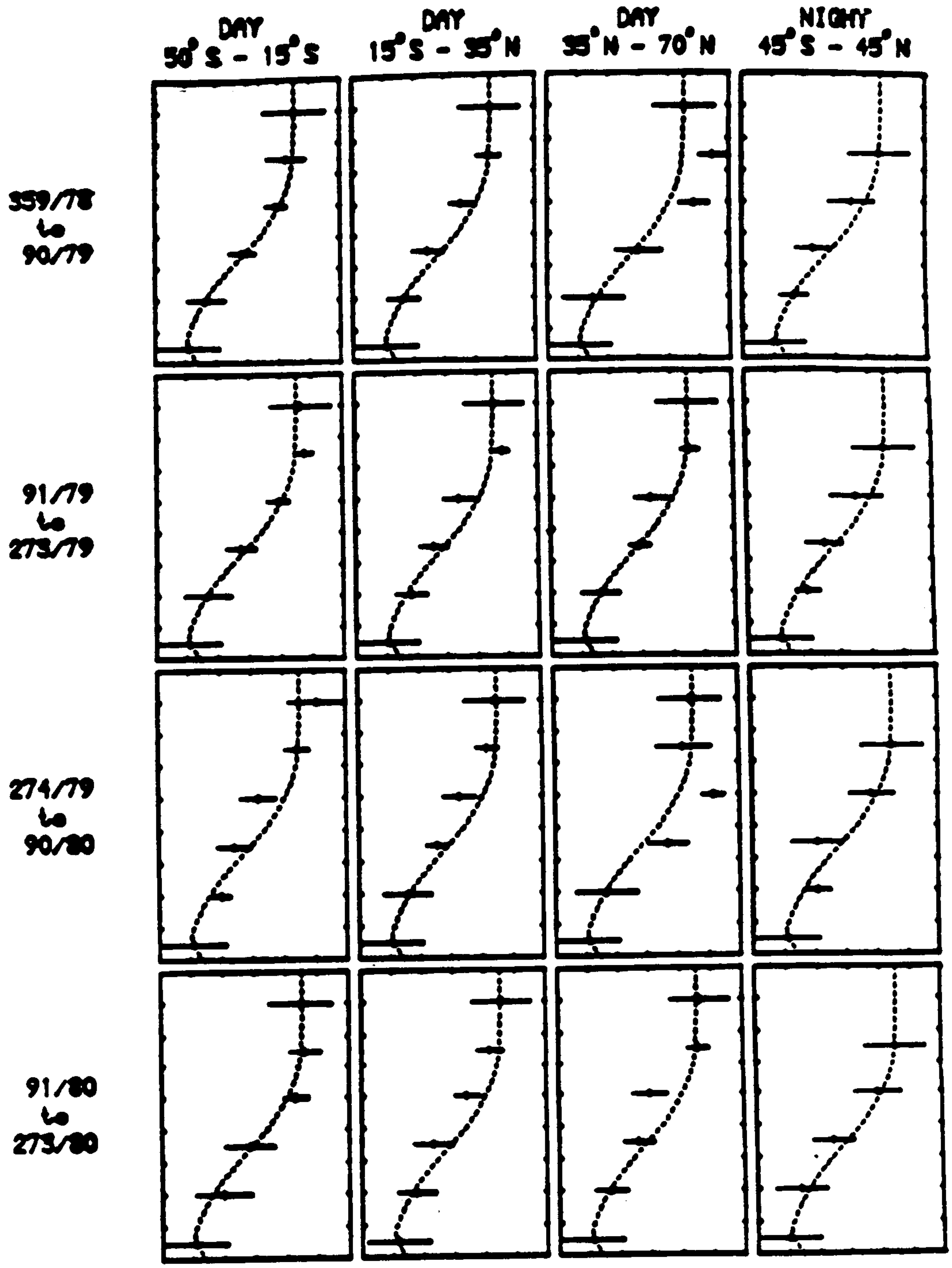

Figure 5-1. Comparison of the retrieved carbon monoxide profiles. Dotted line is the *a priori* profile (identical in all cases). Vertical scale: -ln (pressure/atmospheres) = 2 to 20. Horizontal scales: $\log_{10}$ (volume mixing ratio) = -9 to -3.

because of the geometry of the orbit, the density of observations is greatest at 50° S and 70° N. Consequently, averages for bands that include these latitudes are biased toward them.

The precision (systematic error) of the retrieval is approximately ±25 percent, but the accuracy (random error) is worse, about -57 to +130 percent. The profile is valid over the range 6 to 14 pressure scale heights (about 45 to 100 km).

Although the random errors are high, marked variations can be seen. The most significant feature is that mixing ratios are very high in the mesosphere during the northern hemisphere winter. This effect is clearly seen in the retrievals for the 1978-79 and 1979-80 winters. There is a difference of well over a factor of 10 between summer and winter mixing ratios at some levels. This difference is far too large to be attributed to errors in the measurements or the retrieval process. There is some evidence for a similar effect in the Southern Hemisphere, at about 85 km (12 pressure scale heights), but the most southerly latitude zone extends only to 50° S. The variations between the remaining profiles are generally comparable with the level of errors on the retrievals. The central latitude band shows a profile that exhibits little variation between the data periods, and the mixing ratios are comparable with summertime values in the northern and southern hemisphere zones.

d) A4: nitric oxide.

The nitric oxide in the PMC unexpectedly suffered from a catalytic disproportion reaction on the molecular sieve material, so that the PMC actually contained a mixture of nitrous oxide and a small amount of nitric oxide. Consequently, the data from this channel are of little value. The channel failed mechanically after 520 days in orbit.

e) B1: water vapor 2.7 micron resonance fluorescence.

This channel should provide water concentration in the 65-90 km region, but suffers from poor S/N, as do the other shortwave channels. So far only a limited number of retrievals have been performed for monthly zonal means, in the latitude range of 45° S to 45° N for the months of January, April, July, and October 1979. Processing is in hand to produce similar products for the whole of 1979 and for smaller latitude boxes.

f) B2: water vapor rotation band.

This is the primary water vapor channel, which should produce both zonal means and global distributions of water from 15 to 60 km. However, our retrieved profiles to date have failed to satisfy our validation criteria. The problem appears to be associated with uncertainties in the spectroscopy of water vapor in pressure modulators, and the symptom is that the retrieved profiles show an unreasonably large amount of water at high levels. Laboratory studies are currently being undertaken in an attempt to solve this problem.

Preliminary processing of zonal mean fields for 1979 and 1980 has been completed; similar processing of the remainder of the data and the production of global fields is proceeding. These data can be used only to illustrate the qualitative behavior of the water distribution, however, and will not be archived with NSSDC.

g) C2 and C3: nitrous oxide and methane.

Nitrous oxide and methane have been retrieved from the SAMS radiances for the period January 1, 1979 to December 31, 1981. The data are too sparse during the experimental period before January 1979 to be useful, and 1982 contains both the El Chichon eruption and the scan failure. Some parts of the 1982 data will be retrieved and placed in the archive. Note that because C2 and C3 both use the same detector, only one of the two channels can be used at any one time.

For channels A2/3/4 and C2/3, the wideband measurements are of little use since they were the result of emission from several gases. They were not used in the retrievals. They were, however, affected by the El Chichon dust, and they could be used to study the wavelength dependence of aerosol absorption.

The pattern of use for the instrument is given in Table 5-2. The 'SCAN PROG' column is the internal reference number for the scan program being employed on that day. It is included so that different days when the same program was being used can be identified. Detailed scan patterns can be supplied by the principal investigators at Oxford (Section 1.5) for individual cases on request. The nominal scan range is given in km for the 'D' field of view. Relative to this direction, the A field of view (FOV) is 0.32° above, B is 0.16° above, and C is 0.24° below (approximately 18, 9, and -7 km respectively). The nominal scan range is only an approximate guide to the actual scan range obtained in the atmosphere because of the attitude variations of the spacecraft relative to the horizon. The "sieve setting" number indicates the choice of PMC cell pressure (see Table 5-3), and the "E" indicates which modulator is energized, in those cases where there is more than one modulator associated with a detector.

Table 5-2
Mode Table 1: Launch - day 239, 1982

DATE YEAR	DAY	ORBITS (APPROX)	SCAN PROG	RANGE(KM) (APPROX)	SIEVE SETTINGS A1	A2	A3	B1 B2	C1	C2	C3	
1978	299	32:35	1.1		3E	0E	0	3E	3E	0	1E	WIDE SCAN - LIMB SEARCH
1978	299	35:37	2.2	15:90	1E	0	0	3E	3E	1E	0	
1978	300	37:52	2.2	15:90	1E	0	0	3E	3E	1E	0	
1978	301	52:58	2.7		1E	0	0	3E	3E	0E	1	NO SCAN
1978	301	58:64	2.3	30:105	1E	0	0	2E	3E	1	0E	BEAT B12/CH BEAT C1/C3
1978	302	64:78	2.8	10:85	3E	0	0	3E	3E	1	0E	BEAT C1/C3
1978	303	78:89	2.8	10:85	3E	0	0	3E	3E	1	0E	BEAT C1/C3
1978	303	89:92	2.10	10:85	3E	0	0	3E	3E	1	1E	
1978	304	92:106	2.10	10:85	3E	0	0	3E	3E	1	1E	
1978	305	106:119	2.12	30:105	3E	0	0	1E	3E	0E	1	
1978	305	119:120	2.17		3E	0	0	3E	3E	1E	1	NO SCAN BBODY/SPACE CAL
1978	306	120:130	2.11	29:95	3E	0	0	2E	3E	1E	1	BEAT B12/CH
1978	306	130:134	2.9	10:85	3E	0	0	3E	3E	1E	1	
1978	307	134:148	2.13	30:105	3E	0	0	1E	3E	1	1E	
1978	308	148:163	2.11	20:95	3E	0	0	2E	3E	1E	1	BEAT B12/CH
1978	309	163:175	2.16	25:100	3E	0	0	3E	3E	1	1E	
1978	310	175:189	2.16	25:100	3E	0	0	3E	3E	1	1E	
1978	311	189:203	2.16	25:100	3E	0	0	3E	3E	1	1E	
1978	312	203:210	2.16	25:100	3E	0	0	3E	3E	1	1E	
1978	312	210:213	5.24		3E	0	0	3E	3E	1	1E	MOON SCAN ATTEMPT (PCL PROG ERROR)
1978	312	214:216	2.9	10:85	3E	0	0	3E	3E	1E	1	
1978	313	217:231	3.18	15:35	3E	0	0	2E	3E	1	1	BEAT B12/CH
1978	314	231:245	3.19	25:45	1E	0	0	1E	3E	1E	1	
1978	315	245:258	3.21	-5:30	3E	0	0	3E	3E	1	1E	
1978	316	258:261	3.21	-5:30	3E	0	0	3E	3E	1	1E	
1978	316	261:272	4.20		1E	0	0	0E	3E	0E	1	NO SCAN
1978	317	272:282	4.22		1E	0	0	0E	3E	0E	1	NO SCAN
1978	317	282:286	4.23		1E	0	0	1E	3E	1	1E	NO SCAN COOLER DOOR OPEN 282 ETC 1700Z
1978	318	286:300	4.23		1E	0	0	1E	3E	1	1E	NO SCAN
1978	319	300:315	3.25	5:25	1E	0E	1	3E	3E	1E	1	
1978	320	315:325	3.28	5:40	1E	1E	1	3E	3E	1	1E	
1978	321	337:341	3.28	5:40	1E	1E	1	3E	3E	1	1E	BALLOON FLIGHT
1978	322	341:355	8.29	10:45	1E	1	1E	3E	3E	1	1E	
1978	323	355:368	6.30		1E	0E	1	0E	3E	1	1E	NO SCAN
1978	324	368:383	6.32		0E	1	1	0E	3E	1	1E	NO SCAN
1978	326	397:411	6.31		1E	1	0E	0E	3E	1E	1	NO SCAN
1978	327	411:424	8.33	30:65	3E	1	0E	1E	3E	1E	1	
1978	328	424:438	8.33	30:65	3E	1	0E	1E	3E	1E	1	
1978	330	452:465	8.34	-5:30	3E	1	0E	3E	3E	1E	1	DATUM MAY BE TOO LOW FOR GOOD SPACE VIEW
1978	331	465:480	8.34	-5:30	3E	1	0E	3E	3E	1E	1	DATUM MAY BE TOO LOW FOR GOOD SPACE VIEW
1978	332	480:494	8.35	-5:30	3E	1	1	3E	3E	1	1E	DATUM MAY BE TOO LOW FOR GOOD SPACE VIEW
1978	334	508:521	11.36	-5:50	3E	1	0E	3E	3E	1	1E	
1978	335	521:535	11.36	-5:50	3E	1	0E	3E	3E	1	1E	
1978	336	535:549	11.37	-5:50	3E	1	0E	3E	3E	1E	1	
1978	338	563:576	11.37	-5:50	3E	1	0E	3E	3E	1E	1	
1978	339	578:585	5.38		3E	0	0	3E	3E	1	1E	BAD SCAN PROGRAM
1978	339	586:590	11.39	-5:50	3E	1E	1	3E	3E	1	1E	BEAT A12/A3
1978	340	590:604	11.39	-5:50	3E	1E	1	3E	3E	1	1E	BEAT A12/A3
1978	342	618:627	12.42		3E	1	0E	1E	3E	1E	1	NO SCAN
1978	342	628:633	5.38		3E	0	0	3E	3E	1	1E	BAD DATA
1978	343	634:645	11.40	-5:50	3E	1E	1	3E	3E	1E	1	BEAT A12/A3
1978	344	645:660	11.40	-5:50	3E	1E	1	3E	3E	1E	1	BEAT A12/A3
1978	346	673:688	8.41	25:60	3E	1	0E	2E	3E	1	1E	
1978	347	688:690	0.0		3E	1	0E	2E	3E	1	1E	BAD SCAN PROGRAM
1978	347	696:702	3.28	5:40	1E	1E	1	3E	3E	1	1E	
1978	348	702:715	8.41	25:60	3E	1	0E	2E	3E	1	1E	BEAT B12/CH

DATE YEAR	DAY	ORBITS (APPROX)	SCAN PROG	RANGE(KM) (APPROX)	SIEVE SETTINGS A1	A2	A3	B1 B2	C1	C2	C3	
1978	350	738:743	15.56	-20:35	3E	1	1E	3E	3E	1E	1	
1978	351	743:756	15.44	0:55	3E	1	0E	3E	3E	1E	1	
1978	352	757:770	8.46	25:60	3E	1	0E	2E	3E	1E	1	POSS BEAT B12/CH
1978	354	784:798	108.50	35:70	1E	1	1	1E	3E	0E	1	
1978	355	798:812	108.158	10:45	1E	1	0	1E	2E	1	0E	
1978	356	812:825	108.147	20:55	3E	0E	0	2E	3E	1	1E	POSS BEAT B12/CH
1978	358	839:853	108.148	20:55	3E	1	0	2E	3E	1E	1	POSS BEAT B12/CH
1978	359	854:867	115.161	-5:50	2E	1E	0	3E	3E	1	1E	
1978	360	867:881	115.162	-25:30	2E	1E	0	3E	3E	1	1E	
1978	362	895:908	114.153	50:115	1E	1	0E	0E	3E	0E	1	
1978	363	908:922	114.159	50:115	1E	0E	1	0E	2E	1	0E	
1978	364	922:936	114.155	50:115	0E	1	1	0E	3E	0E	1	
1979	1	950:964	115.156	-25:30	3E	1	0E	3E	3E	1E	1	
1979	2	964:977	115.144	-5:50	3E	1E	0	3E	3E	1E	1	POSS BEAT A12/A3
1979	3	977:982	115.144	-5:50	3E	1E	0	3E	3E	1E	1	POSS BEAT A12/A3
1979	3	982:991	5.43		3E	0	0	3E	3E	1	1E	MOON SCAN
1979	5	1005:1019	108.150	35:70	1E	1	0	1E	3E	0E	1	
1979	6	1019:1037	108.158	35:70	1E	1	0	1E	2E	1	0E	
1979	7	1033:1037	108.158	35:70	1E	1	0	1E	2E	1	0E	
1979	7	1037:1047	5.43		3E	0	0	3E	3E	1	1E	MOON SCAN
1979	9	1060:1075	108.148	20:55	3E	1	0	2E	3E	1E	1	POSS BEAT B12/CH
1979	10	1075:1088	115.161	-5:50	2E	1E	0	3E	3E	1	1E	
1979	11	1088:1102	115.162	-25:30	2E	1E	0	3E	3E	1	1E	
1979	13	1116:1129	114.153	50:115	1E	1	0E	0E	3E	0E	1	
1979	14	1130:1143	114.159	50:115	1E	0E	0	0E	2E	1	0E	
1979	15	1143:1157	114.155	50:115	0E	1	0	0E	3E	0E	1	
1979	17	1171:1186	115.156	-25:30	3E	1	0E	3E	3E	1E	1	
1979	18	1186:1200	115.144	-5:50	3E	1E	0	3E	3E	1E	1	POSS BEAT A12/A3
1979	19	1200:1213	115.144	-5:50	3E	1E	0	3E	3E	1E	1	POSS BEAT A12/A3
1979	21	1226:1240	108.150	35:70	1E	1	0	1E	3E	0E	1	
1979	22	1240:1254	115.145	-5:50	3E	1	0E	3E	3E	1	1E	
1979	23	1254:1263	108.147	20:55	3E	0E	0	2E	3E	1	1E	POSS BEAT B12/CH
1979	23	1263:1268	115.144	-5:50	3E	1E	0	3E	3E	1E	1	POSS BEAT A12/A3
1979	24	1269:1282	108.147	20:55	3E	0E	0	2E	3E	1	1E	STRAT WARMING POSS BEAT B12/CH
1979	25	1282:1297	115.258	25:80	1E	1	0	1E	2E	1	0E	STRAT WARMING POSS BEAT A12/A3
1979	26	1297:1310	115.144	-5:50	3E	1E	0	3E	3E	1E	1	STRAT WARMING POSS BEAT A12/A3
1979	27	1310:1323	115.246	10:65	3E	1	0E	2E	3E	1E	1	STRAT WARMING POSS BEAT A12/A3
1979	28	1323:1337	115.250	25:80	1E	1	0	1E	3E	0E	1	STRAT WARMING POSS BEAT B12/CH
1979	29	1337:1351	115.145	-5:50	3E	1	0E	3E	3E	1	1E	STRAT WARMING
1979	30	1351:1365	115.247	10:65	3E	0E	0	2E	3E	1	1E	STRAT WARMING POSS BEAT B12/CH
1979	31	1365:1379	115.251	25:80	1E	1	0	1E	3E	1	0E	STRAT WARMING POSS BEAT C1/C3
1979	32	1379:1392	115.261	-5:50	2E	1E	0	3E	3E	1E	1	STRAT WARMING
1979	33	1393:1406	115.246	10:65	3E	1	0E	2E	3E	1E	1	STRAT WARMING POSS BEAT B12/CH
1979	34	1407:1420	115.145	-5:50	3E	1	0E	3E	3E	1	1E	
1979	35	1421:1433	115.145	-5:50	3E	1	0E	3E	3E	1	1E	
1979	36	1434:1447	115.145	-5:50	3E	1	0E	3E	3E	1	1E	
1979	37	1448:1461	115.145	-5:50	3E	1	0E	3E	3E	1	1E	
1979	38	1462:1475	115.145	-5:50	3E	1	0E	3E	3E	1	1E	
1979	39	1476:1489	115.145	-5:50	3E	1	0E	3E	3E	1	1E	
1979	41	1504:1516	115.145	-5:50	3E	1	0E	3E	3E	1	1E	
1979	42	1517:1531	115.145	-5:50	3E	1	0E	3E	3E	1	1E	
1979	43	1532:1544	115.145	-5:50	3E	1	0E	3E	3E	1	1E	
1979	45	1558:1572	114.253	40:105	1E	1	0E	0E	3E	0E	1	
1979	46	1572:1586	114.254	40:105	1E	0E	0	0E	3E	1	0E	POSS BEAT C1/C3
1979	47	1586:1600	116.262	-15:50	2E	1E	0	3E	3E	1	1E	
1979	49	1614:1616	116.262	-15:50	2E	1E	0	3E	3E	1	1E	NO SCANNING

DATE YEAR	DAY	ORBITS (APPROX)	SCAN PROG	RANGE(KM) (APPROX)	SIEVE SETTINGS A1	A2	A3	B1 B2	C1	C2	C3	
1979	49	1616:1627	116.262	-15:50	2E	1E	0	3E	3E	1	1E	
1979	50	1627:1640	115.246	10:65	3E	1	0E	2E	3E	1E	1	"NO" ROCKET COVERAGE
1979	51	1640:1655	115.246	10:65	3E	1	0E	2E	3E	1E	1	"NO" ROCKET COVERAGE
1979	53	1669:1683	118.348	-10:90	3E	1	0	2E	3E	1E	1	POSS BEAT B12/CH
1979	54	1683:1696	118.345	-25:75	3E	1	0E	3E	3E	1E	1	
1979	55	1696:1710	118.362	-45:55	2E	1E	0	3E	3E	1	1E	
1979	56	1710:1723	118.346	-10:90	3E	1	0E	2E	3E	1E	1	POSS BEAT B12/CH
1979	57	1724:1738	118.346	-10:90	3E	1	0E	2E	3E	1E	1	POSS BEAT B12/CH
1979	58	1738:1741	118.347	-10:90	3E	0E	0	2E	3E	1	1E	NO SCANNING, POSS BEAT B12/CH
1979	58	1741:1752	118.347	-10:90	3E	0E	0	2E	3E	1	1E	POSS BEAT B12/CH
1979	59	1752:1766	119.355	40:125	0E	1	0	0E	3E	0E	1	FREQ SPACE CAL
1979	61	1779:1793	118.361	-25:75	2E	1E	0	3E	3E	1	1E	
1979	62	1793:1802	118.361	-25:75	2E	1E	0	3E	3E	1	1E	
1979	62	1802:1807	5.143		3E	0	0	3E	3E	1	1E	MOON SCAN
1979	63	1808:1821	118.346	-10:90	3E	1	0E	2E	3E	1E	1	POSS BEAT B12/CH
1979	65	1835:1848	118.350	5:105	1E	1	0	1E	3E	0E	1	
1979	66	1648:1855	118.350	5:105	1E	1	0	1E	3E	0E	1	
1979	66	1855:1863	5.143		3E	0	0	3E	3E	1	1E	MOON SCAN
1979	67	1863:1876	118.347	-10:90	3E	0E	0	2E	3E	1	1E	POSS BEAT B12/CH
1979	69	1890:1904	118.348	-10:90	3E	1	0	2E	3E	1E	1	POSS BEAT B12/CH
1979	70	1904:1918	118.345	-25:75	3E	1	0E	3E	3E	1E	1	
1979	71	1918:1932	118.362	-45:55	2E	1E	0	3E	3E	1	1E	
1979	73	1946:1958	119.453	30:115	1E	1	0E	0E	3E	0E	1	FREQ SPACE CAL
1979	73	1958:1959	119.100		1E	0	0	3E	3E	1	0E	SCAN CAL CHECK
1979	74	1959:1973	119.454	30:115	1E	0E	0	0E	3E	1	0E	FREQ SPACE CAL
1979	75	1974:1986	119.455	30:115	0E	1	0	0E	3E	0E	1	FREQ SPACE CAL
1979	77	2001:2014	118.356	-45:55	2E	1E	0	3E	3E	1E	1	
1979	78	2015:2028	118.361	-25:75	2E	1E	0	3E	3E	1	1E	
1979	79	2029:2042	118.346	-10:90	3E	1	0E	2E	3E	1E	1	POSS BEAT B12/CH
1979	81	2057:2069	118.350	5:105	1E	1	0	1E	3E	0E	1	
1979	82	2070:2083	118.351	5:105	1E	1	0	1E	3E	1	0E	
1979	83	2084:2097	118.347	-10:90	3E	0E	0	2E	3E	1	1E	POSS BEAT B12/CH
1979	85	2112:2125	118.348	-10:90	3E	1	0	2E	3E	1E	1	POSS BEAT B12/CH
1979	86	2125:2139	118.345	-25:75	3E	1	0E	3E	3E	1E	1	
1979	87	2139:2147	118.362	-45:55	2E	1E	0	3E	3E	1	1E	
1979	87	2147:2156	118.364	-25:75	3E	1	0E	3E	3E	1	1E	NORMAL BALLOON MODE
1979	89	2167:2179	119.453	30:115	1E	1	0E	0E	3E	0E	1	FREQ SPACE CAL
1979	90	2180:2194	118.364	-25:75	3E	1	0E	3E	3E	1	1E	NORMAL BALLOON MODE
1979	91	2194:2208	118.364	-25:75	3E	1	0E	3E	3E	1	1E	NORMAL BALLOON MODE
1979	92	2208:2213	118.364	-25:75	3E	1	0E	3E	3E	1	1E	NORMAL BALLOON MODE
1979	92	2214:2218	5.143		3E	0	0	3E	3E	1	1E	MOON SCAN
1979	92	2219:2221	219.455		0E	1	0	0E	3E	0E	1	1 DOPPLER SCAN
1979	93	2222:2235	118.356	-45:55	3E	1	0E	3E	3E	1E	1	
1979	94	2236:2249	118.364	-25:75	3E	1	0E	3E	3E	1	1E	NORMAL BALLOON MODE
1979	95	2250:2263	118.364	-25:75	3E	1	0E	3E	3E	1	1E	NORMAL BALLOON MODE
1979	96	2264:2273	118.364	-25:75	3E	1	0E	3E	3E	1	1E	NORMAL BALLOON MODE
1979	96	2274:2277	118.364	-25:75	3E	1	0E	3E	3E	1	1E	NORMAL BALLOON MODE
1979	97	2278:2291	118.364	-25:75	3E	1	0E	3E	3E	1	1E	NORMAL BALLOON MODE
1979	98	2292:2304	118.364	-25:75	3E	1	0E	3E	3E	1	1E	NORMAL BALLOON MODE
1979	99	2305:2318	118.364	-25:75	3E	1	0E	3E	3E	1	1E	NORMAL BALLOON MODE
1979	100	2319:2332	118.364	-25:75	3E	1	0E	3E	3E	1	1E	NORMAL BALLOON MODE
1979	101	2332:2344	219.455		0E	1	0	0E	3E	0E	1	1 DOPPLER SCAN/ORBIT
1979	102	2345:2360	118.345	-25:75	3E	1	0E	3E	3E	1E	1	
1979	103	2360:2374	118.362	-45:55	2E	1E	0	3E	3E	1	1E	
1979	105	2388:2400	119.453	30:115	1E	1	0E	0E	3E	0E	1	FREQ SPACE CAL
1979	107	2415:2429	119.455	30:115	0E	1	0	0E	3E	0E	1	FREQ SPACE CAL

DATE YEAR	DAY	ORBITS (APPROX)	SCAN PROG	RANGE(KM) (APPROX)	A1	A2	A3	B1 B2	C1	C2	C3	
1979	109	2443:2452	118.356	-45:55	3E	1	0E	3E	3E	1E	1	
1979	109	2453:2457	118.364	-25:75	3E	1	0E	3E	3E	1	1E	NORMAL BALLOON MODE
1979	110	2457:2471	118.361	-25:75	2E	1E	0	3E	3E	1	1E	
1979	111	2471:2484	118.346	-10:90	3E	1	0E	2E	3E	1E	1	POSS BEAT B12/CH
1979	113	2498:2512	118.364	-25:75	3E	1	0E	3E	3E	1	1E	NORMAL BALLOON MODE
1979	114	2512:2522	118.351	5:105	1E	1	0	1E	3E	1	0E	
1979	114	2522:2526	118.364	-25:75	3E	1	0E	3E	3E	1	1E	NORMAL BALLOON MODE
1979	115	2526:2540	118.364	-25:75	3E	1	0E	3E	3E	1	1E	NORMAL BALLOON MODE
1979	117	2553:2567	300.200		3E	1	0E	2E	3E	0E	1	ALT DOPPLER AND LIMB SCANS
1979	119	2582:2595	118.364	-25:75	3E	1	0E	3E	3E	1	1E	NORMAL BALLOON MODE
1979	120	2596:2609	118.364	-25:75	3E	1	0E	3E	3E	1	1E	NORMAL BALLOON MODE
1979	121	2610:2623	118.350	5:105	1E	1	0	1E	3E	0E	1	
1979	122	2624:2630	5.143		3E	0	0	3E	3E	1	1E	MOON SCAN
1979	122	2631:2636	119.453	30:115	1E	1	0E	0E	3E	0E	1	FREQ SPACE CAL
1979	123	2637:2650	119.453	30:115	1E	1	0E	0E	3E	0E	1	FREQ SPACE CAL
1979	125	2678:2685	5.143		3E	0	0	3E	3E	1	1E	MOON SCAN
1979	125	2685:2678	119.454	30:115	1E	0E	0	0E	3E	1	0E	FREQ SPACE CAL
1979	126	2679:2691	119.455	30:115	0E	1	0	0E	3E	0E	1	FREQ SPACE CAL
1979	127	2692:2700	119.454	30:115	1E	0E	0	0E	3E	1	0E	FREQ SPACE CAL
1979	127	2700:2706	118.364	-25:75	3E	1	0E	3E	3E	1	1E	NORMAL BALLOON MODE
1979	129	2719:2736	118.356	-45:55	3E	1	0E	3E	3E	1E	1	
1979	130	2736:2747	118.344	-25:75	3E	1E	0	3E	3E	1	1E	
1979	131	2748:2761	118.346	-10:90	3E	1	0E	2E	3E	1E	1	POSS BEAT B12/CH
1979	132	2761:2774	118.364	-25:75	3E	1	0E	3E	3E	1	1E	NORMAL BALLOON MODE
1979	133	2775:2788	118.364	-25:75	3E	1	0E	3E	3E	1	1E	NORMAL BALLOON MODE
1979	135	2802:2816	118.347	-10:90	3E	0E	0	2E	3E	1	1E	POSS BEAT B12/CH
1979	136	2816:2830	118.364	-25:75	3E	1	0E	3E	3E	1	1E	NORMAL BALLOON MODE
1979	137	2831:2844	118.364	-25:75	3E	1	0E	3E	3E	1	1E	NORMAL BALLOON MODE
1979	138	2844:2857	118.345	-25:75	3E	1	0E	3E	3E	1E	1	
1979	139	2857:2875	118.357	-45:55	3E	1E	0	3E	3E	1	1E	
1979	141	2885:2886	119.100		1E	0	0	3E	3E	1	0E	SCAN CAL CHECK
1979	141	2887:2899	119.453	30:115	1E	1	0E	0E	3E	0E	1	FREQ SPACE CAL
1979	142	2900:2913	119.454	30:115	1E	0E	0	0E	3E	1	0E	FREQ SPACE CAL
1979	143	2913:2926	119.455	30:115	0E	1	0	0E	3E	0E	1	FREQ SPACE CAL
1979	145	2941:2953	118.363	-25:75	3E	1E	0	3E	3E	1E	1	
1979	146	2954:2967	118.361	-25:75	2E	1E	0	3E	3E	1	1E	
1979	147	2968:2981	118.366	-10:90	3E	0E	0	2E	3E	1E	1	
1979	149	2996:3009	118.350	5:105	1E	1	0	1E	3E	0E	1	
1979	150	3010:3023	118.351	5:105	1E	1	0	1E	3E	1	0E	
1979	151	3024:3037	118.347	-10:90	3E	0E	0	2E	3E	1	1E	POSS BEAT B12/CH
1979	152	3049:3052	5.143		3E	0	0	3E	3E	1	1E	MOON SCAN
1979	153	3053:3055	5.143		3E	0	0	3E	3E	1	1E	MOON SCAN
1979	153	3055:3064	118.348	-10:90	3E	1	0	2E	3E	1E	1	POSS BEAT B12/CH
1979	154	3065:3078	118.345	-25:75	3E	1	0E	3E	3E	1E	1	
1979	155	3079:3089	118.362	-45:55	2E	1E	0	3E	3E	1	1E	
1979	155	3090:3092	5.143		3E	0	0	3E	3E	1	1E	MOON SCAN
1979	156	3093:3097	5.143		3E	0	0	3E	3E	1	1E	MOON SCAN
1979	157	3106:3120	300.200		3E	1	0E	2E	3E	0E	1	ALT DOPPLER AND LIMB SCANS
1979	158	3121:3130	300.200		3E	1	0E	2E	3E	0E	1	ALT DOPPLER AND LIMB SCANS
1979	158	3131:3134	118.346	-10:90	3E	1	0E	2E	3E	1E	1	POSS BEAT B12/CH
1979	159	3135:3147	300.201		3E	1	0E	2E	3E	1E	1	DOPPLER SCANS
1979	161	3161:3175	25.101		3E	0E	0	3E	3E	1	1E	
1979	162	3175:3188	118.361	-25:75	2E	1E	0	3E	3E	1	1E	
1979	163	3189:3203	118.366	-10:90	3E	0E	0	2E	3E	1E	1	
1979	165	3217:3230	118.364	-25:75	3E	1	0E	3E	3E	1	1E	NORMAL BALLOON MODE
1979	166	3231:3244	301.202		2E	1	0E	2E	3E	0E	1	ALT DOPPLER AND LIMB SCANS

DATE YEAR	DAY	ORBITS (APPROX)	SCAN PROG	RANGE(KM) (APPROX)	SIEVE SETTINGS A1	A2	A3	B1 B2	C1	C2	C3	
1979	167	3244:3258	26.101		3E	0E	0	3E	3E	1	1E	SPACE VIEW/BB. MIRROR AT AZ BACKWARD LIMIT
1979	169	3272:3285	26.102		3E	0E	0	3E	3E	1	1E	DOPPLER SCANS IN SPACE VIEW
1979	170	3286:3299	118.345	-25:75	3E	1	0E	3E	3E	1E	1	MIRROR AT AZIMUTH BACKWARD LIMIT
1979	171	3300:3313	118.362	-45:55	2E	1E	0	3E	3E	1	1E	MIRROR AT AZIMUTH BACKWARD LIMIT
1979	173	3327:3339	129.475	20:125	0E	1	0	0E	3E	0E	1	FREQ SPACE CAL
1979	174	3340:3341	129.100		1E	0	0	3E	3E	1	0E	SCAN CAL CHECK
1979	174	3342:3355	129.475	20:125	0E	1	0	0E	3E	0E	1	FREQ SPACE CAL
1979	175	3355:3368	129.473	20:125	1E	1	0E	0E	3E	0E	1	FREQ SPACE CAL
1979	177	3383:3396	118.365	-25:75	2E	1E	0	3E	3E	1E	1	
1979	178	3397:3410	118.361	-25:75	2E	1E	0	3E	3E	1	1E	
1979	179	3411:3423	118.366	-10:90	3E	0E	0	2E	3E	1E	1	
1979	181	3438:3451	118.350	5:105	1E	1	0	1E	3E	0E	1	
1979	182	3452:3465	118.351	5:105	1E	1	0	1E	3E	1	0E	
1979	183	3466:3479	118.347	-10:90	3E	0E	0	2E	3E	1	1E	POSS BEAT B12/CH
1979	185	3493:3506	118.348	-10:90	3E	1	0	2E	3E	1E	1	POSS BEAT B12/CH
1979	186	3507:3520	118.345	-25:75	3E	1	0E	3E	3E	1E	1	
1979	187	3521:3535	118.362	-45:55	2E	1E	0	3E	3E	1	1E	
1979	189	3549:3562	129.473	20:125	1E	1	0E	0E	3E	0E	1	FREQ SPACE CAL
1979	190	3563:3575	129.474	20:125	1E	0E	0	0E	3E	1	0E	FREQ SPACE CAL
1979	191	3576:3589	129.475	20:125	0E	1	0	0E	3E	0E	1	FREQ SPACE CAL
1979	193	3606:3617	118.365	-25:75	2E	1E	0	3E	3E	1E	1	
1979	194	3618:3632	118.361	-25:75	2E	1E	0	3E	3E	1	1E	
1979	195	3632:3646	118.366	-10:90	3E	0E	0	2E	3E	1E	1	
1979	197	3669:3672	118.350	5:105	1E	1	0	1E	3E	0E	1	
1979	198	3673:3687	118.351	5:105	1E	1	0	1E	3E	1	0E	
1979	199	3687:3700	118.365	-25:75	2E	1E	0	3E	3E	1E	1	
1979	200	3701:3704	118.365	-25:75	2E	1E	0	3E	3E	1E	1	
1979	201	3714:3728	118.364	-25:75	3E	1	0E	3E	3E	1	1E	NORMAL BALLOON MODE
1979	202	3728:3741	118.345	-25:75	3E	1	0E	3E	3E	1E	1	
1979	203	3742:3758	118.362	-45:55	2E	1E	0	3E	3E	1	1E	
1979	205	3769:3782	129.473	20:125	1E	1	0E	0E	3E	0E	1	FREQ SPACE CAL
1979	206	3783:3784	129.100		1E	0	0	3E	3E	1	0E	SCAN CAL CHECK
1979	206	3785:3797	129.474	20:125	1E	0E	0	0E	3E	1	0E	FREQ SPACE CAL
1979	207	3797:3811	129.475	20:125	0E	1	0	0E	3E	0E	1	FREQ SPACE CAL
1979	209	3828:3838	118.365	-25:75	2E	1E	0	3E	3E	1E	1	
1979	210	3839:3852	118.364	-25:75	3E	1	0E	3E	3E	1	1E	NORMAL BALLOON MODE
1979	211	3852:3867	118.364	-25:75	3E	1	0E	3E	3E	1	1E	NORMAL BALLOON MODE
1979	213	3880:3894	118:350	5:105	1E	1	0	1E	3E	0E	1	
1979	214	3894:3908	118:351	5:105	1E	1	0	1E	3E	1	0E	
1979	215	3908:3922	118.347	-10:90	3E	0E	0	2E	3E	1	1E	POSS BEAT B12/CH
1979	217	3936:3949	118.103	-25:75	3E	0	0	3E	0E	1E	0	
1979	218	3949:3963	118.104	-25:75	3E	0	0	3E	1E	0	1E	SPECTAL C1 PMC CAL MODE
1979	219	3963:3967	118.364	-25:75	3E	1	0E	3E	3E	1	1E	NORMAL BALLOON MODE
1979	219	3968:3977	118:105	-25:75	3E	0	0	1E	2E	0	1E	SPECIAL C1 PMC CAL MODE
1979	221	3991:4004	118.475	20:125	0E	1	0	0E	3E	0E	1	FREQ SPACE CAL
1979	222	4004:4018	118.475	20:125	0E	1	0	0E	3E	0E	1	FREQ SPACE CAL
1979	223	4018:4032	118.475	20:125	0E	1	0	0E	3E	0E	1	FREQ SPACE CAL
1979	225	4047:4060	118.476	20:125	1E	1	0	1E	3E	1	0E	FREQ SPACE CAL
1979	226	4060:4073	118.476	20:125	1E	1	0	1E	3E	1	0E	FREQ SPACE CAL
1979	227	4073:4087	118.476	20:125	1E	1	0	1E	3E	1	0E	FREQ SPACE CAL
1979	229	4101:4115	27.106		3E	0	0	0E	3E	1	0E	WIDE LIMB SCAN FOR WB STRAYS CHECK
1979	230	4115:4129	118.351	5:105	1E	1	0	1E	3E	1	0E	
1979	231	4129:4143	118.347	-10:90	3E	0E	0	2E	3E	1	1E	POSS BEAT B12/CH
1979	233	4156:4171	118.348	-10:90	3E	1	0	2E	3E	1E	1	POSS BEAT B12/CH
1979	234	4171:4184	118.345	-25:75	3E	1	0E	3E	3E	1E	1	
1979	235	4184:4198	118.362	-45:55	2E	1E	0	3E	3E	1	1E	

DATE YEAR	DAY	ORBITS (APPROX)	SCAN PROG	RANGE(KM) (APPROX)	SIEVE SETTINGS A1	A2	A3	B1 B2	C1	C2	C3	
1979	236	4211:4212	129.100		1E	0	0	3E	3E	1	0E	SCAN CAL CHECK
1979	237	4212:4225	129.473	20:125	1E	1	0E	0E	3E	0E	1	FREQ SPACE CAL
1979	238	4225:4238	129.474	20:125	1E	0E	0	0E	3E	1	0E	FREQ SPACE CAL
1979	239	4238:4252	129.475	20:125	0E	1	0	0E	3E	0E	1	FREQ SPACE CAL
1979	241	4267:4281	118.365	-25:75	2E	1E	0	3E	3E	1E	1	
1979	242	4281:4295	118.361	-25:75	2E	1E	0	3E	3E	1	1E	
1979	243	4295:4308	118.366	-10:90	3E	0E	0	2E	3E	1E	1	
1979	245	4323:4336	118.350	5:105	1E	1	0	1E	3E	0E	1	
1979	246	4336:4350	118.351	5:105	1E	1	0	1E	3E	1	0E	
1979	247	4350:4364	118.347	-10:90	3E	0E	0	2E	3E	1	1E	POSS BEAT B12/CH
1979	249	4378:4392	118.348	-10:90	3E	1	0	2E	3E	1E	1	POSS BEAT B12/CH
1979	250	4392:4404	118.345	-25:75	3E	1	0E	3E	3E	1E	1	
1979	251	4405:4418	118.362	-45:55	2E	1E	0	3E	3E	1	1E	
1979	253	4433:4446	129.473	20:125	1E	1	0E	0E	3E	0E	1	FREQ SPACE CAL
1979	254	4447:4461	129.474	20:125	1E	0E	0	0E	3E	1	0E	FREQ SPACE CAL
1979	255	4461:4474	129.475	20:125	0E	1	0	0E	3E	0E	1	FREQ SPACE CAL
1979	257	4488:4502	118.365	-25:75	2E	1E	0	3E	3E	1E	1	
1979	258	4502:4515	118.361	-25:75	2E	1E	0	3E	3E	1	1E	
1979	259	4515:4529	118.366	-10:90	3E	0E	0	2E	3E	1E	1	
1979	261	4546:4558	118.350	5:105	1E	1	0	1E	3E	0E	1	
1979	262	4558:4571	118.351	5:105	1E	1	0	1E	3E	1	0E	
1979	263	4571:4585	118.346	-10:90	3E	1	0E	2E	3E	1E	1	
1979	265	4599:4602	118.348	-10:90	3E	1	0	2E	3E	1E	1	
1979	265	4602:4612	118.348	-10:90	3E	1	0	2E	3E	1E	1	
1979	266	4612:4626	118.345	-25:75	3E	1	0E	3E	3E	1E	1	
1979	267	4626:4640	118.362	-45:55	2E	1E	0	3E	3E	1	1E	
1979	269	4653:4654	129.100		1E	0	0	3E	3E	1	0E	SCAN CAL CHECK
1979	269	4654:4668	129.473	20:125	1E	1	0E	0E	3E	0E	1	SPACE VIEW EACH SCAN CYCLE
1979	270	4668:4682	129.474	20:125	1E	0E	0	0E	3E	1	0E	SPACE VIEW EACH SCAN CYCLE
1979	271	4682:4695	129.475	20:125	0E	1	0	0E	3E	0E	1	SPACE VIEW EACH SCAN CYCLE
1979	273	4709:4723	118.365	-25:75	2E	1E	0	3E	3E	1E	1	
1979	274	4723:4737	118.346	-10:90	3E	1	0E	2E	3E	1E	1	
1979	275	4737:4751	118.366	-10:90	3E	0E	0	2E	3E	1E	1	
1979	277	4765:4778	118.350	5:105	1E	1	0	1E	3E	0E	1	
1979	278	4778:4792	118.351	5:105	1E	1	0	1E	3E	1	0E	
1979	279	4792:4806	118.347	-10:90	3E	0E	0	2E	3E	1	1E	
1979	281	4820:4834	118.348	-10:90	3E	1	0	2E	3E	1E	1	
1979	282	4834:4847	118.345	-25:75	3E	1	0E	3E	3E	1E	1	
1979	283	4847:4861	118.362	-45:55	2E	1E	0	3E	3E	1	1E	
1979	285	4875:4889	129.473	20:125	1E	1	0E	0E	3E	0E	1	SPACE VIEW EACH SCAN CYCLE
1979	286	4889:4903	129.474	20:125	1E	0E	0	0E	3E	1	0E	SPACE VIEW EACH SCAN CYCLE
1979	287	4903:4917	129.475	20:125	0E	1	0	0E	3E	0E	1	SPACE VIEW EACH SCAN CYCLE
1979	289	4930:4944	118.365	-25:75	2E	1E	0	3E	3E	1E	1	
1979	290	4944:4958	118.361	-25:75	2E	1E	0	3E	3E	1	1E	
1979	291	4958:4971	118.366	-10:90	3E	0E	0	2E	3E	1E	1	
1979	293	4986:4999	118.350	5:105	1E	1	0	1E	3E	0E	1	
1979	294	5000:5013	118.351	5:105	1E	1	0	1E	3E	1	0E	
1979	295	5014:5027	118.347	-10:90	3E	0E	0	2E	3E	1	1E	
1979	297	5041:5055	118.348	-10:90	3E	1	0	2E	3E	1E	1	
1979	298	5055:5068	118.345	-25:75	3E	1	0E	3E	3E	1E	1	
1979	299	5068:5082	118.345	-25:75	3E	1	0E	3E	3E	1E	1	
1979	300	5095:5096	129.100		1E	0	0	3E	3E	1	0E	SCAN CAL CHECK
1979	301	5096:5110	129.473	20:125	1E	1	0E	0E	3E	0E	1	SPACE VIEW EACH SCAN CYCLE
1979	302	5110:5124	129.474	20:125	1E	0E	0	0E	3E	1	0E	SPACE VIEW EACH SCAN CYCLE
1979	303	5124:5138	129.475	20:125	0E	1	0	0E	3E	0E	1	SPACE VIEW EACH SCAN CYCLE
1979	305	5152:5165	118.365	-25:75	2E	1E	0	3E	3E	1E	1	

DATE YEAR	DAY	ORBITS (APPROX)	SCAN PROG	RANGE(KM) (APPROX)	A1	A2	A3	B1 B2	C1	C2	C3	
1979	306	5165:5179	118.347	-10:90	3E	0E	0	2E	3E	1	1E	
1979	307	5179:5193	118.366	-10:90	3E	0E	0	2E	3E	1E	1	
1979	309	5208:5220	118.364	-25:75	3E	1	0E	3E	3E	1	1E	
1979	310	5220:5234	118.364	-25:75	3E	1	0E	3E	3E	1	1E	
1979	311	5234:5248	118.364	-25:75	3E	1	0E	3E	3E	1	1E	
1979	313	5262:5276	118.348	-10:90	3E	1	0	2E	3E	1E	1	
1979	314	5276:5290	118.345	-25:75	3E	1	0E	3E	3E	1E	1	
1979	315	5290:5303	118.362	-45:55	2E	1E	0	3E	3E	1	1E	
1979	317	5317:5331	129.473	20:125	1E	1	0E	0E	3E	0E	1	SPACE VIEW EACH SCAN CYCLE
1979	318	5331:5345	118.346	-10:90	3E	1	0E	2E	3E	1E	1	ROCKET FLIGHT COVERAGE
1979	319	5345:5359	129.475	20:125	0E	1	0	0E	3E	0E	1	SPACE VIEW EACH SCAN CYCLE
1979	321	5373:5386	118.365	-25:75	2E	1E	0	3E	3E	1E	1	
1979	322	5386:5400	118.361	-25:75	2E	1E	0	3E	3E	1	1E	
1979	323	5400:5414	118.366	-10:90	3E	0E	0	2E	3E	1E	1	
1979	325	5428:5442	118.350	5:105	1E	1	0	1E	3E	0E	1	
1979	326	5442:5455	118.351	5:105	1E	1	0	1E	3E	1	0E	
1979	327	5455:5469	118.366	-10:90	3E	0E	0	2E	3E	1E	1	
1979	329	5483:5497	118.348	-10:90	3E	1	0	2E	3E	1E	1	
1979	330	5497:5511	118.345	-25:75	3E	1	0E	3E	3E	1E	1	SYNC SLIP
1979	331	5511:5525	118.362	-45:55	2E	1E	0	3E	3E	1	1E	SEVERAL SCAN LOGIC JUMPS
1979	333	5538:5552	118.364	-25:75	3E	1	0E	3E	3E	1	1E	NO SCANNING
1979	334	5552:5566	118.364	-25:75	3E	1	0E	3E	3E	1	1E	
1979	335	5566:5579	118.364	-25:75	3E	1	0E	3E	3E	1	1E	NORMAL BALLOON MODE
1979	337	5594:5596	118.		0	0	0	0	0	0	0	GSFC MESSING ABOUT WITH PCL
1979	337	5597:5607	118.365	-25:75	2E	1E	0	3E	3E	1E	1	
1979	338	5608:5621	118.361	-25:75	2E	1E	0	3E	3E	1	1E	
1979	339	5622:5635	118.366	-10:90	3E	0E	0	2E	3E	1E	1	
1979	340	5635:5649	118.346	-10:90	3E	1	0E	2E	3E	1E	1	POSS BEAT BI2/CH ROCKET FLIGHT MODE
1979	341	5649:5663	118.366	-10:90	3E	0E	0	2E	3E	1E	1	
1979	342	5663:5677	118.351	5:105	1E	1	0	1E	3E	1	0E	
1979	343	5677:5690	118.347	-10:90	3E	0E	0	2E	3E	1	1E	POSS BEAT BI2/CH
1979	345	5704:5718	118.348	-10:90	3E	1	0	2E	3E	1E	1	POSS BEAT BI2/CH
1979	346	5718:5726	118.345	-25:75	3E	1	0E	3E	3E	1E	1	
1979	346	5727:5728	118.345		3E	1	0E	3E	3E	1E	1	NO SCANNING FOLLOWING PCL MALFUNCTION
1979	346	5728:5732	118.345	-25:75	3E	1	0E	3E	3E	1E	1	
1979	347	5732:5746	118.362	-45:55	2E	1E	0	3E	3E	1	1E	
1979	348	5759:5760	129.100		1E	0	0	3E	3E	1	0E	SCAN CAL CHECK
1979	349	5760:5773	129.473	20:125	1E	1	0E	0E	3E	0E	1	FREQ SPACE CAL
1979	350	5773:5787	129.474	20:125	1E	0E	0	0E	3E	1	0E	FREQ SPACE CAL
1979	351	5787:5800	118.346	-10:90	3E	1	0E	2E	3E	1E	1	POSS BEAT BI2/CH ROCKET FLIGHT MODE
1979	352	5800:5814	118.346	-10:90	3E	1	0E	2E	3E	1E	1	POSS BEAT BI2/CH ROCKET FLIGHT MODE
1979	353	5815:5828	118.365	-25:75	2E	1E	0	3E	3E	1E	1	
1979	354	5828:5842	118.361	-25:75	2E	1E	0	3E	3E	1	1E	
1979	355	5842:5856	118.366	-10:90	3E	0E	0	2E	3E	1E	1	
1979	357	5870:5884	118.350	5:105	1E	1	0	1E	3E	0E	1	
1979	358	5884:5898	118.351	5:105	1E	1	0	1E	3E	1	0E	
1979	359	5898:5912	118.347	-10:90	3E	0E	0	2E	3E	1	1E	POSS BEAT BI2/CH
1979	361	5925:5939	118.348	-10:90	3E	1	0	2E	3E	1E	1	POSS BEAT BI2/CH
1979	362	5939:5953	118.345	-25:75	3E	1	0E	3E	3E	1E	1	
1979	363	5953:5966	118.362	-45:55	2E	1E	0	3E	3E	1	1E	
1979	365	5981:5994	129.473	20:125	1E	1	0E	0E	3E	0E	1	FREQ SPACE CAL
1980	1	5994:6008	129.474	20:125	1E	0E	0	0E	3E	1	0E	FREQ SPACE CAL
1980	2	6008:6021	129.475	20:125	0E	1	0	0E	3E	0E	1	FREQ SPACE CAL
1980	3	6021:6022	129.100		1E	0	0	3E	3E	1	0E	SCAN CAL CHECK
1980	4	6036:6049	118.350	5:105	1E	1	0	1E	3E	0E	1	
1980	5	6050:6063	118.351	5:105	1E	1	0	1E	3E	1	0E	

DATE YEAR	DAY	ORBITS (APPROX)	SCAN PROG	RANGE(KM) (APPROX)	STEVE SETTINGS A1	A2	A3	B1 B2	C1	C2	C3	
1980	6	6063:6077	118.347	-10:90	3E	0E	0	2E	3E	1	1E	POSS BEAT BI2/CH
1980	8	6091:6105	118.348	-10:90	3E	1	0	2E	3E	1E	1	POSS BEAT BI2/CH
1980	9	6105:6119	118.345	-25:75	3E	1	0E	3E	3E	1E	1	
1980	10	6119:6133	118.362	-45:55	2E	1E	0	3E	3E	1	1E	
1980	12	6146:6160	129.473	20:125	1E	1	0E	0E	3E	0E	1	FREQ SPACE CAL
1980	13	6160:6174	129.474	20:125	1E	0E	0	0E	3E	1	0E	FREQ SPACE CAL
1980	14	6174:6188	129.475	20:125	0E	1	0	0E	3E	0E	1	FREQ SPACE CAL
1980	16	6202:6215	118.365	-25:75	2E	1E	0	3E	3E	1E	1	
1980	17	6215:6229	118.361	-25:75	2E	1E	0	3E	3E	1	1E	
1980	18	6229:6243	118.366	-10:90	3E	0E	0	2E	3E	1E	1	
1980	20	6257:6271	118.350	5:105	1E	1	0	1E	3E	0E	1	
1980	21	6271:6284	118.351	5:105	1E	1	0	1E	3E	1	0E	
1980	22	6284:6298	118.347	-10:90	3E	0E	0	2E	3E	1	1E	POSS BEAT BI2/CH
1980	24	6312:6326	118.348	-10:90	3E	1	0	2E	3E	1E	1	POSS BEAT BI2/CH
1980	25	6329:6340	118.345	-25:75	3E	1	0E	3E	3E	1E	1	
1980	26	6340:6354	118.362	-45:55	2E	1E	0	3E	3E	1	1E	
1980	28	6367:6381	129.473	20:125	1E	1	0E	0E	3E	0E	1	FREQ SPACE CAL
1980	29	6381:6395	129.474	20:125	1E	0E	0	0E	3E	1	0E	FREQ SPACE CAL
1980	30	6396:6409	129.475	20:125	0E	1	0	0E	3E	0E	1	FREQ SPACE CAL
1980	32	6423:6437	129.365	-25:75	2E	1E	0	3E	3E	1E	1	FREQ SPACE CAL. SEE NOTE 1.
1980	33	6437:6451	129.361	-25:75	2E	1E	0	3E	3E	1	1E	FREQ SPACE CAL. SEE NOTE 1
1980	34	6451:6464	129.366	-10:90	3E	0E	0	2E	3E	1E	1	FREQ SPACE CAL. SEE NOTE 1
1980	36	6478:6492	129.350	5:105	1E	1	0	1E	3E	0E	1	FREQ SPACE CAL. SEE NOTE 1
1980	37	6492:6497	129.351	5:105	1E	1	0	1E	3E	1	0E	FREQ SPACE CAL. NO SCANNING
1980	37	6497:6505	129.351	5:105	1E	1	0	1E	3E	1	0E	FREQ SPACE CAL. SEE NOTES 1 AND 2
1980	38	6505:6519	129.347	-10:90	3E	0E	0	2E	3E	1	1E	FREQ SPACE CAL. SEE NOTES 1 AND 2 AND 3
1980	40	6533:6547	129.348	-10:90	3E	1	0	2E	3E	1E	1	FREQ SPACE CAL. SEE NOTES 1, 2 AND 3.
1980	41	6547:6561	129.345	-25:75	3E	1	0E	3E	3E	1E	1	FREQ SPACE CAL. SEE NOTE 1
1980	42	6561:6575	129.362	-45:55	2E	1E	0	3E	3E	1	1E	FREQ SPACE CAL. SEE NOTE 1
1980	44	6589:6603	129.483	-10:90	1E	1	0E	3E	3E	0E	1	FREQ SPACE CAL.
1980	45	6603:6617	129.484	-10:90	1E	0E	0	3E	3E	1	0E	FREQ SPACE CAL.
1980	46	6617:6629	129.485	-10:90	0E	1	0	0E	3E	0E	1	FREQ SPACE CAL.
1980	46	6629:6630	129.100		1E	0	0	3E	3E	1	0E	SCAN CAL CHECK.
1980	48	6644:6658	118.365	-25:75	2E	1E	0	3E	3E	1E	1	
1980	49	6658:6671	118.361	-25:75	2E	1E	0	3E	3E	1	1E	
1980	50	6671:6685	118.366	-10:90	3E	0E	0	2E	3E	1E	1	
1980	52	6699:6713	118.350	5:105	1E	1	0	1E	3E	0E	1	
1980	53	6713:6727	118.351	5:105	1E	1	0	1E	3E	1	0E	
1980	54	6728:6741	118.347	-10:90	3E	0E	0	2E	3E	1	1E	POSS BEAT B12/CH.
1980	56	6754:6768	118.348	-10:90	3E	1	0	2E	3E	1E	1	POSS BEAT B12/CH.
1980	57	6768:6782	118.345	-25:75	3E	1	0E	3E	3E	1E	1	
1980	58	6782:6796	118.362	-45:55	2E	1E	0	3E	3E	1	1E	
1980	60	6810:6823	129.473	20:125	1E	1	0E	0E	3E	0E	1	FREQ SPACE CAL
1980	61	6823:6837	129.484	-10:90	1E	0E	0	3E	3E	1	0E	FREQ SPACE CAL
1980	62	6837:6851	129.475	20:125	0E	1	0	0E	3E	0E	1	FREQ SPACE CAL
1980	64	6865:6879	118.365	-25:75	2E	1E	0	3E	3E	1E	1	
1980	65	6879:6892	118.361	-25:75	2E	1E	0	3E	3E	1	1E	
1980	66	6893:6907	118.366	-10:90	3E	0E	0	2E	3E	1E	1	
1980	68	6920:6934	118.350	5:105	1E	1	0	1E	3E	0E	1	
1980	69	6934:6948	118.351	5:105	1E	1	0	1E	3E	1	0E	
1980	70	6948:6962	118.347	-10:90	3E	0E	0	2E	3E	1	1E	POSS BEAT BI2/CH
1980	72	6975:6990	118.348	-10:90	3E	1	0	2E	3E	1E	1	POSS BEAT BI2/CH
1980	73	6990:7003	118.345	-25:75	3E	1	0E	3E	3E	1E	1	
1980	74	7003:7017	118.362	-45:55	2E	1E	0	3E	3E	1	1E	BAD SCAN PATTERN ORB.7010
1980	76	7031:7045	129.483	-10:90	1E	1	0E	3E	3E	0E	1	FREQ SPACE CAL
1980	77	7045:7058	129.484	-10:90	1E	0E	0	3E	3E	1	0E	FREQ SPACE CAL

DATE YEAR	DAY	ORBITS (APPROX)	SCAN PROG	RANGE(KM) (APPROX)	SIEVE SETTINGS A1	A2	A3	B1 B2	C1	C2	C3	
1980	78	7058:7071	129.485	-10:90	0E	1	0	0E	3E	0E	1	FREQ SPACE CAL
1980	78	7071:7072	129.100		1E	0	0	3E	3E	1	0E	SCAN CAL CHECK
1980	80	7086:7094	26.101		3E	0E	0	3E	3E	1	1E	
1980	80	7095:7100	26.101		3E	0E	0	3E	3E	1	1E	
1980	81	7100:7114	26.101		3E	0E	0	3E	3E	1	1E	
1980	82	7114:7127	118.366	-10:90	3E	0E	0	2E	3E	1E	1	
1980	84	7141:7155	118.350	5:105	1E	1	0	1E	3E	0E	1	
1980	85	7155:7168	118.351	5:105	1E	1	0	1E	3E	1	0E	
1980	86	7168:7182	118.347	-10:90	3E	0E	0	2E	3E	1	1E	POSS BEAT BI2/CH
1980	88	7196:7210	118.356	-45:55	3E	1	0E	3E	3E	1E	1	
1980	89	7210:7224	118.356	-45:55	3E	1	0E	3E	3E	1E	1	
1980	90	7224:7237	118.356	-45:55	3E	1	0E	3E	3E	1E	1	
1980	92	7251:7265	118.368		3E	1	1E	3E	3E	1E	1	
1980	93	7265:7279	118.368		3E	1	1E	3E	3E	1E	1	
1980	94	7279:7293	118.368		3E	1	1E	3E	3E	1E	1	
1980	95	7293:7307	118.363		3E	1E	0	3E	3E	1E	1	
1980	96	7307:7321	118.365	-25:75	2E	1E	0	3E	3E	1E	1	
1980	97	7321:7335	118.361	-25:75	2E	1E	0	3E	3E	1	1E	
1980	98	7335:7349	118.366	-10:90	3E	0E	0	2E	3E	1E	1	
1980	100	7362:7376	118.350	5:105	1E	1	0	1E	3E	0E	1	
1980	101	7376:7390	118.351	5:105	1E	1	0	1E	3E	1	0E	
1980	102	7390:7404	118.347	-10:90	3E	0E	0	2E	3E	1	1E	POSS BEAT BI2/CH
1980	104	7418:7431	118.348	-10:90	3E	1	0	2E	3E	1E	1	POSS BEAT BI2/CH
1980	105	7431:7445	118.345	-25:75	3E	1	0E	3E	3E	1E	1	
1980	106	7445:7459	118.362	-45:55	2E	1E	0	3E	3E	1	1E	
1980	108	7473:7487	36.101		3E	0E	0	3E	3E	1	1E	BB/SPACE CAL AUX HEATERS ON
1980	109	7487:7500	36.101		3E	0E	0	3E	3E	1	1E	BB/SPACE CAL
1980	110	7500:7513	129.485	20:125	0E	1	0	0E	3E	0E	1	FREQ SPACE CAL
1980	110	7513:7514	129.100		1E	0	0	3E	3E	1	0E	SCAN CAL CHECK
1980	112	7528:7542	118.365	-25:75	2E	1E	0	3E	3E	1E	1	
1980	113	7542:7556	118.361	-25:75	2E	1E	0	3E	3E	1	1E	
1980	114	7556:7570	118.366	-10:90	3E	0E	0	2E	3E	1E	1	
1980	116	7584:7597	118.350	5:105	1E	1	0	1E	3E	0E	1	
1980	117	7597:7611	118.351	5:105	1E	1	0	1E	3E	1	0E	BAD ROLL COMP PHASING
1980	118	7611:7625	118.347	-10:90	3E	0E	0	2E	3E	1	1E	POSS BEAT BI2/CH
1980	120	7639:7653	118.348	-10:90	3E	1	0	2E	3E	1E	1	POSS BEAT BI2/CH
1980	121	7653:7666	118.345	-25:75	3E	1	0E	3E	3E	1E	1	
1980	122	7666:7680	118.362	-45:55	2E	1E	0	3E	3E	1	1E	
1980	124	7694:7708	129.484	20:125	1E	0E	0	3E	3E	1	0E	FREQ SPACE CAL
1980	125	7708:7722	129.484	20:125	1E	0E	0	3E	3E	1	0E	FREQ SPACE CAL
1980	126	7722:7736	129.485	20:125	0E	1	0	0E	3E	0E	1	FREQ SPACE CAL
1980	128	7750:7763	118.365	-25:75	2E	1E	0	3E	3E	1E	1	
1980	129	7763:7777	118.361	-25:75	2E	1E	0	3E	3E	1	1E	
1980	130	7777:7791	118.366	-10:90	3E	0E	0	2E	3E	1E	1	
1980	132	7804:7818	118.350	5:105	1E	1	0	1E	3E	0E	1	
1980	133	7818:7832	118.351	5:105	1E	1	0	1E	3E	1	0E	
1980	134	7832:7846	118.347	-10:90	3E	0E	0	2E	3E	1	1E	POSS BEAT BI2/CH
1980	136	7860:7874	118.348	-10:90	3E	1	0	2E	3E	1E	1	POSS BEAT BI2/CH
1980	137	7874:7887	118.348	-10:90	3E	1	0	2E	3E	1E	1	POSS BEAT BI2/CH
1980	138	7887:7901	118.362	-45:55	2E	1E	0	3E	3E	1	1E	
1980	140	7915:7929	129.484	20:125	1E	0E	0	3E	3E	1	0E	FREQ SPACE CAL
1980	141	7929:7942	129.485	20:125	0E	1	0	0E	3E	0E	1	FREQ SPACE CAL
1980	142	7942:7955	129.485	20:125	0E	1	0	0E	3E	0E	1	FREQ SPACE CAL
1980	142	7955:7956	129.100		1E	0	0	3E	3E	1	0E	SCAN CAL CHECK
1980	144	7970:7984	118.365	-25:75	2E	1E	0	3E	3E	1E	1	
1980	145	7984:7998	118.361	-25:75	2E	1E	0	3E	3E	1	1E	

DATE YEAR	DAY	ORBITS (APPROX)	SCAN PROG	RANGE(KM) (APPROX)	SIEVE SETTINGS A1	A2	A3	B1 B2	C1	C2	C3	
1980	146	7998:8012	118.366	-10:90	3E	0E	0	2E	3E	1E	1	
1980	148	8026:8040	118.350	5:105	1E	1	0	1E	3E	0E	1	
1980	149	8040:8053	118.351	5:105	1E	1	0	1E	3E	1	0E	
1980	150	8053:8066	118.347	-10:90	3E	0E	0	2E	3E	1	1E	POSS BEAT BI2/CH
1980	152	8081:8095	129.506	5:110	3E	0	0	2E	3E	0E	1	FREQ SPACE CAL
1980	153	8095:8109	129.507	5:110	3E	0E	0	3E	3E	1	0E	FREQ SPACE CAL
1980	154	8109:8123	129.508	5:110	3E	0	0	3E	3E	1E	1	FREQ SPACE CAL
1980	156	8136:8150	129.512	20:125	2E	1E	0	1E	3E	1E	1	FREQ SPACE CAL
1980	157	8150:8164	129.513	20:125	2E	0	0	2E	3E	1	1E	FREQ SPACE CAL
1980	158	8164:8178	129.514	5:110	3E	0E	0	3E	3E	1E	1	FREQ SPACE CAL
1980	160	8191:8206	118.500	-10:90	3E	0	0	1E	3E	0E	1	
1980	161	8206:8219	118.501	-10:90	2E	1E	0	2E	3E	1	0E	
1980	162	8219:8233	118.502	-10:90	3E	0	0	3E	3E	1	1E	
1980	164	8247:8261	118.503	-10:90	2E	1E	0	1E	3E	0E	1	
1980	165	8261:8274	118.504	-10:90	3E	0	0	2E	3E	1	1E	
1980	166	8274:8288	118.505	-10:90	3E	0E	0	3E	3E	1E	1	
1980	168	8302:8316	129.506	5:110	3E	0	0	2E	3E	0E	1	FREQ SPACE CAL
1980	169	8316:8330	129.507	5:110	3E	0E	0	3E	3E	1	0E	FREQ SPACE CAL
1980	170	8330:8343	129.508	5:110	3E	0	0	3E	3E	1E	1	FREQ SPACE CAL
1980	172	8357:8371	129.509	40:145	0E	1	0	1E	3E	0E	1	FREQ SPACE CAL
1980	173	8371:8385	129.510	40:145	1E	1	0	1E	3E	1	0E	FREQ SPACE CAL
1980	174	8385:8397	129.511	40:145	1E	1	0	0E	3E	1E	1	FREQ SPACE CAL. SOME BAD DATA
1980	175	8398:8399	129.100		1E	0	0	3E	3E	1	0E	SCAN CAL CHECK
1980	175	8399:8410	129.511	40:145	1E	1	0	0E	3E	1E	1	FREQ SPACE CAL
1980	175	8410:8413	129.511		1E	1	0	0E	3E	1E	1	NO SCANNING
1980	176	8413:8427	118.500	-10:90	3E	0	0	1E	3E	0E	1	
1980	177	8427:8440	118.501	-10:90	2E	1E	0	2E	3E	1	0E	
1980	178	8440:8454	118.502	-10:90	3E	0	0	3E	3E	1	1E	
1980	180	8468:8482	118.503	-10:90	2E	1E	0	1E	3E	0E	1	
1980	181	8482:8496	118.504	-10:90	3E	0	0	2E	3E	1	1E	ROLL COMP SLIP. SOME DATA LOST
1980	182	8496:8509	118.505	-10:90	3E	0E	0	3E	3E	1E	1	
1980	184	8523:8537	129.506	5:110	3E	0	0	2E	3E	0E	1	FREQ SPACE CAL
1980	185	8537:8551	129.507	5:110	3E	0E	0	3E	3E	1	0E	FREQ SPACE CAL
1980	186	8551:8565	129.508	5:110	3E	0	0	3E	3E	1E	1	FREQ SPACE CAL
1980	188	8578:8593	129.512	20:125	2E	1E	0	1E	3E	1E	1	FREQ SPACE CAL. SEE NOTE 5.
1980	189	8593:8606	129.513	20:125	2E	0	0	2E	3E	1	1E	FREQ SPACE CAL. SEE NOTE 6
1980	190	8606:8620	129.514	5:110	3E	0E	0	3E	3E	1E	1	FREQ SPACE CAL
1980	192	8634:8648	118.500	-10:90	3E	0	0	1E	3E	0E	1	
1980	193	8648:8661	118.501	-10:90	2E	1E	0	2E	3E	1	0E	
1980	194	8661:8675	118.502	-10:90	3E	0	0	3E	3E	1	1E	
1980	196	8689:8703	118.363	25:75	3E	1E	0	3E	3E	1E	1	BEAT IN CHANNEL A3P
1980	197	8703:8717	118.504	-10:90	3E	0	0	2E	3E	1	1E	
1980	198	8717:8731	118.505	-10:90	3E	0E	0	3E	3E	1E	1	
1980	200	8745:8758	129.506	5:110	3E	0	0	2E	3E	0E	1	FREQ SPACE CAL
1980	201	8758:8772	129.507	5:110	3E	0E	0	3E	3E	1	0E	FREQ SPACE CAL
1980	202	8772:8786	129.508	5:110	3E	0	0	3E	3E	1E	1	FREQ SPACE CAL
1980	204	8799:8813	129.509	40:145	0E	1	0	1E	3E	0E	1	FREQ SPACE CAL
1980	205	8813:8827	129.510	40:145	1E	1	0	1E	3E	1	0E	FREQ SPACE CAL
1980	206	8827:8840	129.511	40:145	1E	1	0	0E	3E	1E	1	FREQ SPACE CAL
1980	207	8840:8841	129.100		1E	0	0	3E	3E	1	0E	SCAN CAL CHECK
1980	208	8855:8869	118.500	-10:90	3E	0	0	1E	3E	0E	1	
1980	209	8869:8882	118.501	-10:90	2E	1E	0	2E	3E	1	0E	SEE NOTE 4
1980	210	8882:8896	118.502	-10:90	3E	0	0	3E	3E	1	1E	
1980	212	8910:8924	118.503	-10:90	2E	1E	0	1E	3E	0E	1	
1980	213	8924:8938	118.504	-10:90	3E	0	0	2E	3E	1	1E	
1980	214	8938:8952	118.505	-10:90	3E	0E	0	3E	3E	1E	1	

DATE YEAR	DAY	ORBITS (APPROX)	SCAN PROG	RANGE(KM) (APPROX)	A1	A2	A3	B1 B2	C1	C2	C3	
1980	216	8965:8979	129.506	5:110	3E	0	0	2E	3E	0E	1	FREQ SPACE CAL
1980	217	8979:8993	129.507	5:110	3E	0E	0	3E	3E	1	0E	FREQ SPACE CAL
1980	218	8993:9007	129.508	5:110	3E	0	0	3E	3E	1E	1	FREQ SPACE CAL
1980	220	9021:9034	129.512	20:125	2E	1E	0	1E	3E	1E	1	FREQ SPACE CAL
1980	221	9034:9048	129.513	20:125	2E	0	0	2E	3E	1	1E	FREQ SPACE CAL
1980	222	9048:9062	129.513	20:125	2E	0	0	2E	3E	1	1E	FREQ SPACE CAL
1980	224	9076:9090	118.500	-10:90	3E	0	0	1E	3E	0E	1	
1980	225	9090:9104	118.501	-10:90	2E	1E	0	2E	3E	1	0E	
1980	226	9104:9118	118.502	-10:90	3E	0	0	3E	3E	1	1E	
1980	228	9131:9145	118.503	-10:90	2E	1E	0	1E	3E	0E	1	
1980	229	9145:9159	118.504	-10:90	3E	0	0	2E	3E	1	1E	
1980	230	9159:9173	118.505	-10:90	3E	0E	0	3E	3E	1E	1	
1980	232	9186:9200	129.506	5:110	3E	0	0	2E	3E	0E	1	FREQ SPACE CAL
1980	233	9200:9214	129.507	5:110	3E	0E	0	3E	3E	1	0E	FREQ SPACE CAL
1980	234	9214:9228	129.508	5:110	3E	0	0	3E	3E	1E	1	FREQ SPACE CAL
1980	236	9242:9254	129.509	40:145	0E	1	0	1E	3E	0E	1	FREQ SPACE CAL
1980	237	9254:9269	129.510	40:145	1E	1	0	1E	3E	1	0E	FREQ SPACE CAL
1980	238	9269:9281	129.511	40:145	1E	1	0	0E	3E	1E	1	FREQ SPACE CAL
1980	238	9281:9283	129.100		1E	0	0	3E	3E	1	0E	SCAN CAL CHECK
1980	240	9297:9311	118.500	-10:90	3E	0	0	1E	3E	0E	1	
1980	241	9311:9325	118.501	-10:90	2E	1E	0	2E	3E	1	0E	
1980	242	9325:9338	118.502	-10:90	3E	0	0	3E	3E	1	1E	
1980	244	9352:9366	129.506	5:110	3E	0	0	2E	3E	0E	1	FREQ SPACE CAL
1980	245	9366:9380	129.506	5:110	3E	0	0	2E	3E	0E	1	FREQ SPACE CAL AZIM 12 DEG FW
1980	246	9380:9394	129.506	5:110	3E	0	0	2E	3E	0E	1	FREQ SPACE CAL AZIM 9 DEG FW
1980	248	9408:9421	129.506	5:110	3E	0	0	2E	3E	0E	1	FREQ SPACE CAL
1980	249	9421:9436	129.506	5:110	3E	0	0	2E	3E	0E	1	FREQ SPACE CAL AZIM 3 DEG FW
1980	250	9436:9449	129.506	5:110	3E	0	0	2E	3E	0E	1	FREQ SPACE CAL AZIM 6 DEG FW
1980	252	9463:9477	129.506	5:110	3E	0	0	2E	3E	0E	1	FREQ SPACE CAL
1980	253	9477:9490	129.506	5:110	3E	0	0	2E	3E	0E	1	FREQ SPACE CAL AZIM 3 DEG BK
1980	254	9490:9504	129.506	5:110	3E	0	0	2E	3E	0E	1	FREQ SPACE CAL AZIM 6 DEG BK
1980	256	9518:9532	129.506	5:110	3E	0	0	2E	3E	0E	1	FREQ SPACE CAL
1980	257	9532:9545	129.506	5:110	3E	0	0	2E	3E	0E	1	FREQ SPACE CAL AZIM 12 DEG BK
1980	258	9546:9558	129.506	5:110	3E	0	0	2E	3E	0E	1	FREQ SPACE CAL AZIM 9 DEG BK. SEE NOTE 6
1980	260	9572:9586	129.514	5:110	3E	0E	0	3E	3E	1E	1	FREQ SPACE CAL
1980	261	9586:9600	129.514	5:110	3E	0E	0	3E	3E	1E	1	FREQ SPACE CAL AZIM 12 DEG FW
1980	262	9600:9614	129.514	5:110	3E	0E	0	3E	3E	1E	1	FREQ SPACE CAL AZIM 9 DEG FW
1980	264	9629:9641	129.514	5:110	3E	0E	0	3E	3E	1E	1	FREQ SPACE CAL
1980	265	9642:9656	129.514	5:110	3E	0E	0	3E	3E	1E	1	FREQ SPACE CAL AZIM 3 DEG FW
1980	266	9656:9670	129.514	5:110	3E	0E	0	3E	3E	1E	1	FREQ SPACE CAL AZIM 6 DEG FW. SEE NOTE 4
1980	268	9684:9698	129.514	5:110	3E	0E	0	3E	3E	1E	1	FREQ SPACE CAL
1980	269	9698:9712	129.514	5:110	3E	0E	0	3E	3E	1E	1	FREQ SPACE CAL AZIM 3 DEG BK
1980	270	9712:9726	129.514	5:110	3E	0E	0	3E	3E	1E	1	FREQ SPACE CAL AZIM 3 DEG BK
1980	272	9739:9753	129.514	5:110	3E	0E	0	3E	3E	1E	1	FREQ SPACE CAL
1980	273	9753:9767	129.514	5:110	3E	0E	0	3E	3E	1E	1	FREQ SPACE CAL AZIM 12 DEG BK
1980	274	9767:9781	129.514	5:110	3E	0E	0	3E	3E	1E	1	FREQ SPACE CAL AZIM 9 DEG BK
1980	276	9794:9808	129.514	5:110	3E	0E	0	3E	3E	1E	1	FREQ SPACE CAL
1980	277	9809:9822	129.514	5:110	3E	0E	0	3E	3E	1E	1	FREQ SPACE CAL AZIM 6 DEG BK
1980	278	9823:9836	129.514	5:110	3E	0E	0	3E	3E	1E	1	FREQ SPACE CAL AZIM 9 DEG BK
1980	280	9850:9864	129.506	5:110	3E	0	0	2E	3E	0E	1	FREQ SPACE CAL
1980	281	9864:9877	129.507	5:110	3E	0E	0	3E	3E	1	0E	FREQ SPACE CAL
1980	282	9877:9890	129.508	5:110	3E	0	0	3E	3E	1E	1	FREQ SPACE CAL
1980	283	9890:9891	129.100		1E	0	0	3E	3E	1	0E	SCAN CAL CHECK
1980	284	9917:9919	29.513	20:125	2E	0	0	2E	3E	1	1E	FREQ SPACE CAL
1980	285	9919:9933	29.513	20:125	2E	0	0	2E	3E	1	1E	FREQ SPACE CAL
1980	286	9933:9946	29.514	5:110	3E	0E	0	3E	3E	1E	1	FREQ SPACE CAL

DATE		ORBITS	SCAN	RANGE(KM)	SIEVE SETTINGS						
YEAR	DAY	(APPROX)	PROG	(APPROX)	A1	A2	A3	B1 B2	C1	C2	C3
1980	288	9960:9974	118.500	-10:90	3E	0	0	1E	3E	OE	1
1980	289	9974:9988	118.501	-10:90	2E	1E	0	2E	3E	1	OE
1980	290	9988:9996	118.502	-10:90	3E	0	0	3E	3E	1	1E
1980	290	9996:10002	118.363		3E	1E	0	3E	3E	1E	1
1980	292	10016:10030	118.503	-10:90	2E	1E	0	1E	3E	OE	1
1980	293	10030:10043	118.504	-10:90	3E	0	0	2E	3E	1	1E
1980	294	10043:10057	118.505	-10:90	3E	OE	0	3E	3E	1E	1
1980	296	10071:10085	129.506	5:110	3E	0	0	2E	3E	OE	1
1980	297	10085:10098	129.507	5:110	3E	OE	0	3E	3E	1	OE
1980	298	10098:10112	129.508	5:110	3E	0	0	3E	3E	1E	1
1980	300	10126:10140	229.473	20:125	1E	1	OE	OE	3E	OE	1
1980	301	10140:10154	229.474	20:125	1E	OE	0	OE	3E	1	OE
1980	302	10154:10168	229.475	20:125	OE	1	0	OE	3E	OE	1
1980	304	10181:10195	218.500	-10:90	3E	0	0	1E	3E	OE	1
1980	305	10195:10209	218.501	-10:90	2E	1E	0	2E	3E	1	OE
1980	306	10209:10223	218.502	-10:90	3E	0	0	3E	3E	1	1E
1980	308	10237:10251	218.503	-10:90	2E	1E	0	1E	3E	OE	1
1980	309	10251:10265	218.504	-10:90	3E	0	0	2E	3E	1	1E
1980	310	10265:10279	218.505	-10:90	3E	OE	0	3E	3E	1E	1
1980	312	10293:10306	229.506	5:110	3E	0	0	2E	3E	OE	1
1980	313	10306:10320	229.507	5:110	3E	OE	0	3E	3E	1	OE
1980	314	10320:10334	229.508	5:110	3E	0	0	3E	3E	1E	1
1980	316	10347:10361	229.512	20:125	2E	1E	0	1E	3E	1E	1
1980	317	10361:10375	229.513	20:125	2E	0	0	2E	3E	1	1E
1980	318	10375:10389	229.514	5:110	3E	OE	0	3E	3E	1E	1
1980	320	10402:10417	218.500	-10:90	3E	0	0	1E	3E	OE	1
1980	321	10417:10430	218.501	-10:90	2E	1E	0	2E	3E	1	OE
1980	322	10430:10444	218.502	-10:90	3E	0	0	3E	3E	1	1E
1980	324	10458:10472	218.503	-10:90	2E	1E	0	1E	3E	OE	1
1980	325	10472:10486	218.504	-10:90	3E	0	0	2E	3E	1	1E
1980	326	10486:10499	218.505	-10:90	3E	OE	0	3E	3E	1E	1
1980	328	10513:10527	229.506	5:110	3E	0	0	2E	3E	OE	1
1980	329	10527:10541	229.507	5:110	3E	OE	0	3E	3E	1	OE
1980	330	10541:10555	229.508	5:110	3E	0	0	3E	3E	1E	1
1980	332	10568:10582	229.509	40:145	OE	1	0	1E	3E	OE	1
1980	333	10582:10597	229.510	40:145	1E	1	0	1E	3E	1	OE
1980	334	10597:10610	229.511	40:145	1E	1	0	OE	3E	1E	1
1980	336	10624:10638	218.500	-10:90	3E	0	0	1E	3E	OE	1
1980	337	10638:10652	218.501	-10:90	2E	1E	0	2E	3E	1	OE
1980	338	10652:10665	218.502	-10:90	3E	0	0	3E	3E	1	1E
1980	340	10679:10693	218.503	-10:90	2E	1E	0	1E	3E	OE	1
1980	341	10693:10707	218.504	-10:90	3E	0	0	2E	3E	1	1E
1980	342	10707:10720	218.505	-10:90	3E	OE	0	3E	3E	1E	1
1980	344	10734:10748	229.506	5:110	3E	0	0	2E	3E	OE	1
1980	345	10748:10762	229.507	5:110	3E	OE	0	3E	3E	1	OE
1980	346	10762:10776	229.508	5:110	3E	0	0	3E	3E	1E	1
1980	348	10790:10803	229.512	20:125	2E	1E	0	1E	3E	1E	1
1980	349	10803:10817	229.513	20:125	2E	0	0	2E	3E	1	1E
1980	350	10817:10831	229.514	5:110	3E	OE	0	3E	3E	1E	1
1980	352	10845:10859	218.500	-10:90	3E	0	0	1E	3E	OE	1
1980	353	10859:10872	218.501	-10:90	2E	1E	0	2E	3E	1	OE
1980	354	10872:10886	218.502	-10:90	3E	0	0	3E	3E	1	1E
1980	356	10900:10914	218.503	-10:90	2E	1E	0	1E	3E	OE	1
1980	357	10914:10928	218.504	-10:90	3E	0	0	2E	3E	1	1E
1980	358	10928:10941	218.505	-10:90	3E	OE	0	3E	3E	1E	1
1980	360	10955:10969	229.506	5:110	3E	0	0	2E	3E	OF	1

DATE YEAR	DAY	ORBITS (APPROX)	SCAN PROG	RANGE(KM) (APPROX)	SIEVE SETTINGS A1	A2	A3	B1 B2	C1	C2	C3
1980	361	10969:10983	229.507	5:110	3E	0E	0	3E	3E	1	0E
1980	362	10983:10997	229.508	5:110	3E	0	0	3E	3E	1E	1
1980	364	11011:11025	229.509	40:145	0E	1	0	1E	3E	0E	1
1980	365	11025:11039	229.510	40:145	1E	1	0	1E	3E	1	0E
1980	366	11039:11051	229.511	40:145	1E	1	0	0E	3E	1E	1
1980	366	11051:11052	229.107		1E	0	0	3E	3E	1	0E
1981	2	11066:11080	218.500	-10:90	3E	0	0	1E	3E	0E	1
1981	3	11080:11094	218.501	-10:90	2E	1E	0	2E	3E	1	0E
1981	4	11094:11108	218.502	-10:90	3E	0	0	3E	3E	1	1E
1981	6	11122:11135	218.503	-10:90	2E	1E	0	1E	3E	0E	1
1981	7	11135:11148	218.504	-10:90	3E	0	0	2E	3E	1	1E
1981	8	11148:11163	218.505	-10:90	3E	0E	0	3E	3E	1E	1
1981	10	11177:11191	229.506	5:110	3E	0	0	2E	3E	0E	1
1981	11	11191:11205	229.507	5:110	3E	0E	0	3E	3E	1	0E
1981	12	11205:11218	229.508	5:110	3E	0	0	3E	3E	1E	1
1981	14	11232:11246	229.509	40:145	0E	1	0	1E	3E	0E	1
1981	15	11246:11259	229.510	40:145	1E	1	0	1E	3E	1	0E
1981	16	11259:11274	229.511	40:145	1E	1	0	0E	3E	1E	1
1981	18	11288:11301	218.500	-10:90	3E	0	0	1E	3E	0E	1
1981	19	11301:11315	218.501	-10:90	2E	1E	0	2E	3E	1	0E
1981	20	11315:11329	218.502	-10:90	3E	0	0	3E	3E	1	1E
1981	22	11342:11356	218.503	-10:90	2E	1E	0	1E	3E	0E	1
1981	23	11356:11370	218.504	-10:90	3E	0	0	2E	3E	1	1E
1981	24	11370:11384	218.505	-10:90	3E	0E	0	3E	3E	1E	1
1981	26	11398:11412	229.506	5:110	3E	0	0	2E	3E	0E	1
1981	27	11412:11425	229.507	5:110	3E	0E	0	3E	3E	1	0E
1981	28	11425:11439	229.508	5:110	3E	0	0	3E	3E	1E	1
1981	30	11453:11467	229.509	40:145	0E	1	0	1E	3E	0E	1
1981	31	11467:11481	229.510	40:145	1E	1	0	1E	3E	1	0E
1981	32	11481:11494	229.511	40:145	1E	1	0	0E	3E	1E	1
1981	32	11494:11495	229.107		1E	0	0	3E	3E	1	0E
1981	34	11508:11522	218.500	-10:90	3E	0	0	1E	3E	0E	1
1981	35	11522:11536	218.501	-10:90	2E	1E	0	2E	3E	1	0E
1981	36	11536:11550	218.502	-10:90	3E	0	0	3E	3E	1	1E
1981	38	11564:11577	218.503	-10:90	2E	1E	0	1E	3E	0E	1
1981	39	11577:11590	218.504	-10:90	3E	0	0	2E	3E	1	1E
1981	40	11591:11605	218.505	-10:90	3E	0E	0	3E	3E	1E	1
1981	42	11619:11632	229.506	5:110	3E	0	0	2E	3E	0E	1
1981	43	11632:11646	229.507	5:110	3E	0E	0	3E	3E	1	0E
1981	44	11646:11660	229.508	5:110	3E	0	0	3E	3E	1E	1
1981	46	11674:11688	229.509	40:145	0E	1	0	1E	3E	0E	1
1981	47	11688:11702	229.510	40:145	1E	1	0	1E	3E	1	0E
1981	48	11702:11716	229.511	40:145	1E	1	0	0E	3E	1E	1
1981	50	11730:11743	218.500	-10:90	3E	0	0	1E	3E	0E	1
1981	51	11743:11757	218.501	-10:90	2E	1E	0	2E	3E	1	0E
1981	52	11757:11771	218.502	-10:90	3E	0	0	3E	3E	1	1E
1981	54	11785:11798	218.503	-10:90	2E	1E	0	1E	3E	0E	1
1981	55	11798:11812	218.504	-10:90	3E	0	0	2E	3E	1	1E
1981	56	11812:11826	218.505	-10:90	3E	0E	0	3E	3E	1E	1
1981	57	11833:11838	218.502	-10:90	3E	0	0	3E	3E	1	1E
1981	58	11840:11854	218.502	-10:90	3E	0	0	3E	3E	1	1E
1981	59	11854:11867	229.507	5:110	3E	0E	0	3E	3E	1	0E
1981	60	11867:11881	229.508	5:110	3E	0	0	3E	3E	1E	1
1981	62	11895:11909	229.512	20:125	2E	1E	0	1E	3E	1E	1
1981	63	11909:11923	229.513	20:125	2E	0	0	2E	3E	1	1E
1981	64	11923:11937	229.514	5:110	3E	0E	0	3E	3E	1E	1

DATE YEAR	DAY	ORBITS (APPROX)	SCAN PROG	RANGE(KM) (APPROX)	SIEVE SETTINGS A1	A2	A3	B1 B2	C1	C2	C3
1981	66	11951:11964	218.500	-10:90	3E	0	0	1E	3E	0E	1
1981	67	11964:11978	218.501	-10:90	2E	1E	0	2E	3E	1	0E
1981	68	11978:11992	218.502	-10:90	3E	0	0	3E	3E	1	1E
1981	70	12006:12019	218.503	-10:90	2E	1E	0	1E	3E	0E	1
1981	71	12019:12033	218.504	-10:90	3E	0	0	2E	3E	1	1E
1981	72	12033:12047	218.505	-10:90	3E	0E	0	3E	3E	1E	1
1981	74	12061:12075	229.506	5:110	3E	0	0	2E	3E	0E	1
1981	75	12075:12088	229.507	5:110	3E	0E	0	3E	3E	1	0E
1981	76	12088:12102	229.508	5:110	3E	0	0	3E	3E	1E	1
1981	78	12116:12130	229.509	40:145	0E	1	0	1E	3E	0E	1
1981	79	12130:12144	229.510	40:145	1E	1	0	1E	3E	1	0E
1981	80	12144:12157	229.511	40:145	1E	1	0	0E	3E	1E	1
1981	80	12157:12158	229.107		1E	0	0	3E	3E	1	0E
1981	82	12172:12186	218.500	-10:90	3E	0	0	1E	3E	0E	1
1981	83	12186:12200	218.501	-10:90	2E	1E	0	2E	3E	1	0E
1981	84	12200:12214	218.502	-10:90	3E	0	0	3E	3E	1	1E
1981	86	12228:12241	218.503	-10:90	2E	1E	0	1E	3E	0E	1
1981	87	12241:12255	218.504	-10:90	3E	0	0	2E	3E	1	1E
1981	88	12255:12269	218.505	-10:90	3E	0E	0	3E	3E	1E	1
1981	90	12282:12296	229.506	5:110	3E	0	0	2E	3E	0E	1
1981	91	12296:12309	229.507	5:110	3E	0E	0	3E	3E	1	0E
1981	92	12309:12323	229.508	5:110	3E	0	0	3E	3E	1E	1
1981	94	12337:12351	229.512	20:125	2E	1E	0	1E	3E	1E	1
1981	95	12351:12365	229.513	20:125	2E	0	0	2E	3E	1	1E
1981	96	12365:12378	229.514	5:110	3E	0E	0	3E	3E	1E	1
1981	98	12392:12406	218.500	-10:90	3E	0	0	1E	3E	0E	1
1981	99	12406:12420	218.501	-10:90	2E	1E	0	2E	3E	1	0E
1981	100	12420:12434	218.502	-10:90	3E	0	0	3E	3E	1	1E
1981	102	12448:12462	218.503	-10:90	2E	1E	0	1E	3E	0E	1
1981	103	12462:12475	218.504	-10:90	3E	0	0	2E	3E	1	1E
1981	104	12475:12489	218.505	-10:90	3E	0E	0	3E	3E	1E	1
1981	106	12503:12517	229.506	5:110	3E	0	0	2E	3E	0E	1
1981	107	12517:12531	229.507	5:110	3E	0E	0	3E	3E	1	0E
1981	108	12531:12545	229.508	5:110	3E	0	0	3E	3E	1E	1
1981	110	12559:12573	229.509	40:145	0E	1	0	1E	3E	0E	1
1981	111	12573:12587	229.510	40:145	1E	1	0	1E	3E	1	0E
1981	112	12587:12600	229.511	40:145	1E	1	0	0E	3E	1E	1
1981	112	12600:12601	229.107		1E	0	0	3E	3E	1	0E
1981	114	12614:12627	218.500	-10:90	3E	0	0	1E	3E	0E	1
1981	115	12627:12641	218.501	-10:90	2E	1E	0	2E	3E	1	0E
1981	116	12641:12655	218.502	-10:90	3E	0	0	3E	3E	1	1E
1981	118	12669:12682	218.503	-10:90	2E	1E	0	1E	3E	0E	1
1981	119	12682:12696	218.504	-10:90	3E	0	0	2E	3E	1	1E
1981	120	12696:12710	218.505	-10:90	3E	0E	0	3E	3E	1E	1
1981	122	12724:12738	218.505	-10:90	3E	0E	0	3E	3E	1E	1
1981	123	12738:12752	218.505	-10:90	3E	0E	0	3E	3E	1E	1
1981	124	12752:12766	218.505	-10:90	3E	0E	0	3E	3E	1E	1
1981	126	12779:12793	218.505	-10:90	3E	0E	0	3E	3E	1E	1
1981	127	12793:12807	218.505	-10:90	3E	0E	0	3E	3E	1E	1
1981	128	12807:12821	218.505	-10:90	3E	0E	0	3E	3E	1E	1
1981	130	12835:12848	218.500	-10:90	3E	0	0	1E	3E	0E	1
1981	131	12848:12862	218.501	-10:90	2E	1E	0	2E	3E	1	0E
1981	132	12862:12876	218.505	-10:90	3E	0E	0	3E	3E	1E	1
1981	134	12890:12904	218.503	-10:90	2E	1E	0	1E	3E	0E	1
1981	135	12904:12918	218.504	-10:90	3E	0	0	2E	3E	1	1E
1981	136	12918:12931	218.505	-10:90	3E	0E	0	3E	3E	1E	1

DATE YEAR	DAY	ORBITS (APPROX)	SCAN PROG	RANGE(KM) (APPROX)	SIEVE SETTINGS A1	A2	A3	B1 B2	C1	C2	C3
1981	138	12945:12959	229.506	5:110	3E	0	0	2E	3E	OE	1
1981	139	12959:12973	229.507	5:110	3E	OE	0	3E	3E	1	OE
1981	140	12973:12987	229.508	5:110	3E	0	0	3E	3E	1E	1
1981	142	13001:13015	229.509	40:145	OE	1	0	1E	3E	OE	1
1981	143	13015:13029	229.510	40:145	1E	1	0	1E	3E	1	OE
1981	144	13029:13041	229.511	40:145	1E	1	0	OE	3E	1E	1
1981	144	13041:13042	229.107		1E	0	0	3E	3E	1	OE
1981	146	13056:13070	218.500	-10:90	3E	0	0	1E	3E	OE	1
1981	147	13070:13084	218.501	-10:90	2E	1E	0	2E	3E	1	OE
1981	148	13084:13097	218.502	-10:90	3E	0	0	3E	3E	1	1E
1981	150	13111:13125	218.503	-10:90	2E	1E	0	1E	3E	OE	1
1981	151	13125:13139	218.504	-10:90	3E	0	0	2E	3E	1	1E
1981	152	13139:13153	218.505	-10:90	3E	OE	0	3E	3E	1E	1
1981	154	13167:13180	229.506	5:110	3E	0	0	2E	3E	OE	1
1981	155	13180:13194	229.507	5:110	3E	OE	0	3E	3E	1	OE
1981	156	13194:13208	229.508	5:110	3E	0	0	3E	3E	1E	1
1981	158	13222:13236	229.512	20:125	2E	1E	0	1E	3E	1E	1
1981	159	13236:13250	229.513	20:125	2E	0	0	2E	3E	1	1E
1981	160	13250:13264	229.514	5:110	3E	OE	0	3E	3E	1E	1
1981	162	13278:13291	218.500	-10:90	3E	0	0	1E	3E	OE	1
1981	163	13291:13305	218.501	-10:90	2E	1E	0	2E	3E	1	OE
1981	164	13305:13318	218.502	-10:90	3E	0	0	3E	3E	1	1E
1981	166	13333:13346	218.503	-10:90	2E	1E	0	1E	3E	OE	1
1981	167	13346:13360	218.504	-10:90	3E	0	0	2E	3E	1	1E
1981	168	13360:13374	218.505	-10:90	3E	OE	0	3E	3E	1E	1
1981	170	13388:13402	229.506	5:110	3E	0	0	2E	3E	OE	1
1981	171	13402:13416	229.507	5:110	3E	OE	0	3E	3E	1	OE
1981	172	13416:13430	229.508	5:110	3E	0	0	3E	3E	1E	1
1981	174	13444:13457	229.509	40:145	OE	1	0	1E	3E	OE	1
1981	175	13457:13471	229.510	40:145	1E	1	0	1E	3E	1	OE
1981	176	13471:13483	229.511	40:145	1E	1	0	OE	3E	1E	1
1981	176	13483:13484	229.107		1E	0	0	3E	3E	1	OE
1981	178	13498:13512	218.500	-10:90	3E	0	0	1E	3E	OE	1
1981	179	13512:13526	218.501	-10:90	2E	1E	0	2E	3E	1	OE
1981	180	13526:13540	218.502	-10:90	3E	0	0	3E	3E	1	1E
1981	182	13554:13567	218.503	-10:90	2E	1E	0	1E	3E	OE	1
1981	183	13567:13581	218.504	-10:90	3E	0	0	2E	3E	1	1E
1981	184	13581:13595	218.505	-10:90	3E	OE	0	3E	3E	1E	1
1981	186	13609:13622	229.506	5:110	3E	0	0	2E	3E	OE	1
1981	187	13622:13636	229.507	5:110	3E	OE	0	3E	3E	1	OE
1981	188	13636:13650	229.508	5:110	3E	0	0	3E	3E	1E	1
1981	190	13664:13678	229.512	20:125	2E	1E	0	1E	3E	1E	1
1981	191	13678:13692	229.513	20:125	2E	0	0	2E	3E	1	1E
1981	192	13692:13706	229.514	5:110	3E	OE	0	3E	3E	1E	1
1981	194	13720:13733	218.500	-10:90	3E	0	0	1E	3E	OE	1
1981	195	13733:13747	218.501	-10:90	2E	1E	0	2E	3E	1	OE
1981	196	13747:13761	218.502	-10:90	3E	0	0	3E	3E	1	1E
1981	198	13775:13788	218.503	-10:90	2E	1E	0	1E	3E	OE	1
1981	199	13788:13802	218.504	-10:90	3E	0	0	2E	3E	1	1E
1981	200	13802:13816	218.505	-10:90	3E	OE	0	3E	3E	1E	1
1981	202	13830:13843	229.506	5:110	3E	0	0	2E	3E	OE	1
1981	203	13843:13857	229.507	5:110	3E	OE	0	3E	3E	1	OE
1981	204	13857:13871	229.508	5:110	3E	0	0	3E	3E	1E	1
1981	206	13885:13899	229.509	40:145	OE	1	0	1E	3E	OE	1
1981	207	13899:13913	229.510	40:145	1E	1	0	1E	3E	1	OE
1981	208	13913:13925	229.511	40:145	1E	1	0	OE	3E	1E	1

DATE YEAR	DATE DAY	ORBITS (APPROX)	SCAN PROG	RANGE(KM) (APPROX)	STEVE SETTINGS A1	A2	A3	B1 B2	C1	C2	C3
1981	208	13925:13926	229.107		1E	0	0	3E	3E	1	0E
1981	210	13940:13954	218.500	-10:90	3E	0	0	1E	3E	0E	1
1981	211	13954:13968	218.501	-10:90	2E	1E	0	2E	3E	1	0E
1981	212	13968:13982	218.502	-10:90	3E	0	0	3E	3E	1	1E
1981	214	13996:14009	218.503	-10:90	2E	1E	0	1E	3E	0E	1
1981	215	14009:14023	218.504	-10:90	3E	0	0	2E	3E	1	1E
1981	216	14023:14037	218.505	-10:90	3E	0E	0	3E	3E	1E	1
1981	218	14051:14064	229.506	5:110	3E	0	0	2E	3E	0E	1
1981	219	14064:14078	229.507	5:110	3E	0E	0	3E	3E	1	0E
1981	220	14078:14092	229.508	5:110	3E	0	0	3E	3E	1E	1
1981	222	14105:14120	229.512	20:125	2E	1E	0	1E	3E	1E	1
1981	223	14120:14134	229.513	20:125	2E	0	0	2E	3E	1	1E
1981	224	14134:14148	229.514	5:110	3E	0E	0	3E	3E	1E	1
1981	226	14162:14175	218.500	-10:90	3E	0	0	1E	3E	0E	1
1981	227	14175:14189	218.501	-10:90	2E	1E	0	2E	3E	1	0E
1981	228	14189:14203	218.502	-10:90	3E	0	0	3E	3E	1	1E
1981	230	14217:14231	218.503	-10:90	2E	1E	0	1E	3E	0E	1
1981	231	14231:14245	218.504	-10:90	3E	0	0	2E	3E	1	1E
1981	232	14245:14258	218.505	-10:90	3E	0E	0	3E	3E	1E	1
1981	234	14272:14286	229.506	5:110	3E	0	0	2E	3E	0E	1
1981	235	14286:14299	229.507	5:110	3E	0E	0	3E	3E	1	0E
1981	236	14299:14313	229.508	5:110	3E	0	0	3E	3E	1E	1
1981	238	14327:14341	229.509	40:145	0E	1	0	1E	3E	0E	1
1981	239	14341:14355	229.510	40:145	1E	1	0	1E	3E	1	0E
1981	240	14355:14368	229.511	40:145	1E	1	0	0E	3E	1E	1
1981	240	14368:14369	229.511	40:145	1E	1	0	0E	3E	1E	1
1981	242	14383:14396	218.500	-10:90	3E	0	0	1E	3E	0E	1
1981	243	14396:14410	218.501	-10:90	2E	1E	0	2E	3E	1	0E
1981	244	14410:14424	218.502	-10:90	3E	0	0	3E	3E	1	1E
1981	246	14438:14452	218.503	-10:90	2E	1E	0	1E	3E	0E	1
1981	247	14452:14465	218.504	-10:90	3E	0	0	2E	3E	1	1E
1981	248	14465:14479	218.505	-10:90	3E	0E	0	3E	3E	1E	1
1981	250	14493:14507	229.506	5:110	3E	0	0	2E	3E	0E	1
1981	251	14507:14521	229.507	5:110	3E	0E	0	3E	3E	1	0E
1981	252	14521:14535	229.508	5:110	3E	0	0	3E	3E	1E	1
1981	254	14549:14562	229.512	20:125	2E	1E	0	1E	3E	1E	1
1981	255	14562:14576	229.513	20:125	2E	0	0	2E	3E	1	1E
1981	256	14576:14590	229.514	5:110	3E	0E	0	3E	3E	1E	1
1981	258	14604:14618	218.500	-10:90	3E	0	0	1E	3E	0E	1
1981	259	14618:14632	218.501	-10:90	2E	1E	0	2E	3E	1	0E
1981	260	14632:14645	218.502	-10:90	3E	0	0	3E	3E	1	1E
1981	262	14659:14673	218.503	-10:90	2E	1E	0	1E	3E	0E	1
1981	263	14673:14687	218.504	-10:90	3E	0	0	2E	3E	1	1E
1981	264	14687:14701	218.505	-10:90	3E	0E	0	3E	3E	1E	1
1981	266	14715:14728	229.506	5:110	3E	0	0	2E	3E	0E	1
1981	267	14728:14742	229.507	5:110	3E	0E	0	3E	3E	1	0E
1981	268	14742:14756	229.508	5:110	3E	0	0	3E	3E	1E	1
1981	270	14770:14783	229.509	40:145	0E	1	0	1E	3E	0E	1
1981	271	14783:14797	229.510	40:145	1E	1	0	1E	3E	1	0E
1981	272	14797:14810	229.511	40:145	1E	1	0	0E	3E	1E	1
1981	272	14810:14811	329.107		1E	0	0	3E	3E	1	0E
1981	274	14825:14839	218.500	-10:90	3E	0	0	1E	3E	0E	1
1981	275	14839:14853	218.501	-10:90	2E	1E	0	2E	3E	1	0E
1981	276	14853:14867	218.502	-10:90	3E	0	0	3E	3E	1	1E
1981	278	14880:14894	218.505	-10:90	3E	0E	0	3E	3E	1E	1
1981	279	14894:14908	218.505	-10:90	3E	0E	0	3E	3E	1E	1

DATE YEAR	DAY	ORBITS (APPROX)	SCAN PROG	RANGE(KM) (APPROX)	SIEVE SETTINGS A1	A2	A3	B1 B2	C1	C2	C3
1981	280	14908:14922	218.505	-10:90	3E	0E	0	3E	3E	1E	1
1981	282	14936:14950	218.505	-10:90	3E	0E	0	3E	3E	1E	1
1981	283	14950:14963	218.505	-10:90	3E	0E	0	3E	3E	1E	1
1981	284	14963:14977	218.505	-10:90	3E	0E	0	3E	3E	1E	1
1981	286	14991:15004	218.505	-10:90	3E	0E	0	3E	3E	1E	1
1981	287	15004:15018	218.505	-10:90	3E	0E	0	3E	3E	1E	1
1981	288	15018:15032	218.505	-10:90	3E	0E	0	3E	3E	1E	1
1981	290	15046:15060	218.505	-10:90	3E	0E	0	3E	3E	1E	1
1981	291	15060:15074	218.505	-10:90	3E	0E	0	3E	3E	1E	1
1981	292	15074:15088	218.505	-10:90	3E	0E	0	3E	3E	1E	1
1981	294	15101:15115	218.505	-10:90	3E	0E	0	3E	3E	1E	1
1981	295	15115:15129	218.505	-10:90	3E	0E	0	3E	3E	1E	1
1981	296	15129:15143	218.505	-10:90	3E	0E	0	3E	3E	1E	1
1981	298	15157:15170	318.505	-10:90	3E	0E	0	3E	3E	1E	1
1981	299	15171:15185	318.505	-10:90	3E	0E	0	3E	3E	1E	1
1981	300	15185:15198	318.505	-10:90	3E	0E	0	3E	3E	1E	1
1981	302	15212:15226	329.509	40:145	0E	1	0	1E	3E	0E	1
1981	303	15226:15240	329.510	40:145	1E	1	0	1E	3E	1	0E
1981	304	15240:15253	329.511	40:145	1E	1	0	0E	3E	1E	1
1981	304	15253:15254	329.107		1E	0	0	3E	3E	1	0E
1981	306	15268:15281	318.500	-10:90	3E	0	0	1E	3E	0E	1
1981	307	15281:15295	318.501	-10:90	2E	1E	0	2E	3E	1	0E
1981	308	15295:15309	318.502	-10:90	3E	0	0	3E	3E	1	1E
1981	310	15323:15337	318.503	-10:90	2E	1E	0	1E	3E	0E	1
1981	311	15337:15350	318.504	-10:90	3E	0	0	2E	3E	1	1E
1981	312	15350:15364	318.505	-10:90	3E	0E	0	3E	3E	1E	1
1981	314	15378:15392	329.506	5:110	3E	0	0	2E	3E	0E	1
1981	315	15392:15406	329.507	5:110	3E	0E	0	3E	3E	1	0E
1981	316	15406:15420	329.508	5:110	3E	0	0	3E	3E	1E	1
1981	318	15434:15448	329.512	20:125	2E	1E	0	1E	3E	1E	1
1981	319	15448:15461	329.513	20:125	2E	0	0	2E	3E	1	1E
1981	320	15461:15475	329.514	5:110	3E	0E	0	3E	3E	1E	1
1981	322	15489:15502	318.500	-10:90	3E	0	0	1E	3E	0E	1
1981	323	15502:15516	318.501	-10:90	2E	1E	0	2E	3E	1	0E
1981	324	15516:15530	318.502	-10:90	3E	0	0	3E	3E	1	1E
1981	326	15544:15558	318.503	-10:90	2E	1E	0	1E	3E	0E	1
1981	327	15558:15572	318.504	-10:90	3E	0	0	2E	3E	1	1E
1981	328	15572:15585	318.505	-10:90	3E	0E	0	3E	3E	1E	1
1981	330	15599:15613	329.506	5:110	3E	0	0	2E	3E	0E	1
1981	331	15613:15626	329.507	5:110	3E	0E	0	3E	3E	1	0E
1981	332	15626:15640	329.508	5:110	3E	0	0	3E	3E	1E	1
1981	334	15654:15668	329.509	40:145	0E	1	0	1E	3E	0E	1
1981	335	15668:15682	329.510	40:145	1E	1	0	1E	3E	1	0E
1981	336	15682:15695	329.511	40:145	1E	1	0	0E	3E	1E	1
1981	336	15695:15696	329.107		1E	0	0	3E	3E	1	0E
1981	338	15709:15723	318.500	-10:90	3E	0	0	1E	3E	0E	1
1981	339	15723:15737	318.501	-10:90	2E	1E	0	2E	3E	1	0E
1981	340	15737:15751	318.502	-10:90	3E	0	0	3E	3E	1	1E
1981	342	15765:15779	318.503	-10:90	2E	1E	0	1E	3E	0E	1
1981	343	15779:15793	318.504	-10:90	3E	0	0	2E	3E	1	1E
1981	344	15793:15806	318.505	-10:90	3E	0E	0	3E	3E	1E	1
1981	346	15820:15834	329.506	5:110	3E	0	0	2E	3E	0E	1
1981	347	15834:15848	329.507	5:110	3E	0E	0	3E	3E	1	0E
1981	348	15848:15861	329.508	5:110	3E	0	0	3E	3E	1E	1
1981	350	15875:15889	329.512	20:125	2E	1E	0	1E	3E	1E	1
1981	351	15889:15903	329.513	20:125	2E	0	0	2E	3E	1	1E

DATE YEAR	DAY	ORBITS (APPROX)	SCAN PROG	RANGE(KM) (APPROX)	SIEVE SETTINGS A1	A2	A3	B1 B2	C1	C2	C3
1981	352	15903:15917	329.514	5:110	3E	0E	0	3E	3E	1E	1
1981	354	15931:15944	318.500	-10:90	3E	0	0	1E	3E	0E	1
1981	355	15944:15958	318.501	-10:90	2E	1E	0	2E	3E	1	0E
1981	356	15958:15972	318.502	-10:90	3E	0	0	3E	3E	1	1E
1981	358	15986:16000	318.503	-10:90	2E	1E	0	1E	3E	0E	1
1981	359	16000:16013	318.504	-10:90	3E	0	0	2E	3E	1	1E
1981	360	16013:16027	318.505	-10:90	3E	0E	0	3E	3E	1E	1
1981	362	16041:16055	329.506	5:110	3E	0	0	2E	3E	0E	1
1981	363	16055:16069	329.507	5:110	3E	0E	0	3E	3E	1	0E
1981	364	16069:16083	329.508	5:110	3E	0	0	3E	3E	1E	1
1982	1	16097:16111	329.509	40:145	0E	1	0	1E	3E	0E	1
1982	2	16111:16125	329.510	40:145	1E	1	0	1E	3E	1	0E
1982	3	16125:16137	329.511	40:145	1E	1	0	0E	3E	1E	1
1982	3	16137:16138	329.107		1E	0	0	3E	3E	1	0E
1982	5	16151:16166	318.500	-10:90	3E	0	0	1E	3E	0E	1
1982	6	16166:16180	318.501	-10:90	2E	1E	0	2E	3E	1	0E
1982	7	16180:16194	318.502	-10:90	3E	0	0	3E	3E	1	1E
1982	9	16207:16221	318.503	-10:90	2E	1E	0	1E	3E	0E	1
1982	10	16221:16235	318.504	-10:90	3E	0	0	2E	3E	1	1E
1982	11	16235:16248	318.505	-10:90	3E	0E	0	3E	3E	1E	1
1982	13	16262:16276	329.506	5:110	3E	0	0	2E	3E	0E	1
1982	14	16276:16290	329.507	5:110	3E	0E	0	3E	3E	1	0E
1982	15	16290:16303	329.508	5:110	3E	0	0	3E	3E	1E	1
1982	15	16303:16304	329.107		1E	0	0	3E	3E	1	0E
1982	17	16318:16332	329.512	20:125	2E	1E	0	1E	3E	1E	1
1982	18	16332:16345	329.513	20:125	2E	0	0	2E	3E	1	1E
1982	19	16345:16359	329.514	5:110	3E	0E	0	3E	3E	1E	1
1982	21	16373:16387	318.500	-10:90	3E	0	0	1E	3E	0E	1
1982	22	16387:16400	318.501	-10:90	2E	1E	0	2E	3E	1	0E
1982	23	16400:16414	318.502	-10:90	3E	0	0	3E	3E	1	1E
1982	25	16428:16442	318.503	-10:90	2E	1E	0	1E	3E	0E	1
1982	26	16442:16456	318.504	-10:90	3E	0	0	2E	3E	1	1E
1982	27	16456:16470	318.505	-10:90	3E	0E	0	3E	3E	1E	1
1982	29	16483:16497	329.506	5:110	3E	0	0	2E	3E	0E	1
1982	30	16497:16511	329.507	5:110	3E	0E	0	3E	3E	1	0E
1982	31	16511:16525	329.508	5:110	3E	0	0	3E	3E	1E	1
1982	33	16539:16553	329.509	40:145	0E	1	0	1E	3E	0E	1
1982	34	16553:16567	329.510	40:145	1E	1	0	1E	3E	1	0E
1982	35	16567:16580	329.511	40:145	1E	1	0	0E	3E	1E	1
1982	37	16594:16608	318.500	-10:90	3E	0	0	1E	3E	0E	1
1982	38	16608:16622	318.501	-10:90	2E	1E	0	2E	3E	1	0E
1982	39	16622:16636	318.502	-10:90	3E	0	0	3E	3E	1	1E
1982	41	16649:16663	318.503	-10:90	2E	1E	0	1E	3E	0E	1
1982	42	16663:16677	318.504	-10:90	3E	0	0	2E	3E	1	1E
1982	43	16677:16690	318.505	-10:90	3E	0E	0	3E	3E	1E	1
1982	45	16705:16719	329.506	5:110	3E	0	0	2E	3E	0E	1
1982	46	16719:16733	329.507	5:110	3E	0E	0	3E	3E	1	0E
1982	47	16733:16746	329.508	5:110	3E	0	0	3E	3E	1E	1
1982	49	16760:16774	329.512	20:125	2E	1E	0	1E	3E	1E	1
1982	50	16774:16788	329.513	20:125	2E	0	0	2E	3E	1	1E
1982	51	16788:16801	329.514	5:110	3E	0E	0	3E	3E	1E	1
1982	53	16816:16829	318.500	-10:90	3E	0	0	1E	3E	0E	1
1982	54	16829:16843	318.501	-10:90	2E	1E	0	2E	3E	1	0E
1982	55	16843:16857	318.502	-10:90	3E	0	0	3E	3E	1	1E
1982	57	16870:16885	318.503	-10:90	2E	1E	0	1E	3E	0E	1
1982	58	16885:16898	318.504	-10:90	3E	0	0	2E	3E	1	1E

DATE YEAR	DAY	ORBITS (APPROX)	SCAN PROG	RANGE(KM) (APPROX)	SIEVE SETTINGS A1	A2	A3	B1 B2	C1	C2	C3
1982	59	16898:16912	318.505	-10:90	3E	0E	0	3E	3E	1E	1
1982	61	16926:16940	329.506	5:110	3E	0	0	2E	3E	0E	1
1982	62	16940:16954	329.507	5:110	3E	0E	0	3E	3E	1	0E
1982	63	16954:16968	329.508	5:110	3E	0	0	3E	3E	1E	1
1982	65	16981:16995	329.509	40:145	0E	1	0	1E	3E	0E	1
1982	66	16995:17009	329.510	40:145	1E	1	0	1E	3E	1	0E
1982	67	17009:17023	329.511	40:145	1E	1	0	0E	3E	1E	1
1982	69	17036:17050	318.500	-10:90	3E	0	0	1E	3E	0E	1
1982	70	17050:17064	318.500	-10:90	3E	0	0	1E	3E	0E	1
1982	71	17064:17078	318.500	-10:90	3E	0	0	1E	3E	0E	1
1982	73	17092:17106	318.503	-10:90	2E	1E	0	1E	3E	0E	1
1982	74	17106:17119	318.504	-10:90	3E	0	0	2E	3E	1	1E
1982	75	17119:17133	318.505	-10:90	3E	0E	0	3E	3E	1E	1
1982	77	17147:17161	329.506	5:110	3E	0	0	2E	3E	0E	1
1982	78	17161:17174	329.507	5:110	3E	0E	0	3E	3E	1	0E
1982	79	17174:17188	329.508	5:110	3E	0	0	3E	3E	1E	1
1982	81	17202:17216	329.512	20:125	2E	1E	0	1E	3E	1E	1
1982	82	17216:17230	329.513	20:125	2E	0	0	2E	3E	1	1E
1982	83	17230:17244	329.514	5:110	3E	0E	0	3E	3E	1E	1
1982	85	17257:17271	318.500	-10:90	3E	0	0	1E	3E	0E	1
1982	86	17271:17285	318.501	-10:90	2E	1E	0	2E	3E	1	0E
1982	87	17285:17298	318.502	-10:90	3E	0	0	3E	3E	1	1E
1982	89	17312:17326	318.503	-10:90	2E	1E	0	1E	3E	0E	1
1982	90	17326:17340	318.504	-10:90	3E	0	0	2E	3E	1	1E
1982	91	17340:17354	318.505	-10:90	3E	0E	0	3E	3E	1E	1
1982	93	17368:17382	329.506	5:110	3E	0	0	2E	3E	0E	1
1982	94	17382:17396	329.507	5:110	3E	0E	0	3E	3E	1	0E
1982	95	17396:17410	329.508	5:110	3E	0	0	3E	3E	1E	1
1982	97	17424:17438	329.509	40:145	0E	1	0	1E	3E	0E	1
1982	98	17438:17451	329.510	40:145	1E	1	0	1E	3E	1	0E
1982	99	17451:17465	329.511	40:145	1E	1	0	0E	3E	1E	1
1982	101	17479:17493	318.500	-10:90	3E	0	0	1E	3E	0E	1
1982	102	17493:17506	318.501	-10:90	2E	1E	0	2E	3E	1	0E
1982	103	17506:17519	318.502	-10:90	3E	0	0	3E	3E	1	1E
1982	105	17534:17548	318.503	-10:90	2E	1E	0	1E	3E	0E	1
1982	106	17548:17562	318.504	-10:90	3E	0	0	2E	3E	1	1E
1982	107	17562:17576	318.505	-10:90	3E	0E	0	3E	3E	1E	1
1982	109	17589:17603	329.506	5:110	3E	0	0	2E	3E	0E	1
1982	110	17603:17617	329.507	5:110	3E	0E	0	3E	3E	1	0E
1982	111	17617:17629	329.508	5:110	3E	0	0	3E	3E	1E	1
1982	111	17630:17631	329.107		1E	0	0	3E	3E	1	0E
1982	113	17645:17658	329.512	20:125	2E	1E	0	1E	3E	1E	1
1982	114	17658:17672	329.513	20:125	2E	0	0	2E	3E	1	1E
1982	115	17672:17686	329.514	5:110	3E	0E	0	3E	3E	1E	1
1982	117	17700:17714	318.500	-10:90	3E	0	0	1E	3E	0E	1
1982	118	17714:17728	318.501	-10:90	2E	1E	0	2E	3E	1	0E
1982	119	17728:17742	318.502	-10:90	3E	0	0	3E	3E	1	1E
1982	121	17756:17770	318.503	-10:90	2E	1E	0	1E	3E	0E	1
1982	122	17770:17783	318.504	-10:90	3E	0	0	2E	3E	1	1E
1982	123	17783:17797	318.505	-10:90	3E	0E	0	3E	3E	1E	1
1982	125	17811:17825	329.506	5:110	3E	0	0	2E	3E	0E	1
1982	126	17825:17838	329.507	5:110	3E	0E	0	3E	3E	1	0E
1982	127	17838:17852	329.508	5:110	3E	0	0	3E	3E	1E	1
1982	129	17866:17879	329.509	40:145	0E	1	0	1E	3E	0E	1
1982	130	17879:17893	329.510	40:145	1E	1	0	1E	3E	1	0E
1982	131	17893:17907	329.511	40:145	1E	1	0	0E	3E	1E	1

DATE YEAR	DAY	ORBITS (APPROX)	SCAN PROG	RANGE(KM) (APPROX)	SIEVE SETTINGS A1	A2	A3	B1 B2	C1	C2	C3
1982	133	17921:17935	318.500	-10:90	3E	0	0	1E	3E	0E	1
1982	134	17935:17949	318.501	-10:90	2E	1E	0	2E	3E	1	0E
1982	135	17949:17963	318.502	-10:90	3E	0	0	3E	3E	1	1E
1982	137	17977:17990	318.503	-10:90	2E	1E	0	1E	3E	0E	1
1982	138	17990:18004	318.504	-10:90	3E	0	0	2E	3E	1	1E
1982	139	18004:18018	318.505	-10:90	3E	0E	0	3E	3E	1E	1
1982	141	18032:18046	329.506	5:110	3E	0	0	2E	3E	0E	1
1982	142	18046:18060	329.507	5:110	3E	0E	0	3E	3E	1	0E
1982	143	18060:18073	329.508	5:110	3E	0	0	3E	3E	1E	1
1982	145	18087:18100	329.512	20:125	2E	1E	0	1E	3E	1E	1
1982	146	18100:18114	329.513	20:125	2E	0	0	2E	3E	1	1E
1982	147	18114:18126	329.514	5:110	3E	0E	0	3E	3E	1E	1
1982	147	18126:18129	329.514	5:110	3E	0E	0	3E	3E	1E	1
1982	149	18143:18156	318.500	-10:90	3E	0	0	1E	3E	0E	1
1982	150	18156:18170	318.501	-10:90	2E	1E	0	2E	3E	1	0E
1982	151	18170:18184	318.502	-10:90	3E	0	0	3E	3E	1	1E
1982	153	18198:18211	318.503	-10:90	2E	1E	0	1E	3E	0E	1
1982	154	18211:18225	318.504	-10:90	3E	0	0	2E	3E	1	1E
1982	155	18225:18239	318.505	-10:90	3E	0E	0	3E	3E	1E	1
1982	157	18253:18266	329.506	5:110	3E	0	0	2E	3E	0E	1
1982	158	18266:18280	329.507	5:110	3E	0E	0	3E	3E	1	0E
1982	159	18280:18294	329.508	5:110	3E	0	0	3E	3E	1E	1
1982	161	18308:18322	333.631		3E	0	0	3E	3E	1E	1
1982	162	18322:18336	333.631		3E	0	0	3E	3E	1E	1
1982	163	18336:18350	333.631		3E	0	0	3E	3E	1E	1
1982	165	18363:18377	333.632		3E	0	0	2E	3E	1	1E
1982	166	18377:18391	333.632		3E	0	0	2E	3E	1	1E
1982	167	18391:18404	333.632		3E	0	0	2E	3E	1	1E
1982	169	18418:18432	333.631		3E	0	0	3E	3E	1E	1
1982	170	18432:18446	333.631		3E	0	0	3E	3E	1E	1
1982	171	18446:18460	333.631		3E	0	0	3E	3E	1E	1
1982	173	18474:18487	333.633		2E	1E	0	3E	3E	1	1E
1982	174	18487:18501	333.633		2E	1E	0	3E	3E	1	1E
1982	175	18501:18515	333.633		2E	1E	0	3E	3E	1	1E
1982	177	18529:18543	333.631		3E	0	0	3E	3E	1E	1
1982	178	18543:18557	333.631		3E	0	0	3E	3E	1E	1
1982	179	18557:18569	333.631		3E	0	0	3E	3E	1E	1
1982	179	18569:18571	333.137		3E	0	0	3E	3E	1E	1
1982	181	18585:18598	333.632		3E	0	0	2E	3E	1	1E
1982	182	18598:18612	333.632		3E	0	0	2E	3E	1	1E
1982	183	18612:18626	333.632		3E	0	0	2E	3E	1	1E
1982	185	18640:18654	333.634		3E	0	0	3E	3E	0E	1
1982	186	18654:18668	333.634		3E	0	0	3E	3E	0E	1
1982	187	18668:18681	333.634		3E	0	0	3E	3E	0E	1
1982	189	18695:18709	333.635		3E	0	0	1E	3E	1	0E
1982	190	18709:18723	333.635		3E	0	0	1E	3E	1	0E
1982	191	18723:18737	333.635		3E	0	0	1E	3E	1	0E
1982	193	18751:18765	333.631		3E	0	0	3E	3E	1E	1
1982	194	18765:18778	333.631		3E	0	0	3E	3E	1E	1
1982	195	18778:18792	333.631		3E	0	0	3E	3E	1E	1
1982	197	18806:18820	333.632		3E	0	0	2E	3E	1	1E
1982	198	18820:18834	333.632		3E	0	0	2E	3E	1	1E
1982	199	18834:18847	333.632		3E	0	0	2E	3E	1	1E
1982	201	18861:18875	333.631		3E	0	0	3E	3E	1E	1
1982	202	18875:18889	333.631		3E	0	0	3E	3E	1E	1
1982	203	18889:18902	333.631		3E	0	0	3E	3E	1E	1

DATE YEAR	DAY	ORBITS (APPROX)	SCAN PROG	RANGE(KM) (APPROX)	SIEVE SETTINGS A1	A2	A3	B1 B2	C1	C2	C3
1982	205	18916:18930	333.632		3E	0	0	2E	3E	1	1E
1982	206	18930:18944	333.632		3E	0	0	2E	3E	1	1E
1982	207	18944:18957	333.632		3E	0	0	2E	3E	1	1E
1982	208	18957:18971	333.632		3E	0	0	2E	3E	1	1E
1982	209	18971:18985	333.631		3E	0	0	3E	3E	1E	1
1982	210	18985:18998	333.631		3E	0	0	3E	3E	1E	1
1982	211	18998:19012	333.631		3E	0	0	3E	3E	1E	1
1982	211	19012:19013	333.137		3E	0	0	3E	3E	1E	1
1982	212	19013:19027	333.631		3E	0	0	3E	3E	1E	1
1982	213	19027:19042	333.632		3E	0	0	2E	3E	1	1E
1982	214	19042:19055	333.632		3E	0	0	2E	3E	1	1E
1982	215	19055:19068	333.632		3E	0	0	2E	3E	1	1E
1982	216	19068:19082	333.632		3E	0	0	2E	3E	1	1E
1982	217	19082:19096	333.634		3E	0	0	3E	3E	0E	1
1982	218	19096:19110	333.634		3E	0	0	3E	3E	0E	1
1982	219	19110:19124	333.634		3E	0	0	3E	3E	0E	1
1982	220	19124:19138	333.634		3E	0	0	3E	3E	0E	1
1982	221	19138:19151	333.635		3E	0	0	1E	3E	1	0E
1982	222	19151:19165	333.635		3E	0	0	1E	3E	1	0E
1982	223	19165:19179	333.635		3E	0	0	1E	3E	1	0E
1982	224	19179:19193	333.635		3E	0	0	1E	3E	1	0E
1982	225	19193:19207	333.631		3E	0	0	3E	3E	1E	1
1982	226	19207:19221	333.631		3E	0	0	3E	3E	1E	1
1982	227	19221:19234	333.631		3E	0	0	3E	3E	1E	1
1982	228	19234:19248	333.631		3E	0	0	3E	3E	1E	1
1982	229	19248:19262	333.632		3E	0	0	2E	3E	1	1E
1982	230	19262:19276	333.632		3E	0	0	2E	3E	1	1E
1982	231	19276:19289	333.632		3E	0	0	2E	3E	1	1E
1982	233	19303:19317	333.631		3E	0	0	3E	3E	1E	1
1982	234	19318:19331	333.631		3E	0	0	3E	3E	1E	1
1982	235	19331:19344	333.631		3E	0	0	3E	3E	1E	1
1982	237	19358:19372	333.633		2E	1E	0	3E	3E	1	1E
1982	238	19372:19386	333.633		2E	1E	0	3E	3E	1	1E
1982	239	19386:19400	333.633		2E	1E	0	3E	3E	1	1E

NOTE 1: Wrong scan pattern (GSFC error). Space views suspect.

NOTE 2: Bad roll compensation phasing. Some data lost.

NOTE 3: Possible beat (PMC B1/2 and chopper).

NOTE 4: Spikes on data in some orbits.

NOTE 5: C1 signal channel spikes evident on some orbits.

NOTE 6: Large number C1 signal channel spikes. Also some on A23W.

Table 5-3

Mode Table 2: Day 286, 1981 to 160, 1983

This table also contains the start and end times of daily data sets (year, day of year, second of day) and the number of major frames of data in the data set, as well as the sieve setting/-PMC mode as before.

NOMINAL DATE		START TIME			END TIME			16 SEC	PMC MODE							PROCESSING DATE	
YEAR	DAY	YR	DAY	SECS	YR	DAY	SECS	FRAMES	A1	A2	A3	B1 B2	C1	C2	C3	YEAR	DAY
1981	286	1981	286	1668	1981	286	86388	5259	3E	0E	0	3E	3E	1E	1	1983	146
1981	287	1981	287	4	1981	287	86388	5181	3E	0E	0	3E	3E	1E	1	1983	146
1981	288	1981	288	4	1981	289	3412	5474	3E	0E	0	3E	3E	1E	1	1983	146
1981	290	1981	289	86276	1981	290	86388	5357	3E	0E	0	3E	3E	1E	1	1983	146
1981	291	1981	291	4	1981	291	86388	4991	3E	0E	0	3E	3E	1E	1	1983	146
1981	292	1981	292	4	1981	293	1684	5417	3E	0E	0	3E	3E	1E	1	1983	146
1981	294	1981	294	4356	1981	294	86388	4906	3E	0E	0	3E	3E	1E	1	1983	171
1981	295	1981	295	4	1981	295	86388	5338	3E	0E	0	3E	3E	1E	1	1983	171
1981	296	1981	296	4	1981	296	86356	5358	3E	0E	0	3E	3E	1E	1	1983	171
1981	298	1981	298	2564	1981	298	86388	5210	3E	0E	0	3E	3E	1E	1	1983	171
1981	299	1981	299	4	1981	299	86388	5204	3E	0E	0	3E	3E	1E	1	1983	171
1981	300	1981	300	4	1981	301	4532	5064	3E	0E	0	3E	3E	1E	1	1983	171
1981	302	1981	302	788	1981	303	388	5326	0E	1	0	1E	3E	0E	1	1983	172
1981	303	1981	303	1908	1981	304	1508	5354	1E	1	0	1E	3E	1	0E	1983	172
1981	304	1981	304	3028	1981	304	81508	4881	1E	1	0	0E	3E	1E	1	1983	172
1981	306	1981	306	5252	1981	306	85140	4963	3E	0	0	1E	3E	0E	1	1983	172
1981	307	1981	307	116	1981	308	596	5274	2E	1E	0	2E	3E	1	0E	1983	172
1981	308	1981	308	1236	1981	309	900	5293	3E	0	0	3E	3E	1	1E	1983	172
1981	310	1981	310	3460	1981	311	2980	5326	2E	1E	0	1E	3E	0E	1	1983	216
1981	311	1981	311	4580	1981	311	84500	4956	3E	0	0	2E	3E	1	1E	1983	216
1981	312	1981	311	85844	1981	312	85572	5301	3E	0E	0	3E	3E	1E	1	1983	216
1981	314	1981	314	1684	1981	314	37220	2207	3E	0	0	2E	3E	0E	1	1983	216
1981	314	1981	314	43460	1981	315	1220	2744	3E	0	0	2E	3E	0E	1	1983	216
1981	315	1981	315	2804	1981	316	2452	5299	3E	0E	0	3E	3E	1	0E	1983	216
1981	316	1981	316	3908	1981	317	3476	5327	3E	0	0	3E	3E	1E	1	1983	216
1981	318	1981	317	86292	1981	318	85988	5323	2E	1E	0	1E	3E	1E	1	1983	227
1981	319	1981	319	1012	1981	320	676	5138	2E	0	0	2E	3E	1	1E	1983	227
1981	320	1981	320	2132	1981	321	1716	5181	3E	0E	0	3E	3E	1E	1	1983	227
1981	322	1981	322	4356	1981	323	4212	5131	3E	0	0	1E	3E	0E	1	1983	227
1981	323	1981	323	5476	1981	323	85220	4958	2E	1E	0	2E	3E	1	0E	1983	227
1981	324	1981	324	340	1981	324	86260	5309	3E	0	0	3E	3E	1	1E	1983	227
1981	326	1981	326	2596	1981	327	2260	5351	2E	1E	0	1E	3E	0E	1	1983	228
1981	327	1981	327	3684	1981	328	3284	5326	3E	0	0	2E	3E	1	1E	1983	228
1981	328	1981	328	4804	1981	328	84580	4967	3E	0E	0	3E	3E	1E	1	1983	228
1981	330	1981	330	788	1981	331	500	5258	3E	0	0	2E	3E	0E	1	1983	228
1981	331	1981	331	1924	1981	332	1444	5293	3E	0E	0	3E	3E	1	0E	1983	228
1981	332	1981	332	3012	1981	333	2564	5271	3E	0	0	3E	3E	1E	1	1983	228
1981	334	1981	334	5380	1981	334	85140	4852	0E	1	0	1E	3E	0E	1	1983	231
1981	335	1981	335	116	1981	335	86340	5224	1E	1	0	1E	3E	1	0E	1983	231
1981	336	1981	336	1236	1981	336	79796	4805	1E	1	0	0E	3E	1E	1	1983	231
1981	338	1981	338	3460	1981	339	3252	5113	3E	0	0	1E	3E	0E	1	1983	231
1981	339	1981	339	6420	1981	339	84596	4824	2E	1E	0	2E	3E	1	0E	1983	231
1981	340	1981	339	85844	1981	340	85524	4861	3E	0	0	3E	3E	1	1E	1983	231
1981	342	1981	342	1668	1981	343	1204	5281	2E	1E	0	1E	3E	0E	1	1983	234
1981	343	1981	343	2788	1981	344	2356	5289	3E	0	0	2E	3E	1	1E	1983	234
1981	344	1981	344	3908	1981	345	3380	5318	3E	0E	0	3E	3E	1E	1	1983	234
1981	346	1981	346	6132	1981	346	85988	4907	3E	0	0	2E	3E	0E	1	1983	234
1981	347	1981	347	996	1981	348	724	5294	3E	0E	0	3E	3E	1	0E	1983	234
1981	348	1981	348	2132	1981	349	1636	5279	3E	0	0	3E	3E	1E	1	1983	234
1981	350	1981	350	4356	1981	351	3892	5185	2E	1E	0	1E	3E	1E	1	1983	235
1981	351	1981	351	5460	1981	352	5220	5329	2E	0	0	2E	3E	1	1E	1983	235
1981	352	1981	352	6580	1981	353	20	4931	3E	0E	0	3E	3E	1E	1	1983	235
1981	354	1981	354	2564	1981	355	2164	5286	3E	0	0	1E	3E	0E	1	1983	235
1981	355	1981	355	3668	1981	356	3316	5298	2E	1E	0	2E	3E	1	0E	1983	235
1981	356	1981	356	4788	1981	357	4324	5295	3E	0	0	3E	3E	1	1E	1983	235
1981	358	1981	358	772	1981	359	1220	5380	2E	1E	0	1E	3E	0E	1	1983	238

NOMINAL DATE YEAR	NOMINAL DATE DAY	START TIME YR	START TIME DAY	START TIME SECS	END TIME YR	END TIME DAY	END TIME SECS	16 SEC FRAMES	PMC MODE A1	A2	A3	B1 B2	C1	C2	C3	PROCESSING DATE YEAR	PROCESSING DATE DAY
1981	359	1981	359	1892	1981	360	1492	5271	3E	0	0	2E	3E	1	1E	1983	238
1981	360	1981	360	2996	1981	361	244	5182	3E	0E	0	3E	3E	1E	1	1983	238
1981	362	1981	362	5236	1981	362	84964	4728	3E	0	0	2E	3E	0E	1	1983	238
1981	363	1981	363	100	1981	363	86036	5294	3E	0E	0	3E	3E	1	0E	1983	238
1981	364	1981	364	1220	1981	365	884	5255	3E	0	0	3E	3E	1E	1	1983	238
1982	1	1982	1	11771	1982	2	3019	4706	0E	1	0	1E	3E	0E	1	1983	292
1982	2	1982	2	4571	1982	2	84331	4921	1E	1	0	1E	3E	1	0E	1983	292
1982	2	1982	2	21979	1982	2	84331	3855	1E	1	0	1E	3E	1	0E	1983	292
1982	3	1982	3	3499	1982	3	85563	5030	3E	0	0	1E	3E	0E	1	1983	292
1982	5	1982	5	7899	1982	6	1339	4898	3E	0	0	1E	3E	0E	1	1983	292
1982	6	1982	6	2763	1982	7	2459	5297	2E	1E	0	2E	3E	1	0E	1983	292
1982	7	1982	7	3883	1982	7	83803	4947	3E	0	0	3E	3E	1	1E	1983	292
1982	9	1982	8	86251	1982	9	85851	5328	2E	1E	0	1E	3E	0E	1	1983	304
1982	10	1982	10	971	1982	11	539	5198	3E	0	0	2E	3E	1	1E	1983	304
1982	11	1982	11	2091	1982	12	1643	5317	3E	0E	0	3E	3E	1E	1	1983	304
1982	13	1982	13	4331	1982	13	84219	4564	3E	0	0	2E	3E	0E	1	1983	304
1982	14	1982	13	85611	1982	14	85355	5106	3E	0E	0	3E	3E	1	0E	1983	304
1982	15	1982	15	299	1982	15	78827	4818	3E	0	0	3E	3E	1E	1	1983	304
1982	17	1982	17	2539	1982	18	2331	5142	2E	1E	0	1E	3E	1E	1	1983	305
1982	18	1982	18	3643	1982	19	3163	5192	2E	0	0	2E	3E	1	1E	1983	305
1982	19	1982	19	4763	1982	19	84635	4858	3E	0E	0	3E	3E	1E	1	1983	305
1982	21	1982	21	747	1982	22	315	5296	3E	0	0	1E	3E	0E	1	1983	305
1982	22	1982	22	1851	1982	23	1659	5328	2E	1E	0	2E	3E	1	0E	1983	305
1982	23	1982	23	2971	1982	24	2491	5307	3E	0	0	3E	3E	1	1E	1983	305
1982	25	1982	25	5195	1982	26	4763	5314	2E	1E	0	1E	3E	0E	1	1983	308
1982	26	1982	26	6315	1982	26	86251	4910	3E	0	0	2E	3E	1	1E	1983	308
1982	27	1982	27	1179	1982	28	715	5287	3E	0E	0	3E	3E	1E	1	1983	308
1982	29	1982	29	3403	1982	30	2907	5279	3E	0	0	2E	3E	0E	1	1983	308
1982	30	1982	30	4523	1982	30	84411	4880	3E	0E	0	3E	3E	1	0E	1983	308
1982	31	1982	30	85787	1982	31	85563	5308	3E	0	0	3E	3E	1E	1	1983	308
1982	33	1982	33	1611	1982	34	1227	5275	0E	1	0	1E	3E	0E	1	1983	311
1982	34	1982	34	2731	1982	35	2363	5240	1E	1	0	1E	3E	1	0E	1983	311
1982	35	1982	35	3835	1982	35	83643	4835	1E	1	0	0E	3E	1E	1	1983	311
1982	37	1982	36	86219	1982	37	85787	5307	3E	0	0	1E	3E	0E	1	1983	311
1982	38	1982	38	939	1982	39	475	5303	2E	1E	0	2E	3E	1	0E	1983	311
1982	39	1982	39	2107	1982	40	1627	5249	3E	0	0	3E	3E	1	1E	1983	311
1982	41	1982	41	4283	1982	42	3707	5286	2E	1E	0	1E	3E	0E	1	1983	312
1982	42	1982	42	5403	1982	43	5179	5241	3E	0	0	2E	3E	1	1E	1983	312
1982	43	1982	43	6571	1982	43	86171	4864	3E	0E	0	3E	3E	1E	1	1983	312
1982	45	1982	45	2491	1982	46	5419	5529	3E	0	0	2E	3E	0E	1	1983	312
1982	46	1982	46	9851	1982	47	3339	4907	3E	0E	0	3E	3E	1	0E	1983	312
1982	47	1982	47	4715	1982	47	83355	4761	3E	0	0	3E	3E	1E	1	1983	312
1982	48	1982	48	23483	1982	48	23531	4	0E	0E	0	0E	0E	0E	0	1983	312
1982	49	1982	49	827	1982	50	347	5294	2E	1E	0	1E	3E	1E	1	1983	314
1982	50	1982	50	1803	1982	51	1435	5319	2E	0	0	2E	3E	1	1E	1983	314
1982	51	1982	51	2923	1982	52	2491	5154	3E	0E	0	3E	3E	1E	1	1983	314
1982	53	1982	53	5147	1982	53	84923	4894	3E	0	0	1E	3E	0E	1	1983	314
1982	54	1982	54	11	1982	54	86107	5277	2E	1E	0	2E	3E	1	0E	1983	314
1982	55	1982	55	1131	1982	56	139	5194	3E	0	0	3E	3E	1	1E	1983	314
1982	57	1982	57	3355	1982	58	6075	5425	2E	1E	0	1E	3E	0E	1	1983	315
1982	58	1982	58	10715	1982	58	84187	4521	3E	0	0	2E	3E	1	1E	1983	315
1982	59	1982	58	85739	1982	59	85451	5300	3E	0E	0	3E	3E	1E	1	1983	315
1982	61	1982	61	1547	1982	62	4475	5540	3E	0	0	2E	3E	0E	1	1983	315
1982	62	1982	62	8907	1982	63	2363	4924	3E	0E	0	3E	3E	1	0E	1983	315
1982	63	1982	63	3819	1982	64	3259	5257	3E	0	0	3E	3E	1E	1	1983	315
1982	65	1982	64	86155	1982	66	5771	5734	0E	1	0	1E	3E	0E	1	1983	319

NOMINAL DATE YEAR	DAY	START TIME YR	DAY	SECS	END TIME YR	DAY	SECS	16 SEC FRAMES	A1	A2	A3	B1 B2	C1	C2	C3	PROCESSING DATE YEAR	DAY
1982	66	1982	66	7147	1982	67	491	4946	1E	1	0	1E	3E	1	0E	1983	319
1982	67	1982	67	1979	1982	68	2779	5376	1E	1	0	0E	3E	1E	1	1983	319
1982	69	1982	69	2811	1982	69	86395	5173	3E	0	0	3E	3E	1	1E	1983	319
1982	70	1982	70	11	1982	70	86395	5275	3E	0	0	3E	3E	1	1E	1983	319
1982	71	1982	71	11	1982	71	86219	5294	3E	0	0	3E	3E	1	1E	1983	319
1982	73	1982	73	2427	1982	74	2411	5334	2E	1E	0	1E	3E	0E	1	1983	321
1982	74	1982	74	3531	1982	74	83595	4940	3E	0	0	2E	3E	1	1E	1983	321
1982	75	1982	74	84795	1982	76	4107	5567	3E	0E	0	3E	3E	1E	1	1983	321
1982	77	1982	77	619	1982	78	363	5015	3E	0	0	2E	3E	0E	1	1983	321
1982	78	1982	78	1739	1982	79	1307	5305	3E	0E	0	3E	3E	1	0E	1983	321
1982	79	1982	79	2843	1982	79	81723	4876	3E	0	0	3E	3E	1E	1	1983	321
1982	81	1982	80	85227	1982	81	85083	5314	2E	1E	0	1E	3E	1E	1	1983	174
1982	82	1982	81	86347	1982	82	84555	5207	2E	0	0	2E	3E	1	1E	1983	174
1982	83	1982	83	1035	1982	84	3931	5531	3E	0E	0	3E	3E	1E	1	1983	174
1982	85	1982	85	3275	1982	86	2667	5201	3E	0	0	1E	3E	0E	1	1983	174
1982	86	1982	86	4379	1982	86	84251	4926	2E	1E	0	2E	3E	1	0E	1983	174
1982	87	1982	86	85643	1982	88	5019	5711	3E	0	0	3E	3E	1	1E	1983	174
1982	89	1982	89	1483	1982	90	1163	5308	2E	1E	0	1E	3E	0E	1	1983	175
1982	90	1982	90	2571	1982	91	2187	5313	3E	0	0	2E	3E	1	1E	1983	175
1982	91	1982	91	3691	1982	92	3211	5307	3E	0E	0	3E	3E	1E	1	1983	175
1982	93	1982	93	5915	1982	94	75	4860	3E	0	0	2E	3E	0E	1	1983	175
1982	94	1982	94	779	1982	95	811	5354	3E	0E	0	3E	3E	1	0E	1983	175
1982	95	1982	95	1899	1982	96	1563	5323	3E	0	0	3E	3E	1E	1	1983	175
1982	97	1982	97	4123	1982	98	3691	5317	0E	1	0	1E	3E	0E	1	1984	60
1982	98	1982	98	5227	1982	98	85211	4942	1E	1	0	1E	3E	1	0E	1984	60
1982	99	1982	99	6347	1982	99	86203	4891	1E	1	0	0E	3E	1E	1	1984	60
1982	101	1982	101	8571	1982	102	1931	4889	3E	0	0	1E	3E	0E	1	1984	60
1982	102	1982	102	3435	1982	103	2955	5289	2E	1E	0	2E	3E	1	0E	1984	60
1982	103	1982	103	4539	1982	103	84363	4905	3E	0	0	3E	3E	1	1E	1984	60
1982	105	1982	105	523	1982	106	91	5322	2E	1E	0	1E	3E	0E	1	1983	179
1982	106	1982	106	1627	1982	107	1227	5295	3E	0	0	2E	3E	1	1E	1983	179
1982	107	1982	107	2747	1982	108	2347	5316	3E	0E	0	3E	3E	1E	1	1983	179
1982	109	1982	109	4971	1982	109	84843	4962	3E	0	0	2E	3E	0E	1	1983	179
1982	110	1982	109	86235	1982	110	85643	5294	3E	0E	0	3E	3E	1	0E	1983	179
1982	111	1982	111	939	1982	111	79403	4885	3E	0	0	3E	3E	1E	1	1983	179
1982	113	1982	113	3163	1982	114	2891	5317	2E	1E	0	1E	3E	1E	1	1983	180
1982	114	1982	114	4283	1982	115	3915	5297	2E	0	0	2F	3E	1	1E	1983	180
1982	115	1982	115	5403	1982	115	85163	4908	3E	0E	0	3E	3E	1E	1	1983	180
1982	117	1982	117	1371	1982	118	1163	5325	3E	0	0	1E	3E	0E	1	1983	180
1982	118	1982	118	2475	1982	119	5275	5469	2E	1E	0	2E	3E	1	0E	1983	180
1982	119	1982	119	9835	1982	120	3227	4953	3E	0	0	3E	3E	1	1E	1983	180
1982	121	1982	120	85963	1982	121	85627	5336	2E	1E	0	1E	3E	0E	1	1983	181
1982	122	1982	122	683	1982	123	507	5265	3E	0	0	2E	3E	1	1E	1983	181
1982	123	1982	123	1787	1982	124	1483	5303	3E	0E	0	3E	3E	1E	1	1983	181
1982	125	1982	125	4011	1982	126	3723	5313	3E	0	0	2E	3E	0E	1	1983	181
1982	126	1982	126	5131	1982	126	85131	4899	3E	0E	0	3E	3E	1	0E	1983	181
1982	127	1982	126	86395	1982	127	85995	5232	3E	0	0	3E	3E	1E	1	1983	181
1982	129	1982	129	2219	1982	130	1691	5316	0E	1	0	1E	3E	0E	1	1983	182
1982	130	1982	130	3323	1982	131	2955	5282	1E	1	0	1E	3E	1	0E	1983	182
1982	131	1982	131	4443	1982	131	84283	4946	1E	1	0	0E	3E	1E	1	1983	182
1982	133	1982	133	411	1982	133	86299	5336	3E	0	0	1E	3E	0E	1	1983	182
1982	134	1982	134	1515	1982	135	1195	5304	2E	1E	0	2E	3F	1	0E	1983	182
1982	135	1982	135	2651	1982	136	2027	5308	3E	0	0	3E	3E	1	1E	1983	182
1982	137	1982	137	4875	1982	137	84651	4945	2E	1E	0	1E	3E	0E	1	1983	185
1982	138	1982	137	86123	1982	139	3563	5549	3E	0	0	2E	3E	1	1E	1983	185
1982	139	1982	139	7083	1982	140	539	4939	3E	0E	0	3E	3E	1E	1	1983	185

NOMINAL DATE YEAR	NOMINAL DATE DAY	START TIME YR	START TIME DAY	START TIME SECS	END TIME YR	END TIME DAY	END TIME SECS	16 SEC FRAMES	PMC MODE A1	A2	A3	B1 B2	C1	C2	C3	PROCESSING DATE YEAR	PROCESSING DATE DAY
1982	141	1982	141	3051	1982	142	3099	5350	3E	0	0	2E	3E	0E	1	1983	185
1982	142	1982	142	4155	1982	143	3739	5320	3E	0E	0	3E	3E	1	0E	1983	185
1982	143	1982	143	5275	1982	143	77483	4487	3E	0	0	3E	3E	1E	1	1983	185
1982	145	1982	145	1243	1982	146	859	5305	2E	1E	0	1E	3E	1E	1	1983	328
1982	146	1982	146	2363	1982	147	1963	5282	2E	0	0	2E	3E	1	1E	1983	328
1982	147	1982	147	3467	1982	148	3019	5330	3E	0E	0	3E	3E	1E	1	1983	328
1982	149	1982	148	85851	1982	149	85467	5296	3E	0	0	1E	3E	0E	1	1983	328
1982	150	1982	150	555	1982	151	219	5300	2E	1E	0	2E	3E	1	0E	1983	328
1982	151	1982	151	1675	1982	152	1419	5358	3E	0	0	3E	3E	1	1E	1983	328
1982	153	1982	153	3899	1982	154	3483	5295	2E	1E	0	1E	3E	0E	1	1983	329
1982	154	1982	154	5003	1982	154	84955	4953	3E	0	0	2E	3E	1	1E	1983	329
1982	155	1982	154	86267	1982	155	86139	5336	3E	0E	0	3E	3E	1E	1	1983	329
1982	157	1982	157	2091	1982	158	1755	5317	3E	0	0	2E	3E	0E	1	1983	329
1982	158	1982	158	3195	1982	159	2811	5305	3E	0E	0	3E	3E	1	0E	1983	329
1982	159	1982	159	4315	1982	159	84107	4937	3E	0	0	3E	3E	1E	1	1983	329
1982	161	1982	161	283	1982	161	86395	5328	3E	0	0	3E	3E	1E	1	1983	332
1982	162	1982	162	11	1982	162	86395	5358	3E	0	0	3E	3E	1E	1	1983	332
1982	163	1982	163	11	1982	164	1979	5445	3E	0	0	3E	3E	1E	1	1983	332
1982	165	1982	165	4731	1982	165	86395	5012	3E	0	0	2E	3E	1	1E	1983	332
1982	166	1982	166	11	1982	166	86395	5362	3E	0	0	2E	3E	1	1E	1983	332
1982	167	1982	167	11	1982	168	315	5376	3E	0	0	2E	3E	1	1E	1983	332
1982	169	1982	169	2923	1982	169	86395	5152	3E	0	0	3E	3E	1E	1	1983	334
1982	170	1982	170	11	1982	170	86395	5272	3E	0	0	3E	3E	1E	1	1983	334
1982	171	1982	171	11	1982	172	4587	5594	3E	0	0	3E	3E	1E	1	1983	334
1982	173	1982	173	1115	1982	173	86395	5249	2E	1E	0	3E	3E	1	1E	1983	334
1982	174	1982	174	11	1982	174	86395	5278	2E	1E	0	3E	3E	1	1E	1983	334
1982	175	1982	175	11	1982	176	2859	5487	2E	1E	0	3E	3E	1	1E	1983	334
1982	177	1982	177	5563	1982	177	86395	5009	3E	0	0	3E	3E	1E	1	1983	336
1982	178	1982	178	11	1982	178	86395	5353	3E	0	0	3E	3E	1E	1	1983	336
1982	179	1982	179	11	1982	180	1067	5389	3E	0	0	3E	3E	1E	1	1983	336
1982	181	1982	181	3755	1982	181	86395	5051	3E	0	0	2E	3E	1	1E	1983	336
1982	182	1982	182	11	1982	182	86395	5342	3E	0	0	2E	3E	1	1E	1983	336
1982	183	1982	183	11	1982	183	85883	5291	3E	0	0	2E	3E	1	1E	1983	336
1982	185	1982	185	1947	1982	185	86395	5145	3E	0	0	3E	3E	0E	1	1983	339
1982	186	1982	186	11	1982	186	86395	5343	3E	0	0	3E	3E	0E	1	1983	339
1982	187	1982	187	11	1982	188	3627	5560	3E	0	0	3E	3E	0E	1	1983	339
1982	189	1982	189	6395	1982	189	86395	4919	3E	0	0	1E	3E	1	0E	1983	339
1982	190	1982	190	11	1982	190	86395	5327	3E	0	0	1E	3E	1	0E	1983	339
1982	191	1982	191	11	1982	192	1995	5451	3E	0	0	1E	3E	1	0E	1983	339
1982	193	1982	193	4587	1982	193	86395	5051	3E	0	0	3E	3E	1E	1	1983	343
1982	194	1982	194	11	1982	194	86395	5310	3E	0	0	3E	3E	1E	1	1983	343
1982	195	1982	195	11	1982	196	251	5369	3E	0	0	3E	3E	1E	1	1983	343
1982	197	1982	197	2779	1982	197	86395	5142	3E	0	0	2E	3E	1	1E	1983	343
1982	198	1982	198	11	1982	198	86395	5321	3E	0	0	2E	3E	1	1E	1983	343
1982	199	1982	199	11	1982	199	84747	5240	3E	0	0	2E	3E	1	1E	1983	343
1982	201	1982	201	971	1982	201	86395	5269	3E	0	0	3E	3E	1E	1	1983	347
1982	202	1982	202	11	1982	202	86395	5350	3E	0	0	3E	3E	1E	1	1983	347
1982	203	1982	203	11	1982	204	2667	5266	3E	0	0	3E	3E	1E	1	1983	347
1982	205	1982	204	85563	1982	205	86395	5365	3E	0	0	2E	3E	1	1E	1983	347
1982	206	1982	206	11	1982	206	86395	5310	3E	0	0	2E	3E	1	1E	1983	347
1982	207	1982	207	11	1982	207	86395	5322	3E	0	0	2E	3E	1	1E	1983	347
1982	208	1982	208	11	1982	208	86363	5352	3E	0	0	2E	3E	1	1E	1983	347
1982	209	1982	209	3611	1982	209	86395	-1	3E	0	0	3E	3E	1E	1	1983	61
1982	210	1982	210	11	1982	210	86395	-1	3E	0	0	3E	3E	1E	1	1983	61
1982	211	1982	211	11	1982	211	85579	-1	3E	0	0	3E	3E	1E	1	1983	61
1982	212	1982	210	683	1982	212	60795	-1	3E	0	0	3E	3E	1E	1	1983	61

NOMINAL DATE YEAR	DAY	START TIME YR	DAY	SECS	END TIME YR	DAY	SECS	16 SEC FRAMES	A1	A2	A3	B1 B2	C1	C2	C3	PROCESSING DATE YEAR	DAY
1982	213	1982	213	1899	1982	213	86395	-1	3E	0	0	2E	3E	1	1E	1983	61
1982	214	1982	214	11	1982	214	86395	-1	3E	0	0	2E	3E	1	1E	1983	61
1982	215	1982	215	11	1982	215	86395	-1	3E	0	0	2E	3E	1	1E	1983	61
1982	216	1982	216	11	1982	216	85003	-1	3E	0	0	2E	3E	1	1E	1983	61
1982	217	1982	216	86395	1982	217	86395	-1	3E	0	0	3E	3E	0E	1	1983	62
1982	218	1982	218	11	1982	218	86395	-1	3E	0	0	3E	3E	0E	1	1983	62
1982	219	1982	219	11	1982	218	86395	-1	3E	0	0	3E	3E	0E	1	1983	62
1982	220	1982	220	11	1982	221	3019	-1	3E	0	0	3E	3E	0E	1	1983	62
1982	221	1982	221	10667	1982	221	86395	-1	3E	0	0	1E	3E	1	0E	1983	62
1982	222	1982	222	11	1982	222	86389	-1	3E	0	0	1E	3E	1	0E	1983	62
1982	223	1982	223	5	1982	223	86389	-1	3E	0	0	1E	3E	1	0E	1983	62
1982	224	1982	224	5	1982	225	357	-1	3E	0	0	1E	3E	1	0E	1983	62
1982	225	1982	225	2725	1982	225	86389	5154	3E	0	0	3E	3E	1E	1	1983	116
1982	226	1982	226	5	1982	226	86389	5337	3E	0	0	3E	3E	1E	1	1983	116
1982	227	1982	227	5	1982	227	86389	4818	3E	0	0	3E	3E	1E	1	1983	116
1982	228	1982	228	5	1982	228	85717	5297	3E	0	0	3E	3E	1E	1	1983	116
1982	229	1982	229	821	1982	229	86389	5172	3E	0	0	2E	3E	1	1E	1983	116
1982	230	1982	230	5	1982	230	86389	4803	3E	0	0	2E	3E	1	1E	1983	116
1982	231	1982	231	5	1982	232	2661	5496	3E	0	0	2E	3E	1	1E	1983	116
1982	233	1982	233	22661	1982	233	86389	3895	3E	0	0	3E	3E	1E	1	1983	353
1982	234	1982	234	5	1982	234	86389	5358	3E	0	0	3E	3E	1E	1	1983	353
1982	235	1982	235	5	1982	236	1861	5178	3E	0	0	3E	3E	1E	1	1983	353
1982	237	1982	237	3445	1982	237	86389	5122	2E	1E	0	3E	3E	1	1E	1983	353
1982	238	1982	238	5	1982	238	86389	5311	2E	1E	0	3E	3E	1	1E	1983	353
1982	239	1982	239	5	1982	239	86357	5271	2E	1E	0	3E	3E	1	1E	1983	353
1982	241	1982	241	1637	1982	241	86389	5196	3E	0	0	3E	3E	1E	1	1983	354
1982	242	1982	242	5	1982	242	86389	5309	3E	0	0	3E	3E	1E	1	1983	354
1982	243	1982	243	5	1982	244	3893	5566	3E	0	0	3E	3E	1E	1	1983	354
1982	245	1982	244	86229	1982	245	86389	5342	3E	0	0	2E	3E	1	1E	1983	354
1982	246	1982	246	5	1982	246	86389	5349	3E	0	0	2E	3E	1	1E	1983	354
1982	247	1982	247	5	1982	248	1621	5421	3E	0	0	2E	3E	1	1E	1983	354
1982	241	1982	241	1637	1982	241	86389	5196	3E	0	0	3E	3E	1E	1	1984	6
1982	242	1982	242	5	1982	242	86389	5309	3E	0	0	3E	3E	1E	1	1984	6
1982	243	1982	243	5	1982	244	3893	5566	3E	0	0	3E	3E	1E	1	1984	6
1982	245	1982	244	86229	1982	245	86389	5342	3E	0	0	2E	3E	1	1E	1984	6
1982	246	1982	246	5	1982	246	86389	5349	3E	0	0	2E	3E	1	1E	1984	6
1982	247	1982	247	5	1982	248	1621	5421	3E	0	0	2E	3E	1	1E	1984	6
1982	241	1982	241	1637	1982	241	86389	5196	3E	0	0	3E	3E	1E	1	1984	9
1982	242	1982	242	5	1982	242	86389	5309	3E	0	0	3E	3E	1E	1	1984	9
1982	243	1982	243	5	1982	244	3893	5566	3E	0	0	3E	3E	1E	1	1984	9
1982	245	1982	244	86229	1982	245	86389	5342	3E	0	0	2E	3E	1	1E	1984	9
1982	246	1982	246	5	1982	246	86389	5349	3E	0	0	2E	3E	1	1E	1984	9
1982	247	1982	247	5	1982	248	1621	5421	3E	0	0	2E	3E	1	1E	1984	9
1982	249	1982	249	4261	1982	249	86389	5029	3E	0	0	3E	3E	0E	1	1984	10
1982	250	1982	250	5	1982	250	86389	5295	3E	0	0	3E	3E	0E	1	1984	10
1982	251	1982	251	5	1982	251	86341	5219	3E	0	0	3E	3E	0E	1	1984	10
1982	253	1982	253	2453	1982	253	86389	5191	3E	0	0	1E	3E	1	0E	1984	10
1982	254	1982	254	5	1982	254	86389	5314	3E	0	0	1E	3E	1	0E	1984	10
1982	255	1982	255	5	1982	256	4245	5600	3E	0	0	1E	3E	1	0E	1984	10
1982	257	1982	257	645	1982	257	86389	5305	3E	0	0	3E	3E	1E	1	1984	11
1982	258	1982	258	5	1982	258	86389	5354	3E	0	0	3E	3E	1E	1	1984	11
1982	259	1982	259	5	1982	260	2597	5193	3E	0	0	3E	3E	1E	1	1984	11
1982	261	1982	261	13109	1982	261	86389	4542	3E	0	0	2E	3E	1	1E	1984	11
1982	262	1982	262	5	1982	262	86389	5349	3E	0	0	2E	3E	1	1E	1984	11
1982	263	1982	263	5	1982	264	725	5391	3E	0	0	2E	3E	1	1E	1984	11
1982	265	1982	265	3269	1982	265	86389	5136	3E	0	0	2E	3E	1	1E	1984	12

NOMINAL DATE YEAR	DAY	START TIME YR	DAY	SECS	END TIME YR	DAY	SECS	16 SEC FRAMES	PMC MODE A1	A2	A3	B1 B2	C1	C2	C3	PROCESSING DATE YEAR	DAY
1982	266	1982	266	5	1982	266	86389	5314	3E	0	0	2E	3E	1	1E	1984	12
1982	267	1982	267	5	1982	267	85781	5319	3E	0	0	2E	3E	1	1E	1984	12
1982	269	1982	269	6181	1982	269	86389	4974	3E	0	0	2E	3E	1	1E	1984	12
1982	270	1982	270	5	1982	270	86389	5342	3E	0	0	2E	3E	1	1E	1984	12
1982	271	1982	271	5	1982	272	2245	5466	3E	0	0	2E	3E	1	1E	1984	12
Gap due to failure of scan mechanism.																	
1983	44	1983	44	331	1983	44	86395	5040	2E	1E	0	3E	3E	1	1E	1983	110
1983	45	1983	45	11	1983	45	86395	5332	2E	1E	0	3E	3E	1	1E	1983	110
1983	46	1983	46	11	1983	47	2347	5438	2E	1E	0	3E	3E	1	1E	1983	110
1983	48	1983	48	4763	1983	48	86395	5046	3E	0	0	3E	3E	1E	1	1983	110
1983	49	1983	49	11	1983	49	85051	5231	3E	0	0	3E	3E	1E	1	1983	110
1983	50	1983	50	59	1983	50	66187	4097	3E	0	0	3E	3E	1E	1	1983	110
1983	52	1983	52	2939	1983	52	86395	5176	3E	0	0	2E	3E	1	1E	1983	111
1983	53	1983	53	11	1983	53	86395	5324	3E	0	0	2E	3E	1	1E	1983	111
1983	54	1983	54	59	1983	54	84923	5229	3E	0	0	2E	3E	1	1E	1983	111
1983	56	1983	56	1115	1983	56	86395	5240	3E	0	0	3E	3E	0E	1	1983	111
1983	57	1983	57	11	1983	57	86395	5351	3E	0	0	3E	3E	0E	1	1983	111
1983	58	1983	58	11	1983	59	3051	5512	3E	0	0	3E	3E	0E	1	1983	111
1983	60	1983	59	85691	1983	60	86395	5382	3E	0	0	1E	3E	1	0E	1984	13
1983	61	1983	61	11	1983	61	86395	5012	3E	0	0	1E	3E	1	0E	1984	13
1983	62	1983	62	11	1983	63	1035	5391	3E	0	0	1E	3E	1	0E	1984	13
1983	64	1983	64	9963	1983	64	86395	4721	3E	0	0	3E	3E	1E	1	1984	13
1983	65	1983	65	11	1983	65	86395	5328	3E	0	0	3E	3E	1E	1	1984	13
1983	66	1983	66	11	1983	66	85707	5301	3E	0	0	3E	3E	1E	1	1984	13
1983	68	1983	68	1899	1983	68	86395	5212	3E	0	0	2E	3E	1	1E	1984	16
1983	69	1983	69	11	1983	69	86395	5330	3E	0	0	2E	3E	1	1E	1984	16
1983	70	1983	70	11	1983	71	3643	5557	3E	0	0	2E	3E	1	1E	1984	16
1983	72	1983	72	75	1983	72	86395	5162	3E	0	0	3E	3E	1E	1	1984	16
1983	73	1983	73	11	1983	73	86395	5330	3E	0	0	3E	3E	1E	1	1984	16
1983	74	1983	74	11	1983	75	1803	5417	3E	0	0	3E	3E	1E	1	1984	16
1983	76	1983	76	4491	1983	76	86395	5065	2E	1E	0	3E	3E	1	1E	1984	17
1983	77	1983	77	11	1983	77	86395	5320	2E	1E	0	3E	3E	1	1E	1984	17
1983	78	1983	78	11	1983	79	91	5246	2E	1E	0	3E	3E	1	1E	1984	17
1983	80	1983	80	2667	1983	80	86395	5160	3E	0	0	3E	3E	1E	1	1984	17
1983	81	1983	81	11	1983	81	86395	5310	3E	0	0	3E	3E	1E	1	1984	17
1983	82	1983	82	11	1983	82	84651	5207	3E	0	0	3E	3E	1E	1	1984	17
1983	84	1983	84	843	1983	84	86395	5286	3E	0	0	2E	3E	1	1E	1984	19
1983	85	1983	85	11	1983	85	86395	5334	3E	0	0	2E	3E	1	1E	1984	19
1983	86	1983	86	11	1983	87	2635	5486	3E	0	0	2E	3E	1	1E	1984	19
1983	88	1983	88	5275	1983	88	86395	5040	3E	0	0	3E	3E	0E	1	1984	19
1983	89	1983	89	11	1983	89	86395	5325	3E	0	0	3E	3E	0E	1	1984	19
1983	90	1983	90	11	1983	91	827	5388	3E	0	0	3E	3E	0E	1	1984	19
1983	92	1983	92	3451	1983	92	86395	5104	3E	0	0	1E	3E	1	0E	1984	20
1983	93	1983	93	11	1983	93	86395	5354	3E	0	0	1E	3E	1	0E	1984	20
1983	94	1983	94	11	1983	94	85499	5280	3E	0	0	1E	3E	1	0E	1984	20
1983	96	1983	96	7867	1983	96	86395	4862	3E	0	0	3E	3E	1E	1	1984	20
1983	97	1983	97	11	1983	97	86395	5340	3E	0	0	3E	3E	1E	1	1984	20
1983	98	1983	98	11	1983	98	83787	5188	3E	0	0	3E	3E	1E	1	1984	20
1983	100	1983	100	4523	1983	100	86395	5041	3E	0	0	2E	3E	1	1E	1984	23
1983	101	1983	101	11	1983	101	86395	5293	3E	0	0	2E	3E	1	1E	1984	23
1983	102	1983	102	11	1983	103	1499	5429	3E	0	0	2E	3E	1	1E	1984	23
1983	104	1983	104	4219	1983	104	86395	5107	3E	0	0	3E	3E	1E	1	1984	23
1983	105	1983	105	11	1983	105	86395	5362	3E	0	0	3E	3E	1E	1	1984	23
1983	106	1983	106	11	1983	106	86251	5319	3E	0	0	3E	3E	1E	1	1984	23
1983	108	1983	108	8635	1983	108	86395	4810	2E	1E	0	3E	3E	1	1E	1984	24
1983	109	1983	109	11	1983	109	86395	5131	2E	1E	0	3E	3E	1	1E	1984	24

NOMINAL DATE		START TIME			END TIME			16 SEC	PMC MODE							PROCESSING DATE	
YEAR	DAY	YR	DAY	SECS	YR	DAY	SECS	FRAMES	A1	A2	A3	B1 B2	C1	C2	C3	YEAR	DAY
1983	110	1983	110	11	1983	110	84363	5212	2E	1E	0	3E	3E	1	1E	1984	24
1983	112	1983	112	571	1983	112	86395	4965	3E	0	0	3E	3E	1E	1	1984	24
1983	113	1983	113	11	1983	113	86395	5349	3E	0	0	3E	3E	1E	1	1984	24
1983	114	1983	114	11	1983	115	5659	5689	3E	0	0	3E	3E	1E	1	1984	24
1983	116	1983	115	85131	1983	116	86395	5428	3E	0	0	2E	3E	1	1E	1984	25
1983	117	1983	117	11	1983	117	86395	5165	3E	0	0	2E	3E	1	1E	1984	25
1983	118	1983	118	11	1983	119	571	5369	3E	0	0	2E	3E	1	1E	1984	25
1983	120	1983	120	3163	1983	120	86395	5144	3E	0	0	3E	3E	0E	1	1984	25
1983	121	1983	121	11	1983	121	86395	5327	3E	0	0	3E	3E	0E	1	1984	25
1983	122	1983	122	11	1983	122	85179	5268	3E	0	0	3E	3E	0E	1	1984	25
1983	116	1983	115	85131	1983	116	86395	5428	3E	0	0	2E	3E	1	1E	1984	31
1983	117	1983	117	11	1983	117	86395	5165	3E	0	0	2E	3E	1	1E	1984	31
1983	118	1983	118	11	1983	119	571	5369	3E	0	0	2E	3E	1	1E	1984	31
1983	120	1983	120	3163	1983	120	86395	5144	3E	0	0	3E	3E	0E	1	1984	31
1983	121	1983	121	11	1983	121	86395	5327	3E	0	0	3E	3E	0E	1	1984	31
1983	122	1983	122	11	1983	122	85179	5268	3E	0	0	3E	3E	0E	1	1984	31
1983	124	1983	124	1339	1983	124	86395	5211	3E	0	0	1E	3E	1	0E	1984	32
1983	125	1983	125	11	1983	125	86395	5289	3E	0	0	1E	3E	1	0E	1984	32
1983	126	1983	126	11	1983	127	12571	6093	3E	0	0	1E	3E	1	0E	1984	32
1983	128	1983	127	85915	1983	128	86395	5327	3E	0	0	3E	3E	1E	1	1984	32
1983	129	1983	129	11	1983	129	86395	5034	3E	0	0	3E	3E	1E	1	1984	32
1983	130	1983	130	11	1983	131	1515	5453	3E	0	0	3E	3E	1E	1	1984	32
1983	132	1983	132	3931	1983	132	86395	5094	3E	0	0	2E	3E	1	1E	1984	33
1983	133	1983	133	11	1983	133	86395	5279	3E	0	0	2E	3E	1	1E	1984	33
1983	134	1983	134	11	1983	134	85867	5303	3E	0	0	2E	3E	1	1E	1984	33
1983	136	1983	136	2091	1983	136	86395	5189	3E	0	0	3E	3E	1E	1	1984	33
1983	137	1983	137	11	1983	137	86395	5340	3E	0	0	3E	3E	1E	1	1984	33
1983	138	1983	138	11	1983	138	84075	5220	3E	0	0	3E	3E	1E	1	1984	33
1983	140	1983	140	12763	1983	140	86395	4543	2E	1E	0	3E	3E	1	1E	1984	39
1983	141	1983	141	11	1983	141	86395	5357	2E	1E	0	3E	3E	1	1E	1984	39
1983	142	1983	142	11	1983	143	1083	5411	2E	1E	0	3E	3E	1	1E	1984	39
1983	144	1983	144	4683	1983	144	86395	5059	3E	0	0	3E	3E	1E	1	1984	39
1983	145	1983	145	11	1983	145	86395	5301	3E	0	0	3E	3E	1E	1	1984	39
1983	146	1983	146	11	1983	147	251	5346	3E	0	0	3E	3E	1E	1	1984	39
1983	148	1983	148	9099	1983	148	86395	4774	3E	0	0	2E	3E	1	1E	1984	40
1983	149	1983	149	11	1983	149	86395	4925	3E	0	0	2E	3E	1	1E	1984	40
1983	150	1983	150	11	1983	150	84859	5208	3E	0	0	2E	3E	1	1E	1984	40
1983	152	1983	152	1019	1983	152	86395	5264	3E	0	0	3E	3E	0E	1	1984	40
1983	153	1983	153	11	1983	153	86395	5332	3E	0	0	3E	3E	0E	1	1984	40
1983	154	1983	154	11	1983	155	6059	5694	3E	0	0	3E	3E	0E	1	1984	40
1983	156	1983	156	11691	1983	156	86395	4557	3E	0	0	1E	3E	1	0E	1984	41
1983	157	1983	157	11	1983	157	86395	4983	3E	0	0	1E	3E	1	0E	1984	41
1983	158	1983	158	11	1983	158	85547	5210	3E	0	0	1E	3E	1	0E	1984	41
1983	160	1983	160	9867	1983	161	16315	5722	3E	0	0	3E	3E	1E	1	1984	41

SECTION 6

DATA FORMATS

6.1 Format of SAMS Gridded Retrieved Temperature Tapes (GRID-T)

Overall Structure

SAMS GRID-T tapes contain latitude-longitude grids of temperature retrievals as a function of pressure, averaged over northbound and southbound orbits. Zonal mean and climatology values are given. Error bars are also included for some grids.

The data are written on 9-track, half-inch wide magnetic tapes at 6250 bpi. Tapes contain one or more files separated by an end of file mark and are terminated by a double end of file mark. The first file on a tape is a header file consisting of two 630-byte physical records written in EBCDIC. These two records are identical and serve to identify the data type (temperature or composition), data start and end dates, generation date, and software version. The overall file structure is shown in Figure 6-1.

Data files are divided into records, each giving a convenient set of results such as an entire grid or a set of profiles. There is one record per physical tape block. Record lengths (hence block lengths) vary according to the type of data they contain. The maximum block length (for a type 7402 record) is 4882 bytes.

All data are written as 16-bit, twos complement integers (CDC users beware: CDC integers are ones complement). Hence, one word occupies exactly 2 bytes.

The byte ordering within words follows the IBM convention of most significant byte first; note that is the reverse of some machines, (e.g., DEC, which puts the least significant byte first).

Each physical block has the following structure:

Word 1	Length of record in bytes (=2N where N is record length in words).
Word 2	Record serial number (this does not always increment by 1).
Word 3	Record type identifier (uniquely defines format of remainder of record).
Word 4 to N-1	Data section of record.
Word N	Least significant byte is the checksum of words 3 to N-1.
Word N+1	Zero.

Hence, the total length of a physical block is two bytes larger than the record length, i.e., 2N+2 bytes, except for record type 7400, which has a record length of 22 bytes and a block length of 40 bytes. The checksum (the low-order byte of word N of the physical record) is the least significant 8 bits of the sum of bytes of words 3 to N-1; i.e., checksum is between 0 and 255, it is put into byte 2N, and it is the sum of bytes 5 to 2N-2. Note that byte 2N-1 should be ignored.

Example

The following type 7400 block is at the beginning of one of the tapes. It is 12 words (24 bytes) long. Those words in decimal are as follows: 22, 1, 7400, 1, 1979, 281, 7401, 7402, 7403, 0, -13, 0. The bytes (in the order that they are on the tape) are: 0, 22, 0, 1, 28, 232, 0, 1, 7, 187, 1, 25, 28, 233, 28, 234, 28, 235, 0, 0, 255, 243, 0, 0. To verify the checksum we take

$$28+232+0+1+7+1+25+28+234+28+235+0+0=1267;$$
$$1267=4*256+243,$$

so the checksum should be 243, and byte 22, indeed, contains this value.

PRECEDING PAGE BLANK NOT FILMED

PAGE 48 INTENTIONALLY BLANK

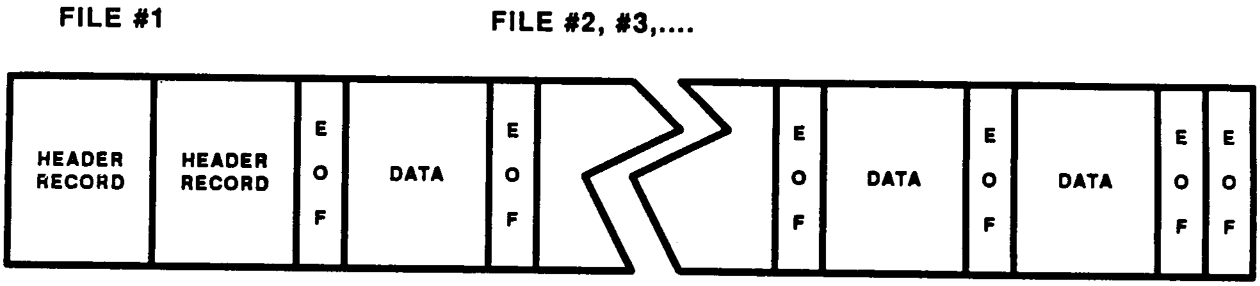

Figure 6-1. Overall structure of SAMS tapes.

Header File Structure

The header file consists of two identical 630-byte physical records that identify a tape as a SAMS product. The format of each of the records is given here. The character "b" indicates a blank, and the character "x" indicates characters that vary from tape to tape.

Characters

bNIMBUS-7bSAMS	(identifies tape as SAMS product)	1 - 14
bXXXXXXXXXXX	(identifies tape type)	15 - 26
bSQbNOb	(sequence number)	27 - 33
XXXXX	(5-digit sequence number)	34 - 38
XX	(redo character and copy number 1 or 2)	39 - 40
bSTARTb19XXbXXX	(data start year and day of year)	41 - 55
bTOb19XXbXXX	(data end year and day of year)	56 - 67
bGENb19XXbXXXbXXXXXX	(year, day of year, and hours, minutes, seconds tape was generated	68 - 87
bPROGRAMbSAMSbXXXXXXXX	(SAMS software version name)	88 - 109
bXX/XX/XX	(software version month, day, year)	110-118
bb.....b	(blanks to fill out the record)	119-630

The following is an example of a SAMS temperature tape header record.

Example

A SAMS temperature tape starting in December 1978 and ending in December 1979 was generated on December 27, 1984 at 19:10:15 using software version VERVS02A.

bNIMBUS-7bSAMSbTEMPERATUREbSQbNOb83581-2bSTARTb1978b358bTOb1979b365bGENb1984b
362b191015bPROGRAMbSAMSbVERVS02Ab12/24/84
followed by 512 blanks.

The SAMS header record tape type, sequence number, redo character, and copy number fields are explained here. The tape type can be one of two values and starts with character 16.

CHARACTERS 16 - 26: This field distinguishes the type of SAMS tapes. TEMPERATURE identifies a tape as a Gridded Retrieved Temperature Tape. COMPOSITION identifies a tape as a Zonal Mean Methane and Nitrous Oxide Composition tape.

The sequence number consists of five digits and starts with character 34 of the record.

CHARACTER 34: The last digit of the year in which data were acquired.

CHARACTERS 35 - 37:	Day of the year on which data were acquired.
CHARACTER 38:	Value is 1 unless necessary to remove ambiguities in the year (character 34), as may occur if data are acquired on or after December 24, 1988.
CHARACTER 39:	Redo character. It will remain as a hyphen unless there is a remake of the tape. In this case, an ascending alpha character will replace the hyphen.
CHARACTER 40:	Tape copy number. The original tape will have a value of 1; the archived copy will have a value of 2.

Data File Structure

GRID-T tape data files have the following types of records:

a) File header record (type 7400).

b) Data records (type 7402 or 7403).

c) End of file mark.

Table 6-1 shows the data file structure.

There is one file per "data day" of data. A "data day" is a period when the instrument is in just one operating mode. Mode changes generally occur near midnight, in which case one data day corresponds to a calendar day. However, this is not always the case and sometimes there will be more than one data day in one calendar day.

Format of File Header Record

Table 6-2 shows the structure of file header records.

Format of latitude-longitude-ln(pressure) retrieved temperatures, block type 7402

This grid contains temperature averaged over day and night at 62 pressure levels. The error bars are not given in this format, but can be obtained for fewer levels (which should be adequate) from 7403 blocks. Table 6-3 shows the block type 7402 format. Detailed comments on selected words follow:

Word	Description
8 + 64(n-1)	Latitude of grid point in degrees N*100 (-5000 to 6750).
9 + 64(n-1)	Longitude of grid point in degrees E*100 (-18000 to 20000) (19000 and 20000 indicate zonal mean and climatological first guess).
10 + 64(n-1) to 71 + 64 (n-1)	Temperature profile; 62 values in K*100 starting at $\ln(p_0/p) = 1.4$, up every 0.2 in $\ln(p_0/p)$ up to 13.6 (p_0=1000).

The value of n ranges from 1 to 38 for each record. There are 64 words for each value of n: latitude, longitude, and temperature for n=1 are for 180°W, those for n=2 are for 170°W, and continuing at 10° intervals to 170°E for n=36. The last two groups of 64 words contain zonal means (n=37) and climatology (n=38). The first record in a type 7402 block contains data for latitude 50°S, the second contains data for 47.5°S, the following records are spaced at 2.5° intervals, and the last record contains data for 67.5°N.

Table 6-1

GRID-T Temperature Tape Data File Structure

Record #		
1	Type 7400	Header Record
2	Type 7402	Retrieved Temperature Grid at - 50.0N
3	Type 7402	Retrieved Temperature Grid at - 47.5N
		⋮
49	Type 7402	Retrieved Temperature Grid at + 67.5N
50	Type 7403	Temperature Grid at Level 2303
51	Type 7403	Error Bars at Level 2303
52	Type 7403	Temperature Grid at Level 3507
53	Type 7403	Error Bars at Level 3507
⋮		⋮
68	Type 7403	Temperature Grid at Level 12717
69	Type 7403	Error Bars at Level 12717
	EOF	

NOTE: Not all these records will necessarily be present.

Table 6-2

GRID-T Temperature Tape Data File Header Record Format

16-Bit Word #	MSB 16	LSB 1
1	Record length	(22 bytes)
2	Serial number	
3	Record type 7400	
4	Data file number	
5	Data year	
6	Data day	
7	7401	
8	7402	
9	7403	
10	Zero fill	
11		Checksum
12-20	Zero fill	

Table 6-3

GRID-T Temperature Tape Latitude-Longitude-1n (Pressure) Record Format Type 7402

16-Bit Word #	MSB 16		LSB 1
1	Record length	4880 bytes	
2	Serial number		
3	Record type 7402		
4	Data day		
5	Data year		
6	Processing day		
7	Processing year		
8	Grid point latitude (degrees *100)		
9	Grid point longitude (degrees *100)		-180 E
10	Temperature (degrees K *100) for 62 pressure levels		
⋮			
71			
72	Grid point latitude degrees *100		
73	Grid point longitude degrees *100		-170 E

Table 6-3

GRID-T Temperature Tape Latitude-Longitude-1n (Pressure) Record Format Type 7402 (continued)

16-Bit Word #	MSB 16	LSB 1
74	Temperature degrees K *100 for 62 pressure levels	
⋮		
135		
136 ⋮	⋮	
2248	Grid point latitude degrees *100	
2249	Grid point longitude degrees *100	+170 E
2250 ⋮	Temperature degrees K *100 for 62 pressure levels	
2311		
2312	Grid point latitude degrees *100	
2313	Grid point longitude degrees *100	+190 E
2314 ⋮	Zonal mean	
2375		

Table 6-3

GRID-T Temperature Tape Latitude-Longitude-1n (Pressure) Record Format Type 7402 (continued)

16-Bit Word #	MSB 16		LSB 1
2376	Grid point latitude degrees *100		
2377	Grid point longitude degrees *100		+200 E
2378	Climatology, i.e., first guess profile		
⋮	⋮		
2439			
2440		Checksum	
2441	Zero fill		

Table 6-4

Grid-T Temperature Tape Latitude-Longitude Grid Record Format Type 7403

16-Bit Word #	MSB 16	LSB 1
1	Record length	3504 bytes
2	Serial number	
3	Record type 7403	
4	Measurement type	(3)
5	Data day	
6	Data year	
7	Processing day	
8	Processing year	
9	Ignore	
10	Scale factor	(divide by this integer)
11	Data type 2 or 102	
12	Pressure level	
13	Ignore	
14	Ignore	
15	Ignore	

Table 6-4

Grid-T Temperature Tape Latitude-Longitude Grid Record Format Type 7403
(continued)

16-Bit Word #	MSB 16 LSB 1
16 ⋮	Zero fill
23	
24 ⋮	Temperatures or error bars for Word 12 level at -50N, -180 E to+170 E
59	
60 ⋮	Temperatures or error bars for Word 12 level at -47.5N, -180 E to +170 E
95 ⋮	⋮
1680	Temperatures or error bars for Word 12 level at +65N, -180 E to +170 E
1715	
1716	Temperatures or error bars for Word 12 level at +67.5N, -180E to +170 E
1751	
1752	Checksum
1753	Zero fill

The climatology should always contain valid data. Bad or missing data are replaced with a fill value of -32768.

Format of latitude-longitude grid block type 7403

These contain grids that extend from 50°S to 67.5°N (every 2.5°) and 180°W to 170°E (every 10°). Each quantity gridded is put into a separate record, which contains a header and then an array of 16-bit integers. Grids of an item and its error count as separate quantities and accordingly are put into different records (adjacent on the tape). All grids are for the mean of northbound and southbound measurements. Table 6-4 shows the format for type 7403 records. Detailed descriptions of selected words follow. In these descriptions, the quantities in brackets (words 9, 13, 14, 15) should be ignored.

Detailed descriptions of block type 7403 words

Word	Description	
3	7403 identifier.	
4	1, 2, or 3 meaning northbound orbits, southbound orbits or combined average (only type 3 present on these tapes).	
5	Day of data.	
6	Year of data.	
9	[address in orbit grid records of quantity gridded].	
10	Scale factor: divide data by this integer.	
11	Data type:	1-eigenfunction coefficient; 2-temperature; 101-error in eigenfunction coefficient; 102-temperature error (only types 2 and 102 present on these tapes).
12	Level:	for type 1 or 101, this is eigenfunction number (1, 2, etc.), for 2 or 102, this is 1000*ln(pressure/p_o) where p_o is 1000 mb.
13	[Format/version number of CAL, RETRIEVE programs, etc.].	
14	[Format/version number of OGRID program].	
15	[Format/version number of LGRID program].	
16-23	Spares, set to 0.	
24-23+36*48	Data array A dimensioned (36,48) in order A(1,1), A(2,1), A(3,1)....A(36,48). -32768 means no information. A(1,1) is for (50°S, 180°W), A(2,1) is (50°S, 170°W),etc.; A(I,J) is for (J-21)*2.5°N, (I-19)*10°E.	

Temperatures are given at the following pressures in mbar (figures in parentheses are the corresponding values of word 12): 100 (2303), 30 (3507), 10 (4605), 3 (5809), 1 (6908), 0.3 (8112), 0.1 (9210), 0.03 (10414), 0.01 (11513), 0.003 (12717).

At the very top pressure levels, the values are primarily climatology. Significant measurements extend up to about 0.03 mb to 0.01 mb (70 to 80 km).

6.2 Format of SAMS Zonal Mean Methane and Nitrous Oxide Composition Tape (ZMT-G)

Overall Structure

The ZMT-G tape contains zonal mean values of nitrous-oxide and methane retrievals and errors expressed as a function of pressure and averaged over 24-hour periods.

The data are written on 9-track, half-inch wide magnetic tapes at 6250 bpi. Tapes contain one or more data files and are terminated by a double end of file mark. Like the SAMS temperature tape, the SAMS composition tape has a tape header file as the first file on the tape. It contains two identical 630-byte physical records written in EBCDIC. The description of header records in Section 6.1 applies to the ZMT-G tapes, as well as to the temperature tapes.

Data files are divided into records, each giving values for 1 day. There is one record per physical tape block. Refer to Table 6-5 for the ZMT-G tape file structure.

All data are written as 16-bit twos complement integers (CDC users beware: CDC integers are ones complement). Hence, one word occupies exactly 2 bytes.

The byte ordering within words follows the IBM convention of most significant byte first; note that is the reverse of some machines, (e.g., DEC, which puts the least significant byte first).

Each physical block has the following structure:

Word 1	Length of record in bytes (=2N where N is record length in words) (2N=5986 in this case).
Word 2	Record serial number.
Word 3	Record type identifier (uniquely defines format of remainder of record) (7405 or 7406 in this case).
Word 4 to N-2	Data section of record.
Word N-1	Least significant byte is the checksum of words 3 to N-2.
Word N	Zero.

Hence, the total length of a physical block is 2N bytes, the same as the record length.

The checksum (the low-order byte of word N-1 of the physical record) is the least significant 8 bits of the sum of bytes of words 3 to N-2; i.e., the checksum is between 0 and 255, it is put into byte 2N-2, and is the sum of bytes 5 to 2N-4. Note that byte 2N-3 should be ignored. An example of checksum computation is given in the description of the overall structure of the temperature tape.

Format of latitude-ln(pressure) zonal mean composition blocks 7405 and 7406

This grid contains zonal 24-hour average (day and night) mean mixing ratios of methane and nitrous oxide at 31 pressure levels. The SAMS cannot measure methane and nitrous oxide simultaneously. Consequently, measurements of only one of the above gases are made during each 24-hour period. Table 6-6 gives the format of block types 7405 and 7406.

Detailed descriptions of selected words follow:

Word	Description
3	Identifier (7405-nitrous oxide; 7406-methane).
6	Enabled channel (8-nitrous oxide; 9-methane).
7	Sieve setting of enabled PMC.
8	Sieve setting of clamped PMC.
9	Sieve setting of A1 PMC (temperature sounding).
10	Sieve setting of channel C1 PMC (temperature sounding).
11	Creation date (day).
12	Creation date (year).
13	Number of elements in each profile.
14	Bottom level ($\ln(P_0/P)*10$).
15	Top level (units as word 14).
15 + 31 (n-1) to 45 + 62 (n-1)	Mixing ratio profile: 31 values (in ppbv*50 for nitrous oxide or ppmv*10000 for methane), starting at $\ln(P_0/P)$= 3.0, every 0.2 in $\ln(P_0/P)$ up to 9.0 (P_0=1013.25 mb); n varies from 1 to 48; n=1 corresponds to 50°S, n=2 to 47.5°S, continuing at 2.5°intervals to 67.5°N for n=31.

Bad or missing data are set to -32768 (note that in 16 bit twos complement arithmetic -32768=32767+1=32768, although +32768 is generally taken to be an invalid number).

There is one block per "data day" of data. A "data day" is a period when the instrument is in just one operating mode. Mode changes generally occur near midnight, in which case one data day corresponds to a calendar day. However, this is not always the case and sometimes there will be more than one data day in one calendar day.

Table 6-5

ZMT-G Composition Tape Data File Structure

Record #	
1	Nitrous oxide (7405) or methane (7406) for one data day
2	Nitrous oxide (7405) or methane (7406) for one data day
3	Nitrous oxide (7405) or methane (7406) for one data day
⋮	⋮
N-1	Nitrous oxide (7405) or methane (7406) for one data day
N	Nitrous oxide (7405) or methane (7406) for one data day
	End of file mark

Table 6-6

ZMT-G Composition Tape Latitude-In (Pressure) Zonal Mean Record Format Types 7405 and 7406

16-Bit Word #	MSB 16 ... LSB 1
1	Record length
2	Serial number
3	Record type: 7405 or 7406
4	Data day
5	Data year
6	Enabled channel
7	Sieve setting enabled PMC
8	Sieve setting clamped PMC
9	Sieve setting A1 PMC
10	Sieve setting C1 PMC
11	Processing day
12	Processing year
13	Number of elements in profile
14	Bottom level

Table 6-6

ZMT-G Composition Tape Latitude-In (Pressure) Zonal Mean Record Format Types 7405 and 7406 (continued)

16-Bit Word #	MSB 16 — LSB 1
15	Top level
16 ⋮	Retrieved mixing ratio at - 50N 31 values
46	
47 ⋮	Retrieved mixing ratio at - 47.5N 31 values
77 ⋮	⋮
1442 ⋮	Retrieved mixing ratio at + 65N 31 values
1447	
1473 ⋮	Retrieved mixing ratio at +67.5N 31 values
1503	

Table 6-6

ZMT-G Composition Tape Latitude-ln (Pressure) Zonal Mean Record Format Types 7405 and 7406 (continued)

16-Bit Word #	MSB 16	LSB 1
1504 ⋮	Mixing ratio errors at - 50N 31 values	
1534		
1535 ⋮	Mixing ratio errors at -47.5N 31 values	
1565 ⋮	⋮	
2930 ⋮	Mixing ratio errors at + 65 N 31 values	
2960		
2961 ⋮	Mixing ratio errors at + 67.5N 31 values	
2991		
2992		Checksum
2993	Zero fill	

REFERENCES

Barnett, J. J., and M. Corney, Temperature comparisons between the Nimbus 7 SAMS, rocket/radiosondes, and the NOAA 6 SSU, *J. Geophys. Res., 89*, 5294-5302, 1984.

Barnett, J. J., M. Corney, A. K. Murphy, R. L. Jones, C. D. Rodgers, F. W. Taylor, E. J. Williamson, and N. M. Vyas, Global and seasonal variability of the temperature and composition of the middle atmosphere, *Nature, 313*, 439-443, 1985.

Chaloner, C. P., Ph.D. Thesis, University of Oxford, 1976.

Chaloner, C. P., J. R. Drummond, J. T. Houghton, R. F. Jarnot and H. K. Roscoe, Infrared measurements of stratospheric composition I. The balloon and water vapour measurements, *Proc. R. Soc. Lond., A364*, 145-159, 1978.

Curtis, P. D., J. T. Houghton, G. D. Peskett, and C. D. Rodgers, Remote sounding of atmospheric temperature from satellites V. The pressure modulator radiometer for Nimbus F, *Proc. R. Soc. Lond., A337*, 135-150, 1974.

Drummond, J. R., J. T. Houghton, G. D. Peskett, C. D. Rodgers., M. J. Wale, J. Whitney, and E. J. Williamson, The stratospheric and mesospheric sounder on Nimbus 7, *Phil. Trans. R. Soc. Lond., A296*, 219-241, 1980.

Drummond, J. R., J. T. Houghton, G. D. Peskett, C. D. Rodgers, M. J. Wale, J. Whitney, and E. J. Williamson, in *The Nimbus-7 User's Guide*, edited by C. R. Madrid, pp. 139-174, Goddard Space Flight Center, Greenbelt, MD, 1978.

Drummond, J. R. and R. F. Jarnot, Infrared measurements of stratospheric composition II. Simultaneous NO and NO_2 measurements, *Proc. R. Soc. Lond., A364*, 237-254, 1978.

Ellis, P. J., G. Holah, J. T. Houghton, T. S. Jones, G. Peckham, G. D. Peskett, D. R. Pick, C. D. Rodgers, H. K. Roscoe, R. Sandwell, S. D. Smith, and E. J. Williamson, Remote sounding of atmospheric temperature from satellites IV. The selective chopper radiometer for Nimbus 5, *Proc. R. Soc. Lond., A334*, 149-170, 1973.

Eyre, J. R., Ph.D. Thesis, University of Oxford, 1978.

Gille, J. C., P. Baily, F. B. House, R. A. Craig, and J. R. Thomas, *The Nimbus-6 User's Guide*, Goddard Space Flight Center, Greenbelt, MD, 1975.

Grose, W. L. and C. D. Rodgers (Eds.), Coordinated study of the behavior of the middle atmosphere in winter: monthly mean comparisons of satellite and radiosonde data and derived quantities, in *Handbook for MAP, Volume 21*, pp. 79-111, edited by C. F. Sechrist, Jr., Urbana, IL, 1986.

Houghton, J. T. and S. D. Smith, Remote sounding of atmospheric temperature from satellites I. Introduction, *Proc. R. Soc. Lond., A320*, 23-33, 1970.

Houghton, J. T. and F. W. Taylor, Remote sounding of artificial satellites and space probes of the atmospheres of the Earth and planets, *Rep. Prog. Phys., 36*, 827-919, 1973.

Houghton, J. T., F. W. Taylor, and C. D. Rodgers, *Remote Sounding of Atmospheres*, Cambridge University Press, 1984.

Jones, R. L. and J. A. Pyle, Observation of CH_4 and N_2O by the NIMBUS-7 SAMS: Comparison with in situ data and two-dimensional numerical model calculations, *J. Geophys. Res.*, *89*, 5263-5279, 1984.

McClatchey, R. A., W. S. Benedict, S. A. Clough, D. E. Burch, and R. F. Calfee, A. F. C. R. L. atmospheric absorption line parameters compilation, AFCRL-TR-73-0096, *Environmental Research*, 1973.

McConnell, J. C., M. B. McElroy, and S. C. Wofsy, Natural sources of atmospheric CO, *Nature*, *233*, 187-188, 1971.

Murray, A. E., Fast refractive infrared and optical systems, *Infrared Phys.*, *2*, 37-47, 1962.

Rodgers, C. D., Retrieval of atmospheric temperature and composition from remote measurements of thermal radiation, *Rev. Geophys. Space Phys.*, *14*, 609-624, 1976.

Rodgers, C. D. (Ed.), Handbook for MAP, Volume 12, 1984*a*.

Rodgers, C. D., Workshops on comparison of data and derived dynamical quantities during Northern Hemisphere winters, *Adv. Space Res.*, Vol. 4, No. 6, pp. 117-125, 1984*b*.

Rodgers, C. D., R. L. Jones, and J. J. Barnett, Retrieval of temperature and composition from NIMBUS-7 SAMS measurements, *J. Geophys. Res.*, 89, 5280-5286, 1984.

Taylor, F. W., Pressure modulator radiometry, *Spectrom. Tech.*, *3*, 137-197, 1983.

Taylor, F. W., J. T. Houghton, G. D. Peskett, C. D. Rodgers, and E. J. Williamson, Radiometer for remote sounding of the upper atmosphere, *Appl. Opt.*, *11*, 135-141, 1972.

Wale, M. J. and G. D. Peskett, Some aspects of the design and behavior of the stratospheric and mesospheric sounder, *J. Geophys. Res.*, *89*, 5287-5293, 1984.

LIST OF ACRONYMS, INITIALS, AND ABBREVIATIONS

A/D	Analog/digital
bpi	Bits per inch (9-track tapes)
CDC	Control Data Corporation
Composition Tape	SAMS Zonal Mean Methane and Nitrous Oxide Composition Tape. Also known as a Trace Species, Constituent or ZMT-G tape.
DEC	Digital Equipment Corporation
EBCDIC	Extended Binary Coded Decimal Interchange Code
EOF	End of file mark
FOV	Field of view
GRID-T	Gridded Retrieved Temperature Tape
GSFC	Goddard Space Flight Center
IBM	International Business Machines
ILT	Image Location Tape
JCL	Job Control Language
JGR	Journal of Geophysical Research
LIMS	Limb Infrared Monitor of the Stratosphere
LSB	Least Significant Bit
LTE	Local Thermodynamic Equilibrium
MSB	Most Significant Bit
MAP	Middle Atmosphere Program
NASA	National Aeronautics and Space Administration
NET	Nimbus Experiment Team
NSSDC	National Space Science Data Center
PMC	Pressure-modulated Channel
PM	Pressure-modulated
PSD	Phase Sensitive Detector

PM Signal	Pressure Modulated Signal (the PM and WB signals are the two radiation components measured by each of the SAMS detectors)
PMR	Pressure Modulator Radiometer
QL	Quick look
SAMS	Stratospheric and Mesospheric Sounder
S/N	Signal-to-Noise
SCOSTEP	Scientific Committee on Solar-Terrestrial Physics
SCR	Selective Chopper Radiometer
STX	ST Systems Corporation
Temperature Tape	A SAMS Gridded Retrieved Temperature Tape (GRID-T)
TGS	Triglycine sulfate
WB	Wideband
WB Signal	Wideband Signal
ZMT-G	Zonal Means Tape - Gas. Same as a Composition Tape

APPENDIX A

SEQUENCE NUMBERS OF SAMS DATA TAPES

This table shows the sequence numbers and start and end dates of SAMS temperature and composition tapes that are archived at the NSSDC. The file column includes tape header and data files.

Type	Sequence	Start	End	Files
Temperature	83581-2	1078/358	1979/365	273
Temperature	00011-2	1980/001	1980/366	273
Temperature	10021-2	1981/002	1981/364	273
Temperature	20021-2	1982/002	1983/160	298
Composition	90011-2	1979/001	1981/364	2

APPENDIX B

FORTRAN SOURCE LISTING OF SAMS TAPE DUMP

This appendix contains the FORTRAN source listing of a program that will enable the user to produce formatted dumps of retrieved temperature data, and methane and nitrous oxide mixing ratios on SAMS GRID-T and ZMT-G tapes, respectively. Figure B-1 is a hierarchy chart showing the relation between dump program modules. The program is written in VS FORTRAN for use on an IBM 3081 system operating under MVS.

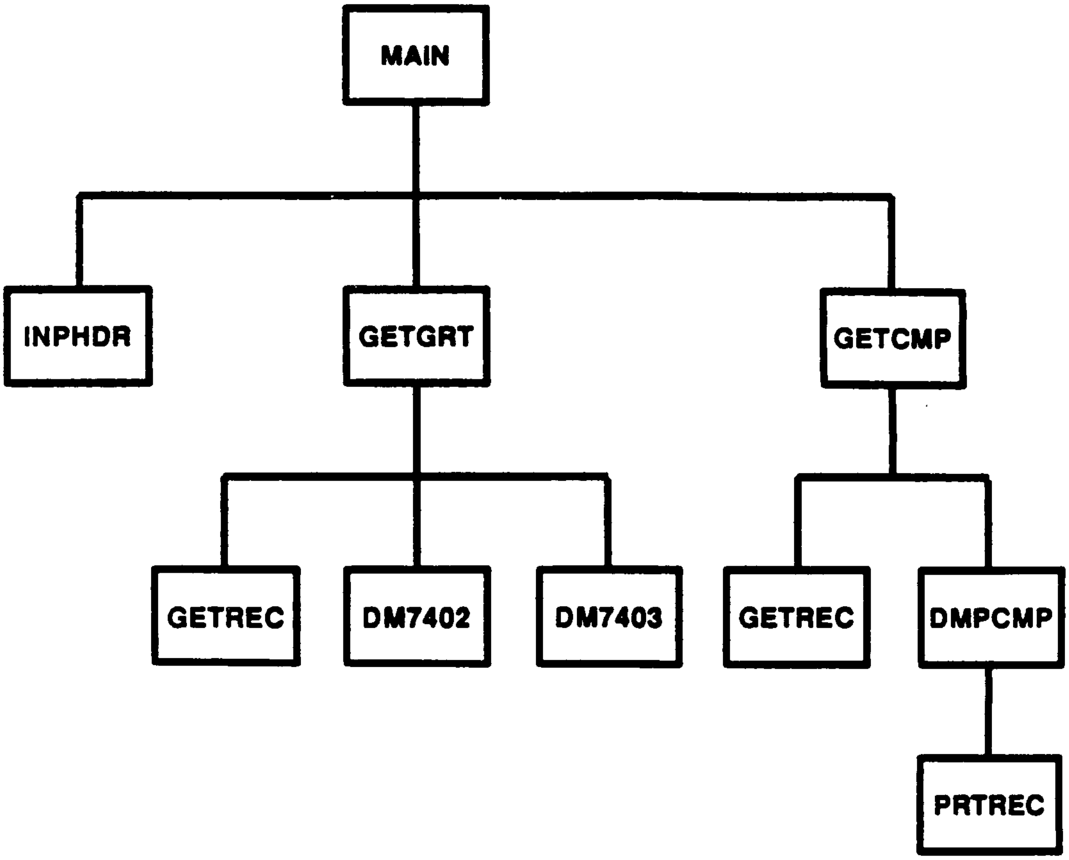

B-1. Hierararchy Chart for SAMS tape dump program.

APPENDIX B

```
*....*...1.........2.........3.........4.........5.........6.........7.*.......8

C***********************************************************************
C PROGRAM - MAIN
C
C PURPOSE - THIS PROGRAM GENERATES A FORMATTED DUMP OF A SAMS GRIDDED
C   RETRIEVED TEMPERATURE TAPE (GRID-T) OR A SAMS ZONAL MEAN METHANE
C   AND NITROUS-OXIDE COMPOSITION TAPE (ZMT-G). THE BYTE ORDERING
C   WITHIN THE 16-BIT WORDS MUST FOLLOW THE IBM CONVENTION.
C
C   <<< WARNING >>> LARGE VOLUMES OF PRINTOUT ARE GENERATED BY DUMPING
C   SAMS TAPES UNLESS DUMPING IS RESTRICTED BY CAREFULLY USING THE
C   DUMP DATES AND DUMP OPTIONS.
C
C   THE PROGRAM READS ONE INPUT CARD WHICH DEFINES THE TAPE VOLSER,
C   DUMP START AND STOP DATES, AND EIGHT DUMP OPTIONS. THE DATES
C   HAVE FORMAT YYDDD WHERE YY ARE THE TWO LOW ORDER DIGITS OF THE YEAR
C   AND DDD IS THE DAY OF YEAR. THE EIGHT DUMP OPTIONS CORRESPOND TO
C   DIFFERENT RECORD TYPES: 7400, 7402, 7403 TEMPERATURE GRID,
C   7403 TEMPERATURE GRID ERRORS, 7405 N2O MIXING RATIOS, 7405 N2O
C   MIXING RATIO ERRORS, 7406 CH4 MIXING RATIOS, 7406 CH4 MIXING RATIO
C   ERRORS. OPTIONS CAN HAVE ONE OF TWO VALUES, 0 FOR NO DUMP,
C   1 FOR DUMP.
C
C   A TYPICAL INPUT CARD WITH THE TAPE VOLSER NUMBER STARTING IN
C   COLUMN ONE WOULD APPEAR AS FOLLOWS:
C     TAP001 79358 80004 0 0 0 0 1 0 1 0
C   THIS WOULD CAUSE THE CH4 AND N2O MIXING RATIOS FOR DAY 358 1979
C   TO DAY 004 1980 TO BE DUMPED.
C
C   THE PROGRAM DETERMINES WHAT TYPE OF TAPE IS BEING PROCESSED:
C   EITHER A GRIDDED RETRIEVED TEMPERATURE TAPE OR AN CH4/N2O ZONAL
C   MEAN TAPE. IT SEARCHES A TAPE FOR RECORDS THAT ARE WITHIN THE
C   START AND STOP DATES GIVEN ON THE INPUT CARD, AND DUMPS RECORDS
C   FOR WHICH OPTIONS ARE SET TO 1.
C
C   THE START AND STOP DATES MUST BE ON OR AFTER 78297 (THE SATELLITE
C   LAUNCH DATE, DAY 297 1978). THE STOP DATE MUST NOT BE LESS THAN
C   THE START DATE, AND MUST NOT BE GREATER THAN 99365, DAY 365
C   (DEC. 31) 1999.
C
C LANGUAGE - VS FORTRAN
C
C COMPUTER - IBM 3081 MVS
C
C DATA SETS -
C   FT05F001 - INPUT DATA CARD
C   FT06F001 - HARDCOPY PRINTOUT
C   FT10F001 - INPUT SAMS TAPE
C
C SUBPROGRAM DEFINITIONS -
C   INPHDR = READ AND CHECK INPUTS, MOUNT TAPE, CHECK HEADER
C   GETGRT = READ RECORDS FROM A TEMPERATURE TAPE
C   GETCMP = READ RECORDS FROM A COMPOSITION TAPE
C   DM7402 = DUMP TYPE 7402 RECORD
C   DM7403 = DUMP TYPE 7403 RECORD (GRID AND GRID ERRORS)
C   DMPCMP = DETERMINE WHICH PART OF TYPE 7405 AND 7406 RECORDS TO DUMP
C   PRTREC = DUMP TYPE 7405 AND 7406 RECORDS
C   GETREC = READ RECORDS FROM SAMS TAPE
C
C LIBRARY SUBPROGRAM DEFINITIONS -
C   MOUNT  = FTIO MOUNT A TAPE (FTIO = FORTRAN INPUT/OUTPUT PACKAGE)
C   POSN   = FTIO POSITION TAPE TO A FILE
C   FREAD  = FTIO READ TAPE RECORDS
C   KCLC   = PERFORMS LOGICAL COMPARISON OF BYTES
C   FMOVE  = STORAGE-TO-STORAGE MOVEMENT OF BYTES
C   ZTIME  = GETS CURRENT DATE AND TIME
C
C SUBROUTINES CALLED - ZTIME,INPHDR,GETGRT,GETCMP
C
C PROGRAMMER - TOM NUTTER 03/05/85 SASC TECHNOLOGIES, INC.
C***********************************************************************
```

```
                 *....*...1.........2.........3.........4.........5.........6.........7.*.......8

ISN      1             CHARACTER*8 VRNAME,VRDATE
ISN      2             CHARACTER*1 RUNDAT(28)
ISN      3             INTEGER TAPTYP,ISTART,ISTOP,FILNUM,OPTION(8),IRETN
ISN      4             DATA TAPTYP/0/,IRETN/0/,VRNAME/'SAMDMP1A'/,VRDATE/'03/15/85'/,
                      FILNUM/1/,OPTION/8*0/,ISTART,ISTOP/2*-99999/
                 C*** GET RUN DATE AND TIME, PRINT JOB HEADING AND VERSION NAME
ISN      5             CALL ZTIME(RUNDAT,3)
ISN      6             WRITE(6,5010) VRNAME,VRDATE,RUNDAT
                 C*** READ AND CHECK CARD INPUTS, MOUNT TAPE, CHECK TAPE HEADER,
                 C*** DETERMINE TAPE TYPE
ISN      7             CALL INPHDR(TAPTYP,ISTART,ISTOP,FILNUM,OPTION,IRETN)
ISN      8             IF (IRETN.GT.0) THEN
ISN      9                WRITE(6,5020) IRETN
ISN     10                STOP 999
ISN     11             ENDIF
                 C*** DUMP A TEMPERATURE TAPE OR A COMPOSITION TAPE
ISN     12             IF (TAPTYP.EQ.1) THEN
ISN     13                CALL GETGRT(ISTART,ISTOP,FILNUM,OPTION,IRETN)
ISN     14                IF (IRETN.GT.0) THEN
ISN     15                   WRITE(6,5030) IRETN
ISN     16                   STOP 999
ISN     17                ENDIF
ISN     18             ELSE
ISN     19                CALL GETCMP(ISTART,ISTOP,FILNUM,OPTION,IRETN)
ISN     20                IF (IRETN.GT.0) THEN
ISN     21                   WRITE(6,5040) IRETN
ISN     22                   STOP 999
ISN     23                ENDIF
ISN     24             ENDIF
                 C*** PRINT JOB COMPLETION MESSAGE
ISN     25             WRITE(6,5050)
ISN     26             STOP
ISN     27       5010  FORMAT(//1X,5('<'),' NIMBUS-7 SAMS TAPE DUMP PROGRAM ',
                 .        5('>')/' PROGRAM VERSION: ',A8,5X,'DATE LAST MODIFIED: ',A8
                 .        /' RUN DATE ',28A1//)
ISN     28       5020  FORMAT(/' *** MAIN *** ERROR CODE OF ',I3,' RETURNED FROM ',
                 .        '"INPHDR" -- ABORT RUN.'/)
ISN     29       5030  FORMAT(/' *** MAIN *** ERROR CODE OF ',I3,' RETURNED FROM ',
                 .        '"GETGRT" -- ABORT RUN.'/)
ISN     30       5040  FORMAT(/' *** MAIN *** ERROR CODE OF ',I3,' RETURNED FROM ',
                 .        '"GETCMP" -- ABORT RUN.'/)
ISN     31       5050  FORMAT(//' END OF DUMP')
ISN     32             END
```

APPENDIX B

```
                  *....*...1.........2.........3.........4.........5.........6.........7.*.......8
ISN     1               SUBROUTINE INPHOR(TAPTYP,ISTART,ISTOP,FILNUM,OPTION,IRETN)
                  C***********************************************************************
                  C SUBROUTINE - INPHOR
                  C
                  C PURPOSE - READ AND ECHO PRINT CARD INPUT, CHECK INPUT VALUES, MOUNT
                  C   TAPE AND CHECK TAPE HEADER, AND DETERMINE TAPE TYPE.
                  C
                  C ARGUMENTS PASSED -
                  C   TAPTYP = TAPE TYPE (1=TEMPERATURE TAPE, 2=CH4-N2O ZONAL MEAN)
                  C   ISTART = START YEAR, DAY OF YEAR (YYDDD) OF DATA TO BE DUMPED
                  C   ISTOP  = STOP YEAR, DAY OF YEAR (YYDDD) OF DATA TO BE DUMPED
                  C   FILNUM = TAPE FILE NUMBER
                  C   OPTION = DUMP OPTIONS FROM INPUT CARD (1=DUMP, 0=NO DUMP)
                  C   IRETN  = ERROR RETURN CODE (IRETN=0 NO ERROR, >0 ERROR)
                  C
                  C SUBPROGRAMS CALLED - MOUNT,FREAD,KCLC
                  C
                  C CALLED BY - MAIN
                  C
                  C PROGRAMMER - TOM NUTTER 03/05/85
                  C***********************************************************************
ISN     2               INTEGER TAPTYP,ISTART,ISTOP,FILNUM,OPTION(8),IRETN
ISN     3               CHARACTER*1 INLINE(80),HEADER(630)
ISN     4               CHARACTER*4 DUMP
ISN     5               CHARACTER*3 DASH
ISN     6               CHARACTER*6 VOLSER
ISN     7               CHARACTER*11 TEMP,COMP,ACTION(8)
ISN     8               CHARACTER*15 SAMSID
                  C*** INITIALIZE VARIABLES
ISN     9               DATA DASH/'---'/,DUMP/'DUMP'/,HEADER/630*' '/
ISN    10               DATA TEMP/'TEMPERATURE'/,COMP/'COMPOSITION'/
ISN    11               DATA SAMSID/' NIMBUS-7 SAMS '/,ACTION/8*'DO NOT DUMP'/
                  C*** READ AND ECHO PRINT INPUT CARDS
ISN    12               WRITE(6,5010)
ISN    13               READ(5,5020,END=900,ERR=910) INLINE
ISN    14               WRITE(6,5030) INLINE
ISN    15               REWIND 5
                  C*** READ INPUTS AGAIN AND CHECK START AND STOP DATES
ISN    16               READ(5,5060,END=900,ERR=910) VOLSER,ISTART,ISTOP,OPTION
ISN    17               IF ((ISTART.LT.78297.OR.ISTOP.LT.78297).OR.(ISTART.GT.ISTOP)) THEN
ISN    18                  IRETN=1
ISN    19                  WRITE(6,5065) ISTART,ISTOP,IRETN
ISN    20                  RETURN
ISN    21               ENDIF
                  C*** CHECK DUMP OPTIONS FOR UNREASONABLE VALUES
ISN    22               DO 200 I=1,8
ISN    23                  IF (OPTION(I).GT.1) THEN
ISN    24                     IRETN=9
ISN    25                     WRITE(6,5070) I,OPTION(I)
ISN    26                  ENDIF
ISN    27         200   CONTINUE
ISN    28               IF (IRETN.GT.0) RETURN
                  C*** MOUNT AND POSITION TAPE TO HEADER FILE, READ AND PRINT HEADER, AND
                  C*** CHECK RECORD LENGTH
ISN    30               CALL MOUNT(1,10,VOLSER,FILNUM)
ISN    31               CALL FREAD(HEADER,10,LENGTH,*920,*930)
ISN    32               WRITE(6,5075) HEADER
ISN    33               IF (LENGTH.NE.630) THEN
ISN    34                  IRETN=2
ISN    35                  WRITE(6,5080) LENGTH,IRETN
ISN    36                  RETURN
ISN    37               ENDIF
                  C*** CHECK IF TAPE IS A SAMS TAPE
ISN    38               IF (KCLC(HEADER,1,SAMSID,1,15).NE.0) THEN
ISN    39                  IRETN=3
ISN    40                  WRITE(6,5090) IRETN
ISN    41                  RETURN
ISN    42               ENDIF
                  C*** DETERMINE WHETHER TAPE IS A TEMPERATURE OR COMPOSITION TAPE, AND
                  C*** PRINT OUT DUMP OPTION TABLE
```

APPENDIX B

```
                *....*...1.........2.........3.........4.........5.........6.........7.*.......8

ISN   43             IYRSTR=ISTART/1000
ISN   44             IDYSTR=ISTART-IYRSTR*1000
ISN   45             IYRSTP=ISTOP/1000
ISN   46             IDYSTP=ISTOP-IYRSTP*1000
ISN   47             DO 300 I=1,8
ISN   48                IF (OPTION(I).EQ.1) ACTION(I)=DUMP
ISN   50       300   CONTINUE
ISN   51             IF (KCLC(HEADER,16,TEMP,1,11).EQ.0) THEN
ISN   52                TAPTYP=1
ISN   53                WRITE(6,5110) TEMP,IDYSTR,IYRSTR,IDYSTP,IYRSTP
ISN   54                WRITE(6,5120) TEMP,(DASH,I=1,7)
ISN   55                WRITE(6,5130) (OPTION(I),ACTION(I),I=1,4)
ISN   56             ELSE
ISN   57                IF (KCLC(HEADER,16,COMP,1,11).EQ.0) THEN
ISN   58                   TAPTYP=2
ISN   59                   WRITE(6,5110) COMP,IDYSTR,IYRSTR,IDYSTP,IYRSTP
ISN   60                   WRITE(6,5120) COMP,(DASH,I=1,7)
ISN   61                   WRITE(6,5140) (OPTION(I),ACTION(I),I=5,8)
ISN   62                ELSE
ISN   63                   IRETN=4
ISN   64                   WRITE(6,5100) IRETN
ISN   65                   RETURN
ISN   66                ENDIF
ISN   67             ENDIF
ISN   68             RETURN
               C*** INPUT CARD END-OF-FILE
ISN   69       900   CONTINUE
ISN   70             IRETN=5
ISN   71             WRITE(6,5050) IRETN
ISN   72             RETURN
               C*** INPUT CARD READ ERROR
ISN   73       910   CONTINUE
ISN   74             IRETN=6
ISN   75             WRITE(6,5040) IRETN
ISN   76             RETURN
               C*** TAPE END-OF-FILE
ISN   77       920   CONTINUE
ISN   78             IRETN=7
ISN   79             WRITE(6,5150) IRETN
ISN   80             RETURN
               C*** TAPE READ ERROR
ISN   81       930   CONTINUE
ISN   82             IRETN=8
ISN   83             WRITE(6,5160) IRETN
ISN   84             RETURN
ISN   85       5010  FORMAT(' INPUT DATA')
ISN   86       5020  FORMAT(80A1)
ISN   87       5030  FORMAT(1X,80A1)
ISN   88       5040  FORMAT(/' *** INPHDR *** READ ERROR ON INPUT DATA CARDS ',
                   .    '-- IRETN= ',I3/)
ISN   89       5050  FORMAT(/' *** INPHDR *** EOF ON INPUT DATA CARDS ',
                   .    '-- IRETN= ',I3/)
ISN   90       5060  FORMAT(A6,1X,2(I5,1X),8(I1,1X))
ISN   91       5065  FORMAT(/' *** INPHDR *** START OR STOP DATES ARE INCORRECT. ',
                   .    'ISTART= ',I8,' ISTOP= ',I8,' IRETN= ',I3/)
ISN   92       5070  FORMAT(/' *** INPHDR *** DUMP OPTION IS NOT VALID. ',
                   .    'OPTION(',I1,')= ',I2)
ISN   93       5075  FORMAT(/' TAPE HEADER RECORD '/5(1X,126A1/))
ISN   94       5080  FORMAT(/' *** INPHDR *** TAPE HEADER RECORD IS NOT 630 BYTES. ',
                   .    'LENGTH= ',I6,' IRETN= ',I3/)
ISN   95       5090  FORMAT(/' *** INPHDR *** TAPE DOES NOT HAVE A SAMS HEADER ',
                   .    'RECORD -- IRETN= ',I3/)
ISN   96       5100  FORMAT(/' *** INPHDR *** TAPE IS NOT A TEMPERATURE OR ',
                   .    'COMPOSITION TAPE -- IRETN= ',I3/)
ISN   97       5110  FORMAT(//' A SAMS ',A11,' TAPE WILL BE DUMPED STARTING WITH ',
                   .    'DAY ',I3,' 19',I2,' AND ENDING WITH DAY ',I3,' 19',I2)
ISN   98       5120  FORMAT(' THE FOLLOWING ',A11,' TAPE DUMP OPTIONS WERE ',
                   .    'SELECTED:'/' RECORD',18X,'DUMP',5X,'ACTION TO'/'  TYPE',
                   .    18X,'OPTION',4X,'BE TAKEN'/1X,2A3,17X,2A3,4X,3A3)
ISN   99       5130  FORMAT(2X,'7400 HEADER RECORDS',6X,I1,6X,A11/
                   .    2X,'7402 RETRIEVED TEMP',6X,I1,6X,A11/
                   .    2X,'7403 TEMP GRID',11X,I1,6X,A11/
                   .    2X,'7403 GRID ERROR',10X,I1,6X,A11)
```

```
                    *....*...1.........2.........3.........4.........5.........6.........7.*.......8
ISN     100    5140  FORMAT( 2X,'7405 N2O MIXING RATIO',4X,I1,6X,A11/                    00001440
                    .   2X,'7405 N2O RATIO ERRORS',4X,I1,6X,A11/                          00001450
                    .   2X,'7406 CH4 MIXING RATIO',4X,I1,6X,A11/                          00001460
                    .   2X,'7406 CH4 RATIO ERRORS',4X,I1,6X,A11)                          00001470
ISN     101    5150  FORMAT(/' *** INPHDR *** UNEXPECTED EOF ON TAPE -- IRETN= ',I3/)     00001480
ISN     102    5160  FORMAT(/' *** INPHDR *** READ ERROR ON TAPE -- IRETN= ',I3/)         00001490
ISN     103          END                                                                00001500
```

APPENDIX B

```
                  *....*...1.........2.........3.........4.........5.........6.........7.*.......8

ISN       1              SUBROUTINE GETGRT(ISTART,ISTOP,FILNUM,OPTION,IRETN)
                  C**********************************************************************
                  C SUBROUTINE - GETGRT
                  C
                  C PURPOSE - READ RECORDS FROM A SAMS TEMPERATURE TAPE AND DUMP THOSE
                  C   THAT FALL BETWEEN THE START AND STOP DATES.
                  C
                  C ARGUMENTS PASSED -
                  C   ISTART = START DATE (YYDDD) FROM INPUT CARD
                  C   ISTOP  = STOP DATE (YYDDD) FROM INPUT CARD
                  C   FILNUM = TAPE FILE NUMBER
                  C   OPTION = DUMP OPTIONS FROM INPUT CARD (1=DUMP, 0=NO DUMP)
                  C   IRETN  = ERROR RETURN CODE (IRETN=0 NO ERROR, >0 ERROR)
                  C
                  C SUBPROGRAMS CALLED - POSN,GETREC,DM7402,DM7403
                  C
                  C CALLED BY - MAIN
                  C
                  C PROGRAMMER - TOM NUTTER 03/05/85
                  C**********************************************************************
ISN       2              INTEGER ISTART,ISTOP,FILNUM,OPTION(8),IRETN,FILDAT
ISN       3              INTEGER*2 IBLOCK(2994),IYEAR,IDAY
ISN       4              LOGICAL EOF,EOV
                  C*** STATEMENT FUNCTION
ISN       5              FILDAT(IYEAR,IDAY)=(IYEAR-(IYEAR/100)*100)*1000+IDAY
                  C*** INITIALIZE END-OF-VOLUME FLAG
ISN       6              EOV=.FALSE.
                  C*** SEARCH THROUGH DATA FILES UNTIL FILE START DATE MATCHES
                  C*** THE REQUESTED DUMP START DATE
ISN       7       100    CONTINUE
                  C***      RESET RECORD COUNTER, END-OF-FILE FLAG, INCREMENT FILE COUNT,
                  C***      POSITION TO NEXT FILE, READ A RECORD
ISN       8                 KNTREC=0
ISN       9                 EOF=.FALSE.
ISN      10                 FILNUM=FILNUM+1
ISN      11                 CALL POSN(1,10,FILNUM)
ISN      12                 CALL GETREC(10,KNTREC,IBLOCK,LEN,NWRD,EOV,EOF,IRETN)
ISN      13                 IF (IRETN.GT.0) THEN
ISN      14                    IRETN=10
ISN      15                    WRITE(6,5010) IRETN
ISN      16                    RETURN
ISN      17                 ENDIF
                  C***      CHECK IF END-OF-VOLUME OCCURRED BEFORE ANY RECORDS WERE DUMPED
ISN      18                 IF (EOV) THEN
ISN      19                    IRETN=11
ISN      20                    WRITE(6,5020) IRETN
ISN      21                    RETURN
ISN      22                 ENDIF
                  C***      VERIFY THAT FIRST RECORD IS A HEADER RECORD (TYPE 7400)
ISN      23                 IF (IBLOCK(3).NE.7400) THEN
ISN      24                    IRETN=12
ISN      25                    WRITE(6,5030) IBLOCK(3),IRETN
ISN      26                    RETURN
ISN      27                 ENDIF
                  C***      CHECK IF FILE START DATE MEETS REQUESTED DUMP LIMITS
ISN      28                 IF (FILDAT(IBLOCK(5),IBLOCK(6)).GT.ISTOP) THEN
ISN      29                    IRETN=15
ISN      30                    WRITE(6,5050) ISTART,ISTOP,FILDAT(IBLOCK(5),IBLOCK(6)),IRETN
ISN      31                    RETURN
ISN      32                 ENDIF
                  C*** GET NEXT FILE HEADER RECORD
ISN      33                 IF (FILDAT(IBLOCK(5),IBLOCK(6)).LT.ISTART) GO TO 100
                  C*** THE FILE WITH THE REQUESTED START DATE HAS BEEN FOUND. DUMP THE
                  C*** HEADER RECORD
ISN      34              WRITE(6,5040) IBLOCK(3),IBLOCK(6),IBLOCK(5)
                  C*** READ THROUGH RECORDS AND DUMP THOSE FOR WHICH THE DUMP
                  C*** OPTION IS SET TO 1
ISN      35       300    CONTINUE
ISN      36                 CALL GETREC(10,KNTREC,IBLOCK,LEN,NWRD,EOV,EOF,IRETN)
ISN      37                 IF (IRETN.GT.0) THEN
```

```
                  *....*...1.........2.........3.........4.........5.........6.........7.*.......8
ISN    38              IRETN=13                                                          00000710
ISN    39              WRITE(6,5010) IRETN                                               00000720
ISN    40              RETURN                                                            00000730
ISN    41           ENDIF                                                                00000740
          C***      POSITION TO NEXT FILE IF END-OF-FILE IS ENCOUNTERED                  00000750
ISN    42           IF (EOF) THEN                                                        00000760
ISN    43              KNTREC=0                                                          00000770
ISN    44              EOF=.FALSE.                                                       00000780
ISN    45              FILNUM=FILNUM+1                                                   00000790
ISN    46              CALL POSN(1,10,FILNUM)                                            00000800
ISN    47              CALL GETREC(10,KNTREC,IBLOCK,LEN,NWRD,EOV,EOF,IRETN)              00000810
ISN    48              IF (IRETN.GT.0) THEN                                              00000820
ISN    49                 IRETN=14                                                       00000830
ISN    50                 WRITE(6,5010) IRETN                                            00000840
ISN    51                 RETURN                                                         00000850
ISN    52              ENDIF                                                             00000860
ISN    53           ENDIF                                                                00000870
          C***      AT END-OF-VOLUME ALL DATA HAS BEEN DUMPED                            00000880
ISN    54           IF (EOV) RETURN                                                      00000890
          C***      GET FILE DATE, DUMP HEADER RECORD OR RETURN IF STOP DATE             00000900
          C***      IS EXCEEDED                                                          00000910
ISN    56           IF (IBLOCK(3).EQ.7400) THEN                                          00000920
ISN    57              IF (FILDAT(IBLOCK(5),IBLOCK(6)).GT.ISTOP) THEN                    00000930
ISN    58                 RETURN                                                         00000940
ISN    59              ELSE                                                              00000950
ISN    60                 WRITE(6,5040) IBLOCK(3),IBLOCK(6),IBLOCK(5)                    00000960
ISN    61              ENDIF                                                             00000970
ISN    62           ENDIF                                                                00000980
          C***      DUMP A TYPE 7402 RECORD                                              00000990
ISN    63           IF (IBLOCK(3).EQ.7402) THEN                                          00001000
ISN    64              IF (OPTION(2).EQ.1) CALL DM7402(IBLOCK)                           00001010
ISN    66           ENDIF                                                                00001020
          C***      DUMP A TYPE 7403 RECORD                                              00001030
ISN    67           IF (IBLOCK(3).EQ.7403) THEN                                          00001040
ISN    68              IF (OPTION(3).EQ.1.AND.IBLOCK(11).EQ.2) CALL DM7403(IBLOCK,2)00001050
ISN    70              IF (OPTION(4).EQ.1.AND.IBLOCK(11).EQ.102) CALL DM7403(IBLOCK,00001060
                          102)                                                           00001070
ISN    72           ENDIF                                                                00001080
          C*** GET NEXT RECORD                                                           00001090
ISN    73        GO TO 300                                                               00001100
ISN    74 5010   FORMAT(/' *** GETGRT *** ERROR FOUND IN GETREC -- IRETN= ',I3)          00001110
ISN    75 5020   FORMAT(/' *** GETGRT *** EOV OCCURRED BEFORE ANY RECORDS ',             00001120
              .     'WERE DUMPED -- IRETN= ',I3)                                         00001130
ISN    76 5030   FORMAT(/' *** GETGRT *** FIRST RECORD IN DATA FILE IS ICORRECT ',       00001140
              .     'TYPE. SHOULD BE 7400, FOUND ',I6,' IRETN= ',I3)                     00001150
ISN    77 5040   FORMAT(///' RECORD TYPE ',I4,' DATA DAY/YEAR ',I3,1X,I4)                00001160
ISN    78 5050   FORMAT(/' *** GETGRT *** THE TAPE START DATE EXCEEDS THE ',             00001170
              .     'REQUESTED DUMP STOP DATE'/' CHECK DUMP DATES AGAINST TAPE ',        00001180
              .     'HEADER DATES. ISTART= ',I6,' ISTOP= ',I6,' TAPE DATE= ',I6,         00001190
              .     ' IRETN= ',I3)                                                       00001200
ISN    79        END                                                                     00001210
```

APPENDIX B

```
             *....*...1.........2.........3.........4.........5.........6.........7.*.......8

ISN    1          SUBROUTINE GETCMP(ISTART,ISTOP,FILNUM,OPTION,IRETN)
             C***********************************************************************
             C SUBROUTINE - GETCMP
             C
             C PURPOSE - READ RECORDS FROM A SAMS COMPOSITION TAPE AND DUMP THOSE
             C   THAT FALL BETWEEN THE START AND STOP DATES.
             C
             C ARGUMENTS PASSED -
             C   ISTART = START DATE (YYDDD) FROM INPUT CARD
             C   ISTOP  = STOP DATE (YYDDD) FROM INPUT CARD
             C   FILNUM = TAPE FILE NUMBER
             C   OPTION = DUMP OPTIONS FROM INPUT CARD (1=DUMP, 0=NO DUMP)
             C   IRETN  = ERROR RETURN CODE (IRETN=0 NO ERROR, >0 ERROR)
             C
             C SUBPROGRAMS CALLED - POSN,GETREC,DMPCMP
             C
             C CALLED BY - MAIN
             C
             C PROGRAMMER - TOM NUTTER 03/05/85
             C***********************************************************************
ISN    2          INTEGER ISTART,ISTOP,FILNUM,OPTION(8),IRETN,RECDAT
ISN    3          INTEGER*2 IBLOCK(2994),IYEAR,IDAY
ISN    4          LOGICAL EOF,EOV
             C*** STATEMENT FUNCTION
ISN    5          RECDAT(IYEAR,IDAY)=(IYEAR-(IYEAR/100)*100)*1000+IDAY
             C*** INITIALIZE RECORD COUNTER, END-OF-FILE FLAG, END-OF-VOLUME FLAG,
             C*** INCREMENT FILE COUNT, POSITION TO NEXT FILE
ISN    6          KNTREC=0
ISN    7          EOF=.FALSE.
ISN    8          EOV=.FALSE.
ISN    9          FILNUM=FILNUM+1
ISN   10          CALL POSN(1,10,FILNUM)
             C*** SEARCH THROUGH DATA RECORDS UNTIL RECORD START DATE MATCHES
             C*** THE REQUESTED INPUT START DATE
ISN   11     100  CONTINUE
ISN   12            CALL GETREC(10,KNTREC,IBLOCK,LEN,NWRD,EOV,EOF,IRETN)
ISN   13            IF (IRETN.GT.0) THEN
ISN   14               IRETN=50
ISN   15               WRITE(6,5010) IRETN
ISN   16               RETURN
ISN   17            ENDIF
             C***     CHECK IF END-OF-VOLUME OCCURRED BEFORE ANY RECORDS WERE DUMPED
ISN   18            IF (EOV) THEN
ISN   19               IRETN=51
ISN   20               WRITE(6,5020) IRETN
ISN   21               RETURN
ISN   22            ENDIF
             C***     POSITION TO NEXT FILE IF AN END-OF-FILE IS ENCOUNTERED
ISN   23            IF (EOF) THEN
ISN   24               KNTREC=0
ISN   25               EOF=.FALSE.
ISN   26               FILNUM=FILNUM+1
ISN   27               CALL POSN(1,10,FILNUM)
ISN   28            ENDIF
             C***     CHECK IF FILE START DATE MEETS REQUESTED DUMP LIMITS
ISN   29            IF (RECDAT(IBLOCK(5),IBLOCK(4)).GT.ISTOP) THEN
ISN   30               IRETN=54
ISN   31               WRITE(6,5030) ISTART,ISTOP,RECDAT(IBLOCK(5),IBLOCK(4)),IRETN
ISN   32               RETURN
ISN   33            ENDIF
             C*** GET NEXT RECORD
ISN   34            IF (RECDAT(IBLOCK(5),IBLOCK(4)).LT.ISTART) GO TO 100
             C*** THE RECORD START DATE NOW FALLS WITHIN THE REQUESTED DUMP LIMITS.
             C*** READ AND DUMP RECORDS UNTIL REQUESTED STOP DATE IS EXCEEDED
ISN   35          CALL DMPCMP(IBLOCK,OPTION)
ISN   36     200  CONTINUE
ISN   37            CALL GETREC(10,KNTREC,IBLOCK,LEN,NWRD,EOV,EOF,IRETN)
ISN   38            IF (IRETN.GT.0) THEN
ISN   39               IRETN=52
ISN   40               WRITE(6,5010) IRETN
```

```
                    *....*...1.........2.........3.........4.........5.........6.........7.*.......8

ISN    41                    RETURN
ISN    42                 ENDIF
                C***      POSITION TO NEXT FILE IF AN END-OF-FILE IS ENCOUNTERED,
                C***      READ THE NEXT RECORD
ISN    43                 IF (EOF) THEN
ISN    44                    KNTREC=0
ISN    45                    EOF=.FALSE.
ISN    46                    FILNUM=FILNUM+1
ISN    47                    CALL POSN(1,10,FILNUM)
ISN    48                    CALL GETREC(10,KNTREC,IBLOCK,LEN,NWRD,EOV,EOF,IRETN)
ISN    49                    IF (IRETN.GT.0) THEN
ISN    50                       IRETN=53
ISN    51                       WRITE(6,5010) IRETN
ISN    52                       RETURN
ISN    53                    ENDIF
ISN    54                 ENDIF
                C***      AT END-OF-VOLUME, OR WHEN RECORD DATE EXCEEDS DUMP STOP DATE,
                C***      ALL DATA HAS BEEN DUMPED
ISN    55                 IF (EOV) RETURN
ISN    57                 IF (RECDAT(IBLOCK(5),IBLOCK(4)).GT.ISTOP) RETURN
                C***      DUMP A RECORD
ISN    59                 CALL DMPCMP(IBLOCK,OPTION)
                C*** GET NEXT RECORD
ISN    60              GO TO 200
ISN    61       5010   FORMAT(/' *** GETCMP *** ERROR FOUND IN GETREC -- IRETN= ',I3)
ISN    62       5020   FORMAT(/' *** GETCMP *** EOV OCCURRED BEFORE ANY RECORDS ',
                     .    'WERE DUMPED -- IRETN= ',I3)
ISN    63       5030   FORMAT(/' *** GETCMP *** THE TAPE START DATE EXCEEDS THE ',
                     .    'REQUESTED DUMP STOP DATE'/' CHECK DUMP DATES AGAINST TAPE ',
                     .    'HEADER DATES. ISTART= ',I6,' ISTOP= ',I6,' TAPE DATE= ',I6,
                     .    ' IRETN= ',I3)
ISN    64              END
```

APPENDIX B

```
                  *....*...1.........2.........3.........4.........5.........6.........7.*.......8

ISN    1           SUBROUTINE GETREC(IUNIT,KNTREC,IBLOCK,LENGTH,NWORDS,EOV,EOF,
                 .    IRETN)
                  C*********************************************************************
                  C SUBROUTINE - GETREC
                  C
                  C PURPOSE - READ A RECORD FROM A SPECIFIED LOGICAL UNIT, INCREMENT
                  C    RECORD COUNTER, AND CALCULATE THE NUMBER OF 32-BIT WORDS IN THIS
                  C    RECORD. DETERMINE END-OF-FILE AND END-OF-VOLUME CONDITIONS
                  C    AS THEY OCCUR.
                  C
                  C ARGUMENTS PASSED -
                  C    IUNIT  = LOGICAL UNIT NUMBER
                  C    KNTREC = RECORDS PER FILE
                  C    IBLOCK = BUFFER INTO WHICH RECORD IS READ
                  C    LENGTH = LENGTH OF RECORD IN BYTES
                  C    NWORDS = NUMBER OF 32-BIT WORDS IN RECORD
                  C    EOV    = END-OF-VOLUME FLAG
                  C    EOF    = END-OF-FILE FLAG
                  C    IRETN  = ERROR RETURN CODE (IRETN=0 NO ERROR, >0 ERROR)
                  C
                  C SUBPROGRAMS CALLED - FMOVE,FREAD
                  C
                  C CALLED BY - GETGRT,GETCMP
                  C
                  C PROGRAMMER - TOM NUTTER 03/05/85
                  C*********************************************************************
ISN    2                 LOGICAL EOV,EOF
ISN    3                 INTEGER IBLOCK(1497)
                  C*** INITIALIZE BUFFER TO 0
ISN    4                 IBLOCK(1)=0
ISN    5                 CALL FMOVE(IBLOCK(2),5984,IBLOCK(1))
                  C*** READ A RECORD, INCREMENT RECORD COUNTER AND CALCULATE THE
                  C*** NUMBER OF 32-BIT WORDS IN THIS RECORD
ISN    6                 CALL FREAD(IBLOCK(1),IUNIT,LENGTH,*800,*930)
ISN    7                 KNTREC=KNTREC+1
ISN    8                 IF (LENGTH.EQ.40 .OR. LENGTH.EQ.3506 .OR. LENGTH.EQ.4882 .OR.
                             LENGTH.EQ.5986) THEN
ISN    9                    NWORDS=LENGTH/4
ISN   10                    IF (MOD(LENGTH,4).GT.0) NWORDS=NWORDS+1
ISN   12                    RETURN
ISN   13                 ELSE
ISN   14                    IRETN=40
ISN   15                    WRITE(6,5010) LENGTH,IRETN
ISN   16                    RETURN
ISN   17                 ENDIF
                  C*** SET END-OF-FILE FLAG AND END-OF-VOLUME FLAG
ISN   18          800    CONTINUE
ISN   19                 EOF=.TRUE.
ISN   20                 IF (KNTREC.LT.1) EOV=.TRUE.
ISN   22                 RETURN
                  C*** READ ERROR
ISN   23          930    CONTINUE
ISN   24                 IRETN=41
ISN   25                 WRITE(6,5020) IUNIT,IRETN
ISN   26                 RETURN
ISN   27          5010   FORMAT(/' *** GETREC *** INVALID RECORD LENGTH OF ',
                       .    I6,' BYTES. IRETN= ',I3/)
ISN   28          5020   FORMAT(/' *** GETREC *** READ ERROR ON UNIT ',I3,
                       .    ' IRETN= ',I3/)
ISN   29                 END
```

APPENDIX B

```
                  *....*...1.........2.........3.........4.........5.........6.........7.*.......8
ISN    1                SUBROUTINE BN7402(IBLOCK)
                  C*************************************************************************
                  C SUBROUTINE - BN7402
                  C
                  C PURPOSE - FORM AND PRINT OUTPUT LINES FOR SAMS GRIDDED RETRIEVED
                  C   TEMPERATURE TYPE 7402 RECORDS.
                  C
                  C ARGUMENTS PASSED -
                  C   IBLOCK = ARRAY CONSISTING OF GRIDDED RETRIEVED TEMPERATURE DATA
                  C
                  C SUBPROGRAMS CALLED - NONE
                  C
                  C CALLED BY - GETGRT
                  C
                  C PROGRAMMER - TOM NUTTER 03/02/85
                  C*************************************************************************
ISN    2                INTEGER*2 IBLOCK(2994),LINE(19)
ISN    3                CHARACTER*4 DASH,LONG(38),HEDLIN(19)
ISN    4                DATA DASH/'----'/
ISN    5                DATA LONG/'-180','-170','-160','-150','-140','-130','-120',
                       .   '-110','-100',' -90',' -80',' -70',' -60',' -50',' -40',
                       .   ' -30',' -20',' -10','   0',' +10',' +20',' +30',' +40',
                       .   ' +50',' +60',' +70',' +80',' +90','+100','+110','+120',
                       .   '+130','+140','+150','+160','+170','+190','+200'/
                  C*** WRITE RECORD HEADING
ISN    6                WRITE(6,5000)
ISN    7                WRITE(6,5010) (IBLOCK(I),I=1,8)
                  C*** FORM AND PRINT OUTPUT LINES FOR TWO LONGITUDE GROUPS -180E TO 0E
                  C*** AND +10E TO +170E, PLUS ZONAL MEAN AND CLIMATOLOGY
ISN    8                DO 300 K=1,2
ISN    9                   ILOG=9
ISN   10                   IF (K.EQ.2) ILOG=1225
                  C***        PRINT HEADING
ISN   12                   CALL FMOVE(HEDLIN(1),76,LONG((K-1)*19+1))
ISN   13                   WRITE(6,5020) HEDLIN,(DASH,I=1,21)
                  C***        FORM AND PRINT OUTPUT LINES FOR 62 PRESSURES
ISN   14                   PLEVEL=1.2
ISN   15                   DO 200 J=1,62
ISN   16                      IOFF=J+ILOG
ISN   17                      DO 100 I=1,19
ISN   18                         LINE(I)=IBLOCK(IOFF)
ISN   19                         IOFF=IOFF+64
ISN   20          100         CONTINUE
ISN   21                      PLEVEL=PLEVEL+0.2
ISN   22                      WRITE(6,5030) PLEVEL,LINE
ISN   23          200      CONTINUE
ISN   24          300   CONTINUE
ISN   25                RETURN
ISN   26          5000  FORMAT(/' RETRIEVED TEMPERATURE GRID')
ISN   27          5010  FORMAT(' RECSIZE',I5,2X,'REC#',I5,2X,'TYPE',I5,2X,
                       .   'DATA DAY/YEAR',1X,I3,1X,I4,2X,'GEN DATE',1X,I3,1X,I4,2X,
                       .   'GRID LAT(X100)',1X,I5)
ISN   28          5020  FORMAT(/' LN(P0/P)',3X,19(A4,2X)/1X,2A4,3X,19(A4,2X))
ISN   29          5030  FORMAT(2X,F4.1,4X,19I6)
ISN   30                END
```

APPENDIX B

```
                    *....*...1.........2.........3.........4.........5.........6.........7.*.......8

ISN     1                 SUBROUTINE DM7403(IBLOCK,DATTYP)
                    C***********************************************************************
                    C SUBROUTINE - DM7403
                    C
                    C PURPOSE - FORM AND PRINT OUTPUT LINES FOR SAMS TYPE 7403 RECORDS -
                    C   TEMPERATURE GRIDS AND TEMPERATURE GRID ERRORS.
                    C
                    C ARGUMENTS PASSED -
                    C   IBLOCK = ARRAY CONSISTING OF TEMPERATURE GRID DATA OR ERRORS
                    C   DATTYP = DATA TYPE DESIGNATING TEMPERATURE GRID OR GRID ERRORS
                    C
                    C SUBPROGRAMS CALLED - NONE
                    C
                    C CALLED BY - GETGRT
                    C
                    C PROGRAMMER - TOM NUTTER 03/01/85
                    C***********************************************************************
ISN     2                 INTEGER DATTYP
ISN     3                 INTEGER*2 IBLOCK(2994)
ISN     4                 CHARACTER*4 DASH,LONG(36),HEDLIN(18)
ISN     5                 CHARACTER*5 LAT(48)
ISN     6                 DATA DASH/'----'/
ISN     7                 DATA LONG/'-180','-170','-160','-150','-140','-130','-120',
                         .    '-110','-100',' -90',' -80',' -70',' -60',' -50',' -40',
                         .    ' -30',' -20',' -10','   0',' +10',' +20',' +30',' +40',
                         .    ' +50',' +60',' +70',' +80',' +90','+100','+110','+120',
                         .    '+130','+140','+150','+160','+170'/
ISN     8                 DATA LAT/'-50.0','-47.5','-45.0','-42.5','-40.0','-37.5','-35.0',
                         . '-32.5','-30.0','-27.5','-25.0','-22.5','-20.0','-17.5','-15.0',
                         . '-12.5','-10.0',' -7.5',' -5.0',' -2.5','  0.0',' +2.5',' +5.0',
                         . ' +7.5','+10.0','+12.5','+15.0','+17.5','+20.0','+22.5','+25.0',
                         . '+27.5','+30.0','+32.5','+35.0','+37.5','+40.0','+42.5','+45.0',
                         . '+47.5','+50.0','+52.5','+55.0','+57.5','+60.0','+62.5','+65.0',
                         . '+67.5'/
                    C*** WRITE RECORD IDENTIFICATION INFORMATION
ISN     9                 WRITE(6,5000) (IBLOCK(I),I=1,8),IBLOCK(10),IBLOCK(11)
ISN    10                 IF (DATTYP.EQ.2) WRITE(6,5010)
ISN    12                 IF (DATTYP.EQ.102) WRITE(6,5020)
                    C*** FORM AND PRINT OUTPUT LINES FOR TWO LONGITUDE GROUPS -180E TO -10E
                    C*** AND 0E TO +170E
ISN    14                 DO 200 J=1,2
ISN    15                    ISTRT=-12
ISN    16                    IF (J.EQ.2) ISTRT=6
                    C***        PRINT HEADING
ISN    18                    CALL FMOVE(HEDLIN(1),72,LONG((J-1)*18+1))
ISN    19                    WRITE(6,5030) IBLOCK(12),HEDLIN,(DASH,M=1,18)
                    C***        FORM AND PRINT OUTPUT LINES FOR LATITUDES -50 N TO +67.5 N
ISN    20                    DO 100 LOOP=1,48
ISN    21                       ISTRT=ISTRT+36
ISN    22                       ISTOP=ISTRT+17
ISN    23                       WRITE(6,5040) LAT(LOOP),(IBLOCK(I),I=ISTRT,ISTOP)
ISN    24           100      CONTINUE
ISN    25           200   CONTINUE
ISN    26                 RETURN
ISN    27           5000  FORMAT(/' RECSIZE',I5,2X,'REC#',I5,2X,'TYPE',I5,2X,'ORBIT TYPE',
                         .    I3,2X,'DATA DAY/YEAR',1X,I3,1X,I4,2X,'GEN DATE',1X,I3,1X,I4,2X,
                         .    'SCALE FACTOR',I3,2X,'DATA TYPE',I4)
ISN    28           5010  FORMAT(/' TEMPERATURE GRID DATA')
ISN    29           5020  FORMAT(/' TEMPERATURE GRID ERRORS')
ISN    30           5030  FORMAT(' PRESSURE LEVEL= ',I5/9X,18(A4,2X)/9X,18(A4,2X))
ISN    31           5040  FORMAT(1X,A5,1X,18I6)
ISN    32                 END
```

APPENDIX B

```
                *....*...1.........2.........3.........4.........5.........6.........7.*.......8
ISN      1            SUBROUTINE DMPCMP(IBLOCK,OPTION)
                C***********************************************************************
                C SUBROUTINE - DMPCMP
                C
                C PURPOSE - PRINT A FORMATTED DUMP OF A SAMS ZONAL MEAN METHANE OR
                C   NITROUS-OXIDE COMPOSITION RECORD.
                C
                C ARGUMENTS PASSED -
                C   IBLOCK = ARRAY CONSISTING OF ZONAL MEAN DATA
                C   OPTION = DUMP OPTIONS FROM INPUT CARD (1=DUMP, 0=NO DUMP)
                C
                C SUBPROGRAMS CALLED - PRTREC
                C
                C CALLED BY - GETCMP
                C
                C PROGRAMMER - TOM NUTTER 03/05/85
                C***********************************************************************
ISN      2            INTEGER OPTION(8)
ISN      3            INTEGER*2 IBLOCK(2994)
                C*** PRINT RECORD IDENTIFYING INFORMATION
ISN      4            WRITE(6,5010) (IBLOCK(I),I=1,15)
                C*** DUMP NITROUS-OXIDE RECORD
ISN      5            IF (IBLOCK(3).EQ.7405) THEN
                C***     DUMP NITROUS-OXIDE MIXING RATIOS
ISN      6              IF (OPTION(5).EQ.1) THEN
ISN      7                 WRITE(6,5020)
ISN      8                 CALL PRTREC(IBLOCK,-480)
ISN      9              ENDIF
                C***     DUMP NITROUS-OXIDE MIXING RATIO ERRORS
ISN     10              IF (OPTION(6).EQ.1) THEN
ISN     11                 WRITE(6,5030)
ISN     12                 CALL PRTREC(IBLOCK,1008)
ISN     13              ENDIF
ISN     14            ENDIF
                C*** DUMP METHANE RECORD
ISN     15            IF (IBLOCK(3).EQ.7406) THEN
                C***      DUMP METHANE MIXING RATIOS
ISN     16               IF (OPTION(7).EQ.1) THEN
ISN     17                  WRITE(6,5040)
ISN     18                  CALL PRTREC(IBLOCK,-480)
ISN     19               ENDIF
                C***      DUMP METHANE MIXING RATIO ERRORS
ISN     20               IF (OPTION(8).EQ.1) THEN
ISN     21                  WRITE(6,5050)
ISN     22                  CALL PRTREC(IBLOCK,1008)
ISN     23               ENDIF
ISN     24            ENDIF
ISN     25            RETURN
ISN     26      5010  FORMAT(/' RECSIZE',I5,2X,'REC#',I5,2X,'TYPE',I5,2X,'DATA DATE',
                     .   1X,I3,1X,I4,2X,'CHAN',I2,2X,'SIEVE SET ENPMC',I2,2X,'CLPMC',
                     .   I2,2X,'A1PMC',I2,2X,'C1PMC',I2,2X,'GEN DATE',1X,I3,1X,I4,2X,
                     .   /' ELEMENTS IN PROFILE',I4,2X,'BOT/TOP LEVELS',I3,1X,I3)
ISN     27      5020  FORMAT(/' NITROUS-OXIDE MIXING RATIOS')
ISN     28      5030  FORMAT(/' NITROUS-OXIDE MIXING RATIO ERRORS')
ISN     29      5040  FORMAT(/' METHANE MIXING RATIOS')
ISN     30      5050  FORMAT(/' METHANE MIXING RATIO ERRORS')
ISN     31            END
```

APPENDIX B

```
                 *....*...1.........2.........3.........4.........5.........6.........7.*.......8
ISN    1               SUBROUTINE PRTREC(IBLOCK,INDEX)
                 C***********************************************************************
                 C SUBROUTINE - PRTREC
                 C
                 C PURPOSE - FORM AND PRINT OUTPUT LINES FOR ZONAL MEAN METHANE OR
                 C   NITROUS-OXIDE COMPOSITION RECORDS.
                 C
                 C ARGUMENTS PASSED -
                 C   IBLOCK = ARRAY CONSISTING OF ZONAL MEAN DATA
                 C   INDEX  = INDEX THAT POSITIONS TO MIXING RATIOS OR MIXING RATIO ERROR
                 C
                 C SUBPROGRAMS CALLED - NONE
                 C
                 C CALLED BY - DMPCMP
                 C
                 C PROGRAMMER - TOM NUTTER 03/02/85
                 C***********************************************************************
ISN    2               INTEGER*2 IBLOCK(2994),LINE(16),IGROUP(496)
ISN    3               CHARACTER*4 DASH
ISN    4               CHARACTER*5 HEDLIN(16),LAT(48)
ISN    5               DATA DASH/'----'/
ISN    6               DATA LAT/'-50.0','-47.5','-45.0','-42.5','-40.0','-37.5','-35.0',
                      . '-32.5','-30.0','-27.5','-25.0','-22.5','-20.0','-17.5','-15.0',
                      . '-12.5','-10.0',' -7.5',' -5.0',' -2.5',' 0.0',' 2.5',' 5.0',
                      . '  7.5',' 10.0',' 12.5',' 15.0',' 17.5',' 20.0',' 22.5',' 25.0',
                      . ' 27.5',' 30.0',' 32.5',' 35.0',' 37.5',' 40.0',' 42.5',' 45.0',
                      . ' 47.5',' 50.0',' 52.5',' 55.0',' 57.5',' 60.0',' 62.5',' 65.0',
                      . ' 67.5'/
                 C*** FORM AND PRINT OUTPUT LINES FOR THREE LATITUDE GROUPS -50.0N TO
                 C*** -12.5N, -10.0N TO +27.5N, +30.0N TO +67.5N
ISN    7               IOFF=INDEX
ISN    8               DO 300 K=1,3
ISN    9                  IOFF=IOFF+496
ISN   10                  CALL FMOVE(IGROUP(1),992,IBLOCK(IOFF))
                 C***     PRINT HEADING
ISN   11                  CALL FMOVE(HEDLIN(1),80,LAT((K-1)*16+1))
ISN   12                  WRITE(6,5000) HEDLIN,(DASH,I=1,18)
ISN   13                  PLEVEL=2.8
ISN   14                  DO 200 J=1,31
ISN   15                     DO 100 I=1,16
ISN   16                        L=(I-1)*31+J
ISN   17                        LINE(I)=IGROUP(L)
ISN   18         100         CONTINUE
                 C***        PRINT OUTPUT LINE
ISN   19                     PLEVEL=PLEVEL+0.2
ISN   20                     WRITE(6,5010) PLEVEL,LINE
ISN   21         200      CONTINUE
ISN   22         300   CONTINUE
ISN   23               RETURN
ISN   24         5000  FORMAT(/' LN(P0/P)',2X,16(A5,1X)/1X,2A4,3X,16(A4,2X))
ISN   25         5010  FORMAT(2X,F4.1,4X,16I6)
ISN   26               END
```

APPENDIX C

THE STRATOSPHERIC AND MESOSPHERIC SOUNDER ON NIMBUS-7

[Reproduced from *Phil. Trans. R. Soc. Lond., A296*, 219-241 (1980).]

Phil. Trans. R. Soc. Lond. A **296**, 219–241 (1980) [219]

Printed in Great Britain

The stratospheric and mesospheric sounder on Nimbus 7

By J. R. Drummond, J. T. Houghton, F.R.S., G. D. Peskett, C. D. Rodgers, M. J. Wale, J. Whitney and E. J. Williamson

Department of Atmospheric Physics, Clarendon Laboratory, Oxford, OX1 3PU

The stratospheric and mesospheric sounder (s.a.m.s.) instrument was launched on the Nimbus G satellite on 24 October 1978. It is designed to measure temperature and concentration profiles of various gases in the height range 20–100 km by detecting either their thermal emission or, in some cases, resonant scattering of sunlight.

The gases selected, CO_2, CO, CH_4, NO, N_2O and H_2O, significantly affect the upper atmosphere energy budget by their influence on the concentration of the primary sunlight absorber, ozone. This influence is disproportionate to their own concentration because of the existence of 'catalytic cycles' which destroy ozone while regenerating the catalyst.

A description of the instrument, its principles of operation and some of the methods of retrieval used is presented, together with some preliminary results from the first 3 months of operations.

1. Introduction

As has been explained earlier in this meeting by Professor Labitzke and by Dr Barnett, during the last 10 years remote sounding observations from satellites of atmospheric temperature have been extended through the stratosphere into the mesosphere. Much extra insight into atmospheric phenomena has arisen through the provision of these observations substantially continuous in time and with near global coverage. The purpose of the stratospheric and mesospheric sounder (s.a.m.s.) on Nimbus 7 is to provide similar coverage in time and space for observations of the concentration of a number of important minor constituents in the stratosphere and mesosphere, all of which are directly or indirectly involved in the chemistry of ozone (cf. Thrush, this symposium). Like previous remote sounding instruments built for Nimbus satellites in which the Oxford University Atmospheric Physics Department has been involved, s.a.m.s. observes infrared radiation emitted by the atmospheric constituents it is required to measure. In this paper, the principles of the techniques employed will first be outlined, then the different measurements being made by s.a.m.s. will be discussed together with a description of the instrument and the method of calibration. Finally, some early results will be presented.

2. Principles of operation

2.1. *Limb-sounding*

The advantages of the limb view (see figure 7) are that emission observations can be made from as long a path through the atmosphere as possible, and that behind the atmospheric path is the cold radiation background of space. Such a limb path possesses an air mass approximately 70 times that in a vertical path above the lowest point of the path. The atmosphere's pressure profile and the geometry of the path both weight the material in the path strongly towards the tangent height giving good vertical resolution. For emission from spectral lines that are

PRECEDING PAGE BLANK NOT FILMED

PAGE 88 INTENTIONALLY BLANK

not saturated at their centres, 60% of the emission from a limb path originates from altitudes within 3 km of the lowest altitude of the path (see figure 4). By contrast, the horizontal resolution of a limb observation is poor, the length of the limb path being of the order of 400 km.

Radiometers carried by balloons or aircraft have, for a long time, observed emission from the atmosphere's limb. Results from the limb radiance inversion radiometer (l.r.i.r.) on Nimbus 6 (Gille *et al.* 1975), the first satellite radiometer to observe radiance from the atmosphere's limb, have demonstrated the vertical resolution which can be achieved in measurements of temperature and ozone (Gille, this symposium).

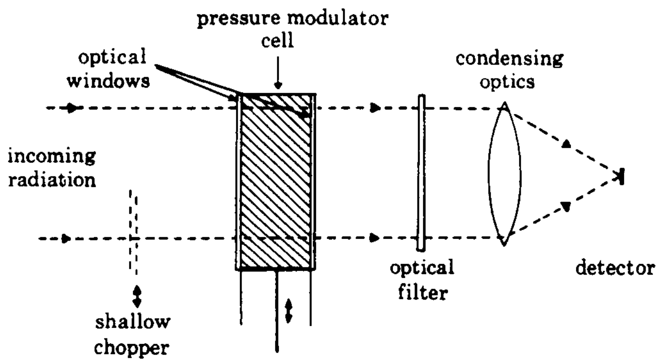

FIGURE 1. Simplified diagram of a p.m.r. optical system employing a 'shallow chopper' which only modulates part of the incoming radiation beam.

2.2. *The pressure modulator*

The pressure modulator is a device which selectively modulates the emission from a gas by using the absorption lines of the same gas as an optical filter. A cell of gas is included in the optical path of the radiometer (figure 1) and its pressure varied cyclically. The transmission of the cell is modulated only at optical frequencies that lie within the absorption lines of the gas, thus selectively modulating emission from the same gas incident on the radiometer. After detection, the signal at the frequency of the modulation may be recovered by phase-sensitive detection. A broad optical filter limits the spectral bandwidth to the appropriate emission band.

The pressure modulator technique is a development from the selective chopper technique employed for temperature sounding instruments on the Nimbus 4 and 5 satellites (Houghton & Smith 1970; Ellis *et al.* 1973). It has previously been flown in a temperature sounder on the Nimbus 6 satellite (Taylor *et al.* 1972; Curtis *et al.* 1974). The advantages of the technique for composition sounding have been described by Chaloner *et al.* (1978), who employed it in a balloon-borne radiometer for the measurement of NO, NO_2 and H_2O in the stratosphere. Further details of the technique are also given in Drummond & Jarnot (1978).

2.3. *Double chopping*

The gas pressure in the pressure modulator cell (p.m.c.) is modulated at the resonant frequency (20–40 Hz) of the mechanical system (see § 4.3). It is also useful to include a conventional chopper at a much higher frequency (*ca.* 240 Hz) in the optical system. This modulates all 'incoming' radiation with the optical filter profile and produces a 'wideband' signal

APPENDIX C

at the detector. The 'wideband' signal, in the absence of emission from other species, provides information for lower in the atmosphere than the p.m.r. signal (see figure 2). The wideband signal may also be used for the elimination of signals from atmsopheric constituents whose absorption bands overlap that of the wanted species (see Drummond & Jarnot 1978), and in the determination of the atmospheric level being observed (§ 3.3). In s.a.m.s. a shallow chopper is employed (see § 4), which chops only *ca.* 2.5 % of the aperture of the system. The shallow chopper is preferred over a conventional 100 % chopper because it does not obstruct the beam for the pressure modulator further back in the optical chain.

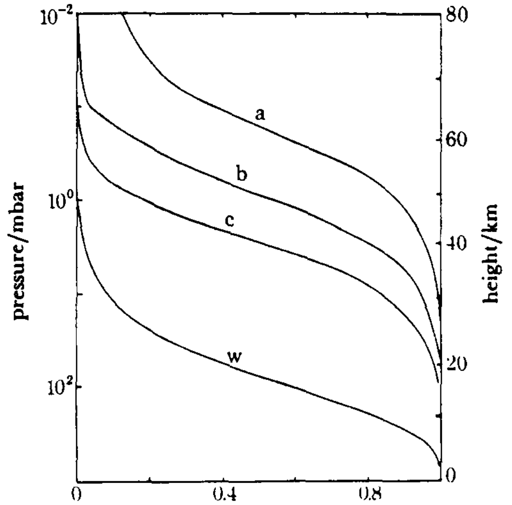

FIGURE 2. The effective emissivity, ϵ (see equation (5)) for water vapour evaluated by using a climatological equatorial temperature profile and a constant volume mixing ratio of 5×10^{-6}. Curves (a), (b) and (c) are for the s.a.m.s. B2 p.m.r. channel with mean cell pressures of 0.87 mbar, 4.48 mbar and 15.3 mbar respectively. Curve (w) is for the corresponding wideband channel and is virtually independent of modulator pressure.

3. Measurements with s.a.m.s.

The radiant power, W, emitted by a limb path at frequency ν and received by one of the s.a.m.s. detectors is given by

$$W = A\Omega \int_0^\infty \int_0^\infty J_\nu(x)\, \tau_{0\nu}\, \tau_{m\nu} \frac{\mathrm{d}\tau_\nu(x)}{\mathrm{d}x}\, \mathrm{d}x\, \mathrm{d}\nu, \tag{1}$$

where A is the aperture of the telescope, Ω the field of view, $\tau_\nu(x)$ the transmission between the satellite and the position along the path described by the coordinate x, $\tau_{0\nu}$ the static component of the optical transmission in the appropriate channel, $\tau_{m\nu}$ the modulated component of the optical transmission, and $J_\nu(x)$ is the source function appropriate to the emission band in question at the location described by the coordinate x. Under conditions of local thermodynamic equilibrium (l.t.e.), the source function is equal to the Planck function $B_\nu(T)$ at the temperature T of the atmosphere at location x.

Integration is along the limb path and over the frequencies where the optical components have any significant transmission.

Calibration of the instrument is carried out by inserting a black-body at temperature T_b in the path when the radiant power W_b received is

$$W_b = A\Omega \int_0^\infty B_\nu(T_b)\, \tau_{0\nu}\, \tau_{m\nu}\, \mathrm{d}\nu. \tag{2}$$

The radiance, L, of an atmospheric path is then defined as

$$L = \frac{W}{W_b} \frac{\int_0^\infty B_\nu(T_b)\, \tau_{0\nu}\, \tau_{m\nu}\, \mathrm{d}\nu}{\int_0^\infty \tau_{0\nu}\, \tau_{m\nu}\, \mathrm{d}\nu}. \tag{3}$$

For channels covering a reasonably narrow frequency interval the ratio of the integrals in equation (3) is $B_{\bar{\nu}}(T_b)$, where $\bar{\nu}$ is the centre frequency of the interval.

To illustrate the radiometric measurements being made it is useful when l.t.e. applies to write a simplified expression for the radiance L measured by a particular channel, namely:

$$L = \epsilon B_{\bar{\nu}}(\overline{T}), \tag{4}$$

where

$$\epsilon = \frac{\int_0^\infty \int_0^\infty \tau_{0\nu}\, \tau_{m\nu} \frac{\mathrm{d}\tau_\nu(x)}{\mathrm{d}x}\, \mathrm{d}x\, \mathrm{d}\nu}{\int_0^\infty \tau_{0\nu}\, \tau_{m\nu}\, \mathrm{d}x} \tag{5}$$

may be defined as the *effective emissivity* of the path and where $\overline{T}$ is a mean temperature for the path.

3.1. *Temperature measurements*

If the radiance is measured from the emission band of an atmospheric constituent whose distribution is accurately known, for any given path the emissivity ϵ in equation (4) may be calculated and hence a mean temperature $\overline{T}$ for that path may be deduced. A set of radiances received from different levels as the instrument scans over the limb may be retrieved to give a temperature profile (see Rodgers (1976) for a review of retrieval methods and § 6.2). In s.a.m.s. two wideband and two pressure modulator channels are included observing emission from the 15 μm band of CO_2, a gas that is substantially uniformly mixed up to at least 90 km altitude. Above about 80 km, local thermodynamic equilibrium no longer applies for this band; the quantity that is then measured is the vibrational temperature of the band, which is of considerable importance because emission from it is the major energy sink in the upper mesosphere and lower thermosphere.

3.2. *Composition measurements*

Given that the atmosphere's temperature structure has been determined by the method of § 3.1, from radiance observations on any other band an effective emissivity ϵ may be determined from equation (4), and hence the distribution of the emitting constituent observed. In figure 2 are curves showing the variation of effective emissivity for emission from the long wave water vapour band as measured by a wide band channel and by channels containing pressure modulator cells with water vapour at different pressures, demonstrating that the water vapour distribution can be measured from the tropopause through into the upper mesosphere. Some results for H_2O from an early orbit of s.a.m.a. are given in § 6.

The method by which a detailed distribution is derived is as follows. First of all, through theoretical calculations on the basis of spectral information about the band in question, together with a programme of laboratory measurements as described in § 5, algorithms describing the transmission of any atmospheric path are derived. A 'first guess' profile for the distribution of the gas in question is then assumed and, on the basis of the temperature profile derived by the method of § 3.1, an expected set of radiances is computed. These computed radiances are then compared with the measured radiances, and by an iterative process a profile of the gas distribution is found for which computed and measured radiances agree.

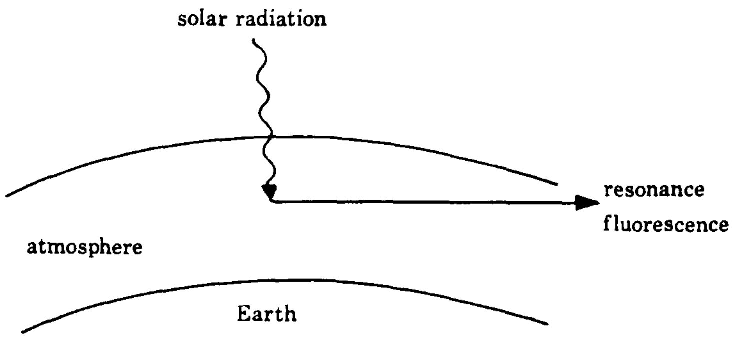

FIGURE 3. The generation of resonance fluorescence signals by scattering of sunlight within the atmosphere.

To acquire information about the distribution of some constituents in the mesosphere and lower thermosphere it is possible to use observations of resonance fluorescence of solar radiation from those molecules which have strong bands in the near infrared (figure 3) (cf. Table 1 for list of bands included in s.a.m.s.). Provided that absorption by solar radiation is the only process of excitation of the band in question, and provided that collisional quenching is negligible, the radiance observed is a function of the solar flux incident on the layer and the number of molecules along the path. In practice, an elaborate radiative transfer calculation has to be carried out for each situation because multiple scattering, excitation by other non-thermal processes (e.g. by particles), and details of quenching processes have also to be considered. Interpretation of measurements from fluorescence channels, therefore, is extremely complex.

3.3. *Reference pressure determination*

Because s.a.m.s. is a limb viewing instrument it is necessary that accurate information is available regarding the pressure of the atmosphere at the levels being viewed at any given time. Consider information such as that contained in figure 2. When, for instance, the effective emissivity of an atmospheric path is about 0.5, a change in signal corresponding to a change in emissivity of 0.01 (equivalent to a change in mixing ratio of *ca.* 6 %) could also result from a change in the level being viewed of 0.15 km, which is equivalent to a change in pressure at the tangent point of *ca.* 2 % or 0.003° in viewing direction.

The attitude of the spacecraft is controlled only to *ca.* 0.5° in all three axes; it is therefore necessary from the measurements made by s.a.m.s. itself to determine the appropriate information about the pressure at the part of the atmosphere being observed.

A method for providing this information arises from comparing the signals from a wideband and a pressure modulator channel in the 15 μm CO_2 band. Under the approximation of equation

APPENDIX C

(4) the two signals will be $\epsilon_w B(\bar{T}_w)$ and $\epsilon_p B(\bar{T}_p)$ where the subscripts w and p respectively denote the wideband and pressure modulator channels. Now it is possible to choose the mean cell pressure in the pressure modulator channel such that over a certain range of altitudes the relative contributions of different segments of the atmospheric path being observed are very similar for the two channels, even though the effective emissivity of the atmosphere for the two channels is very different (figure 4). This means that $\bar{T}_w$ and $\bar{T}_p$ will be almost equal. We then find that the ratio ϵ_p/ϵ_w is almost independent of temperature but strongly dependent on the pressure at the level of observation. Figure 5 illustrates that, for a particular cell pressure, atmospheric pressure over the range between 0.8 mbar and 20 mbar may be derived from the ratio of signals in the two channels. A first order correction for the atmospheric temperature profile can be included, enabling pressure measurement of adequate accuracy (*ca.* 2 %) to be achieved. In § 6 an example of the use of the method with s.a.m.s. data is presented.

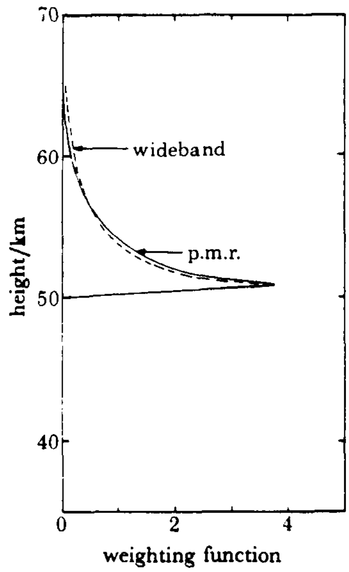

FIGURE 4. A typical pair of CO_2 15 μm weighting functions for the s.a.m.s. attitude-determining channels before the finite field-of-view is accounted for. The tangent height of the line-of-sight is 50 km.

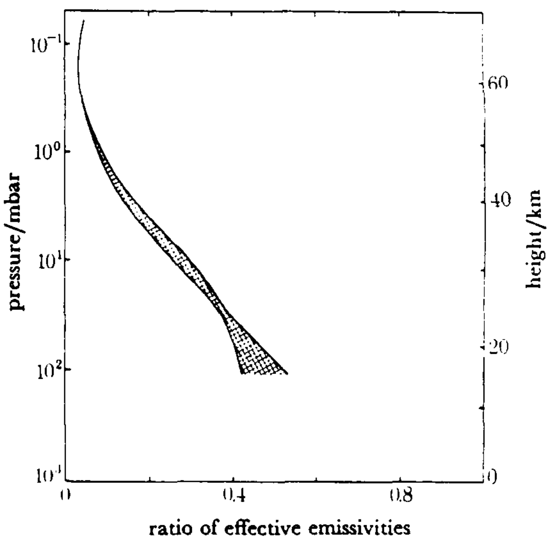

FIGURE 5. Ratio of p.m.r. to wideband emissivities for the 15 μm CO_2 channels C1 at 15 mbar mean cell pressures. The envelope shown is the extreme of a series of curves derived using climatological temperature profiles at 10° latitude intervals from Newell (1977). The effect of the finite instrument field-of-view has also been included in the calculation.

3.4. *Wind determination*

Through the incorporation in the instrument of cells containing the gases whose emission is being detected, the possibility exists of measuring atmospheric motion. If the emitting gas in the atmosphere possesses a significant velocity along the line of sight relative to the gas in the absorbing cells, the emission lines will be shifted relative to the absorbing lines. Figure 6 shows the variation of signal with azimuth angle for a particular case. The direction along which the signal is a maximum is that along which there is zero Doppler shift and hence zero relative velocity of the atmosphere with respect to the spacecraft. If the position of this maximum is determined, knowing the spacecraft velocity vector, and making allowance for the rotation of the Earth, the wind speed along the line of sight can be found. For directions nearly perpendicular to the spacecraft's velocity vector, a change in azimuth direction of 0.1° introduces *ca.* 10 ms^{-1} of the spacecraft's velocity along the line of sight.

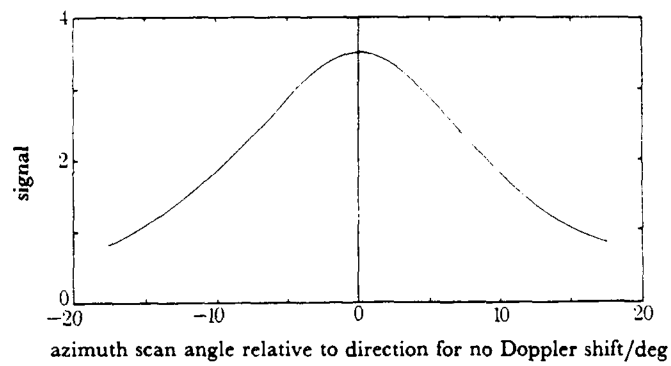

FIGURE 6. Variation of the signal from the 15 μm CO_2 p.m.r. channel with azimuth scan angle relative to the central point where there is no relative motion along the line-of-sight between the atmosphere and the instrument.

So that the influence of atmospheric variations is a minimum, the azimuth scan is carried out at such a rate that during the scan the same part of the atmosphere is kept under observation. A scan over 30° (figure 6) then takes about 240 s. The main problem in carrying out the measurement is that of the maintenance of adequate attitude stability during the period of scan so that the slope of the curve of signal against scan angle is not disturbed by attitude changes. With the Nimbus 7 spacecraft the attitude stability is not adequate for accurate wind determination, although it is hoped that the stability will sometimes be sufficient for the lower mesospheric jet at *ca.* 60 km altitude to be detected.

TABLE 1. S.A.M.S. RADIOMETRIC CHANNELS

field of view	channel	constituent (gas in modulator)	mean cell pressures mbar	spectral band μm	derived quantities and altitude range
A	A1	CO_2	17, 2.4, 0.69, 0.25	15	kinetic temperature 15–80 km; attitude
	A2				ν_2 vibrational temperature 80–100 km
	A3	CO	14.8, 4.5	4–5	
	A4	NO	45, 20		distribution 15–60 km
B	B1	H_2O	16, 4.5, 0.8, 0.5	2.7·	distribution 80–100 km
	B2			25–100	distribution 15–100 km
C	C1	CO_2	36, 11.2, 3.25, 0.87	15	kinetic temperature 15–80 km; attitude
	C2	N_2O	24.4, 7.15	7.7	distribution 15–60 km
	C3	CH_4	47.8, 22.5		

3.5. *Instrument performance*

S.a.m.s. contains a number of channels for various measurements. Some of these channels may be operated simultaneously and some are mutually exclusive. A list of all channels is shown in table 1. Each entry in the constituent column corresponds to a modulator and each entry in the spectral band column to a detector. Since it is only possible to pass one pair of signals (p.m.r. and wideband) through a detector at any one time only one modulator signal using a particular detector may be processed at any time. Therefore, only one of the gases N_2O and CH_4 may be measured at a particular time and only one of CO, NO and 4.3 μm CO_2. A detailed description of how the channels are fitted together in the instrument is given in § 4.

TABLE 2. INSTRUMENT PERFORMANCE FOR TEMPERATURE AND COMPOSITION MEASUREMENTS FROM PRESSURE MODULATOR CHANNELS

gas	CO_2	NO	N_2O/CH_4	CO_2	CO_2	H_2O
band/μm	4.3	5.3	7.7	15	15	25–100
altitude of observation/km	120	40	40	50	100	50
approximate integration time for n.e.e. = 0.03† as measured by s.a.m.s. on Nimbus 7 /s	10000	400	10	4‡	2000	5

† n.e.e. = noise equivalent emissivity. An n.e.e. = 0.03 implies a S/N of 33 when instrument observing black body at atmospheric temperature.
‡ n.e.e. = 0.01 as this is a temperature sounding channel required to measure to ±1 K.

It can be seen from figure 2 that over a large part of the sensitive region for composition sounding a 10% change in composition produces a change of about 3% in the observed signal. In table 2 some typical integration times required to detect such a change are tabulated for various channels in the instrument at typical heights in the atmosphere.

4. The s.a.m.s. instrument

The s.a.m.s. radiometer instrument consists of two modules: the sensor housing containing the optics, mechanisms and detectors, and a separate electronics module. The overall size of the sensor (see figure 8) is 55 cm × 30 cm × 55 cm and it weighs 23.6 kg. The electronics module weighs 6.7 kg. The average power consumption is about 20 W.

There are a total of twelve radiometric channels: six pressure modulator and six wideband channels distributed between three fields-of-view denoted A, B and C. The relation between the three fields is fixed by the geometry of the instrument optics and is illustrated in figure 7. Some of the channels may be used to sense one of several constituents selected by programmable control logic within the instrument (see § 4.7). Figure 7 also shows the scanning range of the instrument for limb views and space calibration.

4.1. *Optical system*

The optical system may be conveniently subdivided into two sections:

(*a*) the front optics comprising scan mirror, telescope, calibration system and wideband chopper;

(*b*) the rear optics comprising field separator mirror, pressure modulator cells, detectors and optical relay components. The front optics is shown in figure 9. Incident radiation is first reflected from the scanning mirror (M1), which can rotate about two axes for both limb (vertical) and azimuth (horizontal) scanning (see § 4.5). It is then reflected from the main paraboloid (M2) to the primary focus forming a telescope of 177 cm^2 area and 22 cm focal length.

During in-flight calibration a small black body is rotated into the beam at the primary focus to give a known input radiance to the rest of the optical system.

After the primary focus the beam is directed by ellipsoid (M3) and plane (M4) mirrors through the fast, shallow chopper (see § 4.4) to the secondary focus at the field separation mirror

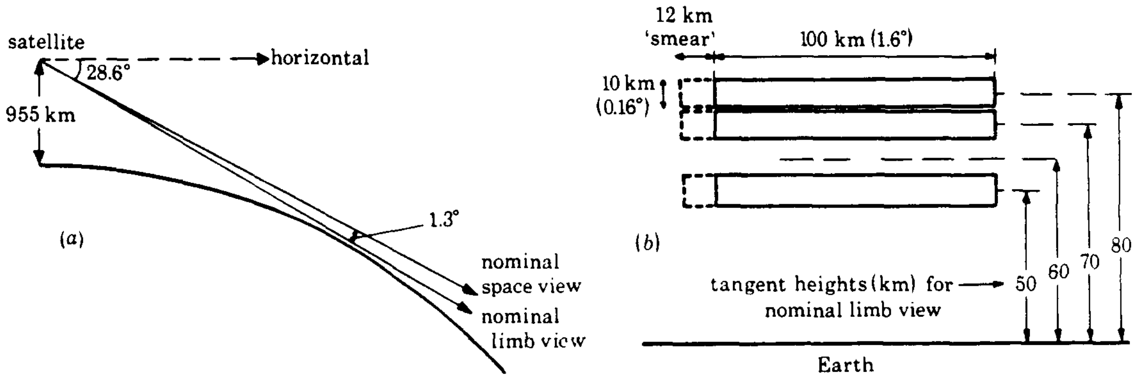

FIGURE 7. (*a*) The geometry of the s.a.m.s. viewing direction. Note that only very small angular moments are necessary to scan the entire atmosphere. As drawn the satellite velocity is into the paper. (*b*) The relative positions of the three fields-of-view A, B and C viewed along the direction of the line of sight in the 'nominal limbview' position. The horizontal smear is caused by spacecraft motion during a 2 s measurement period.

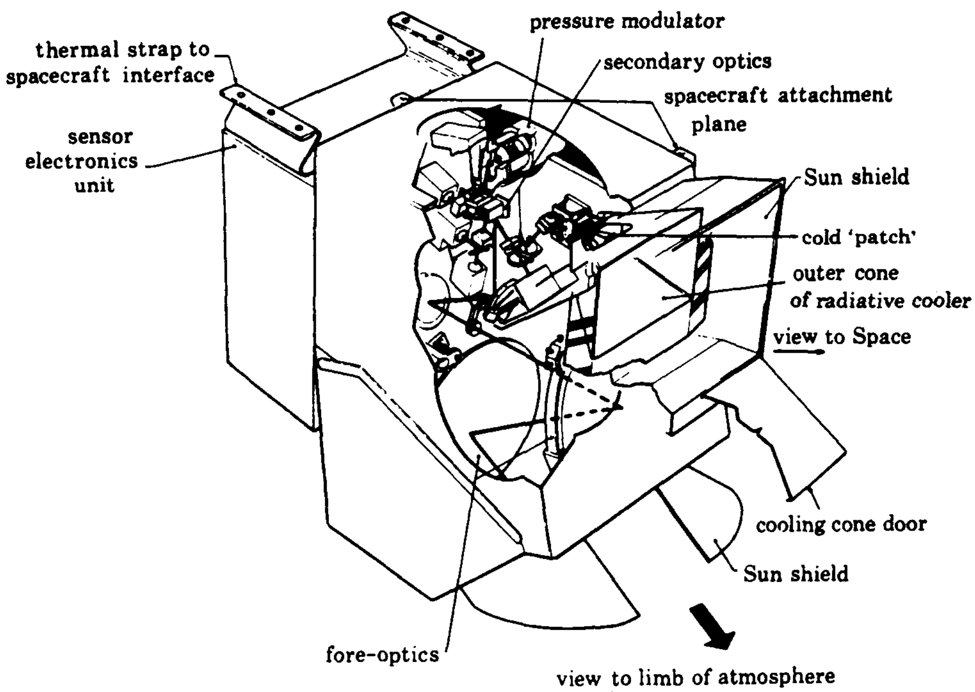

FIGURE 8. Cutaway diagram of the s.a.m.s. sensor unit showing the relative orientation of the optical components, pressure modulators and radiative cooler. The whole unit is located on the sensor ring below the satellite.

15-2

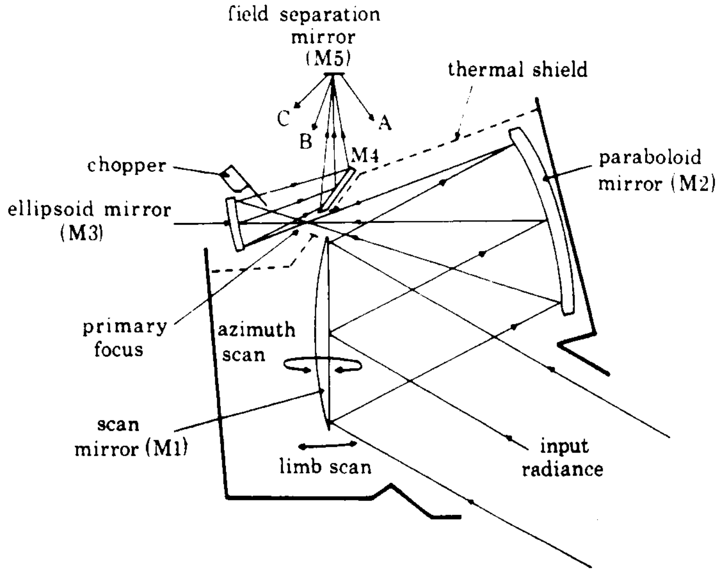

FIGURE 9. The fore-optics of s.a.m.s. in plan view. The calibration black body (not shown) is inserted into the beam at the primary focus. The thermal shield isolates the secondary optics compartment at 25 °C from the front optics compartment at 0 °C.

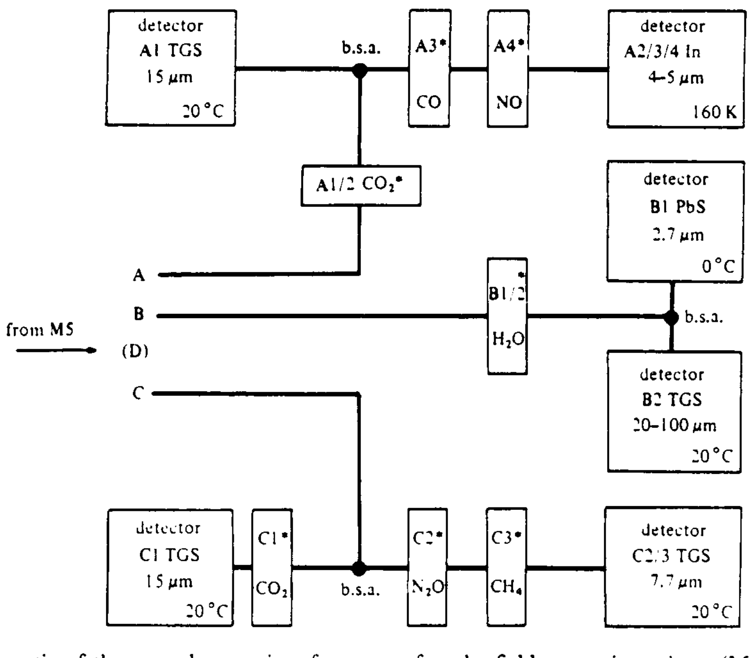

FIGURE 10. Schematic of the secondary optics of s.a.m.s. after the field-separation mirror (M5). The dichroic beamsplitters are marked b.s.A, b.s.B and b.s.C. Secondary mirrors relay lenses and other optical components have been omitted for clarity. The beam marked (D) corresponds to a facet of M5 that reflects the input beam back through the front optics and is used for optical alignment. The pressure modulator cells are identified by an asterisk (*).

(M5). The use of an ellipsoid in the M3 position cancels some of the aberrations of the off-axis paraboloid (M2).

Thermal isolation of the compartment containing the first two mirrors, i.e. those before the primary focus and calibration point, allows these mirrors to be run at a somewhat lower temperature (0 °C) than the rest of the instrument, thus reducing the thermal strays from this area and increasing the reliability of the calibration.

The rear optics are shown in the correct spatial orientation in figure 8 and in schematic form in figure 10. Field separation occurs at three of the four facets of the mirror M5 which are angled to direct parts of the beam into one of three separate optical chains, and curved to image M3 on the detector aperture stop. Each of the fields so defined is rectangular and subtends an angle in the instrument line-of-sight $0.16° \times 1.6°$, a solid angle of 7.8×10^{-5} sr (figure 7).

Broad spectral selection for the different molecular bands is achieved by dichroic beam-splitters (b.s.A, b.s.B, b.s.C) and filter packs of up to three separate components on the various detectors. The pressure modulator windows are either anti-reflexion coated or are made of low refractive index materials. In all there are about 40 individual optical components in the system after M5. High optical transmission in the system is maintained by the use of anti-reflexion coatings. As an example, the overall transmission of the C2/3 chain with 19 surfaces is still 67 % at band centre.

The rear optics, modulators and detectors are mechanically and, except for the 2.7 μm PbS and 4–5 μm InSb detectors (B1 and A2/3/4), thermally attached to the main optics plate made of aluminium 1 cm thick giving good thermal uniformity and capacity as well as mechanical stability.

4.2. *Detectors*

There are six detectors in s.a.m.s., four triglycine sulphate (TGS), one lead sulphide (PbS) and one indium antimonide (InSb). Each detector flake is imaged by its optical system on to one of the facets of M5 and, therefore, the aspect ratio of the detectors is the aspect ratio of the field of view. Each detector is 3.12 mm × 0.312 mm, giving an area of approximately 1 mm^2.

The detectors are each assembled and tested as sub-assemblies consisting of detector, pre-amplifier, condensing optical system and filters before being integrated with the rest of the instrument. A TGS sub-assembly is shown in figure 11. The condensing optical doublet, consisting of a meniscus and a plano-convex lens (see Murray 1962), is made of anti-reflexion coated germanium (except in the case of the 25–100 μm H_2O channel (B2) where silicon is used). The package consisting of the meniscus lens detector and mounting flange is evacuated to protect the detectors from moisture during ground operations.

The sub-assemblies for the cooled detectors are more complicated than those for the TGS because of the need to isolate the detector thermally while mechanically attaching it to the optics plate. The B1 and A2/3/4 detectors are cooled radiatively, the B1 to 0 °C by a radiator in the fore optics compartment and the A2/3/4 to 160 K by a separate radiative cooler (see § 4.6).

4.3. *Pressure modulator assemblies*

The pressure modulators used in s.a.m.s. are a development of those used in the Nimbus 6 p.m.r. instrument (see Curtis *et al.* 1974). The pressure of the gas in the optical cell is altered by means of a piston oscillating at between 25 and 40 Hz in a connecting volume (figure 12). A pressure variation over the cycle of the order 2:1 is achieved in this design, the exact value depending on the dimensions of the particular optical cell and the mean cell pressure. The principal

APPENDIX C

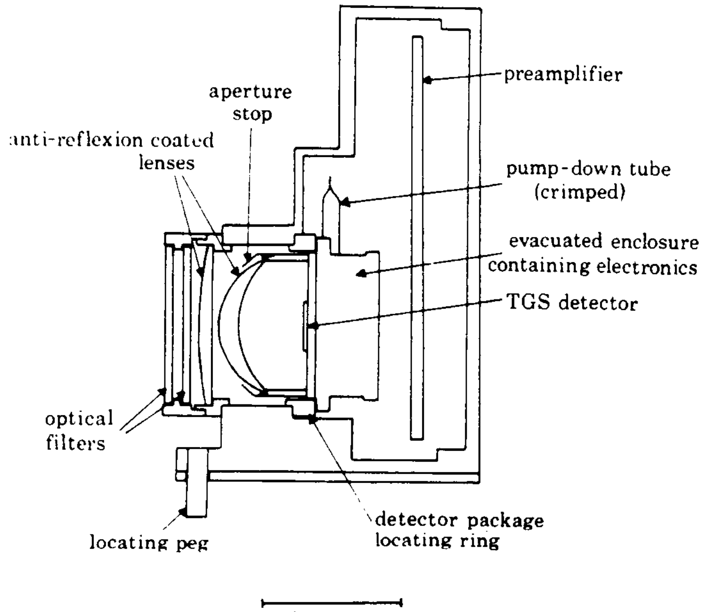

FIGURE 11. S.a.m.s. detector sub-assembly (TGS). Because the impedance of a TGS detector is very high and the signal small, part of the preamplifier is built into the back of the detector package within the evacuated enclosure. Precise optical alignment is essential, both of the package to the sub-assembly and of the sub-assembly to the secondary optics mounting plate. In the former case a close-fitting ring is used and in the latter a precision locating peg.

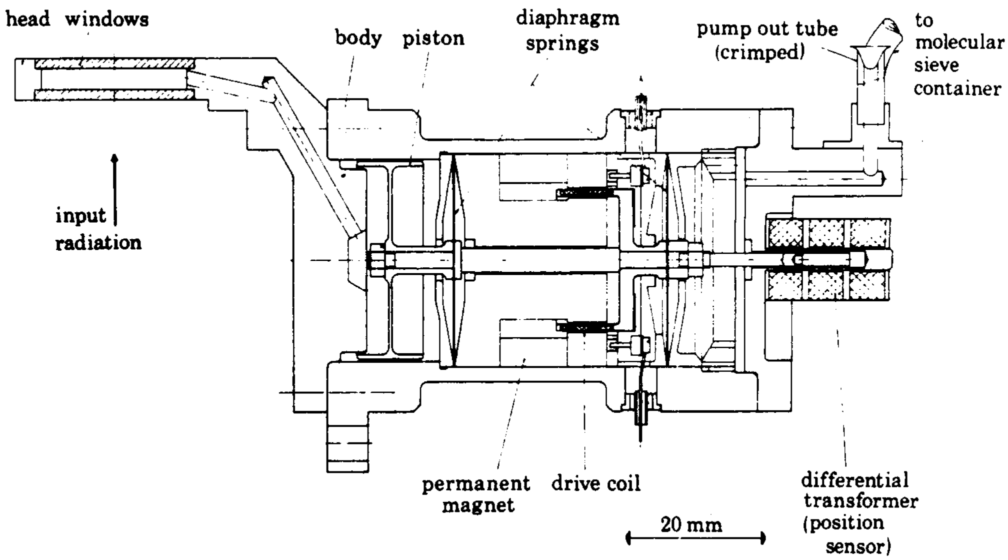

FIGURE 12. Cross section of a p.m.r. assembly. The body of the PMR is made of titanium with gold 'O' ring seals at each end. The support springs and coil lead-outs are made of beryllium–copper. The thermostatted container of molecular sieve is not shown.

changes from the devices used in the Nimbus 6 instrument are a reduction of size by a factor of approximately 2 and the use of a moving coil drive leading to better amplitude control and electrical efficiency. Other improvements have made the modulators easier to manufacture and assemble. It is necessary, as was observed in § 3.2, to alter the pressure of gas in the cell in flight, the pressure selected depending on the altitude range being scanned. This is achieved in the s.a.m.s. modulators as follows. The gas in the cell is in equilibrium with a much larger amount adsorbed on a zeolite molecular sieve material in a reservoir (figure 12). In this system the mean pressure of gas is determined by the temperature of the sieve, and provision has therefore been made for programmable temperature control of the sieve container. Each modulator is provided with two or four pressure settings, which may encompass a range of over 20:1, corresponding to a thermostat temperature range of 30–120 °C. These settings are selected by the program control logic. The adsorption and desorption of gas from the sieve is entirely reversible and the system provides good pressure stabilization. Measurement of the oscillation frequency, which changes rapidly with pressure, is used as the primary method of determining cell pressure since slow variations in gas amount, such as might be caused by a leak in a modulator, could not be detected by monitoring the sieve temperature.

4.4. *Fast chopper assembly*

The fast chopper used on s.a.m.s. only modulates 2.5 % of the beam for reasons described above (see § 2.3). It consists of two etched, black-painted copper grids, mounted one above the other. One grid is fixed to the mount but the other is free to move on the end of a flat cantilever leaf spring. Oscillation, at the mechanical resonant frequency of the spring–grid assembly, is maintained by an electronic loop using redundant pairs of piezoelectric ceramic plates as both drive and position sensors. Oscillation is at a frequency of approximately 245 Hz with a peak-to-peak amplitude of 2 mm.

4.5. *Scan mirror assembly*

The scan mirror must be rotated with high positional accuracy in two mutually perpendicular directions to produce limb and azimuth scanning. This is realized by supporting the mirror in two frames, one within the other, for the two scan directions. Each mirror drive consists of a lead-screw directly driven by a 45° stepping motor. Coupling to the mirror is by means of a recirculating-ball nut, which is lubricated by a lead coating. The axis of rotation of the mirror is defined by a pair of cross-leaf springs (flexipivots). The step sizes of the drive system, expressed in terms of motion of the line-of-sight, are 4.8 arc min in the limb direction and 7.3 arc min in azimuth.

Mirror position is independently sensed in both directions by a linear variable differential transformer (l.v.d.t.), actuated directly by the mirror, and associated electronics. The output of the limb l.v.d.t. is digitized with a resolution of 0.045 arc min and the azimuth l.v.d.t. to 1.8 arc min. It is therefore possible to monitor the limb position of the mirror to a very much higher accuracy than the step size. The limb position is under full control of the program control logic (p.c.l.) (see § 4.7), whereas the azimuth scan can only be programmed as a continuous scan or stepped.

Limit detectors, both optical and mechanical, are provided for resynchronizing the control logic and preventing damage under fault conditions.

4.6. *Radiation cooler*

The indium antimonide detector is cooled by a two stage radiation cooler, the first high-capacity stage forming a cone around the second stage as shown in figure 13. The first stage cools the front lens of the optical doublet (see § 4.2) as well as pre-cooling the rear lens and detector. In orbit, the inner and outer cooler temperatures are typically 160 K and 190 K.

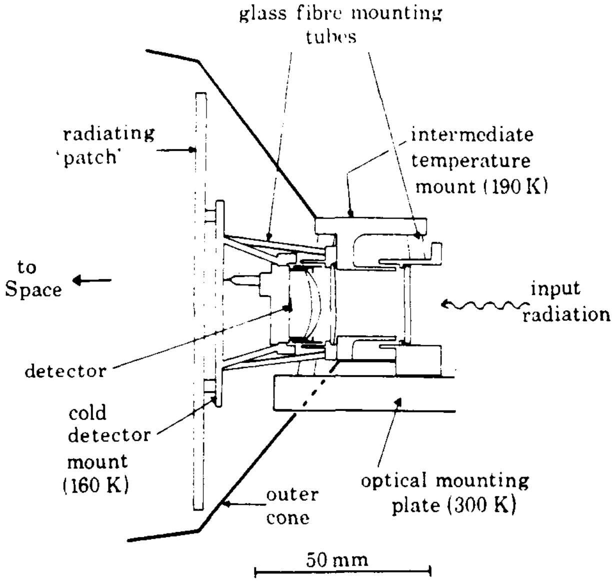

FIGURE 13. The s.a.m.s. cold detector assembly (InSb). The mount is in three parts: the detector mount at 160 K, the intermediate lens mount at 190 K and the mechanical interface at 298 K. The parts are interconnected by 8 glass fibre tubes, some of which may be seen in the diagram. The relative sizes of the 'radiating patch', which is black-painted, and the outer cone, which is coated with vapour deposited aluminium, can be seen in figure 8.

The cooler has been designed to minimize the effects of contamination on the optics as the spacecraft outgases; however, provision has been made to heat the detector and optics electrically to remove the debris as necessary. The cooler surfaces were protected during launch and the first 3 weeks of orbit by a door which was opened on 13 November 1978. The door cannot be closed again and will remain open for the duration of the mission.

4.7. *Electronics*

The electronics of s.a.m.s. is considerably more complicated than that of previous instruments built at Oxford for three reasons:

(*a*) there are more signal channels (twelve in all) and modulator drives (seven);

(*b*) the increased number of signal channels and drives means that more care must be taken to ensure that coupling and cross-talk, both electrical and mechanical, is minimized.

(*c*) The scan and calibration control system is considerably more flexible than previous instruments allowing in-flight programming.

The major changes in construction details since previous instruments are the use of integrated circuit amplifiers in the linear electronics and CMOS in the digital electronics. A full block diagram of the system is shown in figure 14.

APPENDIX C

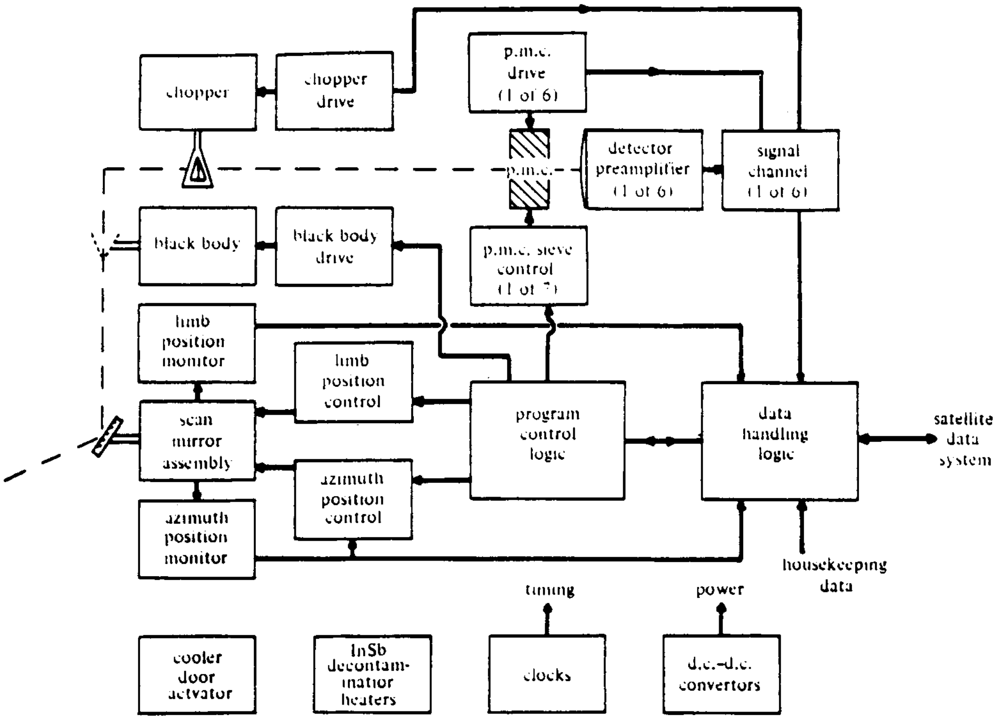

FIGURE 14. Block diagram of the s.a.m.s. electronics subsystems.

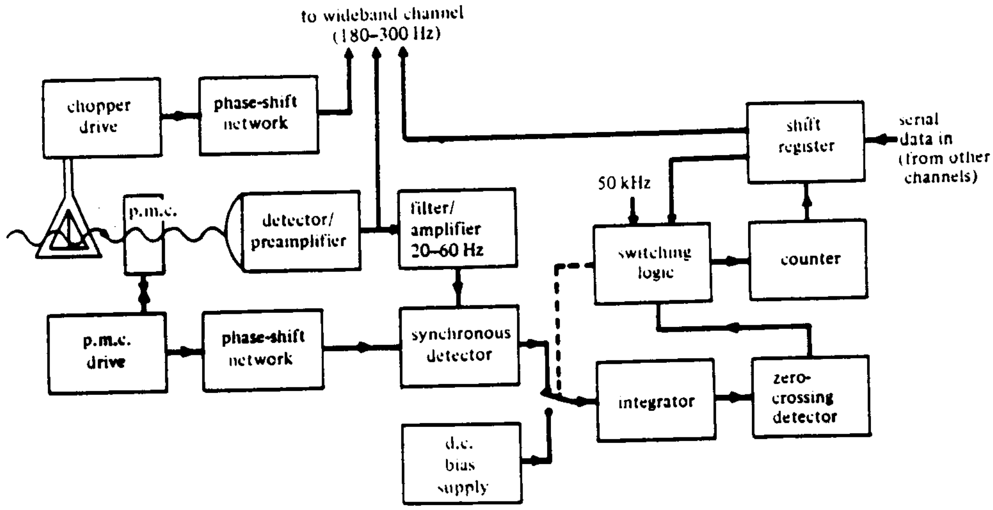

FIGURE 15. Block diagram of one half of a signal channel. Data from all channels is transferred to the data handling system in a single serial stream.

(*a*) *Signal channels*

The signal processing electronics follows the pattern of the system used for a previous balloon radiometer (see Chaloner *et al.* 1978). The high and low frequencies (wideband and pressure modulated signals respectively) present at the detector output are processed by separate channels as shown in the block diagram in figure 15. The output integrator of each channel is also made to act as a dual-slope analogue-to-digital converter. This is achieved by integrating the signal, plus a small offset to ensure that the result is positive, for 1.8 s, and then integrating a fixed negative signal until the result is zero. By timing the second integration period with the use of the 50 kHz spacecraft clock, a resolution of 1 part/10^4 is obtained in the remaining 200 ms of the 2 s period. Only 12 bits are actually telemetred to the ground but the 13th can be inferred, if necessary, by context. The 200 ms period while the signals are evaluated is also used to step the scan mirror.

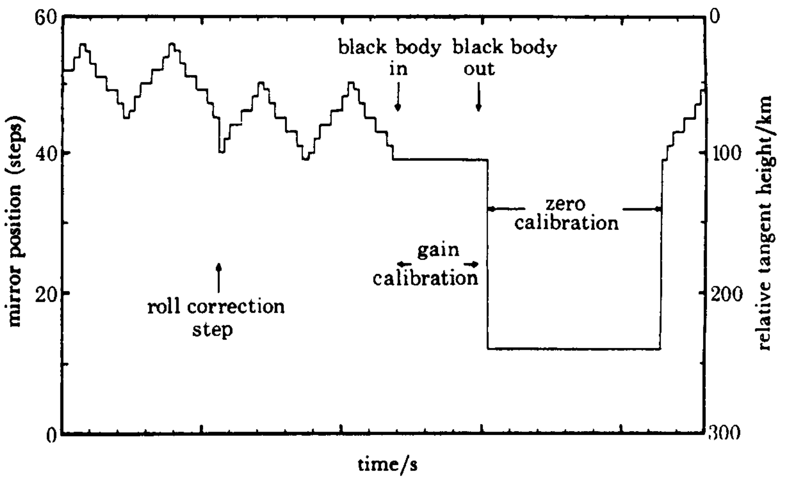

FIGURE 16. A typical scan program. There are 18 scans (up and down ramps) between calibration sequences leading to an interval between calibrations which is not synchronous with the orbital period. Roll correction is applied independently, synchronous with the orbital period.

(*b*) *Pressure modulator drives*

The drive circuits for the pressure modulators are considerably more complex than those used for the Nimbus 6 p.m.r. or the balloon instrument. The complexity is necessary because of the need to maintain a constant amplitude despite large internal pressure variations, which in turn lead to large changes in frequency and power requirements. The use of a moving coil drive, with its inherently tighter coupling than the previous moving magnet drive, assists with amplitude control and also allows active damping to be employed when a modulator is inhibited. Active damping is useful in multiple channels with only one detector (e.g. A2/3/4) since unwanted mechanical energy could otherwise be coupled into the 'off' modulators and appear as unwanted modulation in the detector output. This can be prevented by switching the drive from positive (oscillating) to negative (damping) feedback when the modulator is inhibited.

(*c*) *Program control logic* (*p.c.l.*)

The extremely large number of possible operating modes for s.a.m.s. using various combinations of modulators, scanning ranges and mean cell pressures, and the need to correct the scanning sequences for any predictable orbital roll of the spacecraft, made a programmable operating mode very desirable. The system used operates the scan mirror, modulators, molecular sieves, thermostats and calibration black body by reference to a stored 'program' in a 128×10 bit memory which may be reloaded from the ground. The instruction set of the p.c.l. also includes jump, wait, synchronizing and timing instructions to allow program loops to be constructed which operate in a fixed relationship to the spacecraft data system. The variations of scanning and calibration are, therefore, infinite and it is possible to adapt the scanning sequence to partially compensate for orbital roll. It is also possible to scan outside the atmosphere, for example, to locate the moon for calibration purposes.

A typical scan sequence is shown in figure 16. This program is designed to scan a height range of 55 km in 10 km steps with regular calibration sequences not related to the orbital period. A roll correction step can also be seen.

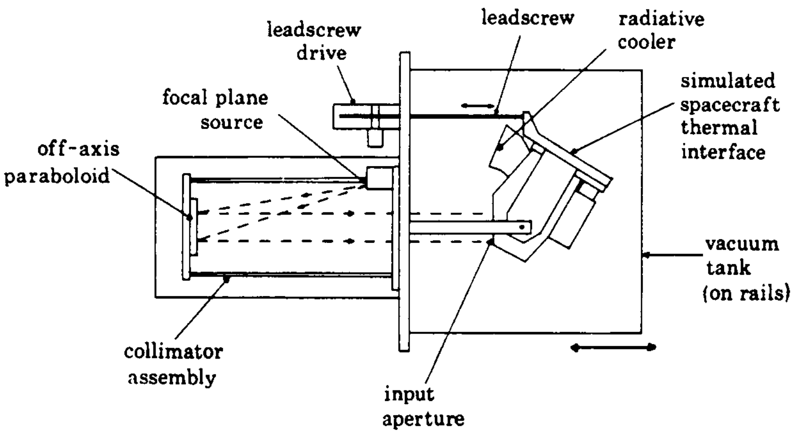

FIGURE 17. S.a.m.s. environmental test chamber at Oxford. Baffles, cooled by liquid nitrogen, surround the instrument to simulate radiative loss to space but these have been omitted for clarity. Access is provided by rolling the main vacuum tank away on rails. The collimator assembly is shown in position. The black body assembly (see text) may be substituted for the collimator when required.

5. Verification and calibration performance

In addition to the tests that were necessary to prove the design of the instrument and the environmental tests specified by N.A.S.A., s.a.m.s. has undergone the following series of measurements intended to facilitate the interpretation of data when in orbit.

(*a*) The response of the instrument to known black body radiance inputs has been measured, and a calibration scheme devised to take account of variations in operating conditions.

(*b*) The response of the instrument to emission from gases in the atmosphere has been determined, using a simulated atmospheric path, in order to verify the spectroscopic calculations by which atmospheric quantities are deduced.

(*c*) The field of view profiles of all the channels and their interrelation has been measured.

(*d*) The scan mirror position telemetry (see § 4.5) has been accurately calibrated in terms of the instrument line-of-sight. A combined vacuum and thermal environment chamber at Oxford provides correct simulation of the spacecraft interface and orbital conditions. Various additional radiation sources are also available within the chamber for calibration purposes (see figure 17).

5.1. *Radiometric calibration*

The response of the instrument is determined for a range of accurately known black body radiances in order to

(*a*) verify that the instrument response is linear and has the correct gain and noise levels;

(*b*) check that the spectral selection of the optics is correct and that there are no unknown spectral 'leaks' in the overall response;

(*c*) provide a basis for the model of the instrument used in the in-flight calibration scheme;

(*d*) determine the magnitude of any stray responses, particularly those which depend on either azimuth or limb scan angle. The source used for this test is a large, baffled black-body cone, completely filling the instrument aperture, whose temperature may be held constant and uniform at any temperature between 77 K and 320 K. The input radiance is, therefore, very precisely calculable. There are in fact two sources, one on the instrument axis viewed with the azimuth scan centralized and one off-axis viewed at the limit of the azimuth scan. By using both targets, the variations of strays with azimuth scan angle may be established.

Variations with limb-scan angle are measured by tilting the whole instrument using a precision lead-screw, thus varying the relative position of the on-axis target and the instrument.

The sensor temperature is held constant during measurements of stray radiation but may be varied or cycled over a considerable range (-5 to $+40$ °C), in order to dynamically evaluate the temperature coefficients of the response. By simulating the orbital temperature variations of the spacecraft experience is gained of the likely instrument temperature variations in orbit – a verification of the sensor thermal design.

5.2. *Response of p.m. channels to atmospheric paths*

The response of the channels to paths of gas is checked by measurment of the transmission of simulated atmospheric paths in the laboratory, using either the actual sensor modulators, filters and detectors before finaL assembly of devices identical in design and construction. The apparatus consists of a multiple-pass absorption white cell which provides paths of up to 10 m, which may be used at temperatures down to 240 K (see Houghton & Taylor 1973). Transmissions of isothermal paths of the required absorber or absorber/nitrogen mixtures measured with this equipment as a function of pressure are then compared with the response calculated from line data, and information from both sources is combined in the transmission model used in the final attitude, temperature and composition retrievals.

5.3. *Field of view*

The attitude of the sensor line of sight is determined in orbit from the ratio of the pressure modulator and wideband signals in the CO_2 channels (see § 3.3). The line-of-sight of the other channels, therefore, needs to be measured with respect to these. The details of the field profiles, especially the shape of the lower edge, also critically affect the weighting function of the channels and must also be determined.

For field of view determination the black cones are replaced by a collimator (see figure 17). This consists of an off-axis paraboloid mirror, with a narrow slit illuminated by a hot ceramic filament in the focal plane. The lead screw system is used to rotate the s.a.m.s. sensor through the parallel beam of radiation from the collimator at a precisely known rate, and the field response is thus determined.

The collimator assembly and leadscrew are also used for various optical checks and in particular for the calibration of the l.v.d.t. system used for limb scan angle telemetry. The lead screw is driven slowly and continuously while the p.c.l. is programmed to step the s.a.m.s. scan mirror so that the edge of the field of view of a selected channel passes through the collimated beam once per step. By matching the respective points on the field response, the l.v.d.t. system is calibrated directly in terms of the line-of-sight. This test and the primary field of view determination are carried out at several temperatures over the desired operating range.

5.4. *In-flight calibration*

A two point calibration is provided in flight as follows.

(*a*) The scan mirror may be programmed to move so that the tangent height viewed in the atmosphere is sufficiently high that the atmospheric radiance is insignificant ('space' view). This is arranged in operational programs such that the minimum tangent height for the lowest field of view (the C channels) is at least 150 km.

(*b*) The black body (see § 4.1) may be placed in the optical path to provide a standard radiance at approximately 295 K. This is also under the control of the p.c.l.

In practice the estimate of the space view signal is much more important than the measurement of gain, as many of the measurements made are of small differences from the zero radiance level. Operational p.c.l. programs are therefore arranged to have a higher proportion of space view calibration than of black body view as shown in figure 16.

In flight the zero offset and radiometric gain are calculated from instrument housekeeping data by means of a model, the parameters of which have been obtained by combining the results of ground tests and in-flight calibration measurements.

6. Preliminary results

Calibrated radiance data from s.a.m.s. is processed in the following sequence. A preliminary estimate is obtained of the tangent pressure of the line-of-sight of all three fields-of-view at all times using the method described in § 3.3. Then the atmospheric temperature profile and a better estimate of the tangent pressure are derived from the preliminary estimate of tangent pressure and the CO_2 channel radiances. Finally, this information is used, together with radiances from the other channels, to retrieve constituent profiles. These three steps are described in some detail below.

6.1. *Attitude determination*

As has already been shown in § 3.3 the tangent pressure of the line-of-sight of the CO_2 channels can be determined from the ratio of the wideband to p.m.r. radiances assuming that the tangent height is within a suitable range (approximately 20–50 km). Since the space-craft roll rate is reasonably low and the orbital period long compared to the rate of sounding (1 every 2 s), smoothing along the orbit path, i.e. in time, is applied using a linear sequential estimator (Kalman–Bucy filtering, see Rodgers 1976). To achieve this the tangent pressure is converted, using a climatological temperature profile and the scan mirror position, to the tangent height of a reference scan mirror position. This tangent height estimate is then smoothed.

The estimator is stepped forwards along the orbit and for each new observation a smoothed estimate of the tangent height and its uncertainty are calculated given the observation and its error, the previous smoothed estimate and its error, the variation in scan mirror position measured by the l.v.d.t., the time between observations and a knowledge of the likely maximum roll rate. The process is repeated backwards along the orbit and the two results at each observation point are combined to derive a best estimate of the roll angle at any point. The smoothed roll-angle is then reconverted to tangent pressure for each field of view. The results for a typical orbit are shown in figure 18.

The smoothing process is capable of dealing automatically with missing data caused either by bad soundings or a tangent height out of the range where attitude determination is possible. Prolonged loss of information produces a steadily increasing uncertainty in the attitude.

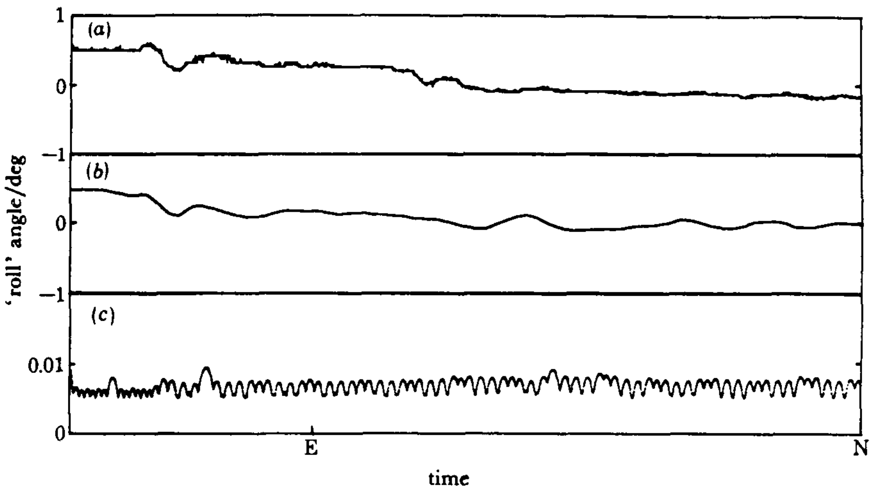

FIGURE 18. A comparison of the 'roll' angle derived as described in the text with the output of the spacecraft attitude control system (for part of orbit 135 of Nimbus 7). For reasons described in the text these are not necessarily comparable but short timescale features should be reproduced. The error in the derived roll error is in a scale magnified 100× relative to the other two plots. E = equator, N = most northerly latitude of orbit. (*a*) Spacecraft attitude control system roll output; (*b*) s.a.m.s. derived 'roll'; (*c*) s.a.m.s. derived 'roll' error.

6.2. *Temperature retrieval*

The short wave channels are particularly sensitive to atmospheric temperature (5 % per degree for the 5 μm channel) so accurate temperature retrievals are of particular importance for making good constituent measurements. It is also possible to improve further upon the attitude determination described above which assumed climatological temperature profiles. Temperature profiles and an improved attitude are, therefore, retrieved simultaneously.

Since there are a large number of possible scan patterns in use, the retrieval method must be able to handle any pattern selected and must, therefore, be very flexible. Were the instrument quickly scanning up and down through the whole atmosphere, complete sets of radiances for a scan could be assembled and the retrieval performed by simpler methods. But there is a need to incorporate observations when and where they occur, essentially at random, and a sequential estimator is again used. For economy of computation the retrieval solution is represented by coefficients of 12 eigenfunctions, giving the deviation of source function at 15 μm from the climatological mean (interpolated linearly from monthly means at 10° latitude intervals). They are eigenfunctions of the covariance matrix

$$C_{ij} = \exp\left(-(z_i - z_j)^2/\alpha^2\right) \frac{dB(z_i)}{dT}\,\frac{dB(z_j)}{dT},$$

where z_i is the scale height of level i and $dB(z_i)/dT$ is the differential with respect to temperature at level z_i. This is the Planck function covariance resulting from a set of wave perturbations in

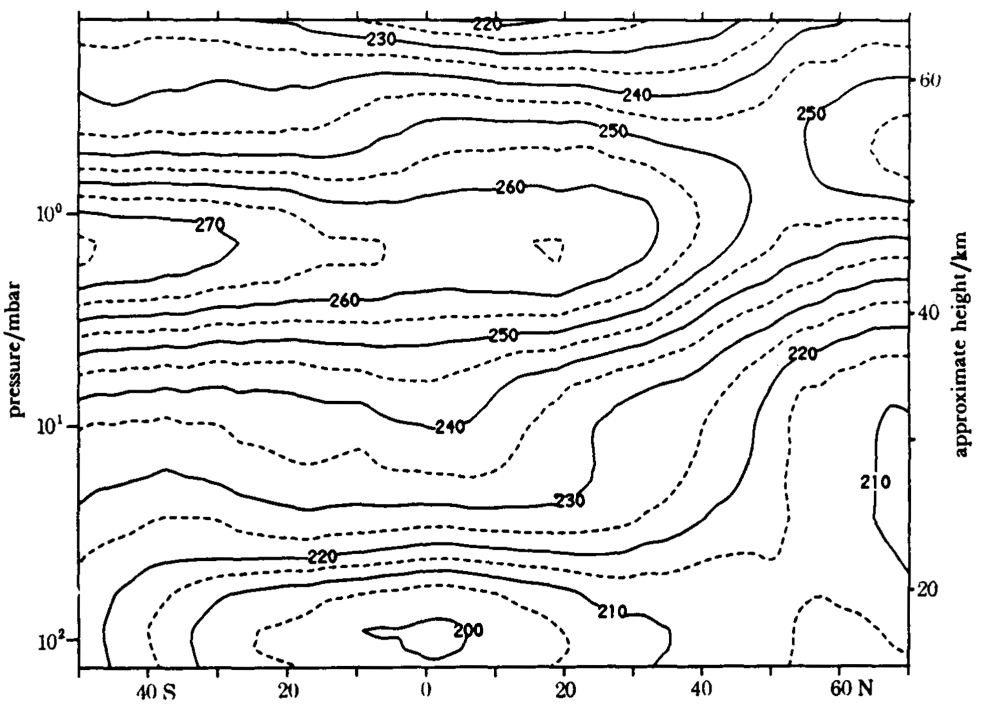

FIGURE 19. Zonal mean temperature cross section for 6 November 1978 derived entirely from Nimbus 7 s.a.m.s. data.

the vertical with a Gaussian spectrum and temperature amplitude independent of height. Using the estimate of attitude derived as above, the deviation of observed radiance from its climatological value can be represented linearly in terms of the solution which consists of the eigenfunction coefficients and the attitude. By these means a linear sequential estimator can be employed in a similar manner to the attitude determination described above. In the absence of input data the solution is made to decay exponentially with time towards zero (i.e. towards its climatological value) so that when there is no information about some or all levels, any deviations for those levels are slowly forgotten. When run forwards along the orbit the estimator is recursive and one-sided, using just past and present data to give the solution. However, an independent set of estimates is obtained by running the estimator backwards along the orbit. At $2\frac{1}{2}°$ latitude intervals along the orbit both estimates are combined in accordance with their uncertainties and the result retained for derivation of temperatures and analysis on latitude–longitude grids. A typical zonal mean cross section is shown in figure 19.

6.3. *Concentration retrievals*

Using the derived tangent heights and temperatures it is now possible to obtain concentration profiles from the data. Figure 20 shows some typical results for the H_2O rotation band (channel B2) in both the p.m.r. and wideband cases.

The solid lines were calculated using the temperature data derived using the methods described above, water vapour band data from McClatchey *et al.* (1973) and Chaloner (1976) and a computer program to simulate atmospheric signals due to Eyre (1978).

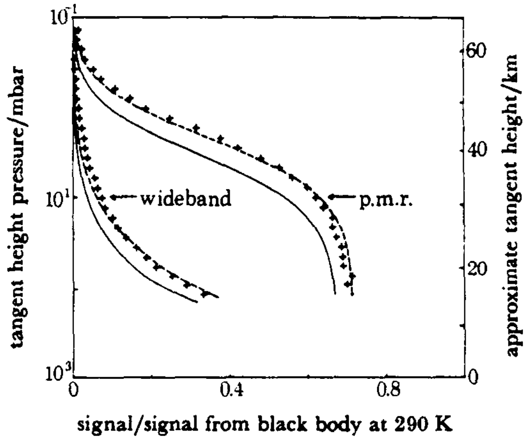

FIGURE 20. Water vapour signal from s.a.m.s. (on 6 November 1978 for latitudes between 20° N and 20° S) compared with signals calculated for constant volume mixing ratio profiles. It can be seen that the p.m.r. signals indicate a slight fall in mixing ratio from 50 to 30 km which becomes pronounced in the wideband signal between 30 and 18 km where there are uncertainties due to clouds and other effects associated with the tropopause. +, S.a.m.s. data; ---, 5 parts/10^6 by volume; —, 2 parts/10^6 by volume.

Because the data is of a preliminary nature, a profile of concentration versus altitude is not presented. However, it can be seen that the results are inconsistent with a constant mixing ratio profile but would be consistent with a slow rise starting at 20 km levelling off above 35 km. This type of behaviour would be expected if the photolytic destruction of CH_4 were a source of H_2O in the middle stratosphere (McConnell *et al.* 1971).

The project has been supported by the Science Research Council. We particularly acknowledge the invaluable work of the Project Manager, Mr K. H. Davies. Technical support at Oxford was given by Dr P. Curtis, Mr M. Clarke, Mr S. Werrett, Mr M. W. Johnson, Mr I. Colbeck and Mrs C. E. Holt. Substantial assistance in several areas was given by the Rutherford Laboratory, in particular by Mr H. Hadley, Mr J. Parker, Mr R. Wolfenden, Mr G. Stapleton, Mr T. Morgan, Mr R. Elsey and Mr P. Gear. The optical filters and windows were made by Dr J. S. Seeley and Mr R. Hunneman of Reading University. Hawker Siddeley Dynamics (now British Aerospace) at Stevenage built the flight models; we thank in particular Mr G. W. Cocks, Mr J. Bonsor, Mr C. Collins and Mr I. White. Mr W. Andiario has been the experiment representative at the General Electric Company, Valley Forge, during integration of the experiment in the spacecraft. The experiment representative with Nimbus Project, N.A.S.A., was Mr R. White. We gratefully acknowledge the generous cooperation of all members of the Nimbus Project, N.A.S.A.

APPENDIX C

REFERENCES (Drummond *et al.*)

Chaloner, C. P. 1976 D. Phil. Thesis, University of Oxford.
Chaloner, C. P., Drummond, J. R., Houghton, J. T., Jarnot, R. F. & Roscoe, H. K. 1978 *Proc. R. Soc. Lond.* A **364**, 145–159.
Curtis, P. D., Houghton, J. T., Peskett, G. D. & Rodgers, C. D. 1974 *Proc. R. Soc. Lond.* A **337**, 135–150.
Drummond, J. R. & Jarnot, R. F. 1978 *Proc. R. Soc. Lond.* A **364**, 237–254.
Ellis, P. J., Holah, G., Houghton, J. T., Jones, T. S., Peckham, G., Peskett, G. D., Pick, D. R., Rodgers, C. D., Roscoe, H. K., Sandwell, R., Smith, S. D. & Williamson, E. J. 1973 *Proc. R. Soc. Lond.* A **334**, 149–170.
Eyre, J. R. 1978 D.Phil. Thesis, University of Oxford.
Gille, J. C., Bailey, P., House, F. B., Craig, R. A. & Thomas, J. R. 1975 *The Nimbus* 6 *user's Guide*. Goddard Space Flight Center, Greenbelt, Maryland.
Houghton, J. T. & Smith, S. D. 1970 *Proc. R. Soc. Lond.* A **320**, 23–33.
Houghton, J. T. & Taylor, F. W. 1973 *Rep. Prog. Phys.* **36**, 827–919.
McClatchey, R. A., Benedict, W. S., Clough, S. A., Burch, D. E. & Calfee, R. F. 1973 *A.F.C.R.L. atmospheric absorption line parameters compilation*. AFCRL-TR-73-0096 Environmental Research.
McConnell, J. C., McElroy, M. B. & Wofsy, S. C. 1971 *Nature, Lond.* **223**, 187–188.
Murray, A. E. 1962 *Infrared Phys.* **2**, 37–47.
Rodgers, C. D. 1976 *Rev. Geophys. Space Sci.* **14**, 609–624.
Taylor, F. W., Houghton, J. T., Peskett, G. D., Rodgers, C. D. & Williamson, E. J. 1972 *Appl. Opt.* **11**, 135–141.

APPENDIX D

RETRIEVAL OF TEMPERATURE AND COMPOSITION FROM NIMBUS-7 SAMS MEASUREMENTS

[Reproduced from *Journal of Geophysical Research, 89,* 5280-5286 (1984).]

JOURNAL OF GEOPHYSICAL RESEARCH, VOL. 89, NO. D4, PAGES 5280-5286, JUNE 30, 1984

Retrieval of Temperature and Composition From NIMBUS 7 SAMS Measurements

C. D. Rodgers, R. L. Jones, and J. J. Barnett

Clarendon Laboratory, University of Oxford

A general purpose stochastic sequential estimator is described, which allows the inverse problem of remote sounding to be solved in an optimum manner. The use of a sequential estimator allows continuity in the horizontal or in time to be included, making the a priori estimate close to the final solution, so that iteration is not required. The scan pattern in which measurements are made is not used and need not be known, so that the problem of spacecraft attitude stability is minimized. The method gives both a solution profile and its error covariance. It is applied to both temperature and composition sounding from a limb scanning instrument, the SAMS on NIMBUS 7.

1. Introduction

The Stratospheric and Mesospheric Sounder (SAMS) on NIMBUS 7 is described in detail by *Drummond et al.* [1980]. It is designed to measure temperature and concentration profiles of various gases in the height range of 15-100 km by detecting thermal emission or, in some cases, resonantly scattered sunlight. It obtains information about vertical distribution by scanning the limb and uses the technique of gas correlation by pressure modulation to select the required spectral signal from the gases being measured. A summary of the spectral channels used and the characteristics of these channels is given in Table 1. There are three fields of view, A, B, and C, separated in the vertical, with A highest in the atmosphere. All the fields of view are approximately Gaussian, with a vertical width of about 8 km.

In the technique of pressure modulation, a cell of the gas whose emission is to be measured is used as a filter, in conjunction with an interference filter to select the appropriate spectral band. The pressure in the cell is modulated, and the transmitted radiation is detected at the modulation frequency to give a measurement of radiation originating near the line centers, integrated over the whole spectral interval. By chopping the beam with a black chopper at a different frequency, a parallel measurement of emission over the whole band (excluding the line centers) is obtained. These measurements are known as pressure modulated (PM) and wide band (WB), respectively.

The radiance $L_i(h)$ received at the instrument from the limb (Figure 1) can be written

$$L_i(h) = \int_{-\infty}^{\infty} B[\nu, T(x)] \frac{d\tau}{dx}(\nu, x)\, dx$$

where h is the tangent height of the line of sight, $B[\nu, T]$ is the Planck function at wave number ν and temperature T, and $\tau(\nu, x)$ is the transmittance from position x to the instrument.

The retrieval (inverse) problem divides into two parts, temperature and composition. The temperature profile is determined from the two 15 μm CO_2 PM channels and the two corresponding WB channels in the A and C fields of view which are separated by 0.56° (about 35 km). The composition profile is determined from radiances in the remaining channels but requires the temperature profile as input.

Paper number 3D1686.
0148-0227/84/003D-1686$05.00

The limb scanning temperature retrieval problem has some complications that make it less linear than its nadir sounding counterpart. The most serious complication is that the attitude of the spacecraft is not adequately measured or controlled, so that the tangent height of the line of sight is not known accurately enough to compute the corresponding transmittance function. However, there is enough information in the radiances to determine both temperature profile and tangent height. The composition retrieval is nonlinear because the unknown enters the equation of transfer nonlinearly as an argument of the transmittance function.

Our approach to both retrieval problems is to linearize the direct equation about an a priori profile and to use a statistically optimum estimator [*Rodgers*, 1976] to find the most likely solution. The question of iteration is avoided by ensuring that the a priori profile is sufficiently close to the solution that the linearization is adequate. In the case of temperature this is achieved by using a sequential maximum-likelihood estimator, in which the retrieval corresponding to time t, and its error covariance matrix, are used to construct the a priori and its error covariance at time $t + \Delta t$, where Δt (typically 2 s) is the time interval between measurements. For composition retrieval it has proved necessary to average the data, for example, zonally, in order to improve the signal to noise ratio and to reduce computing time. In this case, the previous day's retrieval for the same averaging box is used to construct the a priori.

2. Radiance Emitted From a Limb Path

To simplify the equations, we will consider first the case of an infinitesimal field of view. The radiant flux $\Phi(h)$ emitted by a limb path with a tangent height h and reaching the detector of the radiometer may be written as

$$\Phi(h) = A\Omega \iint F(\nu)B[\nu, T(x)] \frac{d\tau_h}{dx}(\nu, x)\, d\nu\, dx \qquad (1)$$

where A is the aperture of the telescope, Ω the (infinitesimal) instrument field of view, $F(\nu)$ the spectral response of the channel in question (including the modulated component of the cell transmittance in the case of PMR channels), and $\tau_h(\nu, x)$ is the monochromatic transmittance of the atmosphere at the frequency ν from the satellite to the location described by the coordinate x. Provided that the molecular bands being observed are in local thermodynamic equilibrium at the atmo-

PRECEDING PAGE BLANK NOT FILMED

PAGE 112 INTENTIONALLY BLANK

APPENDIX D

TABLE 1. SAMS Spectral Channels

Channel	Gas	Spectral Region, cm^{-1}	Purpose
A1	CO_2	600–800	temperature, attitude
A2	CO_2	1700–2700	non-LTE
A3	CO	1700–2700	composition
A4	NO	1700–2700	composition
B1	H_2O	3650–4250	composition
B2	H_2O	170–330	composition
C1	CO_2	600–800	temperature, attitude
C2	N_2O	1180–1350	composition
C3	CH_4	1180–1350	composition

spheric levels of interest, the source function in equation (1) is the Planck function $B(\nu, T)$.

Explicit integrations along the limb path and over the instrument pass band both involve substantial amounts of computation so that if a direct calculation is to be made sufficiently fast, some more rapid and hence necessarily approximate means of evaluating $\Phi(h)$ must be found.

We first simplify equation (1) by dividing by $A\Omega \int F(\nu)\, d\nu$, obtaining

$$L(h) = \iint \bar{F}(\nu) B[\nu, T(x)] \frac{d\tau_h}{dx}(\nu, x)\, d\nu\, dx$$

where $L(h)$ has the units of spectral radiance and $\bar{F}(\nu)$ is the normalized spectral response of the instrument. As the internal calibration is made by viewing a black body at a known temperature of about 290 K, we find it convenient to express the measured radiance as a fraction of that from a black body at $T = 290$ K. The radiance seen by the instrument from a black body at temperature T is

$$L_B(T) = \int B(\nu, T) \bar{F}(\nu)\, d\nu$$

so that the normalized radiance $I(h)$ is

$$I(h) = L(h)/L_B(T_0) = \iint \frac{L_B[T(x)]}{L_B[T_0]} f(\nu, T(x)) \frac{d\tau_h}{dx}(\nu, x)\, d\nu\, dx$$

where $f(\nu, T) = B(\nu, T)\bar{F}(\nu)/L_B(T)$ is a weight which depends mainly on the instrumental spectral response, but also varies slightly with the temperature of the atmospheric path. We can now formally remove the frequency integration by writing

$$I(h) = \int \bar{B}(T(x)) \frac{d\bar{\tau}_h}{dh}(x, T)\, dx \qquad (2)$$

where $\bar{B}(T) = L_B(T)/L_B(T_0)$ is a known function of temperature and

$$\bar{\tau}_h(x, T) = \int f(\nu, T) \tau_h(\nu, x)\, d\nu \qquad (3)$$

This spectrally integrated transmittance must be precomputed and parameterized for CO_2, so that equation (2) can be solved for the temperature profile. The functional form of the transmittance must be parameterized for the trace gases so that equation (2) can be solved for their concentration.

2.1. *Integration Along the Path*

The integration along the line of sight is carried out by dividing the atmosphere into a number of concentric shells, with $z = \ln(p_0/p)$ as the vertical coordinate (p is pressure and p_0 is one atmosphere) and equal shell thicknesses of $\Delta z = 0.2$ (about 1.4 km). Each limb path thus falls naturally into a number of segments, each bounded by the shell boundaries (see Figure 1). We now replace the integration along the limb path by a summation over the N segments, with the gradient of path transmittance being evaluated by finite differences so that the emission from the limb path may be written

$$I(h) = \sum_1^N \bar{B}(\bar{T}_i)(\bar{\tau}_i - \bar{\tau}_{i-1})$$

where T is the mean (mass weighted) temperature of the ith segment.

The next step is to use a version of the Curtis-Godson approximation (C.G.) to replace each inhomogeneous path with a homogeneous path that has an equivalent absorption. The required equivalence is obtained by matching the absorber amounts and the mass weighted mean pressures and temperatures of each pair of paths. Details are not given here, but it may be shown, by considering the spectroscopic domains where the C.G. approximation is exact, the spectroscopy of the bands concerned, and the expected atmospheric distributions of the gases, that errors in the transmittance of paths arising from the use of the C.G. approximation are negligible in this instance. Typical errors are found to be $\ll 0.2\%$ for methane and $\ll 0.5\%$ for nitrous oxide at 50% transmittance [*Jones*, 1983].

Using this approximation, the mean atmospheric path transmittance $\bar{\tau}_i$ (equation (3)) may be written as a function of four variables, the absorber mass $\bar{u}_i$, mean pressure $\bar{p}_i$, mean temperature $\bar{T}_i$, and the local temperature T_i; that is,

$$\bar{\tau}_i = \bar{\tau}(T_i, \bar{u}_i, \bar{p}_i, \bar{T}_i) \qquad (4)$$

The mean path temperature and the local temperature are in general not equal, but, in practice, the mean path transmittance depends only weakly on the local temperature T_i. We have therefore taken T_i to be equal to $\bar{T}_i$ in equation (4), thereby reducing the number of independent variables describing the state of any path to three. Such an assumption only has the effect of weighting the mean path transmittance by the frequency dependence of the Planck function of a slightly wrong temperature. The error due to this effect depends on a number of factors, principally the gradient of the Planck func-

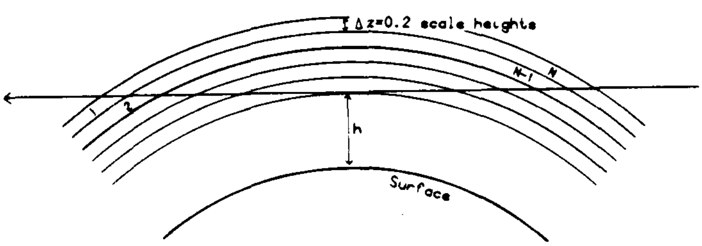

Fig. 1. The geometry of limb sounding.

APPENDIX D

TABLE 2. The Effect of Planck Function Weighting on Calculated Pressure Modulated Transmittance in Two Sample Cases

Local temperature, T	Pressure Modulated Transmittance CH_4 21.2 mbar	N_2O 23.9 mbar	$B(1150, T)/B(1350, T)$
195 K	0.6103	0.6731	2.57
220 K	0.6083	0.6730	2.19
245 K	0.6067	0.6729	1.93
270 K	0.6045	0.6728	1.74

The C.G. parameters for the absorbing path are $u = 10^{18}$ mols/cm, $p = 10$ mbar, $T = 195$ K. The modulator length is 3 mm, its temperature is 296 K, and its mean pressures are as in the table.

tion across the passband and the distribution of the spectral lines. For the pressure modulated CH_4 and N_2O sensing channels in SAMS, the resulting errors in transmittance are shown in Table 2 for an arbitrarily chosen path. Despite the substantial change of the Planck function gradient with local temperature (column 4), the calculated N_2O channel transmittances (column 3) remain almost constant (due to the high degree of symmetry of the P and R branches about the band center) while for the CH_4 channel (column 2), the changes in transmittance, although larger, are small (<0.5% in transmittance).

Precomputing a data base of homogeneous transmittances for suitable ranges of the C.G. equivalent u, p, and T is practical, and the costly line-by-line integration across the instrument passband is thus avoided by parameterizing the data base in terms of simple, readily evaluated functions (called the "transmittance functions") of the three independent variables.

2.2. *Transmittance Function Parameterization*

The path transmittances are found to depend only weakly on the mean path temperature $\bar{T}$, allowing their temperature dependence to be treated in a simple manner. A suitable functional form for a transmittance function is as a number of bivariate polynomial surfaces in log $(\bar{u})$ and log $(\bar{p})$ at a number of preselected temperatures T_m, $m = 1, \cdots M$, each of the form

$$\ln(-\ln(\bar{\tau}_i)) = \sum_{ij} A_{ij}^m (\ln \bar{p})^i (\ln \bar{u})^j$$

with linear interpolation between the temperatures. The coefficients A_{ij}^m were obtained by fitting a bivariate Chebyshev series to $\ln(-\ln(\tau))$ at values of $\log_{10}(\bar{u})$ and $\log_{10}(\bar{p})$ in intervals of 0.5 (i.e., $\bar{u}$ and $\bar{p}$ spaced by factors of $\sqrt{10}$), and path temperatures between 170 K and 320 K in intervals of 25 K. The degrees of the polynomials needed depend on the application and intended coverage, a seventh order fit in log $(\bar{u})$ and between a third and seventh order fit in log $(\bar{p})$ being used for the pressure modulated channels.

The homogeneous path transmittance computations use a line-by-line integration across the instrument passband. The spectral data used in these calculations were based on those available from the spectral data compilations of *McClatchey et al.* [1973] and *Rothman* [1981], with modifications required to fit a series of laboratory measurements on simulated atmospheric paths in the case of methane and nitrous oxide [*Jones*, 1983].

2.3. *Incorporation of the FOV*

The discussion has up to this point been restricted to radiances from a single tangent height. SAMS in fact possesses an approximately Gaussian field of view with a width at the tangent point of about 8 km at half height (measurement of the instrument's fields of view forms an important part of the prelaunch calibration program and is described by *Wale and Peskett* [this issue]). The effects of the finite field of view may be accounted for by convolving the field of view with the radiance profile. This is done to good precision in the case of constituent retrieval by computing the infinitesimal field of view radiances at each shell boundary (i.e., every 0.2 scale heights or 1.4 km) and performing a weighted average. In the case of temperature retrieval, weighting functions are used in the linearization. The infinitesimal field of view weighting function is calculated and then convolved with the actual field of view.

3. TEMPERATURE RETRIEVAL

The SAMS views at right angles to the direction of satellite travel, thus the variation of the roll angle causes corresponding changes of the observation tangent level. As a consequence of the uncertainty in satellite roll angle, the tangent height corresponding to any measurement is not known a priori with adequate accuracy. Therefore, the temperature retrieval process must estimate roll as well as the temperature profile.

The retrieval is a sequential maximum likelihood estimator. At each observation time (i.e., each point in the scan) several pieces of information are known about the unknown quantities, roll angle, and temperature profile. These are (1) the wide band and PMR radiances at two different altitudes (channels A1 and C1), (2) the look angle relative to the spacecraft, (3) the roll angle and rate derived from the spacecraft attitude control system (for NIMBUS 7 these are 2 or 3 orders of magnitude less accurate than needed for specifying the tangent level), (4) the retrieved profile, roll angle, and roll rate at the previous observation time, 2 s earlier, (5) the climatological temperature distribution.

If we make some assumptions about the statistics of the horizontal variation of the temperature profile, and the time evolution of roll, then item 4 can be used to provide an a priori estimate of these quantities at the observation time. All these pieces of information have error estimates, and they are all combined by using a statistically optimum maximum likelihood estimator [*Rodgers*, 1976] to provide the best estimate

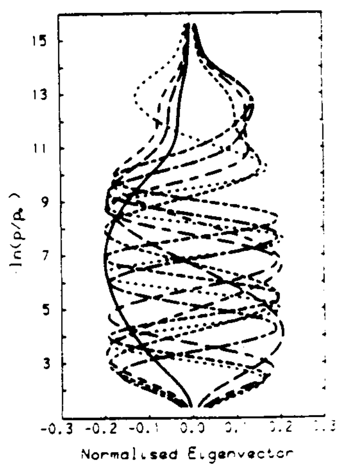

Fig. 2. Eigenfunctions of the solution covariance that have been used as an efficient representation for the temperature profile.

APPENDIX D

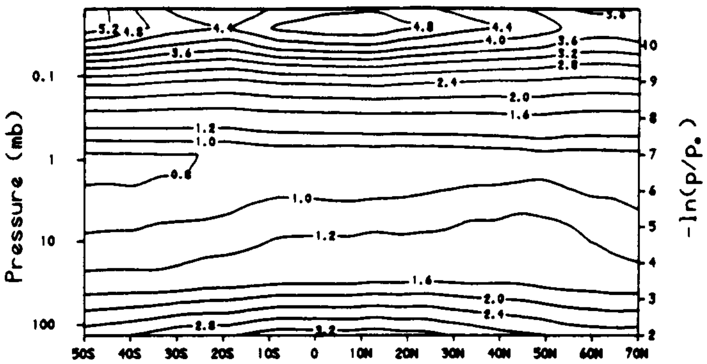

Fig. 3. An estimate of the rms precision of the retrieved temperature (K) for one particular day, February 5, 1981, as a function of latitude and altitude. This estimate is obtained by using equation (7b) and includes both instrumental noise and "unseen structure."

of the unknown profile and roll at the observation time, together with the error statistics of this estimate.

3.1. *The Temperature Profile Representation*

To minimize computing time, it is important to use the most efficient representation possible for the temperature profile. This has been done here by using a set of empirical orthogonal functions which represent an ensemble of retrieved profiles most efficiently, rather than functions representing an ensemble of actual profiles. If the covariance of an ensemble of actual profiles is S, and the instrument has weighting function matrix K and noise covariance S_ϵ, then it is straightforward to show that the covariance of the ensemble of maximum likelihood retrieved profiles S^R is

$$S^R = SK^T(KSK^T + S_\epsilon)^{-1}KS$$

The representation with least error of a member of this ensemble, for a given number N of coefficients, is as a linear combination of those eigenvectors of S^R which correspond to the N largest eigenvalues.

SAMS does not have a fixed set of weighting functions, nor is the atmospheric covariance S known adequately for our range of heights. Nevertheless, we have used the above representation as a reasonably efficient one for our purpose. For the elements of S we have assumed

$$S_{ij} = S_0 \exp(-(i-j)^2/a^2)$$

where i and j are level numbers, with levels spaced at intervals of 0.2 scale height, a^2 is 50, and S_0 is 0.0625 in units of the square the radiance of a 290 K black body. This assumes that the atmosphere is correlated over a range of about 3–4 km and ignores longer-range correlation. For the matrix K in this calculation we have used a set of weighting functions corresponding to tangent heights from 2.3 to 8.3 scale heights for the wide band channels and from 4.7 to 13.5 scale heights for the PMR, both in steps of 0.4 scale heights. The resulting set of eigenfunctions are shown in Figure 2.

3.2. *Stochastic Equation for Roll*

The instrument datum used is the direction of the D field of view when the vertical scan mirror is at step 41, its central position. The fields of view of each channel were determined relative to channel 1 during prelaunch tests, and the mirror angle relative to step 41 is known continuously to high accuracy by telemetry.

Roll angle θ_t at time t is defined for the purpose of the retrieval as the angle of the datum above the direction which has a tangent point at pressure level p where $\ln(p_0/p) = 7$ (about 0.92 mbar). A roll rate r is also defined such that $r_t = \theta_t - \theta_{t-1}$. Time t is expressed in units of observation intervals of 2 s. Given estimates $\hat{\theta}_{t-1}$ and $\hat{r}_{t-1}$ at time $t - 1$, we assume an a priori estimate at time t given by

$$\theta_t^0 = \hat{\theta}_{t-1} + \hat{r}_{t-1} + \delta_r$$

$$r_t^0 = \beta\hat{r}_{t-1} + \delta_r$$

where δ_r is a gaussian random change of roll rate and β is a constant between 0 and 1 which represents the long-term control of mean roll rate to be zero. This stochastic equation is equivalent to assuming that the torque on the spacecraft is random and uncorrelated on a time scale of 2 s. This is a conservative assumption, but it appears to be adequate for our purposes.

3.3. *Stochastic Equation for Temperature*

Temperature is represented by a vector x of coefficients of eight eigenfunctions of the deviation of profile of Planck function at 675 cm^{-1} from the climatology interpolated to the appropriate latitude and day. This wave number was chosen because the Planck function at that frequency most closely matched the spectrally weighted black body radiances $L_B(T)$ for the two PMR CO_2 channels.

We assume that the coefficients obey a first-order stochastic process thus:

$$\mathbf{x}_t = \alpha\mathbf{x}_{t-1} + \boldsymbol{\delta}_x \quad (5)$$

where $\boldsymbol{\delta}_x$ is a gaussian random vector and α represents the fact that in the long term $\bar{\mathbf{x}} \rightarrow 0$.

A relationship between the coefficient α and S_δ, the covariance of $\boldsymbol{\delta}_x$, can be found by taking the covariances of both sides of (5) to be equal to S^R:

$$S^R = E\{\mathbf{x}_t\mathbf{x}_t^T\} = E\{(\alpha\mathbf{x}_{t-1} + \boldsymbol{\delta}_x)(\alpha\mathbf{x}_{t-1} + \boldsymbol{\delta}_x)^T\}$$

therefore

$$S^R = \alpha^2 S^R + S_\delta$$

hence

$$S_\delta = (1 - \alpha^2)S^R$$

APPENDIX D

A second (or higher) order stochastic process would clearly be more representative, but leads to excessively large computing requirements.

3.4. *Construction of the A Priori Information*, $\mathbf{u}_t^0$

We define the state vector $\mathbf{u}$ as $(\mathbf{x}, \theta, r)$. The stochastic equations for roll and temperature can be written jointly as

$$\mathbf{u}_t^0 = \mathbf{A}\hat{\mathbf{u}}_{t-1} + \mathbf{\Delta}$$

where

$$\mathbf{A} = \begin{pmatrix} 1 & 0 & & \\ 0 & & 1 & 1 \\ & & 0 & \beta \end{pmatrix}$$

and

$$\mathbf{\Delta} = (\boldsymbol{\delta}_x, \boldsymbol{\delta}_r, \boldsymbol{\delta}_r)$$

If the covariance matrix of $\hat{\mathbf{u}}_{t-1}$ is $\hat{\mathbf{S}}_{t-1}$ then the covariance matrix of the a priori $\mathbf{u}_t^0$ is given by

$$\mathbf{S}_t^0 = \mathbf{A}\hat{\mathbf{S}}_{t-1}\mathbf{A}^T + \mathbf{\Delta}\mathbf{\Delta}^T = \mathbf{A}\hat{\mathbf{S}}_{t-1}\mathbf{A}^T + \mathbf{S}_\Delta$$

3.5. *Linearization of the Direct Model*

When the a priori profile is close to the retrieved profile, as is the case with this sequential estimator, linearization is likely to be an accurate approximation to the direct model. This allows the usual linear theory to be used without iteration. The linearization for temperature retrieval takes place in two stages. Equation (2) is sufficiently linear in $\bar{B}$ that it can be adequately linearized once and for all with respect to Planck function about a climatological (time and space dependent) distribution. However the nonlinearity due to roll is so large that this linearization must be done about the a priori at each observation time.

Radiances are calculated as functions of pressure for climatological mean profiles taken every 10° latitude and every month and are interpolated to the exact latitude and day. Differential weighting functions $\mathbf{W}(h)$ relating radiance from tangent height h to the coefficient of the representation are calculated numerically by finding the changes of radiance resulting from separate small changes in each of the coefficients and averaging over all climatological profiles.

$$W_i(h) = \{I(h, x_i + \Delta x_i) - I(h, x_i)\}/\Delta x_i$$

The radiance profile is therefore related to tangent height h and eigenvector coefficients by

$$I(h) = I_c(h) + \mathbf{W}^T(h)\mathbf{x} \qquad (6)$$

where $I_c(h)$ is the climatological radiance profile. If we linearize (6) with respect to h about a nominal value h_0 we obtain

$$I(h) = I_c(h_0) + \mathbf{W}^T(h_0)\mathbf{x} + \left\{\frac{\partial I_c}{\partial h}(h_0) + \frac{\partial \mathbf{W}^T}{\partial h}(h_0)\mathbf{x}\right\}(h - h_0) + O(h - h_0)^2$$

This can be put in the form

$$\Delta I = \mathbf{M}^T\Delta\mathbf{u}$$

where $\Delta I = I - I_c(h_0) - \mathbf{W}^T(h_0)\mathbf{x}$ is the deviation of the observation from that expected using $\mathbf{x}_0$ and θ_0, $\Delta\mathbf{u}$ is the vector $(\mathbf{x} - \mathbf{x}_0, \theta - \theta_0, r - r_0)$ and $\mathbf{M}$ is a vector of coefficients, the last of which is zero as radiance does not depend on roll rate.

Given an a priori estimate $\mathbf{u}^0$ with covariance $\mathbf{S}^0$, we can update this to find an improved estimate $\hat{\mathbf{u}}$ with covariance $\hat{\mathbf{S}}$ by using the observed ΔI and its variance σ^2 with equations of *Rodgers* [1976]

$$\hat{\mathbf{u}} = \mathbf{u}^0 + \mathbf{S}^0\mathbf{M}(\mathbf{M}^T - \mathbf{S}^0\mathbf{M} + \sigma^2)^{-1}\Delta I \qquad (7a)$$

$$\hat{\mathbf{S}} = \mathbf{S}^0 - \mathbf{S}^0\mathbf{M}(\mathbf{M}^T - \mathbf{S}^0\mathbf{M} + \sigma^2)^{-1}\mathbf{M}^T\mathbf{S}^0 \qquad (7b)$$

For this application we have up to four observations at each time (two WB/PM pairs), but because the number varies (mainly because one or more of the channels may be viewing outside its useful height range) we choose to apply equations (7a) and (7b) separately for each channel as a scalar, using the new $\hat{\mathbf{u}}$ and $\hat{\mathbf{S}}$ from one update as the $\mathbf{u}^0$ and $\mathbf{S}^0$ of the next, including using the revised roll angle to provide an improved tangent height linearization point.

3.6. *Practical details*

We have initially available for each observation time an approximate estimate of the roll angle determined by a sequential estimation process which uses the ratio of wide band to PM radiances and the output of the satellite attitude control system. This method gives roll angle sufficiently accurately to be a starting point from which the full retrieval can converge. It is only necessary at the start of sets of atmospheric data (e.g., after data gaps).

Data are normally processed in sets of about 24 hours. The retrieval algorithm is applied to a whole 24 hour period which is available in sequential order. The estimator is started at a point 10 min from the start of data and run back to the start, the results being discarded except for the estimates of x and θ for the first observation. The estimator is then run forward through the data set, θ and its variance being stored every observation time (every 2 s), and x and θ and their covariances being stored at every crossing of a 2.5° latitude line. At the end of the data set the final x and θ are used as starting values and the estimator run backward along the orbit to the start. This time the backward estimate of θ is combined with the forward estimate previously stored, weighted by the reciprocals of their variances. Similarly at 2.5° latitude intervals combined values of x are also produced in accordance with the covariances. At the start of both the forward and backward runs $\mathbf{S}^0$ is set to a large value representing no data. When forward and backward are combined no attempt is made to combine roll rate (since it is not required) or to use its covariance since, for a given time for which x and θ are applicable, the forward and backward values of r correspond to times separated by one time interval.

The approximate first estimate roll angle is incorporated into the full estimate as a pseudo observation (with relatively large standard deviation of 0.4°) every time slot. It is only effective during long periods when there is no atmospheric data sufficient to constrain the solution.

3.7. *Sequential Estimation of Space-Radiance Offset*

The precision of calibration of radiances near zero limits the lowest values of atmospheric emissivity, and thus the highest altitude of measurement, that can be used. For example, an emissivity of 0.1 when viewing an atmosphere at 240 K would give a radiance 0.05 of that of the 290 K internal black body. Since with the SAMS implementation of pressure modulation the channels chop against references at instrument temperatures (about 290 K), changes of gain and instrument temperature cause apparent changes of radiance when viewing space. Instrument scan patterns are chosen to give views of space

APPENDIX D

well above the atmosphere at about 10 min intervals. In addition, every scan cycle (32 s) the channels view levels sufficiently high in the atmosphere for the radiance to be regarded as zero. Only the retrieval algorithm has knowledge of whether these are high enough to be usable as a zero calibration. Therefore, an estimator of space view radiance offset is run in parallel with the attitude and temperature estimator, using the roll angle estimate to provide estimates of radiance correction for each channel.

4. Composition Retrieval

The retrieval of the distribution of trace gases could in principle be carried out in the same way as the temperature retrieval, by linearizing the direct model at every observation time and by updating the profile estimate and its covariance with the measured radiance. However, because the direct model is much more complicated in this case, the computing requirements of this method are prohibitive. Furthermore, the signal to noise in the composition channels is relatively low, so that this approach would be rather like taking a sledgehammer to crack a nut. We have therefore chosen to analyze the radiances in a relatively coarse grid before retrieving profiles, thus considerably reducing the number of profiles retrieved. The details of the grid vary with the gas, depending on the signal to noise ratio.

4.1. *Use of Sequential Estimation*

The starting point for a composition retrieval is a radiance profile sampled at a fixed interval in $-\ln(p)$, usually 0.2 scale heights. The profile to be retrieved is modeled by straight line segments in the logarithm of mixing ratio against $-\ln(p)$, using a relatively small number, n, of points to determine the profile. Thus the problem is over constrained, and does not, in principle, need an a priori estimate. In practice, of course, a rather good first guess is needed as a linearization point, and to prevent the solution behaving badly at those altitudes where there is little information in the measurements.

The profile is retrieved, starting at the top, by sequentially updating the coefficients $\mathbf{x}$ representing the profile and its covariance $\mathbf{S}$ with each measured radiance I_i(and its variance σ_i) in turn, thus

$$\mathbf{x}_i = \mathbf{x}_{i-1} + \mathbf{S}_{i-1}\mathbf{W}_i \Delta I_i^m/(\mathbf{W}^T\mathbf{S}_{i-1}\mathbf{W}_i + \sigma_i^2)$$

$$\mathbf{S}_i = \mathbf{S}_{i-} - \mathbf{S}_{i-1}\mathbf{W}_i\mathbf{W}_i^T\mathbf{S}_{i-1}/(\mathbf{W}_i^T\mathbf{S}_{i-1}\mathbf{W}_i + \sigma_i^2)$$

where subscript i refers to the radiance level being used for the update, $i-1$ is the result of the previous stage, $\mathbf{W}_i$ is a vector of weighting functions, and ΔI_i^m is the departure of the measured radiance from that calculated for level i using the retrieval of stage $i-1$:

$$\Delta I_i^m = I_i^m - I_i^{i-1}(\text{calc})$$

The weighting functions $\mathbf{W}_i$ are calculated by finite differences at each stage

$$\mathbf{W}_i = \frac{\Delta \mathbf{I}_i}{\Delta \mathbf{x}}$$

$\mathbf{W}_i$ depends on the temperature structure, the a priori concentration profile, and the pressure of gas in the PMC.

The final solution of this iteration $\hat{\mathbf{x}}$ and $\hat{\mathbf{S}}$ are equal to $\hat{\mathbf{x}}_n$ and $\hat{\mathbf{S}}_n$, respectively. This solution has second-order convergence and is usually found to converge adequately in one step. If further iterations are required, the covariance $\mathbf{S}^0$ is reinitialized to the first guess, the a priori absorber distribution $\mathbf{x}^0$ is set equal to $\hat{\mathbf{x}}$, and the weighting function matrix is reevaluated by linearizing about the new initial guess $\mathbf{x}^0$.

4.2. *Practical Details*

The CH_4 and N_2O sensing channels on SAMS share the same detector and thus cannot both be enabled at any one time. To maximize the coverage obtained, the CH_4 and N_2O PM channels are thus generally arranged to operate on alternate 24 hour periods. It is thus convenient, and in fact appropriate from signal to noise considerations, to treat each 24 hour period independently. Although the longitudinal variations of CH_4 and N_2O are being investigated, the quantities processed for archiving are zonal mean mixing ratio cross sections. After calibration and removal of space view offset, the radiances are zonally averaged into 10° latitude bands and in 0.2 scale height intervals using the retrieved attitude and the tangent point latitude. Radiances with estimated attitude errors greater than 0.15 scale heights are rejected at this point. At the same time the corresponding zonal mean temperature profiles are obtained by averaging the Planck function at 1290 cm^{-1} (the center of the CH_4 and N_2O channels) and retrieved temperatures over the same bands. The zonal mean radiances and temperatures are then archived as an intermediate product.

To retrieve a given data set, latitude dependent a priori estimate of the CH_4 and N_2O zonal mean mixing ratios are determined using the Oxford two-dimensional model [*Harwood and Pyle*, 1975] assuming large covariances (implying uncertainties of 25 and 100% in the CH_4 and N_2O mixing ratios, respectively). Starting a month into the data set, and working backward in time, each day's data is retrieved by using a single iteration. At the completion of each day, the a priori estimate for the species being measured that day (either CH_4 or N_2O) is then replaced with the retrieved zonal mean mixing ratio cross section, and the covariance is reinitialized. This process is repeated until the start of the data set is reached, whereupon the retrieval is run forward through the data set in the same manner with the zonal mean cross sections and their covariances now being stored.

5. Error Analysis

Random errors arise mainly from the contribution of detector noise to the measured radiances. One reason for using the optimal estimation equations is to treat this component of the total error correctly and automatically, obtaining the covariance matrix of the random error of the solution (equation (7b)) as one of the outputs of the system. Thus every retrieved profile has its own error estimate attached. An example of this error estimate is given in Figure 3, which shows contours of temperature error in a zonal cross section. Note that this error includes contributions from both instrument noise and "unseen structure" (i.e., fine structure in the temperature profile (as expressed in its covariance matrix) which is invisible at the vertical resolution of the instrument).

Systematic errors arise from many sources, some of which have already been touched on:

1. Calibration error: gain, space offset, temperature dependences, etc.

2. Instrumental: PMC pressure, field of view profile, spectral filter profile.

3. Location error: tangent height (for composition), lati-

APPENDIX D

tude, time. Winds and spacecraft yaw stability (via Doppler shift).

4. Spectroscopy: line strengths, widths, temperature dependences, air broadening, and self broadening. C.G. approximation. Transmittance parameterization. Overlap with other gases.

5. Retrieval: zonal averaging (for composition). Stochastic prediction equation. Use of eigenvectors as a representation. Nonlinearity. Temperature errors in the case of constituent retrieval.

Error analysis may in principle be carried out by perturbing the retrieval equations in a way appropriate to the error source, to determine the effect on the resulting profile. The details are straightforward but tedious. A discussion of these errors in the case of temperature is given by *Barnett and Corney* [this issue] and in the case of methane and nitrous oxide by *Jones and Pyle* [this issue].

6. Discussion

Retrieval of temperature and composition profiles from SAMS presents both theoretical and logistical problems. The inverse problem for temperature is nonlinear both because of the temperature dependence of the transmittance and because the scan is geometrical, while the atmospheric mass distribution with height varies according to the hydrostatic equation. The inverse problem for composition is more nonlinear because the absorber distribution to be measured appears as an argument of the transmittance function. Logistical problems arise because the scan pattern of SAMS is programable and therefore arbitrary and because the attitude control of the spacecraft is inadequate. Furthermore, owing to the satellite's horizontal motion during the vertical scan, the radiance profile is along a slant path, not a vertical path, so that vertical profiles are not measured directly. The problems are further compounded by the low signal/noise ratio in some channels.

In the case of temperature, the retrieval method presented here retrieves all the unknowns, including roll angle and rate, at every observation time, using a single radiance and the optimal estimation equations. This may appear unlikely but is no different in principle from retrieving a continuous vertical profile from perhaps 10 simultaneous nadir sounding channels. In practice, up to four channels are used at any one observation time, two PM and two WB CO_2 15 μm radiances. Continuity along the tangent track is provided by way of a stochastic equation which provides the a priori profile using that retrieved at the previous observation time. Forward and backward estimates are combined so that continuity is used in both directions.

Apart from the question of statistical optimality, the method has a number of practical advantages, which follow:

1. The a priori is always close to the solution, so that problems of nonlinearity and iteration are minimized.
2. Horizontal continuity is incorporated via the stochastic equation.
3. The scan pattern need not be pre-specified.
4. The first stage of global gridding is done automatically.
5. Objective interpolation is automatically carried out over data gaps.

We have not included in this paper examples of retrieved cross sections of temperature and composition and their accuracy and precision. For these we refer the reader to the two companion papers, *Barnett and Corney* [this issue] and *Jones and Pyle* [this issue]. Barnett and Corney discuss the validation of the temperature profiles in comparison with Tiros-N SSU and rocket measurements, while Jones and Pyle present methane and nitrous oxide cross sections in comparison with those computed by the Oxford two-dimensional model.

References

Barnett, J. J., and M. Corney, Temperature comparisons between the NIMBUS 7 SAMS and Rocket/radiosondes and the NOAA-6 SSU, *J. Geophys. Res.*, this issue.

Drummond, J. R., J. T. Houghton, G. D. Peskett, C. D. Rodgers, M. J. Wale, J. Whitney, and E. J. Williamson, The stratospheric and mesopheric sounder on NIMBUS 7, *Phil. Trans. R. Soc. London Ser. A*, *296*, 219–241, 1980.

Harwood, R. S., and J. A. Pyle, A two dimensional mean circulation model for the atmosphere below 80 km, *Q. J. R. Meteorol. Soc.*, *101*, 723–748, 1975.

Jones, R. L., Measurement of the atmospheric distributions of CH_4 and N_2O from satellites, D. Phil. Thesis, Univ. of Oxford, Oxford, 1983.

Jones, R. L., and J. A. Pyle, Observations of CH_4 and N_2O by the NIMBUS 7 SAMS: A comparison with in situ and two-dimensional numerical model calculations, *J. Geophys. Res.*, this issue.

McClatchey, R. A., W. S. Benedict, S. A. Clough, D. E. Burch, and R. F. Calfee, AFCRL atmospheric absorption line parameters, *AFCRL-TR-73-0096*, U.S. Air Force Cambridge Res. Lab., Cambridge, Mass., 1973.

Rodgers, C. D., Retrieval of atmospheric temperature and composition from remote measurements of thermal radiation, *Rev. Geophys. Space Sci.*, *14*, 609–624, 1976.

Rothman, L. S., AFGL atmospheric absorption line parameters compilation: 1980 version, *Appl. Opt.*, *20*, 791–795, 1981.

Wale, M. J., Development of spectroscopic instrumentation for the remote sounding of the atmosphere, D. Phil. Thesis, Oxford Univ., Oxford, 1981.

Wale, M. J., and G. D. Peskett, Some aspects of the design and behavior of the stratospheric and mesospheric sounder, *J. Geophys. Res.*, this issue.

J. J. Barnett, R. L. Jones, and C. D. Rodgers, Department of Atmospheric Physics, University of Oxford, Clarendon Laboratory, Parks Road, Oxford OX1 3PU, United Kingdom.

(Received April 20, 1983;
revised October 10, 1983;
accepted October 17, 1983.)

APPENDIX E

TEMPERATURE COMPARISONS BETWEEN THE NIMBUS-7 SAMS, ROCKET/RADIOSONDES, AND THE NOAA-6 SSU

[Reproduced from *Journal of Geophysical Research, 89*, 5294-5302 (1984).]

Temperature Comparisons Between the NIMBUS 7 SAMS, Rocket/Radiosondes and the NOAA 6 SSU

J. J. BARNETT AND M. CORNEY

Department of Atmospheric Physics, Clarendon Laboratory, University of Oxford

The stratospheric and mesospheric sounder (SAMS) on the NIMBUS 7 satellite is a limb sounder measuring infrared thermal emission from gases in the earth's atmosphere. Carbon dioxide measurements near 15 μm are used to determine the temperature profile and satellite roll angle. These temperature fields are compared with measurements by the NOAA 6 SSU and radio/rocketsondes over a 13-month period in 1980/81. Consistent patterns of bias between the instruments are found but are generally less than 2 K. Some of these are attributed to atmospheric tides, but others appear to indicate errors, including a problem caused by atmospheric ozone affecting lower-stratosphere SAMS measurements. Remarkably good agreement is found between variations measured by the three sensors, with standard deviations of difference typically of 1 K and correlation coefficients of up to 0.994 over the whole period.

1. INTRODUCTION

The stratospheric and mesospheric sounder (SAMS) is a limb-scanning infrared radiometer carried on board the NIMBUS 7 satellite, which was launched in October 1978. The SAMS worked well until October 1982, when the scan mechanism began to malfunction, thus giving 4 years of continuous data; several months of good data were also obtained in 1983.

This study was undertaken to see how well the SAMS temperature measurements agreed with those of rockets, radiosondes, and the TIROS-N series stratospheric sounder units. The temperature field is an important product of the SAMS measurements for the study of atmospheric thermal structure, radiation, and dynamics, but it is also an essential input for the retrieval of the SAMS minor constituent channels.

1.1 *The SAMS*

The SAMS hardware was described in detail by *Drummond et al.* [1980] and by *Wale and Peskett* [this issue], who also discuss the SAMS calibration and its operation in space.

The SAMS radiometer uses the technique of pressure modulation to select emission from a specified part of the band for a given gas. The principals are outlined by *Taylor et al.* [1972] and *Curtis et al.* [1974], and its advantages for limb composition sounding are described by *Chaloner et al.* [1978] and *Drummond and Jarnot* [1978]. The pressure modulator selectively modulates the emission from a gas in the atmosphere by using the absorption lines of the same gas as an optical filter. A cell containing the gas to be measured is included in the optical path of the radiometer. The gas pressure is varied so that the transmission of the cell is modulated at frequencies in the range 20–40 Hz. Pressure modulation is sensitive to emission at higher altitudes. By using a conventional black chopper in series with the pressure modulator at a much higher frequency (approximately 240 Hz), it is possible to obtain information from as low in the atmosphere as does a simple wideband radiometer. By combining the two methods of modulation, known as pressure modulation (PM) and wideband (WB) modulation, data have been obtained over altitudes from 10 to 100 km.

Paper number 3D1991
0148-0227/84/003D-1991$05.00

Pressure level and temperature sounding is accomplished by two such optical paths in the SAMS: C1, which uses ~30 mbar of CO_2 in a 10-mm long cell; A1, which uses ~12 mbar of CO_2 in a 3-mm long cell. Both pairs measure emission from the whole 15-μm υ_2 band with similar filters, hence the wideband measurements are nearly identical. However the A1 pair are offset to view 0.56° (approximately 30 km) above the C1 pair. The A1 cell pressure is sometimes set to much lower values than above; in this case the signal-to-noise ratio of the pressure-modulated measurement is too poor for it to be useful other than in the zonal mean, and only the C1 measurements are used.

The weighting functions (i.e., the Frèchet derivatives of the measured radiance with respect to the vertical radiance coordinate) for these channels are shown in Figure 1. The retrieval method is described in detail by *Rodgers et al.* [this issue]. It uses a sequential estimator in which the retrieved profile at each observation time is used as the a priori profile for the retrieval at the next observation time, 2 s later (an observation is a single tangent height, not a complete scan—the scan takes about 32 s). This allows continuity in the horizontal to be included and makes the a priori profile so close to the solution at each stage that linearization is adequate and iteration is not required. The profiles are stored at every 2.5° of latitude along the tangent track, thus automatically doing the first stage of gridding, the "orbit grid." At a later stage, values are interpolated in longitude onto a regular grid with 10° longitude and 2.5° latitude intervals. The northbound and southbound orbits are gridded separately but are then combined to give an average field for the day derived from all values between 0000 and 2400 Z.

1.2 *The SSU*

The stratospheric sounder unit (SSU) is a temperature sounder provided by the British Meteorological Office and carried on the NOAA operational TIROS-N series satellites. It measures thermal emission from carbon dioxide by using three pressure modulator channels. Although scanning sideways by ±35°, it is essentially a nadir sounder, providing measurements of a fundamentally different type from the SAMS. The weighting functions peak near 28 km, 36 km, and 43 km for channels 25, 26, and 27, respectively, and are about 15-km broad (see Figure 1). The data were processed by the Meteorological Office and were supplied in the form of analyses on a

APPENDIX E

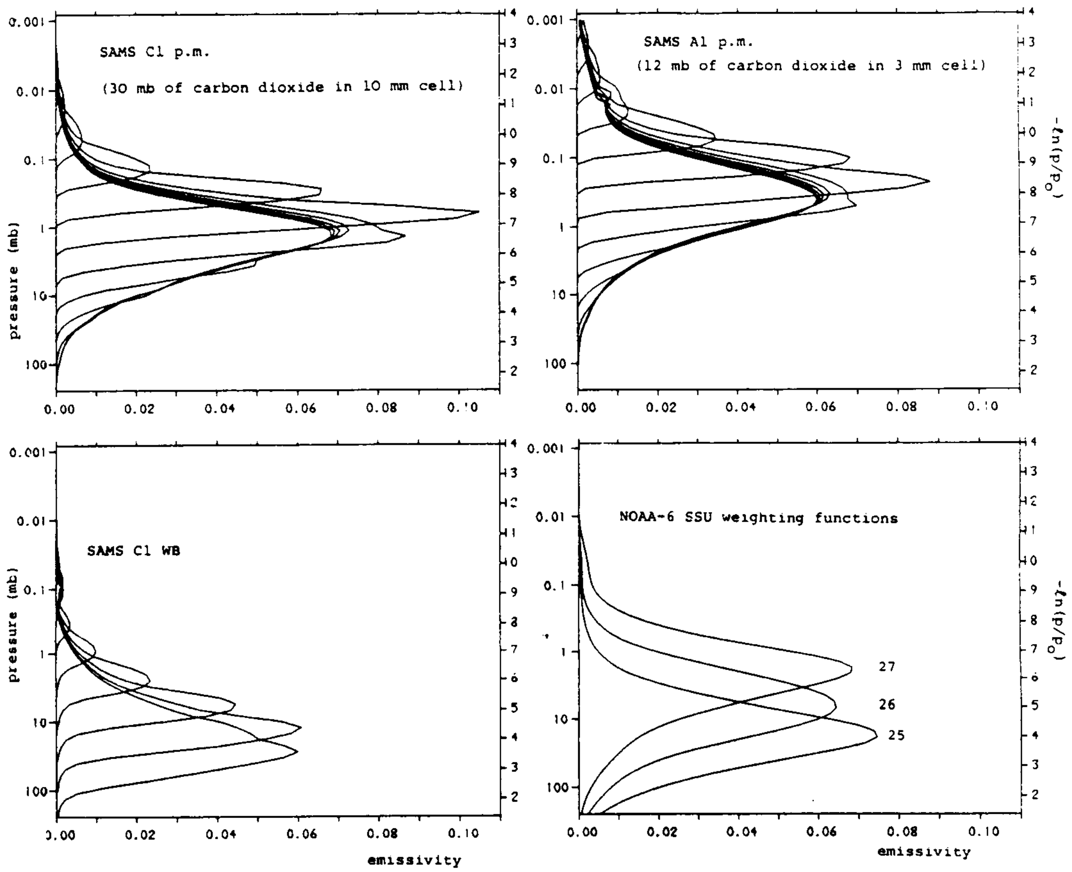

Fig. 1. Weighting functions for SAMS C1 PM, C1 WB, and A1 PM channels and for the NOAA 6 SSU. SAMS weighting functions are given for tangent pressures of the center of the field of view at intervals of 1.0 in $\ln(p/p_0)$.

5° by 5° latitude/longitude grid interpolated in time to 1200 Z for each day. Two types of data were used: (1) radiances for each SSU channel (corrected to exact nadir view); (2) thickness analyses from 100 mbar to various levels, derived by the Meteorological Office by regression, and incorporating, to some extent, measurements by the HIRS-II infrared and MSU microwave vertical sounders on the same satellite. For this study, data from the NOAA 6 satellite were used. This has equatorial crossing times of approximately 0730 and 1930 local mean time (see Table 1). Of the SSUs launched so far, this is probably the best understood and the most stable. The quality of the measurements were discussed in detail by *Nash and Brownscombe* [1983]. They show the overall radiometric precision for channels 25, 26, and 27 to be 0.15, 0.15, and 0.2 mw m^{-2} $ster^{-1}$ $(cm^{-1})^{-1}$, respectively, with an additional component of 0.06, 0.1, and 0.3, respectively, arising from the uncertainty of cell pressure, implying a weighting function mean height uncertainty. At this wavelength these units are approximately equivalent to K for atmospheric temperatures. *Pick and Brownscombe* [1981], *Brownscombe and Schlapp* [1983], and *Miller et al.* [1980] give additional information about the SSU's and their data.

1.3 *Rocket/Radiosonde Measurements*

These were prepared by the Meteorological Office as part of their SSU comparison program and supplied on magnetic tape. The rocket sensors were Super Loki datasondes, which measure temperature to a precision of 1.0–2.5 K over the 20–60 km height range. The rocket data were originally taken from teletype Rocobs messages and corrected where necessary for dynamic and radiative heating. They were combined with nearly coincident radiosonde profiles and interpolated to give temperature, geopotential height, and wind as functions of pressure. The radiosonde provided both temperature data below 50-mbar pressure and a pressure and height near that level to enable the rocket temperature measurements, which are measured as a function of height, to be obtained on a pressure scale that is the fundamental vertical coordinate for the satellite measurements. Rocket temperature was used exclusively above 10 mbar and radiosonde below 50 mbar, a smooth transition being made in any overlap region between these pressures. In this region the standard levels are 50, 30, 20, and 10 mbar. Where there was no overlap such that one or more levels was missing between the two parts of the profile, no further attempt was made to use the profile. For this study, data from three rocketsonde stations were used. In every case the radiosonde ascent was from the same station. At Ascension Island (8°S, 14°W) the 1200-Z radiosonde was always used, and rocket launches were typically within 2 hours and always within 4 hours. At Kwajalein Island (9°N, 168°E) the 0000-Z radiosonde was always used with rocket measurements typically within 2 hours but up to 5 hours away. At Primrose

APPENDIX E

TABLE 1. Approximate Local Times of SAMS and SSU Observations

	SAMS			SSU		
Latitude	Ascending	Descending	Bias, %	Ascending	Descending	Bias, %
50°S	1657	1842	97	2015	0644	−7
40°S	1517	2021	88	2002	0658	−5
20°S	1414	2125	59	1944	0716	−2
0°	1349	2150	50	1930	0730	0
20°S	1342	2157	47	1917	0743	2
40°N	1353	2146	51	1859	0801	5
50°N	1412	2126	58	1842	0817	8
60°N	1451	2048	71	1825	0834	11
67°N	1604	1934	90	1758	0902	15

SAMS times are for the tangent point location, whereas for the SSU they relate to the NOAA 6 subsatellite point (times in hours and minutes). The bias is explained in section 3.

Lake (55°N, 110°W) the rocket launches were all at about 1800 Z, and either the 0000-Z or 1200-Z radiosonde was used, whichever was more appropriate; the biggest time difference was 8 hours.

2. RADIANCE AND THICKNESS COMPARISONS

2.1 *Comparisons at Rocket Stations*

For this comparison we have studied in detail three rocket stations for which there were particularly frequent launches. Satellite data were interpolated to these locations from the gridpoint analyses. A 406-day period was used for the comparison to give a complete annual cycle plus some overlap. SSU data were available for most days, but the SAMS is routinely switched off for one complete day every fourth, giving 300 days of data. For rocket/radiosonde data the number of profiles available at Primrose Lake and Kwajalein and Ascension Islands were 103, 75, and 83, respectively. Thicknesses of the 100–20 mbar, 20–5 mbar, 5–1 mbar layers were calculated for all sensors at the three rocket stations. In Figure 2 we show a time sequence plot for the three layers at Primrose Lake. Agreement between all sensors appears best in the layer 20–5 mbar, with SAMS being slightly warmer than SSU at 5–1 mbar but cooler at 100–20 mbar. With almost continuous data the SAMS and SSU values appear to track each other extremely well, both traces exhibiting the same short-term variations. It is more difficult to follow these variations with the rocket data, but when they are sufficiently frequent, e.g., during days 1–80 and 300–350, 1980, there is good correlation.

Figure 3(*a*–*c*) and Table 2 summarize the comparisons. Here the three data types have been compared for the whole period in pairs, using days when both types of data were present. Using days when all three types of data were available would in some ways have been preferable but would have substantially reduced the number of comparisons. Thickness differences and standard deviations are plotted as equivalent mean temperatures by using lines that span the entire layer. Temperature profiles are compared at the standard rocket/radiosonde levels, but *no* SSU profiles were available. SSU radiances were compared with simulated radiances calculated from SAMS and rocket/radiosonde profiles. Weighting functions appropriate to the NOAA 6 SSU were used; they were not varied in time, since this radiometer is sufficiently stable for this to be unnecessary. They were appropriate to a global annual mean temperature profile, and no account was taken

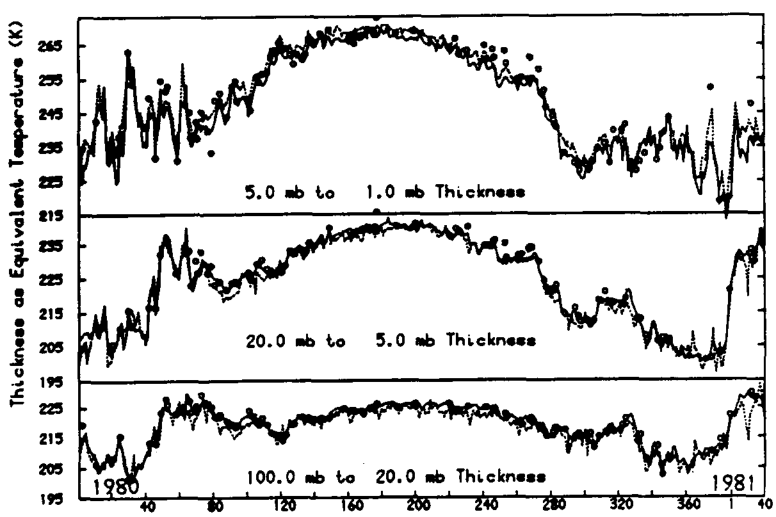

Fig. 2. SSU (solid line), SAMS (dashed line), and rocket (open circles) thicknesses expressed as equivalent layer mean temperature over Primrose Lake rocket station (55°N, 110°W).

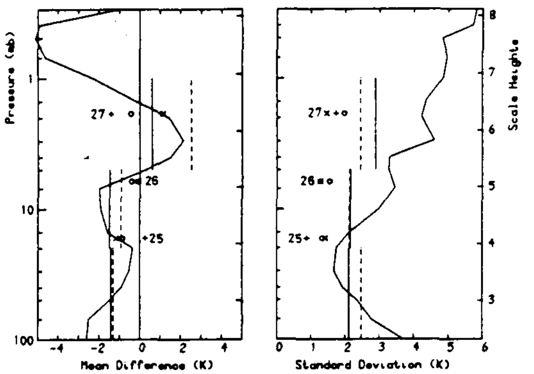

Fig. 3a

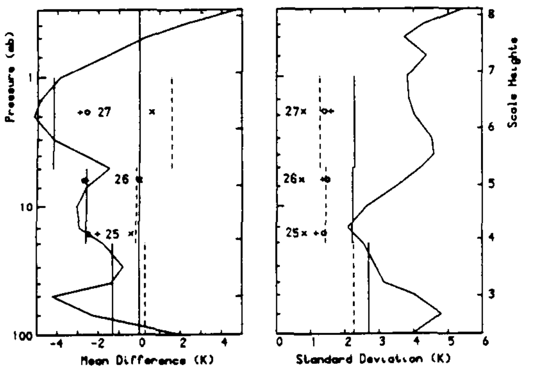

Fig. 3b

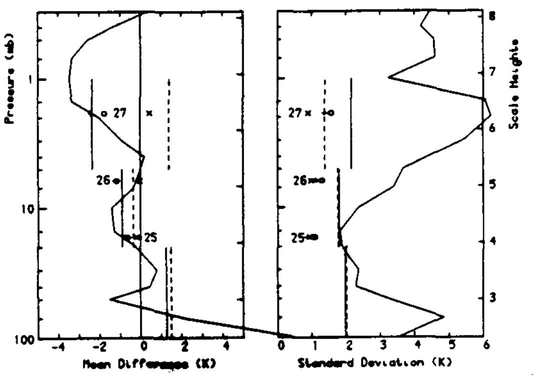

Fig. 3c

Fig. 3. Comparison of SAMS, SSU, and rockets expressed as equivalent temperatures. The profile is SAMS-rocket given at the standard levels of 100, 70, 50, 40, 30, 20, 15, 10, 7, 5, 4, 3, 2, 1.5, 1, 0.7, 0.5, 0.4, 0.2, 0.15, and 0.1 mbar (the ticks on the pressure scale); the bars are mean layer temperature differences (100–20 mbar, 20–5 mbar, 5–1 mbar) of SAMS-rocket (solid line) and SAMS-SSU (dashed line); the spot points are at SSU weighting function maxima SAMS-rocket (open circles), SAMS-SSU (×), and SSU-rocket (+) for (*a*) Primrose Lake, (*b*) Ascension Island, and (*c*) Kwajalein Island.

of temperature dependence, an approximation that may lead to errors of up to about 1 K. Radiances were converted to brightness temperature each day before differencing and averaging. The differences are plotted at the levels of weighting function maxima.

The mean differences for radiances, temperatures, and thickness are consistent with each other. Standard deviations are also consistent: the smallest variations occur with radiances, which average over the broadest layers. The largest variations occur with temperature profiles, where the SAMS is unable to resolve the fine structure, which itself may change rapidly within the time scale of a day and which would be reduced by horizontal averaging.

Table 2 shows that at Primrose Lake the standard deviation of temperature over the period was 7 to 14 K, depending on the level and the layer. Correlation coefficients are all larger than 0.97, except for the SAMS components of the 100–20 mbar thickness. Correlations are generally higher for radiance than for thickness, being 0.988–0.993 for SAMS vs. SSU and 0.985–0.994 for SAMS vs. rocket (becoming worse with increasing height). The gradients of least squares fit straight lines are given, in each case using first one then the other variable of a pair as the independent (assumed noise-free) variable; this was done because the relative errors of each were unknown. With perfect correlation the two gradients would be equal, while for zero correlation the first would be zero and the second infinite. Ideally, they would both be 1, indicating that both sensors of a pair show the same magnitude of response to a change. At Kwajalein and Ascension Islands the standard deviation of temperature is 1–2 K over the period. This is little more than the standard deviation between the instruments, so correlation coefficients are much poorer, being as low as 0.39. For the same reason the gradients at these places are of little value and are given only for completeness.

The mean differences given in Table 2 show interesting patterns, which will be discussed in section 3. The three differences for a given channel or layer at a single station do not add to zero because different sets of days were used for each comparison, as already discussed. In the middle and upper stratosphere, standard deviations of difference are generally smallest for SAMS-SSU and largest for SAMS-rocket, indicating that the SSU shows the smallest and the rocket the largest variation about some compromise "truth." This interpretation must be treated with caution, since errors may be correlated between sensors, e.g., this could result from error-free rocket measurements but with SAMS and SSU both having offset errors that vary seasonally together. Estimates of the absolute standard deviation of each sensor can be obtained from the variances and covariances between differences (preferably using only days when all three measurements are present), but too few days were available for this to be done reliably.

Figure 4 shows the scatter between channel 27 SSU and SAMS at Primrose Lake; days with and without A1 PM available are shown separately, but there is no suggestion that these two classes of measurement fall on separate lines. The line of points tends to be slightly curved, falling closer to the SAMS–SSU line in the middle 230–250 K range than at higher or lower temperatures. From Table 2*a* the mean and standard deviation of SAMS-SSU for this set of measurements is 1.14 K and 1.46 K, respectively.

2.2 *SAMS and SSU Comparisons as a Function of Latitude*

Zonal mean SAMS-SSU brightness temperatures have been calculated for each day. They show consistent seasonal variations, changing smoothly from month to month. Figure 5 gives monthly means at 3-month intervals as being representative of the behavior. Differences of up to 3 K occur, usually peaking toward either pole and being smallest in the

TABLE 2. Radiance and Thickness Comparisons at Primrose Lake, Ascension Island, and Kwajalein Island

Channel Layer	Overall Standard Deviation, K	Difference, x y	Number of Pairs	Mean, K	Standard Deviation, K	Correlation Coefficient	dy/dx x independent	dy/dx y independent
			Primrose Lake					
Channel 25	8.0	SAMS-SSU	262	−1.16	1.42	0.988	1.002	1.027
		SAMS-Rocket	74	−0.86	1.33	0.987	1.005	1.031
		SSU-Rocket	94	0.26	0.88	0.994	1.006	1.019
Channel 26	9.5	SAMS-SSU	262	−0.26	1.27	0.993	1.003	1.017
		SAMS-Rocket	74	−0.42	1.54	0.988	1.002	1.026
		SSU-Rocket	94	−0.07	1.27	0.991	1.005	1.024
Channel 27	9.8	SAMS-SSU	262	1.14	1.46	0.990	0.988	1.008
		SAMS-Rocket	74	−0.44	1.97	0.982	1.007	1.043
		SSU-Rocket	94	−1.42	1.73	0.985	1.010	1.042
100–20 mbar	7.0	SAMS-SSU	261	−1.32	2.47	0.936	1.027	1.172
		SAMS-Rocket	74	−1.43	2.13	0.941	1.018	1.149
		SSU-Rocket	94	−0.22	1.44	0.971	0.963	1.021
20–5 mbar	12.2	SAMS-SSU	261	−0.92	2.13	0.985	0.991	1.022
		SAMS-Rocket	74	−1.49	2.18	0.980	0.978	1.019
		SSU-Rocket	94	−0.60	1.55	0.989	1.011	1.034
5–1 mbar	14.2	SAMS-SSU	261	2.53	2.45	0.985	1.021	1.052
		SAMS-Rocket	74	0.61	2.91	0.979	1.030	1.075
		SSU-Rocket	94	−1.73	2.97	0.976	1.001	1.050
			Ascension Island					
Channel 25	1.4	SAMS-SSU	268	−0.40	0.81	0.939	0.80	1.14
		SAMS-Rocket	66	−2.49	1.39	0.677	0.79	1.73
		SSU-Rocket	76	−2.02	1.12	0.810	1.13	1.72
Channel 26	1.8	SAMS-SSU	268	0.01	0.73	0.894	0.96	1.21
		SAMS-Rocket	66	−2.71	1.48	0.706	0.95	1.90
		SSU-Rocket	76	−2.61	1.34	0.785	0.99	1.62
Channel 27	1.9	SAMS-SSU	268	0.60	0.79	0.878	1.00	1.30
		SAMS-Rocket	66	−2.58	1.40	0.698	0.86	1.77
		SSU-Rocket	76	−2.94	1.60	0.680	0.73	1.58
100–20 mbar	1.8	SAMS-SSU	270	0.29	2.26	0.403	0.32	1.99
		SAMS-Rocket	65	−1.30	2.72	0.389	0.31	2.06
		SSU-Rocket	73	−1.77	1.56	0.695	0.86	1.79
20–5 mbar	2.1	SAMS-SSU	270	−0.15	1.45	0.788	0.71	1.14
		SAMS-Rocket	66	−2.59	2.24	0.657	0.82	1.89
		SSU-Rocket	74	−2.29	1.87	0.768	1.07	1.81
5–1 mbar	2.0	SAMS-SSU	270	1.59	1.28	0.842	0.71	1.00
		SAMS-Rocket	66	−4.21	2.30	0.676	0.81	1.76
		SSU-Rocket	74	−5.55	2.07	0.740	1.02	1.86
			Kwajalein Island					
Channel 25	1.8	SAMS-SSU	267	−0.20	0.93	0.839	0.83	1.18
		SAMS-Rocket	48	−0.73	1.08	0.824	0.82	1.20
		SSU-Rocket	69	−0.59	0.88	0.876	0.91	1.19
Channel 26	2.0	SAMS-SSU	267	−0.02	0.98	0.842	0.91	1.53
		SAMS-Rocket	48	−1.16	1.30	0.823	0.98	1.44
		SSU-Rocket	69	−1.24	1.13	0.873	1.01	1.32
Channel 27	2.1	SAMS-SSU	267	0.46	0.90	0.872	0.92	1.21
		SAMS-Rocket	48	−1.75	1.58	0.799	0.96	1.51
		SSU-Rocket	69	−2.42	1.37	0.845	1.03	1.44
100–20 mbar	2.1	SAMS-SSU	267	1.51	2.03	0.626	0.54	1.36
		SAMS-Rocket	48	1.28	2.00	0.673	0.82	1.81
		SSU-Rocket	69	−0.53	1.49	0.829	1.02	1.48
20–5 mbar	2.3	SAMS-SSU	267	−0.35	1.76	0.752	0.66	1.17
		SAMS-Rocket	48	−0.91	1.81	0.796	0.76	1.20
		SSU-Rocket	69	−0.42	1.61	0.820	0.88	1.31
5–1 mbar	2.2	SAMS-SSU	267	1.41	1.38	0.823	0.73	1.08
		SAMS-Rocket	48	−2.36	2.19	0.809	1.00	1.53
		SSU-Rocket	69	−4.12	1.94	0.880	1.31	1.69
			Kwajalein (Not A1 12-mbar days)					
Channel 27	1.8	SAMS-SSU	112	0.69	1.10	0.817	0.89	1.33
		SAMS-Rocket	24	−1.79	1.99	0.722	0.91	1.75
			Kwajalein (Only A1 12-mbar days)					
Channel 27	1.8	SAMS-SSU	155	0.29	0.68	0.924	0.97	1.14
		SAMS-Rocket	24	−1.71	1.06	0.893	1.01	1.26

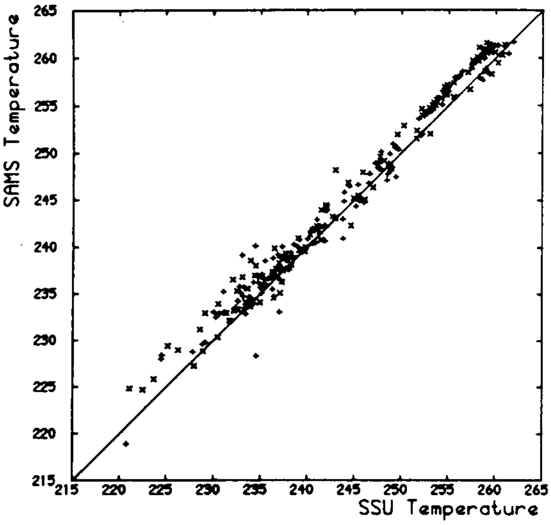

Fig. 4. SAMS and SSU brightness temperatures for SSU channel 27 over Primrose Lake rocket station (55°N, 110°W) for January 1, 1980 to February 11, 1981; + and × denote days with and without A1 PM data for 12 mbar available.

tropics. The locations of Primrose Lake, Kwajalein Island, and Ascension Island are marked, and it can be seen that the overall means for these places are approximately consistent with mean SAMS-SSU values given in Table 2. Channels 25 and 27 appear to show quite different patterns, with channel 26 behaving in an intermediate way. Channel 27 shows large differences toward 50°S; these are shown in more detail in Figure 6 togeher with 50°N and 67.5°N for comparison. The differences at 50°S are seen to be 2.5–3 K from August to January, with no counterpart in the northern hemisphere. Conversely, for Channel 25 the differences are more symmetric about the equator, with maximum difference occurring in autumn in each hemisphere.

3. DISCUSSION

Since this paper is primarily intended to discuss the SAMS-derived temperatures, possible problems with the SSU or rocket/radiosonde will not be discussed. There are several potential problems with the SAMS retrievals: (1) motional chopping in the wideband channels and field of view uncertainties, (2) horizontal gradient effects in pressure-modulated channels at levels where the emissivity is near unity, (3) Doppler shifts caused by the earth's rotation affecting pressure-modulated channels, (4) inadequate allowance for ozone effects in the wideband channels, (5) solar tides, given the consistent differences between measurement times.

Table 3 gives values for the magnitudes of some of these effects. For Doppler shift they are the errors introduced in the tropics by neglecting the earth's rotation, and they were found by analyzing at the equator a special sequence of data when the SAMS was viewing with azimuth angles up to 12° away from the normal giving Doppler Shifts of up to 1600 m s^{-1}. To quantify other problems a single day (8 February 1981) was taken and processed several times with different assumptions.

3.1. *Field of View Uncertainty and Motional Chopping*

The SAMS fields of view are approximately Gaussian in the vertical, with a thickness at half peak value of about 8 km. They were measured during prelaunch tests and, for CO_2, are subject to an error of the level of the center of $\pm 0.003°$ (0.2 km) [*Wale and Peskett*, this issue]. However, there is also a potential error caused by motional chopping. This is the result of vibration of the scan mirror (or some other part of the optics) in synchrony with the radiometric chopper. In the case of wideband channels, motional chopping has the effect of changing the field of view. The components were measured during test and have an effect similar to a downward shift of the field of view by 0.02°. The temperature retrieval uses wideband fields of view that include motional chopping on the assumption that it was unchanged between prelaunch test and operation in space. *Wale* [1981] has shown that for the pressure-modulated channels motional chopping effects should be much smaller than for the wideband. Table 3 gives the effect of changing wideband motional chopping by 100%; it is reasonable to allow possible errors of half of this, giving errors of up to 1 K. Motional chopping is discussed further by Wale and Peskett.

3.2 *Horizontal Weighting Function Shifts*

The weighting functions are primarily functions of log-(pressure). The emission originates within about 200 km horizontally of the tangent point in cases where the total absorption along the tangent path is less than about 0.5 (the optically thin case). However, for absorption near unity the emission is centered about a point nearer the satellite than the tangent point; for the range of data used in the temperature retrieval this horizontal displacement can be up to 300 km. Temperature is assumed constant on pressure surfaces along the line of sight. The net effects of this approximation are (1) the temperature derived for the upper stratosphere and lower mesosphere corresponds to a point roughly 100 km nearer the satellite than the tangent point; (2) the pressure registration

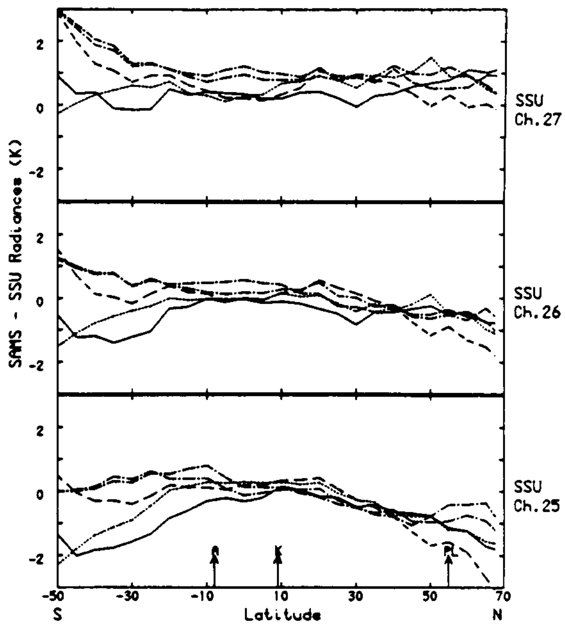

Fig. 5. Monthly zonal mean SAMS-SSU brightness temperatures for SSU channels 25, 26, and 27: (dashed dotted line) January 1980, 1981; (dotted line) April 1980; (solid line) July 1980; (dashed line) October 1980.

will be in error where there is a strong horizontal temperature gradient in the atmosphere. For zonal means the effects cancel at latitudes where the SAMS views primarily east-west, errors only arising north of about 60°N and south of 40°S. In this case a temperature error corresponding to the change in about 100 km is to be expected, thus approximately ±0.5 to ±1 K, depending on season and pressure, with corresponding tangent height errors of 125 to 250 m (0.002° to 0.004°).

3.3 *Doppler Shift*

The SAMS views perpendicular to the direction of motion of the satellite, so the radiation suffers no Doppler shift as a result of satellite velocity, except for relatively minor errors caused by the orientation of the satellite. However, the earth's rotation causes a Doppler shift of about ±400 m s^{-1} in the tropics, falling to zero at extreme northerly and southerly latitudes. In the case of the CO_2 channels the effects are small, and no attempt is made to allow for them.

3.4 *Ozone Contamination*

The mid-latitude annual mean ozone profile given by *Krueger and Minzner* [1976] was used to correct the wideband channels. Table 3 shows the effect of reducing the ozone mixing ratio in the model by 30% at all levels. Consequently, the retrieved temperature increases in the stratosphere to account for the observed emission. Minor decreases occur in the mesosphere because of compensation associated with the pressure-modulated channels being unaffected by ozone. These changes in temperature are to be expected from 30% ozone mixing ratio increases in the atmosphere (more ozone giving a higher apparent temperature). Ozone mixing ratios given by *Heath* [1980] show maximum deviations of this magnitude about the mean model, with a lower and mid-stratospheric maximum in the tropics and minima at the poles. This would adequately explain the behavior of SAMS-SSU as a function of latitude (Figure 5) for channel 25, although only if the curve is moved upward by about 1 K.

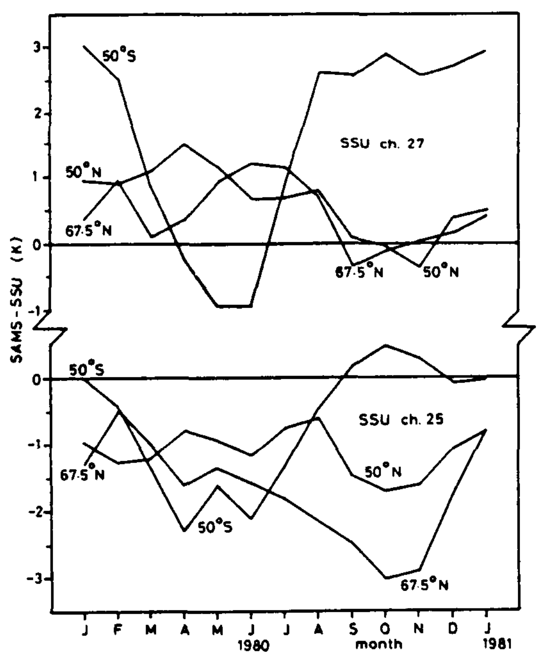

Fig. 6. Monthly zonal mean SAMS-SSU brightness temperature for SSU channels 25 and 27 at 50°S, 50°N, and 67.5°N.

TABLE 3. Changes in Temperature Retrieval (*K*) Resulting From Changes in Assumed Conditions

	Level (ln (p_0/p))				SSU Channel		
	2–4	4–6	6–8	8–10	25	26	27
Ozone less 30%	1.1	1.9	−0.4	−0.3	1.3	1.2	0.4
C1 WB shifted up 0.02°	−0.1	2.2	−0.6	−1.0	1.0	1.5	0.7
A1 PM not used	0.2	0.5	−0.3	6.3	0.4	0.3	0.0
Doppler shift corrected at equator	−0.4	−0.3	0.4	0.9			

3.5 *The Effects of Tides*

SSU measurements from two satellites measuring both temperature and its east-west gradient every 6 hours have shown solar tides of up to 3 K amplitude (J. L. Brownscombe and J. Nash, private communication, 1983) for channel 27. Model calculations by C. F. Rogers et al. (private communication, 1983) indicate that in the tropics the semidiurnal tides averaged over the SSU weighting function have amplitudes of ~1 K, whereas the diurnal oscillation, because its phase changes rapidly with height, should have a much smaller amplitude. However, at mid-latitudes the diurnal wave would be expected to dominate, with a maximum temperature at about 1800 hours local time. These calculations appear to be confirmed quite well by SSU measurements. Table 1 shows the biases of SAMS and SSU zonal means produced by a diurnal sine wave peaking at 1800 hours. For each satellite the northbound and southbound measurements are assumed to be averaged together, and deviations from the true mean arise because, in general, the two measurements for a given satellite at a given latitude are not 12 hours apart. At 50°S the bias of the SAMS relative to the SSU daily mean is expected to be 104% of the diurnal amplitude, whereas at 50°N, where comparable tidal amplitudes can be expected (in the corresponding season), the bias is only 50%—consistent with the much smaller channel 27 SAMS-SSU differences found there. Thus it is reasonable to ascribe these differences to tides. At 67.5°N, where the bias would be 75% of the tidal amplitude, smaller tidal amplitudes are expected, so the smaller discrepancies there are reasonable. Tidal amplitudes are believed to increase rapidly with height in the stratosphere, so although tides may explain discrepancies in channel 27, their effects should be very much smaller at channel 25 levels, and much less than the observed discrepancies. The SAMS measurements show little difference (~1 K) between northbound and southbound measurements, consistent with a diurnal tide peaking at 1800 hours local time, since the SAMS measurements are symmetrically placed about that time.

Brownscombe and Schlapp [1983] have shown that the lunar semidiurnal tide is detectable in SSU channel 27 data, with a maximum amplitude of about 0.2 K in January and February and a mean of 0.15 K averaged over the year investigated (1980/81). The amplitude is smaller for lower channels. This would have the effect of modulating the differences with a period of 14 days and a zero mean. A simple calculation, using the times given in Table 1, shows that this would cause an rms SAMS-SSU component of 0.15 K in the tropics (averaged over the year). Compared with the smallest observed standard

APPENDIX E

deviation for channel 27, which is 0.79 K at Ascension Island, the lunar tide contributes only 4% of the variance. Hence it has been ignored in this study.

3.6 *Comparisons Between Satellites and Rockets*

Comparing mean differences between the three sensors at the three rocket stations shows that at Primrose Lake the differences are considerably smaller than at Kwajalein or Ascension Islands. *Nash and Brownscombe* [1983] found a similar effect, comparing the TIROS-N and the NOAA 6 SSU's with rockets for different periods. They found good agreement to ~1 K at mid and high latitudes of the northern hemisphere, but going further south, the rocket-SSU difference progressively increased, being larger at Ascension Island than at Kwajalein Island. The results presented here (see Table 2) support those findings, with the SAMS and SSU generally agreeing with each other but not with the rocket. At Kwajalein Island the difference is only marked for channel 27, but at Ascension Island, differences are evident at all levels. Several potential problems with the SAMS have been outlined, but the offsets they can introduce should all be identical within a fraction of a degree at both tropical stations. This is also true for the SSU, but also no doubt for the rocket measurements, both rocket stations measuring at about the same local time.

4. CONCLUSIONS

There are various, quite different uses to which temperature fields derived from the SAMS measurements will be put, and they determine the types of error that are acceptable:

(1) The temperature fields are used directly as the source of data for study of the dynamical and radiative properties of the atmosphere, e.g., calculation of momentum fluxes. For this application, slow changes of bias with height and latitude of the magnitude found are probably not too serious.

(2) They may be used to monitor long-term trends related to climate change or the solar cycle; here biases do not matter, provided they do not change. Some of the sources of error discussed here can, in principle, drift (notably motional chopping), but there are also others, such as mirror surface degradation and second-order effects associated with CO_2 cell pressure and satellite temperature drifts, that are discussed by *Wale and Peskett* [this issue]. Thus long-term changes of bias must be expected, with a probable magnitude of 1–2 K.

(3) For many studies it is advantageous to combine SAMS with SSU and other data because each measures over different time and space domains with different resolution. However, this is difficult where they do not agree, whether because of temporal effects or instrument errors, because sharp gradients far more serious than the absolute error of either alone arise at the interfaces.

(4) The pressure-scale of the SAMS scan is determined from CO_2 meaurements by a process intimately linked with the temperature sounding such that they both depend strongly on each other. The SAMS minor constituent measurements rely on correct registration of the scan, and since there is no way to verify this, a level of confidence can only be obtained indirectly from the instrument's performance as a temperature sounder. Based on discrepancies found in this comparison, it appears that the pressure-scale registration may have a bias of up to $\pm 0.006°$ in satellite roll angle, corresponding to about 360 m at the limb. The implication of pressure-scale errors on the constituent sounding are outlined by *Jones and Pyle* [this issue].

(5) Temperature measurements are a necessary input for constituent sounding, since thermal emission measured by the minor constituent channels is proportional to the Planck function. The effect of temperature errors is discussed by *Jones and Pyle* [this issue] for the 7-μm CH_4/N_2O channel. At this wavelength, at 240 K the Planck function changes by 3% K^{-1}, and the temperature uncertainties are a limiting factor.

The SAMS has been compared with other sensors in the stratosphere, and differences with random components of 1–2 K have been bound. Mean differences show marked patterns that, to some extent, are understood. They indicate that SAMS temperature measurements are probably subject to biases (excluding those due to tides) of up to 2 K in the low stratosphere and 1 K in the upper stratosphere. The difference is perhaps to be expected, since the upper stratosphere is the middle of the SAMS temperature retrieval range and is the lower level for which the temperature is measured by the pressure modulator channels.

Acknowledgments. We gratefully acknowledge the work done by the NIMBUS project of NASA in their provision of SAMS data and the U.S. Air Force for their detailed sequences of rocket soundings. We are also particularly grateful to those at the Meteorological Office associated with the SSU, both for their data and for their many valued discussions. Several people have been involved with processing SAMS data at Oxford: their help is greatly appreciated. This work was supported by grants from the Science and Engineering Research Council and the Meteorological Office.

REFERENCES

Brownscombe, J. L., and D. Schlapp, The lunar semi-diurnal tide observed by stratospheric sounder units on the TIROS-N series of satellites, *J. Atmos. Terr. Phys.*, *45*, 27–32, 1983.

Chaloner, C. P., J. R. Drummond, J. T. Houghton, R. F. Jarnot, and H. K. Roscoe, Infra-red measurements of stratospheric composition, 1, The balloon instrument and water vapour measurements, *Proc. R. Soc. London*, *A364*, 145–159, 1978.

Curtis, P. D., J. T. Houghton, G. D. Peskett, and C. D. Rodgers, Remote sounding of atmospheric temperature from satellites, 5, The pressure modulator radiometer for Nimbus F, *Proc. R. Soc. London*, *A337*, 135–150, 1974.

Drummond, J. R., and R. F. Jarnot, Infrared measurements of stratospheric composition, 2, Simultaneous NO and NO_2 measurements, *Proc. R. Soc. London*, *A364*, 237–254, 1978.

Drummond, J. R., J. T. Houghton, G. D. Peskett, C. D. Rodgers, M. J. Wale, J. Whitney, E. J. Williamson, The stratospheric and mesospheric sounder on Nimbus 7, *Phil. Trans. R. Soc. London*, *A296*, 219–241, 1980.

Heath, D. F., Spatial and temporal variability of ozone as seen from space, Proceedings of NATO Advanced Study Institute on Atmospheric Ozone, *Publ. FAA-EE-80-20*, U.S. Dep. Transp., Washington, D.C., 1980.

Jones, R. L., and J. A. Pyle, Observations of CH_4 and N_2O by the NIMBUS 7 SAMS: A comparison with in-situ and two-dimensional numerical model calculations, *J. Geophys. Res.*, this issue.

Krueger, A. J., and R. A. Minzner, A mid-latitude ozone model for the 1976 U.S. Standard Atmosphere, *J. Geophys. Res.*, *81*, 4477–4481, 1976.

Miller, D. E., J. L. Brownscombe, G. P. Carruthers, D. R. Pick, and K. H. Stewart, Operational temperature sounding of the stratosphere, *Phil. Trans. R. Soc. London*, *A296*, 65–71, 1980.

Nash, J., and J. L. Brownscombe, Validation of the stratospheric sounding unit, *Adv. Space Res.*, *2*(6), 59–62, 1983.

Pick, D. R., and J. L. Brownscombe, Early results based on the stratospheric channels of TOVS on the Tiros-N series of operational satellites, *Adv. Space Res.*, *1*(4), 247–260, 1981.

Rodgers, C. D., R. L. Jones, and J. J. Barnett, Retrieval of temperature and composition from NIMBUS 7 SAMS measurements, *J. Geophys. Res.*, this issue.

Taylor, F. W., J. T. Houghton, G. D. Peskett, C. D. Rodgers, and E. J.

APPENDIX E

Williamson, Radiometer for remote sounding of the upper stratosphere, *Appl. Opt.*, *11*, 135–141, 1972.
Wale, M. J., Development of spectroscopic instrumentation for the remote sounding of the atmosphere, Ph.D. thesis, Oxford Univ., Oxford, England, 1981.
Wale, M. J., and G. D. Peskett, Some aspects of the design and behavior of the stratospheric and mesospheric sounder, *J. Geophys. Res.*, this issue.

J. J. Barnett and M. Corney, Department of Atmospheric Physics, Clarendon Laboratory, University of Oxford, Oxford OX1 3PU, Great Britain.

(Received April 25, 1983;
revised October 11, 1983;
accepted December 23, 1983.)

APPENDIX F

OBSERVATIONS OF CH4 AND N2O BY THE NIMBUS-7 SAMS: A COMPARISON WITH IN SITU DATA AND TWO-DIMENSIONAL NUMERICAL MODEL CALCULATIONS

[Reproduced from *Journal of Geophysical Research, 89*, 5263-5279 (1984).]

Observations of CH_4 and N_2O by the NIMBUS 7 SAMS: A Comparison With In Situ Data and Two-Dimensional Numerical Model Calculations

R. L. Jones

Department of Atmospheric Physics, Clarendon Laboratory

J. A. Pyle

Rutherford Appleton Laboratory

Monthly mean, zonal mean measurements of CH_4 and N_2O for 1979 made by the stratospheric and mesospheric sounder (SAMS) on the NIMBUS 7 satellite are presented for the first time. Comparison with in situ and other available data confirms a general pattern of mixing ratios decreasing with height and of maxima, at a given pressure level, in low latitudes. The SAMS data, by virtue of its extensive coverage, reveals new features. These include during certain months a "double peak" when, along a constant pressure surface, mixing ratio maxima are found in low latitudes of both hemispheres with a local minimum at the equator. In the upper stratosphere are found regions of weak and strong horizontal gradients. Comparison with a two-dimensional model shows many areas of agreement, especially for CH_4, and the model is used to interpret atmospheric behavior. The model overestimates the observed N_2O in the upper stratosphere. This is investigated in terms of a possible underestimation of the photochemical sink. We believe strongly, however, that uncertainties in transport representation cannot be ruled out.

1. Introduction

The stratospheric and mesospheric sounder (SAMS) instrument launched on the NIMBUS 7 satellite in October 1978 is a multi-channel infrared limb scanning radiometer employing conventional chopping and pressure modulation techniques to measure atmospheric temperature and the abundances of a number of minor constituents by detecting either their thermal emission or, in some cases, resonantly scattering sunlight. In this paper we present monthly mean cross sections of CH_4 and N_2O for 1979 derived from SAMS measurements. The satellite data provide a great increase in spatial and temporal coverage compared with previous measurements and many features which could not be resolved by limited in situ measurements become accessible to investigation. Since the production of CH_4 and N_2O is at the ground and the photochemical sink is weak in the stratosphere, the satellite data should prove particularly useful for tracing atmospheric motions. Comparison of the zonal mean data with a two-dimensional model places a strong constraint on the transport and photochemical schemes used by the model. In areas of good agreement the model can be used diagnostically to make inferences about atmospheric processes. For the comparison we have used the two-dimensional circulation model developed initially at the University of Oxford.

In the following sections, the CH_4 and N_2O channels of the SAMS instrument are briefly described. An error analysis of the retrieval of the radiance data to give mixing ratio profiles is summarized. The data for 1979 are then presented and a comparison with other measurements made. This is followed by a brief description of the numerical model. After a comparison with the model results, a number of particular features shown by the data are discussed in more detail.

Paper number 3D1644.
0148-0227/84/003D-1644$05.00

2. The CH_4 and N_2O Sensing Channel on SAMS

A detailed description of the SAMS instrument has been given by *Drummond et al.* [1980]. Broad spectral selection for the CH_4 and N_2O (C2/3) sensing channel is provided by a dichroic beam splitter and a filter consisting of three separate components, which together define a spectral passband with maximum transmission at 7.8 μm (1280 cm^{-1}) and half heights at 7.5 μm (1340 cm^{-1}) and 8.3 μm (1200 cm^{-1}). Atmospheric emission in this region of the spectrum arises primarily from the P and Q branches of the ν_4 band of CH_4 and the ν_1 band system of N_2O, with minor additional contributions from CO_2, H_2O, SO_2, O_3, and HNO_3. Atmospheric radiant energy directed into the C2/3 channel passes through two pressure modulated cells (PMCs), the first containing N_2O gas and the second CH_4 gas, which act as optical filters allowing emission from each of these species to be detected selectively [see *Drummond et al.*, 1980]. The mean pressure of gas in each modulator can be set to either of two preselected pressures (see Table 1) extending the useful vertical coverage that may be obtained with each channel. To illustrate this effect, in Figure 1 are curves showing the variation with height of the emissivity of the CH_4 and N_2O channels for the two available mean PMC pressures. The best measurements are obtained over the height range where the emissivity gradient is large, with little useful information being obtained from the levels where the emissivity is close to zero or unity. By altering the mean PMC pressure, the spectral response of the pressure modulated channel is moved closer to or further from the centers of emission lines, shifting the region of maximum emissivity gradient in the vertical. The effect is evident in the curves shown in Figure 1 (compare curves a and b and curves c and d). The emissivity curves of the N_2O channel tend to zero at lower levels than those of the CH_4 channel because of the much more rapid drop-off of N_2O with height.

Because the CH_4 and N_2O PMCs share a common detector, only one channel can be enabled at any one time so that

APPENDIX F

TABLE 1. Nominal Mean PMC Pressures in the CH_4 and N_2O Pressure Modulators

Channel	Mode	Mean PMC Pressure and Estimated Error, mbar
C2 (N_2O)	C2S0	7.15 (±3.5%)
	C2S1	24.4 (±2.0%)
C3 (CH_4)	C3S0	22.5 (±1.0%)
	C3S1	47.8 (±1.0%)

Cell length 3 mm, approximate compression ratio: 1.7.

simultaneous measurements of both gases are not possible. Normally, therefore, measurements of CH_4 and N_2O are made on alternate days and this, together with the SAMS duty cycle of 3 days on and 1 day off, means that measurements of each species are possible for ~40% of the time (~12 days a month).

3. RETRIEVALS

The signal-to-noise ratio of the measured radiances was not in general sufficient to obtain individual profiles of CH_4 and N_2O. Normally, therefore, we derived zonal mean mixing ratio profiles directly from zonally averaged radiance profiles and effective zonal mean temperature profiles. To account for the nonlinearity of the Planck function at 7.8 μm, at each level we first average zonally the Planck function at this wavelength using the SAMS derived temperatures [see *Barnett and Corney*, this issue]. Each zonal mean Planck function profile is then inverted to give an effective temperature profile for each latitude band. Some error does result through averaging zonally rather than by using smaller longitudinal segments and then averaging the retrieved profiles but, as is discussed further in section 4.3, we found this to be minor when compared with other systematic errors.

Normally, we averaged radiances over 10° latitude bands and 0.2 scale height (~1.4 km) intervals. The choice of these values is somewhat subjective, with these representing a suitable compromise between latitudinal resolution and the computation time required for the retrievals. The signal-to-noise ratios of the zonal mean radiance profiles depend greatly on the atmospheric temperature structure (see Figure 2) and the instrument channel used. Signal-to-noise ratios reached typically ~30 in the low stratosphere. The restrictions that this places on the accuracy of retrieved solutions are discussed in section 4.5.

The retrieval method employed a sequential estimator to update an a priori profile and covariance. To ensure rapid convergence, the most recent previous measurement at each latitude was used for the a priori profile with an overestimated variance. This method is described in detail elsewhere in this issue [*Rodgers et al.*, this issue].

4. ACCURACY AND PRECISION OF THE SAMS CH_4 AND N_2O MEASUREMENTS

An important feature of atmospheric measurements made from a satellite-mounted instrument such as SAMS is that spatial and temporal variations in atmospheric state become accessible to measurement. It is particularly important, therefore, that those errors that may introduce spurious features of these kinds are well understood and their magnitudes known. In the following discussion of error sources we have attempted, where possible, to distinguish between the errors of this type and those which to first order only lead to constant biases in the retrieved fields. Where the distinction cannot be made reliably, we have, if anything, erred on the conservative side.

Systematic errors in the retrieved constituent fields fall broadly into four categories: uncertainties in the spectroscopy of the absorbing gases; instrumental uncertainties; limitations and simplifications in the retrieval method and algorithm (e.g., uncompensated Doppler shifts and errors associated with the zonal averaging of radiances and temperatures); and inaccurate knowledge of the atmospheric state (primarily of the temperature field). These various error sources and their impacts

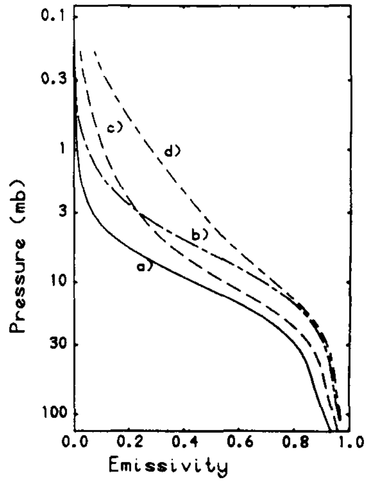

Fig. 1. Variation of emissivity with pressure level for the SAMS N_2O and CH_4 channels assuming typical equatorial mixing ratio and temperature profiles. Curves a and b are for the N_2O channel for mean PMC pressures of 24.4 and 7.15 mbar, respectively, and curves c and d are for the CH_4 channel, 47.8 and 22.5 mbar, respectively.

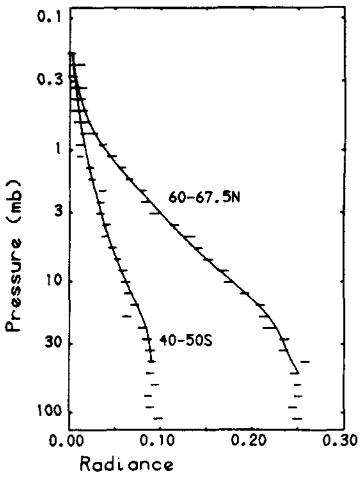

Fig. 2. Examples of zonal mean radiance profiles for July 2, 1979 (expressed as a fraction of the signal observed from a black body at 290 K). The horizontal bars denote measurements and their (±1σ) errors, and the solid curves are synthetic profiles computed from the retrieved mixing ratio profile. The difference between the profiles is mainly due to the large interhemispheric temperature gradient present at the time.

TABLE 2*a*. Summary of Error Budget for the C3 (CH_4) Sensing Channel on SAMS

Pressure Level	20 mbar	7 mbar	2 mbar	0.6 mbar	0.2 mbar
1. Spectroscopy	±7%	±7%	±5%	±5%	±5%
2. Field of view	±2%	±1%	±3%	±6%	±3%
3. Mean PMC pressure	±3%	±2%	±6%	±6%	±3%
4. Uncompensated Doppler shifts	±1.5%	±1%	±1.5%	±6%	±7%
5. Zonal averaging	±8%	±8%	±8%	±8%	±8%
6. Interference of N_2O	±5%	±2%	±0.5%	—	—
7. Temperature (±2 K)	±50%	±15%	±10%	±10%	±10%
8. Line-of-sight attitude (±0.006°)	±4%	±2%	±6%	±10%	±6%
9. RSS of latitude and time dependent errors	±51%	±15%	±12%	±17%	±14%
10. RSS of bias errors	±9%	±6%	±8%	±10%	±7%
11. Net RSS accuracy	±52%	±18%	±17%	±21%	±17%
12. Precision of monthly mean cross section	±5–15%	±3–10%	±3–13%	±4–13%	±20–40%

on the retrieved constituent fields are described below. Other more minor error sources also exist, and, although these are not discussed individually below, their effects have been included in the error budget summaries given in Tables 2*a* and 2*b*.

To compute the magnitudes of systematic errors, a synthetic radiance profile was computed for typical mixing ratio and temperature profiles, with all the uncertain parameters set to their nominal values. This data set was then retrieved with each uncertain parameter offset in turn within its limit of uncertainty, and the retrieval is then compared with the original. Several tests were performed that demonstrated that the errors were sufficiently insensitive to the temperature and mixing ratio profiles used for the results presented below to be of general applicability.

4.1. *Spectroscopic Errors*

Uncertainty in the atmospheric absorptions of CH_4 and N_2O was minimized by measuring in the laboratory the response of sensors, identical in design and construction to those used in the flight instrument, to simulated atmospheric limb paths containing these gases. Corresponding line-by-line transmission calculations were then performed, using spectral data from the compilations of *McClatchey et al.* [1973] and *Rothman* [1981], which demonstrated that minor improvement and modifications to the spectral data were required [*Jones*, 1983]. Using the modified spectral data, residual uncertainty in the absorptions of CH_4 and N_2O is estimated to be equivalent to bias error of $\sim \pm 5$–7% in the retrieved mixing ratios of both CH_4 and N_2O (Tables 2*a* and 2*b*, row 1).

4.2. *Instrumental Uncertainties*

The CH_4/N_2O channel field of view was measured as an integral part of the prelaunch testing to be approximately Gaussian in the vertical with a half width at half height of ~4 km. Some uncertainty is present in this measurement which may be thought of as being approximately equivalent to an uncertainty in view angle of ±0.003° or approximately ±0.2 km at the tangent point. The effect of such an error is to change the vertical gradient of the retrieved profiles, leading to biases of up to ±5% in the retrieved mixing ratios of CH_4 and up to ±7% in those of the N_2O (see Tables 2*a* and 2*b*, row 2).

The mean pressure of gas in a PMC is critical in defining the spectral response of that channel (refer for example to Figure 1); any error leads to both a vertical gradient change and an offset in the derived fields. The gas pressures in the CH_4 modulator are known to ±1% and those in the N_2O modulator to ±3.5% and ±2% for the low and high mean cell pressures, respectively (see Table 1). These lead to bias

TABLE 2*b*. Summary of Error Budget for the C2 (N_2O) Sensing Channel on SAMS

Pressure Level	20 mbar	7 mbar	2 mbar	0.6 mbar
1. Spectroscopy	±7%	±7%	±5%	±5%
2. Field of view	±2%	±4%	±7%	±8%
3. Mean PMC pressure	±3%	±2%	±17%	±21%
4. Uncompensated Doppler shifts	±3%	±2%	±45%	±15%
5. Zonal averaging	±8%	±8%	±8%	±8%
6. Interference of CH_4	±8.5%	±2%	±5%	±25%
7. Temperature (±2 K)	±50%	±15%	±10%	±20%
8. Line-of-sight attitude (±0.006°)	±4%	±8%	±12%	±3%
9. RSS of latitude and time dependent errors	±51%	±17%	±48%	±35%
10. RSS of bias errors	±9%	±7%	±20%	±24%
11. Net RSS accuracy	±52%	±20%	±50%	±43%
12. Precision of monthly mean cross section	±12–20%	±6–17%	±10–24%	±50–100%

errors of up to $\pm6\%$ in the retrieved CH_4 mixing ratios (Table 2*a*, row c) and up to $\pm25\%$ in those of N_2O (Table 2*b*, row 3).

4.3. *Limitations in the Retrieval Method*

A problem inherent in using a gas correlated device such as a pressure modulator is the Doppler shifting of atmospheric emission lines relative to those in the PMC on the orbiting spacecraft. In normal operation the instrument line-of-sight is nominally perpendicular to the direction of spacecraft motion so that the shift is due to the combined effects of the earth's rotation and atmospheric winds. In practice, an additional component arises because of yaw angle errors in the spacecraft orientation (estimated to be $\pm0.6°$). The dominant component—that due to the earth's rotation—can be precomputed from a knowledge of the instrument viewing geometry and is therefore included explicitly in the model for calculating atmospheric radiances. The other sources cannot be dealt with reliably and have not been allowed for. This results in uncertainties of up to $\sim5\%$ in the CH_4 abundances and up to $\sim\pm30\%$ at higher levels in those of N_2O (see Tables 2*a* and 2*b*, row 4).

As was stated above, zonal mean mixing ratio cross sections have been derived directly from zonal mean radiance and temperature and cross sections. While this approach is likely to be satisfactory when the temperature and constituent fields are zonally symmetric (frequently the case in the summer hemisphere), significant errors might arise during more active winter periods when large waves in temperature and constituent concentration may be present around a latitude circle. A direct test of the accuracy of this approach was therefore made, using as an example a single days data (February 9, 1981). At this time a large temperature wave was present at high northern latitudes with an amplitude in excess of 30 K peak-to-peak between 30 and 1 mbar. In contrast, the temperature field in the summer (southern) hemisphere was almost zonally symmetric. Radiances in the latitude bands from 60°N to 67.5°N and from 50°S to 40°S were retrieved by using different numbers of boxes around each latitude circle, namely, (1) one 360° longitude box (the standard), (2) four 90° longitude boxes, and (3) twelve 30° longitude boxes.

A mixing ratio profile was retrieved for each box. A zonal mean mixing ratio profile was then obtained for each test by averaging the individual boxes together with due regard for their uncertainties. As expected, the zonal mean profiles for the band between 50°S and 40°S were almost indistinguishable, while those for the 60°N–67.5°N band showed minor differences, with an rms scatter of between 3.5 and 8% at different heights. However, in spite of these differences the important features were faithfully reproduced in all three profiles. We have taken an error of $\pm8\%$ as being the maximum error incurred through the zonal averaging of radiances (Tables 2*a* and 2*b*, row 5). This, of course, represents a worst case, appropriate only when large deviations from a zonally symmetric atmospheric state are present.

4.4. *Uncertainties in the Atmospheric State*

Atmospheric thermal emission in the 7.8 μm region of the spectrum arises predominantly from CH_4 and N_2O, with minor additional contributions from CO_2, H_2O, O_3, SO_2, and HNO_3. The use of a gas correlated technique like pressure modulation virtually excludes emission from the minor contributors, although the mutual overlap of the CH_4 and N_2O bands is such that a small correction caused by absorption by the other must be applied in the retrieval of both species. As the atmospheric distributions of both species are of course measured by the SAMS, we have applied a correction using the most recent previous measurement of the abundance of the interfering gas at that latitude. Uncertainties in abundances of the contaminating gas lead to uncertainties of $\pm5\%$ in the retrieved mixing ratios of CH_4 at low levels, decreasing rapidly with height, and $<6\%$ over most of the stratosphere for N_2O, increasing to $\sim25\%$ at the stratopause level (see Tables 2*a* and 2*b*, row 6).

An error in the assumed atmospheric temperature structure leads to an anti-correlated error in the retrieved minor constituent fields. The atmospheric temperatures used in the retrievals are derived from SAMS measurements of thermal emission from the 15-μm band of CO_2 in a coupled temperature/line-of-sight attitude retrieval. Uncertainty in the retrieved temperature field is estimated to be ±2 K [*Barnett and Corney*, this issue] and $\pm0.006°$ in attitude, equivalent to $\pm$ 0.37 km at the tangent point (J. J. Barnett, private communication, 1983), both with possibly significant latitudinal and seasonal components. An uncertainty in temperature of ±2 K translates to a mixing ratio error of $\gtrsim\pm15\%$ (See Tables 2*a* and 2*b*, row 7), while an uncertainty in attitude of $\pm0.006°$ gives rise to an error of $\lesssim10\%$ (Tables 2*a* and 2*b*, row 8).

4.5. *Random Errors*

Random errors on the retrieved solutions are predominantly due to radiance noise. We can determine the effects of radiance noise on the retrieved mixing ratio profiles straightforwardly from the diagonal elements of the error covariance matrix obtained from the retrieval process [see *Rodgers et al.*, this issue]. Typical values for the random errors on a monthly mean cross section obtained in this way are shown in Tables 2*a* and 2*b*, row 12. A precise value cannot be given as this would depend on the atmospheric temperature structure (which as can seen from Figure 2 largely determines the signal-to-noise ratios of the radiance measurements) and to a lesser extent on the temporal coverage obtained during each month. Errors obtained in this way are overestimates in that they take no account of the correlations that are present between the retrieved mixing ratios at the various levels.

4.6. *Summary of Errors*

For both channels, insufficiently accurate knowledge of the atmospheric temperature structure and to a lesser extent of the line-of-sight attitude are potentially significant sources of spurious latitudinal or seasonal features. For the N_2O channel, uncompensated Doppler shifts are another potentially serious problem, particularly in the upper stratosphere (see Table 2*b* row 4) where the emission lines of N_2O at 7.8 μm are Doppler broadened and hence narrow. Comparison of Tables 2*a* and 2*b*, rows 9 and 10 shows that purely bias errors are generally small in comparison.

The net RSS accuracies of the CH_4 and N_2O measurements made by the SAMS are shown in percentage terms at various heights in Tables 2*a* and 2*b* row 11. Over much of the stratosphere the CH_4 measurements are seen to be superior to those of N_2O with an RSS accuracy of $\lesssim20\%$ compared with 25–50% for the latter. This is a consequence of the greater sensitivity of the N_2O channel to unwanted Doppler shifts and to interference by CH_4 in the upper stratosphere and is offset to some extent by the more rapid vertical drop-off of N_2O mixing ratio with height and the consequential increase, in percentage terms, of the features observed (e.g., latitudinal gradients) in the cross sections. These values are to be compared with the precisions at various heights obtained on a monthly mean cross section (Tables 2*a* and 2*b* row 12).

The vertical extent of useful CH_4 and N_2O measurements made by the SAMS is influenced by a number of factors. The spectrocopy and the atmospheric distributions of each species, together with the spectral response of each channel, couple to define the height range over which information may in principle be obtained (refer for example to Figure 1). In practice, however, the finite signal-to-noise ratio of the radiance measurements and the sensitivity of the retrievals to systematic errors reduce the useful coverage. We feel that useful measurements of monthly zonal mean cross sections of CH_4 are made between 20 mbar ($\sim$30 km) and 0.2 mbar ($\sim$60 km) and of N_2O between 20 mbar ($\sim$30 km) and 0.6 mbar ($\sim$53 km). The data presented below have been restricted to within these confidence limits.

5. THE DATA SET

Since launch in October 1978, over 4 years of CH_4 and N_2O radiance measurements have been accumulated. Data from the whole of 1979 and a 3 month period in early 1981 have been retrieved and studied extensively. In the following discussion we will concentrate our attention on the first full year of data. In Figures 3*a*–3*l* and 4*a*–4*l* are shown monthly mean, zonal mean cross sections of N_2O and CH_4 for January–December 1979. Mixing ratios are plotted only between the confidence limits discussed in the previous section. Note that the coverage is asymmetric about the equator, extending from 50°S to 70°N. The gross structure suggested by these cross sections is of a low latitude, low stratosphere maximum, with the mixing ratios of both CH_4 and N_2O decreasing with height throughout the stratosphere, the former by a factor of $\sim$6, the latter much more strongly, by a factor of $\sim$60. Superimposed on this basic structure are large, apparently seasonal, changes. Of particular note is the marked correlation between the changes observed in the CH_4 and N_2O cross sections throughout the year (simple inspection of Figures 3 and 4 is sufficient to reveal this).

During January (refer to Figures 3*a* and 4*a*) the distributions of CH_4 and N_2O showed a marked asymmetry about the equator, with a region of elevated mixing ratios extending throughout the stratosphere, tilting from the equator at $\sim$20 mbar into the summer (southern) hemisphere, reaching a latitude of $\sim$20°S at the stratopause level. By way of contrast, at this time a more rapid drop-off of mixing ratio was evident in low northern (winter) latitudes with a region of weaker gradients above. This structure persisted through February (Figures 3*b* and 4*b*)), but during March and April (Figures 3*c* and 3*d* and 4*c* and 4*d*) the southern hemisphere maximum began to subside, and a second similar feature began to develop in the northern hemisphere, giving by May (Figures 3*e* and 4*e*) an almost symmetric pattern. This "double peak" structure in which two low latitude maxima, on a fixed pressure surface, are separated by a local mixing ratio minimum near the equator will be discussed in detail below.

By July, the pattern was a reversal of that of January, with an area of elevated mixing ratio now extending into the northern hemisphere with again an area of weaker vertical gradients in the winter mid-stratosphere (Figures 3*g* and 4*g*). The structure during the second half of 1979 differed in many respects from that of the first. During August and September throughout the middle stratosphere there existed a pronounced maximum at low latitudes. At high northern latitudes very little height variation of the mixing ratio is evident in the upper stratosphere (Figures 3*h* and 3*i* and 4*h* and 4*i*). Coverage does not extend sufficiently far into the southern hemisphere to establish the existence of a corresponding feature 6 months earlier. By October, the maximum had subsided somewhat, although the region of uniform mixing in the vertical still persisted. The "double peak" structure evident during May was not observed. In the final months of 1979, the maximum continued to subside giving, by December, an almost symmetric distribution (Figures 3*l* and 4*l*).

The high degree of correlation between the distributions of CH_4 and N_2O is expected because both originate in the troposphere, and their long photochemical lifetimes (of the order of many months for both gases in the mid-stratosphere) mean that the distributions of both species are determined in large part by the same dynamical processes. It is important to note that because of the more rapid vertical decrease of N_2O, the errors required to introduce similar spurious features into the distributions of both species are radically different. However, the sensitivities of both species to known errors are of comparable size or do not influence the CH_4 distribution significantly (see Tables 2*a* and 2*b*), and we therefore have considerable confidence that the features evident in Figures 3 and 4 are substantially real and are not artifacts of the instrument calibration or the retrieval algorithm.

6. COMPARISON WITH OTHER MEASUREMENTS

Vertical profiles of CH_4 and N_2O have been measured on numerous occasions over the last decade, the majority by local sampling using either evacuated grab samplers or cryosamplers although several remote measurements using infrared absorption techniques have also been made [see *World Meteorological Organization*, 1982] (WMO). These data do not provide uniform spatial coverage, being strongly weighted to latitudes of 32°N, 44°N, and 52°N for CH_4 and to equatorial latitudes and 44°N for N_2O.

Because of the large variability evident in the profiles of CH_4 and N_2O measured by other workers (much larger than the precisions of 2–5% quoted by the individual experimenters) and the absence of any clearly defined seasonal trends, we feel that a comparison of SAMS zonal mean CH_4 and N_2O profiles with the few profiles measured during 1979 would be of dubious value. Instead, in Figures 5–10 we compare all the available measurements made using in situ and other remote techniques (as presented in *WMO* [1982]) with annual mean profiles of CH_4 and N_2O for 1979 measured by SAMS at various latitudes and leave a discussion of the observed seasonal changes to section 8.

As the SAMS measurements are made with respect to pressure coordinates while those of other workers are generally quoted in relation to geometric height, we have used a climatological annual mean, zonal mean temperature cross section kindly provided by J. J. Barnett (private communication, 1983) to relate the two.

For CH_4, SAMS and other measurements are consistent where overlap occurs (the SAMS measurements extend to much higher levels). At low latitudes ($<10°$), there are too few measurements to draw firm conclusions, but the SAMS profile and the one available in situ measurement are consistent

APPENDIX F

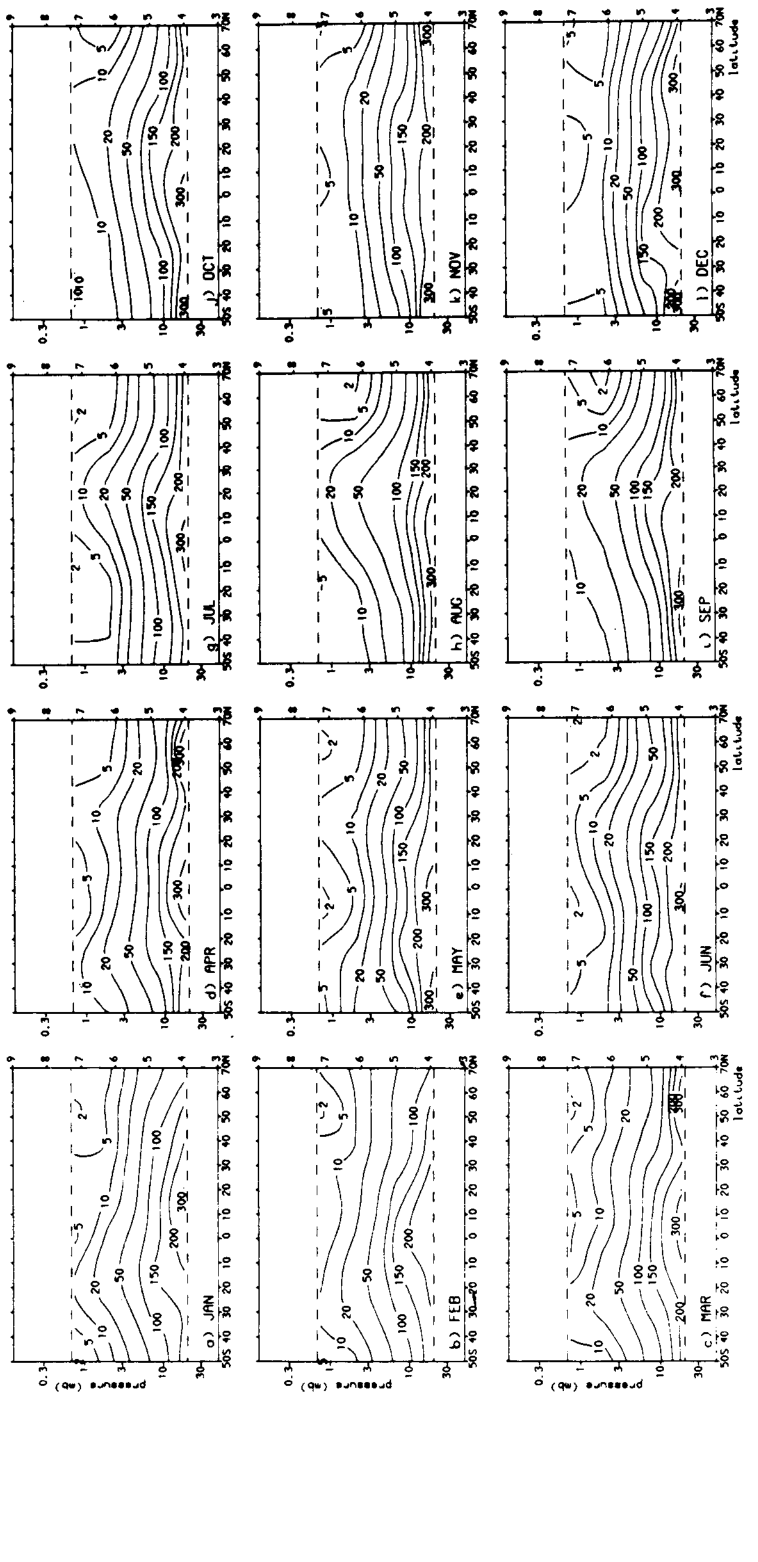

Fig. 3. Monthly mean cross section of N_2O (ppbv) between 50°S and 70°N for 1979 measured by the NIMBUS 7 SAMS. The error budget is shown in Table 2*a*.

APPENDIX F

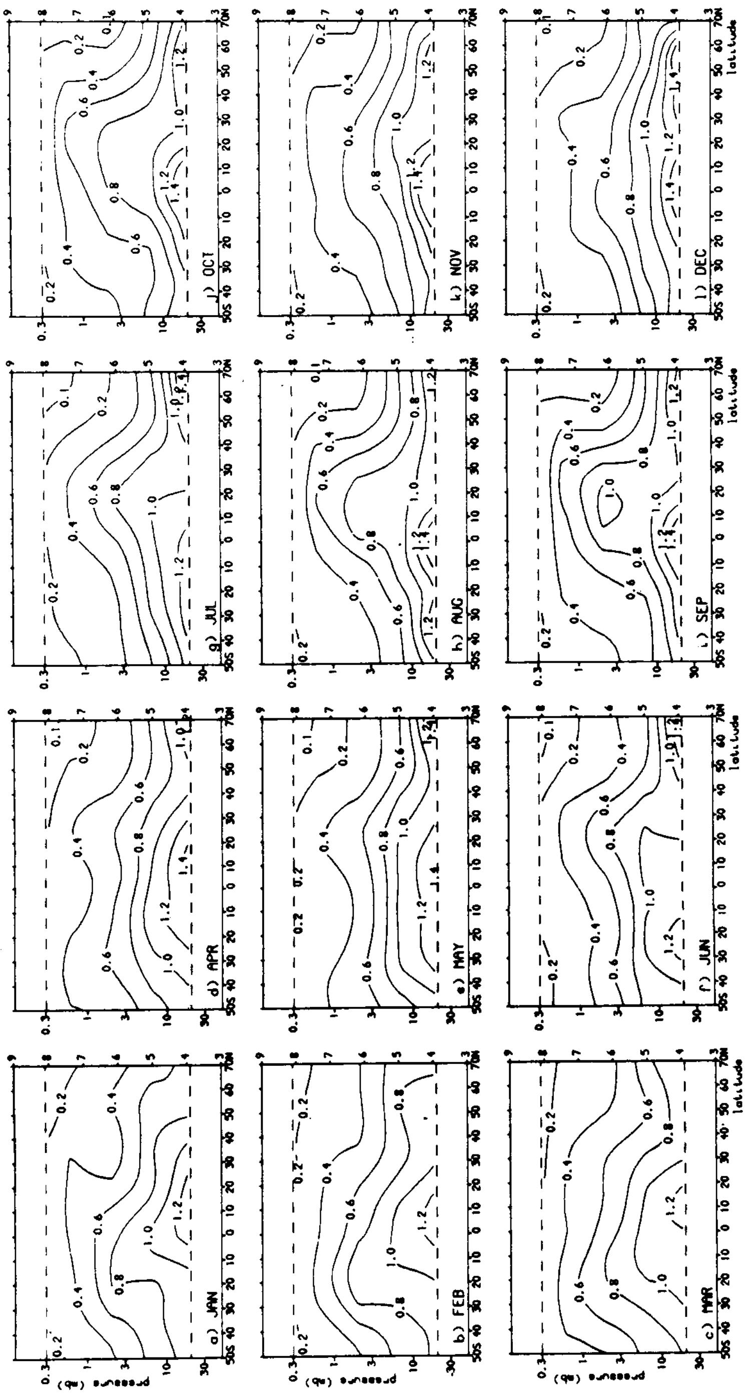

Fig. 4. Monthly mean cross section of CH_4 (ppmv) between 50°S and 70°N for 1979 measured by the NIMBUS 7 SAMS. The error budget is shown in Table 2b.

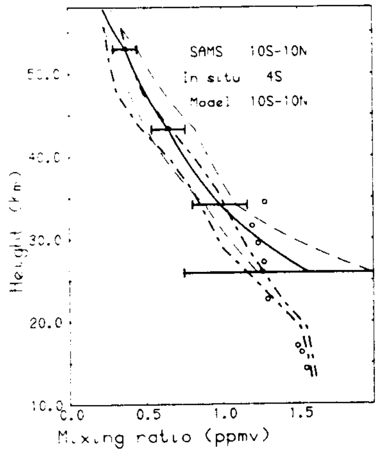

Fig. 5. Comparison of the SAMS CH_4 annual mean profile (solid line) for 10°S to 10°N with other measurements (circle, *WMO* [1982]). The dashed envelope (dashed line) shows the standard deviation of the montly mean profiles for the latitude band and the horizontal bars the estimated accuracy. The heavy dot-dash envelope shows the annual variation of the model profiles over the indicated latitude band.

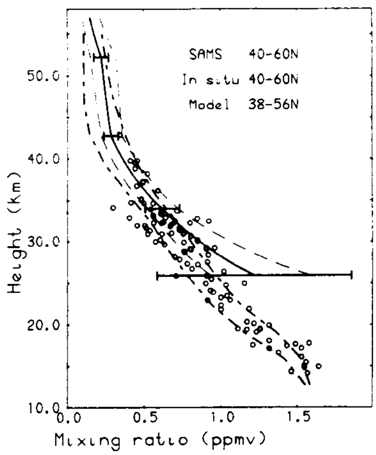

Fig. 7. As Figure 5, except at 40°–60°N.

(Figure 5). Between 25°N and 35°N, many more measurements have been performed. These show an almost linear drop-off of mixing ratio with height from 1.6 ppmv at 15 km to 0.5 ppmv at 40 km, although with much greater variability than at other latitudes. A similar drop-off is evident in the SAMS measurements, reaching a somewhat higher mixing ratio of 0.7 ppmv at 40 km, with a region of weaker vertical gradients above (Figure 6). Between 40°N and 60°N (Figure 7), the in situ measurements show a rather more rapid, although still approximately linear drop-off of mixing ratio with height up to 35 km. The SAMS measurements reproduce well the vertical gradient, showing the drop-off extending to above 40 km with, again, a region of weak vertical gradient above. The SAMS measurements are also consistent with the one profile measured at 65°N (Figure 8).

For N_2O, at equatorial latitudes (Figure 9) above 30 km the SAMS measurements agree well with other measurements both in terms of vertical gradient and absolute amount. Below 30 km the SAMS measurements are biased high, but nevertheless the two data sets are consistent to within their estimated accuracies. At 45°N (Figure 10), although the SAMS measurements reproduce fairly well the vertical gradient suggested by the in situ measurements, they appear biased high relative to the latter, by 20–30% at 30 km and rather more below. It is conceivable that this discrepancy is exacerbated by a combination of the more rapid vertical drop-off of N_2O compared with that of CH_4 and inaccuracies in relating the geometric height and pressure scales of the two data sets.

Overall, the SAMS measurements reproduce well the gross features shown by other measurements, namely, the low stratosphere, low latitude maxima, the almost linear decrease of CH_4 with height at mid- and high latitudes, and the much more rapid vertical drop-off of N_2O. There is some indication of a bias (SAMS higher than other measurements), particularly in the low stratosphere at high latitudes, although the two data sets are consistent to within their estimated accuracies.

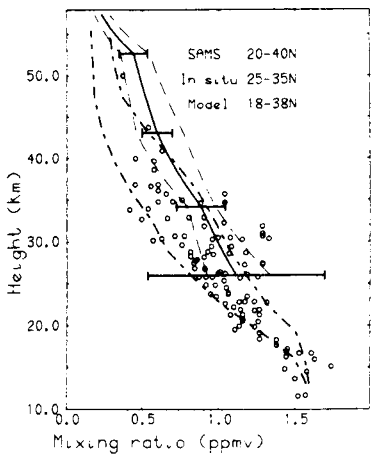

Fig. 6. As Figure 5, except at 20°–40°N.

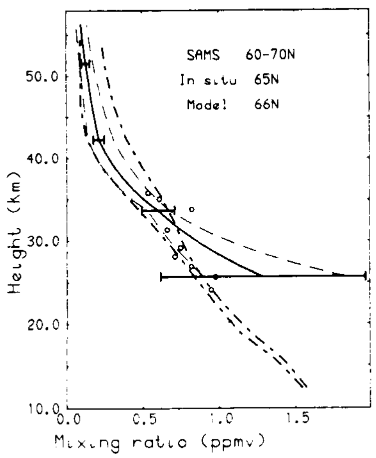

Fig. 8. As Figure 5, except at 60°–70°N.

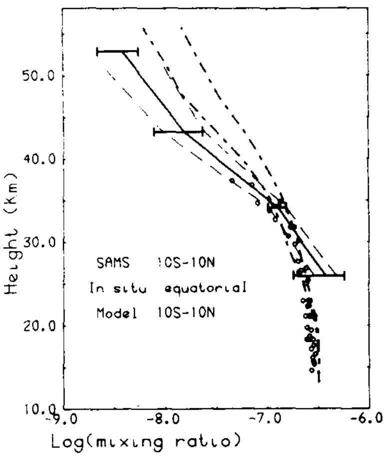

Fig. 9. As Figure 5, except the SAMS N_2O is plotted for the 10°S–10°N latitude band.

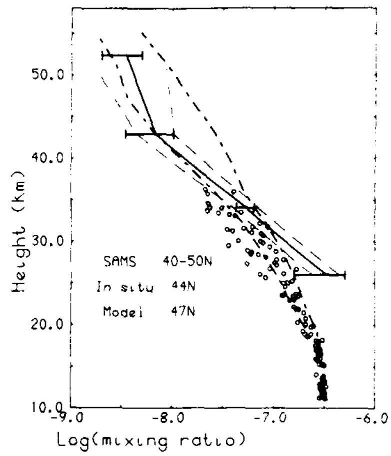

Fig. 10. As Figure 9, except at 40°–50°N.

7. MODEL

The model used in this study is the two-dimensional circulation model described by *Harwood and Pyle* [1975]. The model calculates the zonal mean values of temperature, wind components, and chemical constituent mixing ratios with a resolution of $\pi/19$ in latitude, 0.5 in ln (p_0/p) (approximately 3.5 km) in the vertical and with a 6 hour time step. A second-order partial differential equation is solved for the meridional stream function given the forcing by radiative and other diabatic heating and eddy heat and momentum fluxes. The dynamical and radiative formulation employed is that described by *Haigh and Pyle* [1982].

The horizontal eddy momentum fluxes are derived from data from the selective chopper radiometer flown on NIMBUS 5. Monthly means of the 1973 values are used. The eddy fluxes of heat and tracers are calculated by using the K coefficients derived by *Luther* [1973] and based on atmospheric statistics. It is clear that by using these data we should not expect the model to reproduce the behavior of any particular month's synoptic situation, still less that it should reproduce behavior on a shorter time scale. Neither will the model necessarily reproduce long-term average behavior since, for example, the momentum fluxes were obtained from just one year of data. However, experiments using different K coefficients and momentum fluxes [*Harwood and Pyle*, 1980] still preserve the main features of the month-to-month changes in the model and maintain the broad agreement found on comparison with observations. Thus, we are confident that the model development is at least representative of some mean atmospheric behavior. This should be borne in mind when considering the comparisons presented later.

The photochemical scheme is based on that used by *Haigh and Pyle* [1982] in which family groupings are employed. The kinetic data have been updated by the recommendations of *WMO* [1982] and *Baulch et al.* [1980]. HO_2NO_2 and HOCl are now included in the photochemical scheme, and in this case continuity equations are also solved for CH_4 and N_2O with sinks calculated using the reactions in Table 3. At the bottom boundary the mixing ratios of CH_4 and N_2O are fixed at their tropospheric values. The upper boundary at approximately 60 km is a rigid lid to tracers. Unlike in Haigh and Pyle, the photochemical model used here contains a source of chlorine which simulates the natural background.

We have discussed above some of the problems related to comparing model and observations arising from the representativeness of the model transport fields. For non-conservative tracers, like CH_4 and N_2O, the comparison will also depend, for example, on how well the model reproduces the fields of $O(^1D)$, Cl, and OH, with which CH_4 and N_2O react. A detailed analysis of the behavior of all the model constituent fields and their budgets is beyond the scope of this paper, and, indeed, for the important radicals the data base is not adequate to allow latitudinal and seasonal comparisons. Nevertheless, it can be stated that for OH and Cl there is reasonable agreement between model profiles and the very limited number of observations.

8. COMPARISON WITH A TWO-DIMENSIONAL MODEL

8.1. *Model Behavior*

In Figures 11 and 12 are shown cross sections of the CH_4 and N_2O volume mixing ratios for equinox and solstice from a model run, run A. Notice that the model domain covers the entire globe. There is a broad similarity in the two distributions, as would be expected for gases that originate at the surface and are transported into the stratosphere where their lifetimes against photochemical destruction are long.

The model exhibits much less variability than the observations on "short" spatial (<20° latitude) and temporal (< month) scales. This is to be expected since the model is driven by, for example, radiative heating rates and eddy fluxes which are either smoothly varying or monthly averaged.

TABLE 3. Model Photochemical Sinks for CH_4 and N_2O

	Rate Constants
$N_2O + h\nu \rightarrow N_2 + O$	
$N_2O + O(^1D) \rightarrow 2NO$	7.2×10^{-11}
$N_2O + O(^1D) \rightarrow N_2 + O_2$	4.4×10^{-11}
$CH_4 + O(^1D) \rightarrow CH_3 + OH$	1.4×10^{-10}
$CH_4 + Cl \rightarrow CH_3 + HCl$	$2.4 \times 10^{-12} \exp(-1710/T)$
$CH_4 + OH \rightarrow CH_3 + H_2O$	$9.6 \times 10^{-12} \exp(-1350/T)$

Rate constants are in units of cm^3 $molec^{-1}$ s^{-1}.

APPENDIX F

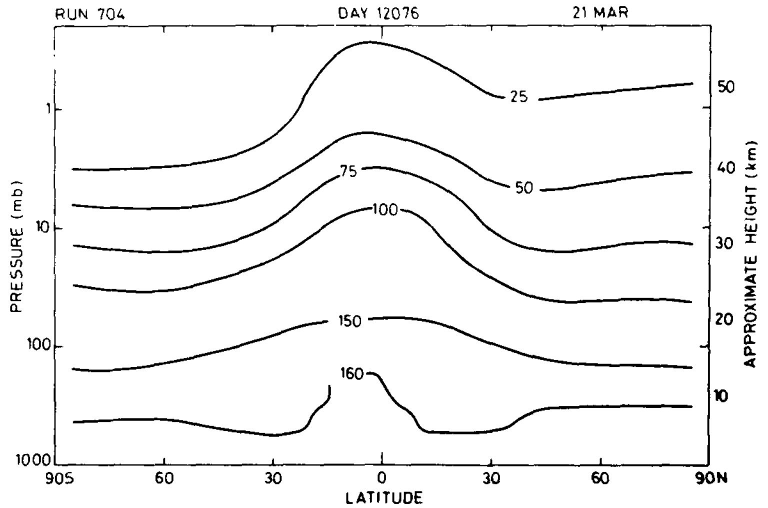

Fig. 11*a*

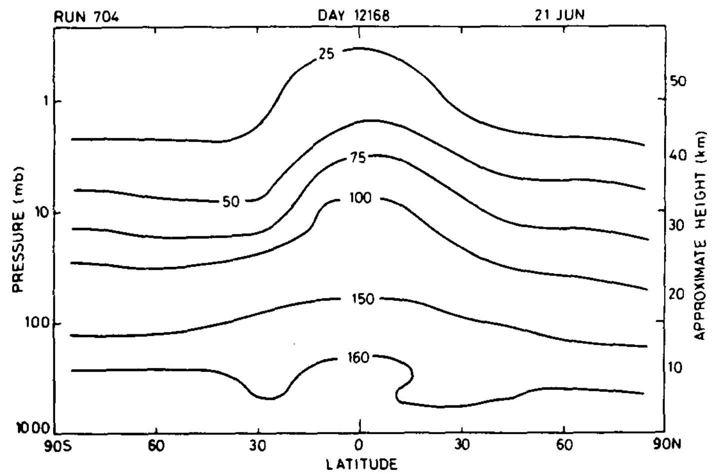

Fig. 11*b*

Fig. 11. Model distributions of CH_4 mixing ratio (ppmv × 100) for (*a*) March, (*b*) June, (*c*) September, (*d*) December.

Short-term or small-scale features, which might have a significant influence on the monthly mean observations for a particular month, should not be expected to be reproduced by the model. It should be noted, for example, that there is much larger variation in the monthly observations than found between successive months of the model. The fact of atmospheric variability must be borne in mind when considering the comparisons discussed below.

The model behavior is quite simple. For any constant pressure surface the maximum mixing ratios are generally found throughout the year in equatorial latitudes. The latitudinal excursions of this maximum are small with the maximum confined to within 10° of the equator. The model does not produce a "double peak," a point discussed in more detail below.

The distributions for the solstices (Figures 11*b*, 11*d*, 12*b*, and 12*d*) are quite symmetric. In contrast, there are significant hemispheric differences in the upper stratosphere at the equinoxes (Figures 11*a*, 11*c*, 12*a*, and 12*c*). For example, in March (Figure 12*a*) the upper stratospheric N_2O mixing ratio decreases from about 25 ppbv at the equator to less then 5 ppbv at the southern pole. The photochemical lifetime of N_2O decreases in the upper stratosphere, being a few weeks at 1 mbar, and the decrease of N_2O in the high latitudes of the sunlit upper stratosphere is, at least in part, due to the integrated photochemical destruction there throughout the polar summer. Six months later the pattern is reversed with a mixing ratio at the southern hemisphere stratopause of about 10 ppbv, produced by transport from the summer hemisphere and the much reduced loss by photochemical processes.

An interesting feature of the model behavior (see, e.g., Figure 11*d*) is the presence of a mixing ratio minimum in middle latitudes of the midstratosphere. This appears to be produced when the reverse mean meridional circulation is established in high latitudes, carrying high mixing ratios aloft at the pole and bringing down air relatively poor in CH_4 and N_2O into middle latitudes. This Eulerian circulation is op-

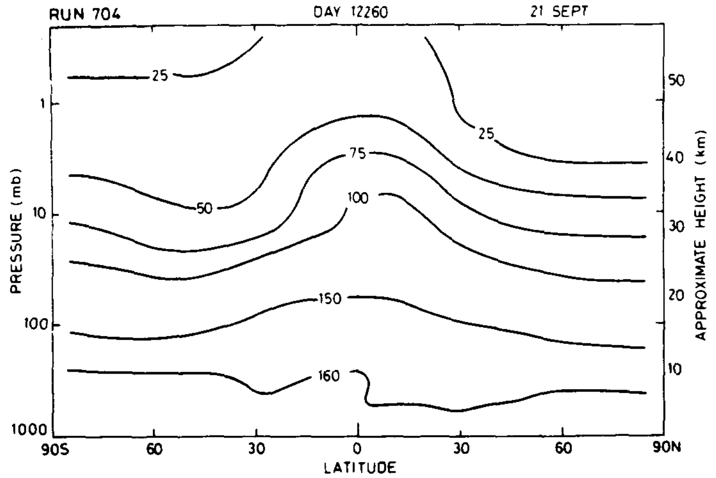

Fig. 11*c*

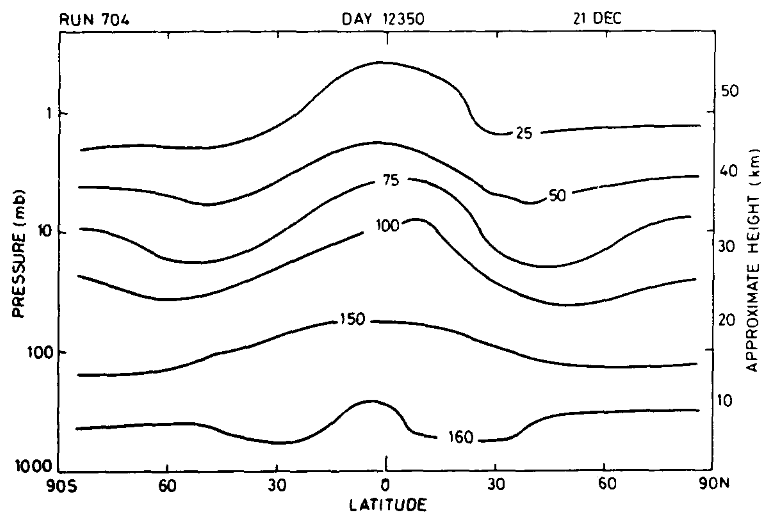

Fig. 11*d*

posed by eddy transports. Nevertheless, the net effect in the model is to produce the mid-latitude minimum.

8.2. *Comparison With Data*

When the model and data are compared, there is satisfactory agreement with respect to the gross features. For both gases there is a decrease of mixing ratio with altitude, this decrease being most pronounced in high latitudes. Both model and data have equatorial or low latitude maxima associated with upward transport in the stratospheric extension of the Hadley cell.

In both observations and calculations the decrease with height is more pronounced for N_2O which has a much shorter photochemical lifetime than CH_4 in the upper stratosphere. This also results in a greater dynamically produced variability of N_2O in the summer upper stratosphere, as discussed above in connection with the model fields and confirmed by the observations. Thus, transport in the meridional plane converts the large N_2O vertical gradients into correspondingly large horizontal gradients. CH_4 is more nearly mixed. For example, there is a factor of 20 difference between N_2O mixing ratios in low and high northern latitudes at about 2 mbar in September, compared with a factor of only about 2 for CH_4 (Figures 11*c* and 12*c*).

As discussed above, the model, at certain times of the year, produces mid-latitude minima in N_2O and CH_4 in the middle stratosphere. As a consequence of the more limited latitudinal coverage provided by the data it is not possible to confirm this feature with confidence, although there are suggestions of such a feature in, for example, Figure 4*c*.

To consider more quantitative aspects of the comparison, the range of CH_4 and N_2O mixing ratios over a model year has been plotted at a number of latitudes in Figures 5–10 along with the SAMS data and the other available observations. For CH_4 the agreement between model and SAMS is generally extremely good (Figures 5, 7, 8). In the low stratosphere the model gives mixing ratios below those observed, but these appear to be biased high when compared with the in

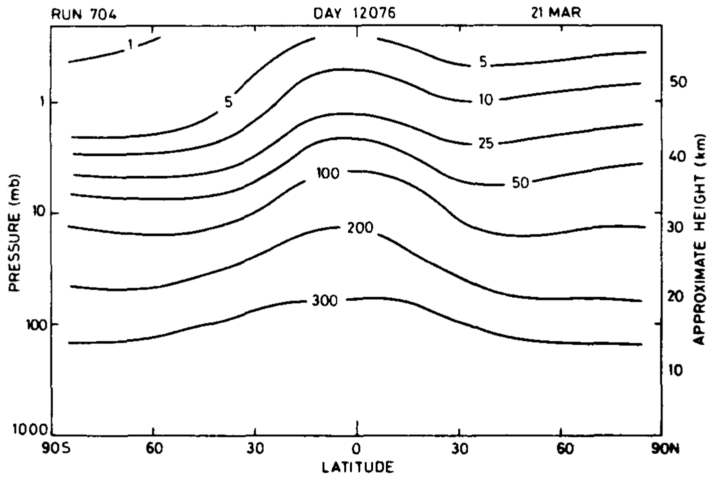

Fig. 12*a*

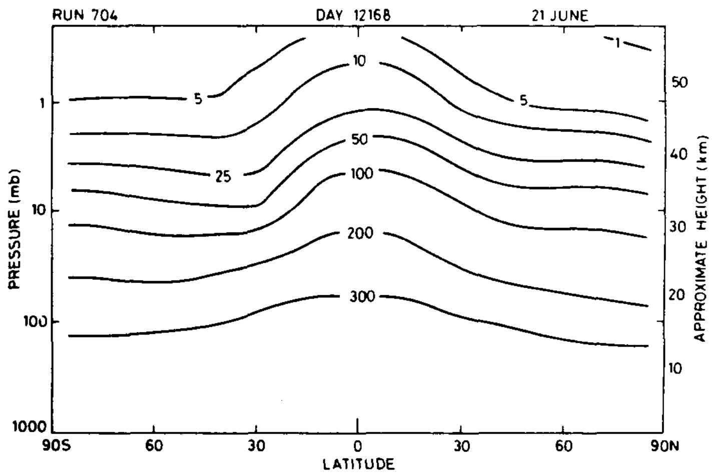

Fig. 12*b*

Fig. 12. Model distributions of N_2O mixing ratio (ppbv) for (*a*) March, (*b*) June, (*c*) September, (*d*) December.

situ measurements. The upper stratospheric values agree well. Notice that the model reproduces the change in the vertical gradient found between 40 and 45 km. We have also found this feature in a model whose vertical domain extended to 80 km, thus ruling out spurious boundary effects.

Agreement is least satisfactory between 20°N and 40°N (Figure 6) where the SAMS observations excede the model results throughout the middle and upper stratosphere. At these latitudes the model shows a minimum, compared with higher and lower latitudes, throughout much of the stratosphere. While this feature, as stated above, appears possibly to be present in some of the observations it cannot be identified unambiguously and is clearly not so pronounced as in the model. Data from other years need to be analyzed before it can be said that this represents a serious discrepancy between the model and data. In the model, the minimum is associated with downward transport, which shows only slow latitudinal variation with time. It is possible that, on the average, downward motion in the atmosphere covers a greater latitudinal extent, thus producing a less strong minimum.

For N_2O the agreement is less satisfactory than in the case of CH_4. At the equator (Figure 9), where for CH_4 there is excellent agreement between model and observations, the decrease of the mixing ratio with height is significantly underestimated in the model. On the other hand, the comparison at 47°N (Figure 10) is somewhat more satisfactory.

The variability of the data makes comparison with an averaged model difficult, even when the annual range is plotted. By choosing specific latitudes it is possible that agreement will appear more satisfactory or disagreements more serious than is the case. A comparison of the two-dimensional distributions should provide a good complementary test, and this has been attempted in Figures 13 and 14 for the month of February.

For CH_4 (Figure 13) there are many satisfactory areas of agreement. The data exhibit a low latitude maximum, dis-

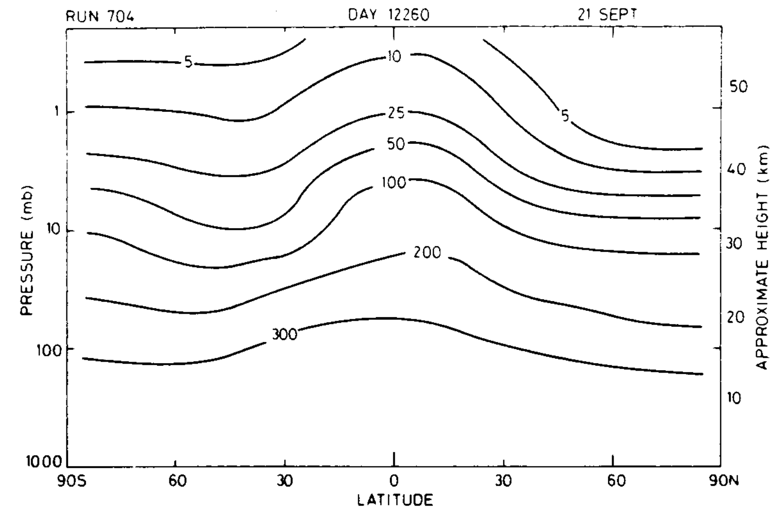

Fig. 12*c*

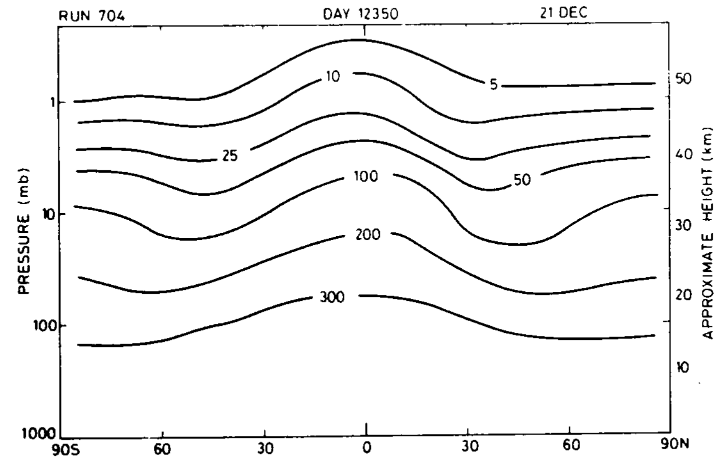

Fig. 12*d*

placed toward the summer hemisphere compared with the model. The slopes of the contours in middle latitude of the model northern hemisphere compare well with the observations, and there is a suggestion in the data of a mid-latitude minimum in the midstratosphere, although this is not a strong feature of the model in this month. Around the stratopause the data have less strong latitudinal gradients, suggesting perhaps a stronger horizontal transport than found in the model. On the whole, the agreement is good.

Although the basic distributions are similar, there are more areas of discrepancy for N_2O (Figure 14). For example, the observed mixing ratios decrease more rapidly with height than the model would indicate, although a comparison at about 25°S would suggest reasonably good agreement up to 1 mbar. The data show a minimum in low latitudes in the upper stratosphere and the double peak discussed earlier. As with CH_4, the horizontal gradients in the upper stratosphere are weaker in the observations than those found in the model.

While the gross features of the observations are satisfactorily reproduced by the model, there are important differences of detail. The variability exhibited by the satellite data emphasizes the difficulty of comparing averaged models with observations. In this regard, notice the sharp horizontal gradients which sometimes exist. For example, at about 30°N where many observations are made there are often large gradients in CH_4 in the middle statosphere (see Figure 4*i*). Furthermore, this is the latitude at which many one-dimensional models are run. These variations indicate the problem of using a limited number of vertical profiles to infer coefficients for vertical transfer.

In one-dimensional models the problem of satisfactorily modeling CH_4 and N_2O (and, for example, $CFCl_3$) simultaneously with a single eddy diffusion profile has been apparent for some time. It has been suggested that a major source of the discrepancy for N_2O, which tends to be over estimated in the upper stratosphere when reasonable CH_4 mixing ratios are reproduced, may be an underestimation of the photochemical sink. *Froidevaux and Yung* [1982] have recently considered model sensitivity to the absorption cross sections of molecular oxygen around 200 nm. By using average data in agreement

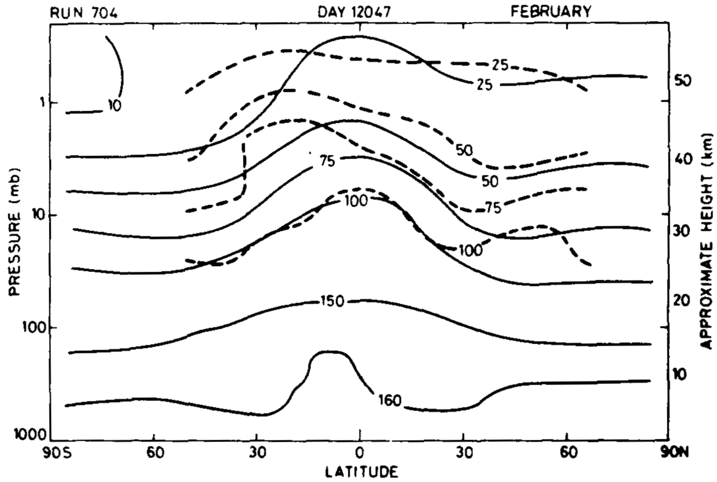

Fig. 13. A comparison of model (solid line) and SAMS (dashed line) CH_4 cross sections for February 1979.

with the observations of *Herman and Mentall* [1982] and more in line with those suggested by *Brewer and Wilson* [1965], they were able to improve their model representation of various trace gases.

We have performed a similar study within the two-dimensional model. Between 196 and 225 nm the oxygen absorption cross sections were reduced by a factor of 0.55. This gives values a little lower than those calculated by *Brewer and Wilson* [1965]. Since our primary aim is to investigate the model sensitivity, the use of this constant factor is justifiable, particularly as the value of the cross sections in still the subject of debate.

Figure 15 shows equatorial profiles for two model runs, run A and a run including the modified oxygen cross section, run B. Both profiles are for the northern hemisphere winter solstice. Also plotted are SAMS data. To emphasize again the variability shown by the data, equatorial profiles for the December and January means are plotted. It is clear that the calculations in run A excede the observations in the upper stratosphere. The discrepancy is reduced in run B where the agreement with the January observed profile is good. On the other hand, the December observations are still exceeded by the model.

Changes in the oxygen absorption cross sections do not simply influence N_2O. The varying penetration of ultraviolet around 200 nm influences many other species, as well as affecting the radiation balance. The impact of all these processes needs to be considered. Such detailed investigation is beyond the scope of this paper. However, to summarize the comparison of runs A and B, it appears that changing the O_2 absorption cross section has both a positive and negative influence. For example, the ozone distribution in run B is less satisfac-

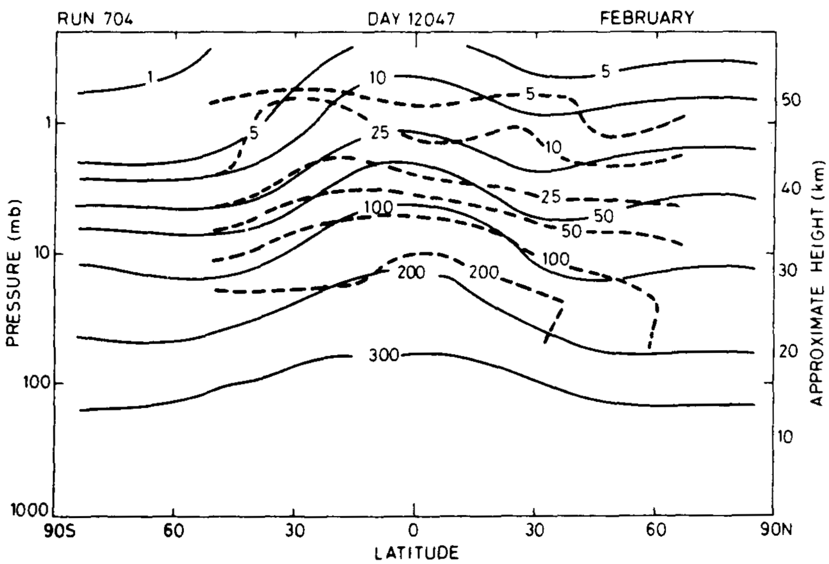

Fig. 14. A comparison of model (solid line) and SAMS (dashed line) N_2O cross sections for February 1979.

APPENDIX F

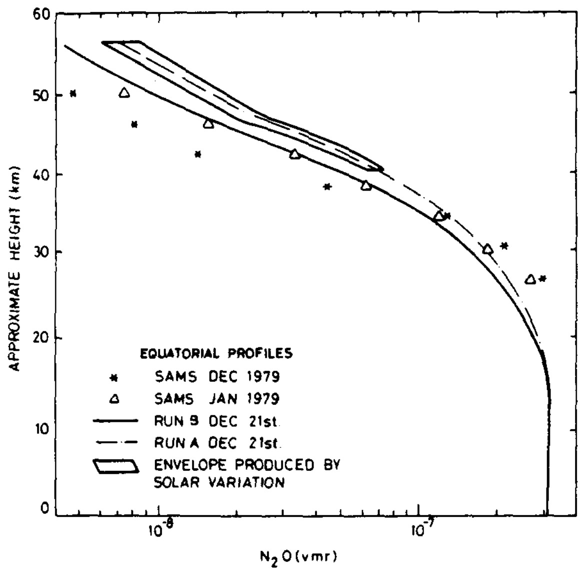

Fig. 15. SAMS equatorial N_2O profiles compared with various model runs.

tory. The total column amounts are increased by 20–30 Dobson Units, depending on the latitude, leading to a significantly overestimated ozone column in low latitudes. The changes in the ozone column amount arise from increases in ozone in the low stratosphere which more than compensates for decreases in the upper stratosphere. These changes will also affect the penetration of ultraviolet radiation. In fact, the changes in ultraviolet heating lead to a somewhat improved model temperature and zonal wind fields. Following the changes in ozone, the temperatures are reduced in the upper stratosphere and increased in the lower stratosphere. Latitudinal variations in these changes lead to reductions in the stratospheric jets which tend to be overestimated in the model.

Since the N_2O profile is sensitive to the penetration of radiation around 200 nm, any solar cycle variations at these wavelengths may be significant. To study to what extent the solar cycle variations, or simply uncertainty in the solar flux, might affect the comparison of model and observations we have imposed on the model the solar variability suggested by *Brasseur and Simon* [1981] for the 11 year sunspot cycle, and these results are also plotted in Figure 15, the envelope indicating the ensuing variations in N_2O.

In reasonable agreement with Brasseur and Simon we find a variation of N_2O during the solar cycle of more than 30% in the upper stratosphere. The decrease in N_2O when the flux is maximum does not appear to be sufficient to explain the observed profiles.

In some respects, model experiments including the lower oxygen cross sections and solar flux variations can lead to an improvement in modeled N_2O; they clearly indicate the necessity of establishing these parameters accurately before N_2O can be modeled with confidence. Nevertheless, this should not be taken to mean that the discrepancy is necessarily photochemical in origin. The lower chemical activity of methane results in much weaker gradients than for N_2O. Its distribution is therefore much less sensitive to transport processes. The modeled methane will be more robust to the representation of transport (just as an inert, uniformly mixed gas with no net sources would be completely insensitive to transport). In consequence, while the overestimate of the N_2O mixing ratio in the model could plausibly be ascribed to an underestimation of the sink, we believe that this is yet to be conclusively demonstrated.

9. DISCUSSION

The year of results presented here provide an enormous increase in our knowledge of the distributions of CH_4 and N_2O and will clearly be the subject of much detailed analysis in the future. For the present we comment on just a small number of the more obvious features that require explanation. These are the maxima found in low latitudes, the double peak structure found in the midstratosphere during a few months of the data and the uniform region sometimes found in midlatitudes in the upper stratosphere.

The low latitude peak we have attributed to the stratospheric extension of the Hadley circulation. It is interesting to ask what velocities are implied by the changes in the monthly mean mixing ratios. For example, if we compare the methane cross sections for January and February, the 1 ppmv contour of CH_4 at the equator, situated near 10 mbar, ascends by approximately 0.5 pressure scale heights between January and February. This corresponds to a vertical velocity of about 1.4 mm s^{-1} which is comparable with that calculated in the two-dimensional model. Of course, this can only be regarded as a very rough estimate since horizontal motion and photochemistry, both of which would be important, have been ignored. We believe that the data are sufficiently good that we will be able to use them to trace stratospheric motions, and this work is already underway.

The double peak structure is most strongly evident in the upper stratosphere between February and May. It does not appear to be present during the southern hemisphere spring. It is not clear yet whether it would be present in a climatology of CH_4 and N_2O; analysis of further data is clearly required. Although the model does not produce a double peak, we believe that some insight into its development can be gained with the help of the model. Figure 16 overlays the model N_2O cross sections for January and July. While the peak mixing ratios are always found in equatorial latitudes, it is evident that there are significant seasonal variations at around 30° latitude. The increase in January at 30°S is consistent with the fluxes marked by the arrows. Such a flux could well give rise to the maximum seen in the data which characteristically tilt with height. Of course the model results are also consistent with a predominantly horizontal flow in the middle atmosphere. The model mean circulation, however, would not support this interpretation. If we accept the view shown in Figure 16 then the double peak will arise when the sun crosses the equator, and the upward motion is predominantly in the northern hemisphere.

It is unclear why there should be a minimum at the equator or, alternatively, why the southern hemisphere ascending branch should preserve its identity. It would appear from the data that if this is a plausible explanation, the stratosphere is more stable in the horizontal than the model indicates.

At these latitudes the rising motion in the model is driven by radiative heating which varies only slowly with latitude. It is likely that the lower stratosphere is much more variable than in the model, and, consequently, the radiative heating and associated motions will also show greater structure which might be needed to explain the observations.

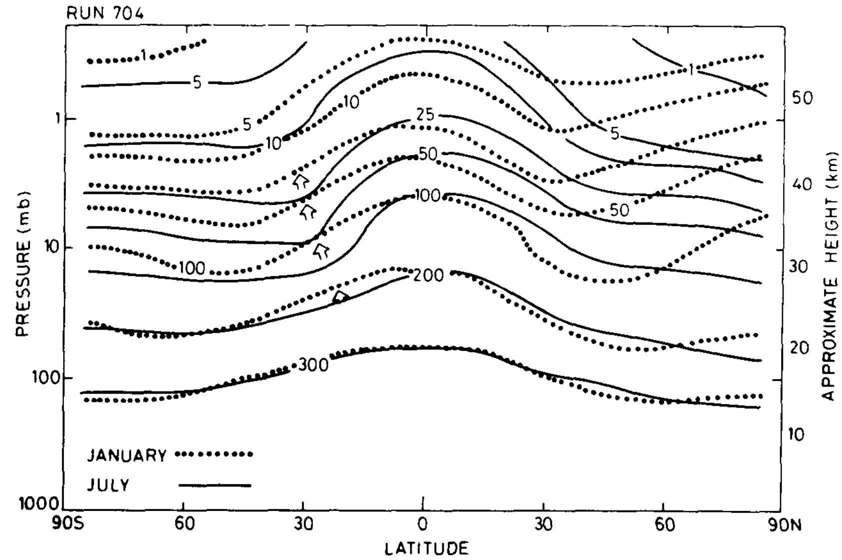

Fig. 16. Model cross-section of N_2O mixing ratio (ppbv) for January (dotted line) and July (solid line). Tentative fluxes are shown by the arrows.

It is interesting to note another feature in Figure 16 commented on above. In the southern hemisphere middle and high latitude mid-stratosphere the contours of constant mixing ratio are at a greater height in January than in July. This is due to the predominantly rising motion found throughout the summer stratosphere transporting high mixing ratios upward. However, at about 1 mbar the pattern changes with the summer hemisphere having less N_2O, a reflection of the fact that the photochemical time constant is decreasing with height.

A number of the observed cross sections show a region in the upper stratosphere of the summer hemisphere across which there is a strong horizontal gradient, while in the winter hemisphere the horizontal gradient is small. The area of marked horizontal gradient is also the region, commented on earlier, where the vertical gradient becomes very small (see, e.g., Figures 3*h* and 4*h* at ~40°N and 2 mbar).

The behavior involves both transport and photochemistry. We identify the area of very small vertical gradient as a transition region. Equatorward of this the high mixing ratios are produced by strong upward transport confined to low latitudes. The horizontal flow in the upper stratosphere is from the summer to the winter hemisphere. The weak horizontal gradients in the winter hemisphere are thus produced by strong horizontal transport from low latitudes. Poleward of the transition region the air has low mixing ratios of N_2O and CH_4. This can be thought of as old stratospheric air, having been at high altitudes for sufficient time for the slow photochemistry of N_2O and CH_4 to reduced the mixing ratios. This air is transported equatorward. The transition region arises when the vertical transport becomes of comparable importance to the horizontal.

The model produces these features, although less markedly than does the data. This was discussed in section 8.2. Figure 17 shows profiles of N_2O at 47°N for February and October. In October, representative of late summer/early autumn, the features found in the data are reproduced, namely, a sharpening of the gradient in the low stratosphere and a much weaker vertical gradient found in the upper stratosphere.

10. CONCLUSIONS

In this paper, monthly mean, zonal mean mixing ratios of CH_4 and N_2O for 1979 obtained from the SAMS instrument on NIMBUS 7 have been presented for the first time, with a coverage from 67.5°N to 50°S and including most of the stratosphere. These data represent a vast increase in the knowledge of the behavior of the two gases in the upper atmosphere.

The data have been compared with the small number of available measurements. At low altitudes, there appears to be a consistent difference between the two data sets with the satellite data higher by ~10–40%. Nevertheless, the two sets of data are consistent within their estimated errors.

The SAMS data confirm the broad features revealed by in situ and other remote measurements. In particular, the decrease of the mixing ratios with height is more rapid in middle latitudes then in the tropics. Many new features are revealed by the satellite data. The large variability from month to month and with latitude is of interest and emphasizes the problems of comparing theoretical models with single observed profiles for a particular day.

For any pressure level in the stratosphere, maximum mixing ratios, as we have stated, are found in low latitudes and are associated with upward transport. Between February and May 1979 a double peak is found with maxima in the sub tropics in the middle stratosphere and a local minimum at the equator. This feature is not found in the model, but the seasonal change in the model fields does suggest a somewhat similar behavior with upward transport following the sun. In the model, horizontal transport prevents the occurrence of an equatorial minimum. It will be of great interest to see if the double peak is found in subsequent years. These data are yet to be analyzed. A more detailed investigation of the double

APPENDIX F

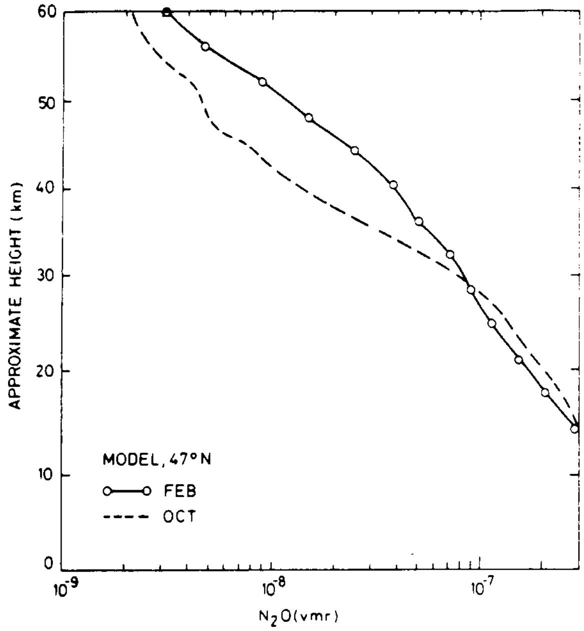

Fig. 17. Model N_2O profile at 47°N for February and October.

peak in which the velocity fields are diagnosed is also important.

Another feature discovered in the data is a region of very strong horizontal gradients, and weak vertical gradients in the mixing ratios, found in the upper stratosphere summer hemisphere. A similar, if less pronounced feature, is found in the model. This transition region marks a loose boundary between air of high mixing ratio, which is being transported upward and into the winter hemisphere, and low mixing ratio air which has been in the stratosphere for a sufficiently long time for the slow photochemistry to produce low mixing ratios of CH_4 and N_2O.

Comparison of the data with the model has proved a very useful exercise. The broad features agree well, suggesting that the gross behavior of the model is satisfactory. One feature found in the model is a middle latitude minimum. Although suggestions of this are found in the data, the coverage is not sufficient for an unambiguous identification. As discussed above, investigation of the model has helped in understanding the double peak and transition regions found in certain months.

The quantitative comparison for CH_4 is extremely good; the model agrees with the data very well. For N_2O the agreement is not so satisfactory with the model results tending to exceed the observed values in the upper stratosphere. Such a disagreement has been found in other models and for other species (e.g., $CFCl_3$). It could be suggested that because the agreement of CH_4 is generally good, the model's failure to reproduce the N_2O profile may be due to an underestimation of the stratosphere sink. We have considered two possibilities, a reduced oxygen absorption cross section around 200 nm and solar flux variations. While both cases can help to reduce the discrepancy, the results are not conclusive. Since the CH_4 gradients are weak, it is less sensitive to transport than N_2O. We believe that inaccuracies in the representation of the transport cannot be ruled out as a cause of the discrepancy.

Finally, we stress again the advantages provided by this large data set. Although the absolute accuracy is not high compared with some in situ measurements, this disadvantage is more than offset by the spatial and temporal coverage. We believe much useful analysis on the interaction of transport and photochemistry is possible by using the data.

Acknowledgments. This work was supported by grants from the Science and Engineering Research Council, the Natural Environment Research Council, and the Commission of the European Communities. We gratefully acknowledge the work done by NIMBUS Project at NASA and the assistance of many people at Oxford.

REFERENCES

Barnett, J. J., and M. Corney, Temperature comparisons between the NIMBUS 7 SAMS, rocket/radiosondes and the NOAA-6 SSU, *J. Geophys. Res.*, this issue.

Baulch, D. L., R. A. Cox, R. F. Hampson, Jr., J. A. Kerr, J. Troe, and R. T. Watson, Evaluated kinetic and photochemical data for atmospheric chemistry, *J. Phys. Chem. Ref. Data*, *9*, 295–471, 1980.

Brasseur, G., and P. C. Simon, Stratospheric chemical and thermal response to long-term variability in solar UV irradiance, *J. Geophys. Res.*, *86*, 7343–7362, 1981.

Brewer, A. W., and A. W. Wilson, Measurements of solar ultraviolet radiation in the stratosphere, *Q. J. R. Meteorol. Soc.*, *91*, 452–461, 1965.

Drummond, J. R., J. T. Houghton, G. D. Peskett, C. D. Rodgers, M. J. Wale, J. Whitney, and E. J. Williamson, The stratospheric and mesospheric sounder on NIMBUS 7, *Phil. Trans. R. Soc. London Ser. A*, *296*, 219–241, 1980.

Froidevaux, L., and Y. L. Yung, Radiation and chemistry in the stratosphere: Sensitivity to O_2 absorption cross sections in the Herzberg continuum, *Geophys. Res. Lett.*, *9*, 854–857, 1982.

Haigh, J. D., and J. A. Pyle, Ozone perturbation experiments in a two-dimensional circulation model, *Q. J. R. Meteorol. Soc.*, *108*, 551–574, 1982.

Harwood, R. S., and J. A. Pyle, A two-dimensional mean circulation model for the atmosphere below 80 km, *Q. J. R. Meteorol. Soc.*, *101*, 723–748, 1975.

Harwood, R. S., and J. A. Pyle, The dynamical behaviour of a two-dimensional model of the stratosphere, *Q. J. R. Meteorol. Soc.*, *106*, 395–420, 1980.

Herman, J. R., and J. E. Mentall, O_2 absorption cross sections (187–225 nm) from stratospheric solar flux measurements, *J. Geophys. Res.*, *87*, 8967–8975, 1982.

Jones, R. L., Measurement of the atmospheric distributions of CH_4 and N_2O from satellites, Ph.D. thesis, University of Oxford, Oxford, Great Britain, 1983.

Luther, F. M., Monthly mean values of eddy diffusion coefficients in the lower stratosphere, paper presented at AIAA-AMS Conference, Sponsor, Denver, Colo., 1973.

McClatchey, R. A., W. S. Benedict, S. A. Clough, D. E. Burch, R. F. Calfee, K. Fox, L. S. Rothman, and J. S. Garing, AFCRL atmospheric absorption line parameters compilation, *Environ. Res. Pap. 434, AFCRL-TR-73-0096*, Air Force Cambridge Res. Lab., Bedford, Mass., 1973.

Rodgers, C. D., R. L. Jones, and J. J. Barnett, Retrieval of temperature and composition from NIMBUS 7 SAMS measurements, *J. Geophys. Res.*, this issue.

Rothman, L. S., AFGL atmospheric absorption line parameters compilation, 1980 version, *Appl. Opt.*, *20*, 791–795, 1981.

World Meteorological Organization, The stratosphere 1981: Theory and measurements, *Rep. 11*, Geneva, 1982.

R. L. Jones, Department of Atmospheric Physics, Clarendon Laboratory, Oxford, OX1 3PU, Great Britain.

J. A. Pyle, Rutherford Appleton Laboratory, Chilton, Didcot, Oxfordshire OX11 OQX, Great Britain.

(Received April 19, 1983;
revised September 6, 1983;
accepted October 4, 1983.)

APPENDIX G

SOME ASPECTS OF THE DESIGN AND BEHAVIOR OF THE STRATOSPHERIC AND MESOSPHERIC SOUNDER

[Reproduced from *Journal of Geophysical Research, 89,* 5287-5293 (1984).]

Some Aspects of the Design and Behavior of the Stratospheric and Mesospheric Sounder

M. J. WALE[1] AND G. D. PESKETT

Department of Atmospheric Physics, Clarendon Laboratory, University of Oxford

The measuring task, the engineering constraints, and the resulting design of the stratospheric and mesospheric sounder are described in broad terms. The calibration system and its performance are discussed in more detail. One significant side effect in the design and its impact on the fields of view is also discussed. The major lessons for future pressure modulator radiometer designs are summarized.

1. INTRODUCTION

The rapid development of remote sounding techniques has meant that new instruments are rarely simple developments of older designs. Radiometers such as the stratospheric and mesospheric sounder (SAMS) consist of optical, electronic, mechanical, and thermal systems that are related to one another in complex ways. Consequently, the designer who, after having optimized the various trade-offs to produce the best overall performance, does not find when the instrument has been built that his decisions have led to unexpected side effects may count himself as being very fortunate. Particularly troublesome are those side effects whose magnitudes may be different in orbit (e.g., owing to the change to a zero *g* environment). Such effects cannot be characterized satisfactorily in the laboratory, and ideally they should be eliminated by redesign, but this may not be possible because of constraints of finance or of schedule. We feel that a discussion of some of these aspects of the SAMS radiometer may be of interest to geophysicists engaged on the analysis of SAMS data as well as to others involved with the design of instruments. This paper should be read in conjunction with the description of the SAMS instrument given by *Drummond et al.* [1980].

2. BASIC DESIGN AIMS AND THEIR REALIZATION

The basic task of the SAMS radiometer is to measure the thermal emission from chosen molecular species present in atmospheric limb paths whose tangent point altitudes range upward from 20 km. Since the radiometer is itself a significant source of radiation, it is necessary to label the incoming radiation. In some of the channels in SAMS this function is combined with the spectral selection of the part of the incoming radiation which has been emitted by the desired constituent.

The problem of spectral selection has two main aspects: the separation of the wanted lines from other atmospheric emission and the minimizing of the contribution due to components of the instrument's own optical system. (Variations in the instrumental emission can often decide the minimum detectable radiance.) Both objectives would be achieved if a spectral response profile limited to just those very narrow regions embracing the wanted lines could be realized.

A good approximation to the ideal spectral response is obtained in SAMS by employing multilayer dielectric filters to isolate the desired parts of the chosen emission bands, combined with pressure modulators [*Curtis et al.*, 1974] which provide the necessary detailed spectral selectivity. A pressure modulator is an optical absorption cell which is filled with the gas whose emission is to be measured. The pressure of the gas is modulated at a few tens of Hertz, resulting in cyclic transmission variations which are confined to spectral regions within the absorption lines of the molecule in question. The desired output from the detector is extracted by "lock-in" type electronic signal processing referenced to the frequency and phase of the pressure cycling. In the channels where pressure modulation is not used (the so-called wideband channels) a vibrating black vane chopper is used to label the incoming radiation, and lock-in techniques are again employed.

As the tangent height of the atmospheric limb path is increased, the signal observed in a radiometer channel falls toward zero and is eventually lost in instrumental noise. In order to sound the widest possible altitude range, therefore, it is necessary to use the best available detectors and to maximize the energy gathered by the telescope by employing the largest practical aperture and field of view.

The choice of detectors for SAMS was constrained by the limited cooling technology then available for long missions, and only two of them were cooled. These were an indium antimonide photovoltaic detector covering the 4 to 5-μm region, cooled by a two-stage radiation cooler, and a lead sulphide photoconductor for 2.5–2.7 μm, cooled by a simpler radiator. The remaining detectors were triglycine sulphate (TGS) pyroelectric devices operated at room temperature. These offered the highest radiometric sensitivity which could be achieved without cooling, but they also showed unwelcome microphonic behavior, which will be discussed later. The costs of increasing the aperture of the telescope become disproportionately high once a mirror diameter of about 20 cm is exceeded, bearing in mind that the signal to noise ratios obtained are proportional to the diameter (not the area) of the collecting optics when, as in SAMS, the detector area is matched to the collecting area. The field of view in the vertical direction is determined largely by the requirements of vertical resolution and is usually of the same order as the natural height range of a limb path (about 4 km), while for a number of reasons the horizontal width of the field of view is best limited to at most 10 times the vertical height. The telescope in SAMS had an aperture of 177 cm^2 and a field of view of $0.16^\circ \times 1.6^\circ$ (nominally 10 km × 100 km at the tangent point).

Since the objective of a limb emission sensor such as SAMS is to measure radiances that range down to those that are barely distinguishable from zero radiance (space view) it is

[1] Now at Plessey Research (Caswell) Ltd.

Paper number 3D1831.
0148-0227/84/003D-1831$05.00

APPENDIX G

essential to measure the atmospheric radiances as differences from the zero radiance level, so that low frequency noise (drifts) in the instrument response can be eliminated. Difference measurements could in principle be made either by rotating the whole instrument between the chosen limb path orientation and a clear view to space or by using an additional tilting mirror. The former approach would require a high precision mechanism capable of rotating the whole instrument sufficiently rapidly to provide adequate coverage with minimal loss of observing time, a difficult engineering requirement. In addition, the associated angular momentum changes would have had a significant effect on the roll attitude of the spacecraft, to the detriment of other limb viewing instruments. Consequently, a scanning mirror system was chosen, in spite of its disadvantages, which are that the optical system must contain an additional component and that the system is unavoidably changed as the mirror is tilted. The mirror tilt required to achieve a clear space view is, however, only of the order of 2°, and, as will be shown later, this does not cause significant changes in instrument response.

Standard calibration radiances for the various channels are provided by introducing a black-body source into the optical path. The most straightforward way of achieving this would be to move a large black body cavity into place across the viewing aperture. This approach would, however, have given rise to difficulties in achieving adequate temperature stability and uniformity, and, indeed, accommodation of such a system on the spacecraft would not have been at all straightforward. An alternative scheme of introducing a small black body at the first focal point of the telescope was therefore chosen. The implications of this are discussed in section 4.

3. Zero Radiance (Space View) Signal

There are a number of contributions to the zero-radiance signal. The main ones are listed below.

1. Emission from the optical components situated in front of the modulators makes a contribution which depends on the temperatures of the components and their emissivities.

2. Radiation enters the beam in front of the modulators as a result of scattering from imperfections in the optical surfaces and through optical aberrations and diffraction.

3. When the pressure modulator (or chopper) in any given SAMS channel is at the point in its modulation cycle where the transmission is low (or zero), it acts as a room temperature radiation source of high emissivity. Consequently, the modulated (or chopped) radiance at the detector has the largest amplitude when the incoming atmospheric radiance is zero, and this amplitude will change as the temperature of the modulator (chopper) changes.

4. The pressure oscillation in the pressure modulator cell is unavoidably accompanied by an oscillation in the gas temperature. These temperature variations lead to an oscillating radiance at the detector which is synchronous with the pressure modulation, yielding an offset in the signal channel output which is dependent on the modulation depth, on the mean pressure in the modulator, and on the temperature of the cell.

Finally, a system employing lock-in type signal processing will respond to any synchronous input, including those not related to the modulated radiance. For example, vibrations in the instrument structure excited by the mechanical modulators may be picked up by microphonic detectors. The TGS detectors in SAMS have a large microphonic response and significant offsets due to this occur in both the pressure modulated and wideband channels. Another source of offsets of this type is electrical pick-up of phase sensitive detector (PSD) reference or modulator drive waveforms.

The difference method of measuring small signals discussed in section 2 relies on all the contributions to the zero radiance signal mentioned above (and also the gain) remaining constant when the scan mirror is moved between space view and the atmospheric limb view. (In addition, the contributions must drift sufficiently slowly that the zero radiance signal can be estimated with the necessary accuracy between space views.)

In general, the instrument is designed such that the temperature changes that affect the instrument response occur only slowly; similarly, the signal offsets due to temperature cycling in the modulator cell and electrical synchronous pickup would also be expected to be stable in the short term. Our attention should therefore be focused on the stray radiation reaching the detector as a result of optical system imperfections and on the microphonic component of the synchronous pickup. Both of these effects may vary as the scan mirror is tilted, the variation in the microphonic case being due to changes in mechanical couplings between the various parts of the instrument. The variations likely to be encountered in orbit are not easily assessed in the laboratory before launch, because it is difficult to arrange for the radiation environment of the instrument to be sufficiently well simulated and because the mechanical couplings responsible for the microphonic component may well change when the sensor is in zero-g. A check obtained in orbit that the zero-radiance offset does not depend on scan mirror position is therefore of special value.

Ideally, we should like to be able to tilt the spacecraft about its roll axis, so that the instrument has a clear view to space throughout the entire scan range: we could then investigate the variation in offset with scan angle directly. It has unfortunately not been possible to do this with NIMBUS 7, but a clear view to space is nonetheless available over a scan range of about 2.5° in the line of sight.

Figure 1 shows the variation in space view offset with scan mirror position in channel A1 WB (a temperature sounding wideband channel operating near 15 μm in the ν_2 band of CO_2) during a typical orbit. The data were obtained as follows. The instrument was programed to perform a uniform up and down scan of 2.9° amplitude in the nominal space view region of the scan range, with occasional excursions to view the middle atmosphere so that a check on the attitude of the spacecraft could be obtained by using the CO_2 channel radiances [see *Barnett et al.* this issue]. The data are presented in Figure 1 in terms of the tangent height of the atmospheric path viewed at any given time, determined from these attitude checks. The dependence of the observed radiance on scan angle is very weak, typically less than 0.1% of the radiance, which would be received from a 290 K black body (or about 0.2% of the radiance received from an atmospheric path of low transmission and stratospheric temperatures (240 K)). It should be noted that this is much less than the noise level in a normal measurement sequence.

4. Gain Calibration

As mentioned earlier, gain calibration is achieved in SAMS by introducing a small black-body source at the first focal point of the telescope. The temperature of this source is very close to the temperature of the secondary optics components which accept its emitted radiation. Consequently, the emiss-

APPENDIX G

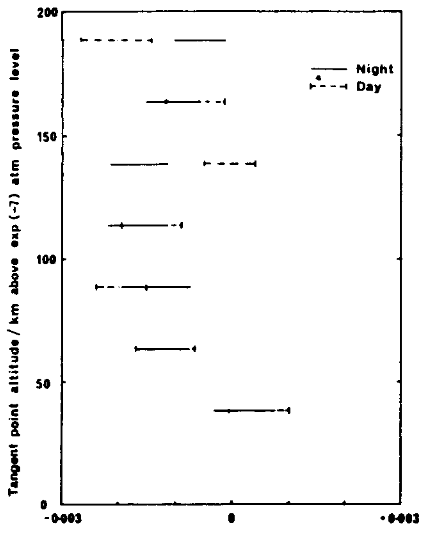

Fig. 1. Radiance profiles observed in channel A1 WB (CO_2, 15 μm band) in the space view region of the scan range. The data shown are taken from the portion between latitudes 50°N and 90°N of a single orbit of NIMBUS 7. The bars indicate 1σ error. "Day" and "night" indicate the ascending and descending parts of the orbit, respectively.

ivity of the source does not have to be very high, since any radiation which is reflected by it is of the same temperature as the radiation emitted by the source itself. *Wale* [1981] has shown that the gain error resulting from the assumption that the SAMS internal black body is of unity emissivity should be less than 0.1% under all normal operating conditions.

The main drawback to the use of a calibration black body that is not at the front of the whole optical system is that corrections need to be made for emission from the scan mirror and objective mirror, which are excluded from the system when the black body is in the beam. It should be noted, however, that if the mirror temperatures are close to the black body temperature the corrections are small, tending to zero in the case of an isothermal instrument. In SAMS the error in the correction may be as large as 30% before the error in the temperature measured by the 15-μm band carbon dioxide channels exceeds 0.1 K.

It is possible that the level of microphonic synchronous pickup is dependent upon whether the black body is in or out of the beam. The black-body mechanism is a small one, and the only change in configuration involved in moving the source into the beam is slight, but other small perturbations (e.g., the opening of the solar door on the ERB instrument) did have an observable effect in ground test. Since, however, we have no way of quantifying the effect, we have no choice but to ignore it. The ultimate test is comparison with results from other instruments [see *Barnett and Corney*, this issue].

5. MOTIONAL CHOPPING

One of the sets of measurements carried out during ground testing was designed to determine the shape of the field of view of each channel. This was achieved by rotating the whole instrument in such a way that the line of sight elevated slowly through a nearly parallel beam of radiation from a collimator.

The measurements revealed unexpected features: The profiles were found to be asymmetric, and they often showed spikes at the edges. A typical profile is shown in Figure 2. The general features are similar in all of the channels, both wide band and pressure modulated, although the positions of the negative and positive peaks are reversed in some cases. The spikes arise from vibrations at the edge of the scanning or telescope mirrors at modulator or chopper frequency, resulting in unwanted synchronous scanning about the roll axis. Estimates of the effective reaction mass of the instrument and its mountings and a knowledge of the uncompensated momentum of the pressure modulators and chopper indicate that motions of the required amplitude (of the order of 1 μm) are to

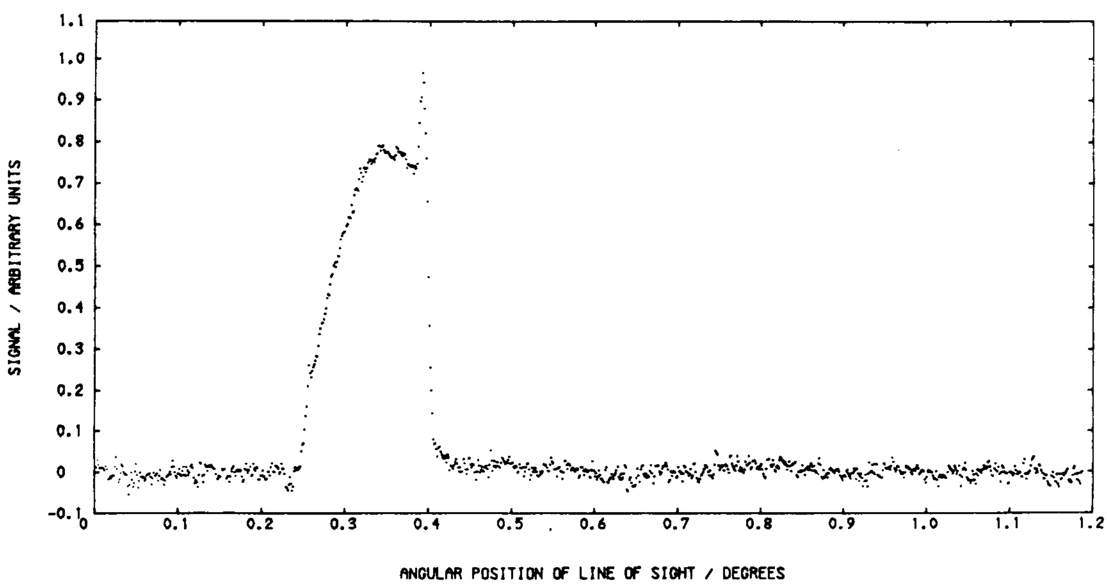

Fig. 2. Field of view response profile of channel C1 PMR, measured during ground testing.

be expected. The question arises as to what are the "real" fields of view.

Consider the situation shown in Figure 3, where a source of very limited angular extent (the collimator beam) is filling the aperture of the sensor. If the field of view is described by the function $F(\theta)$, a small movement $\Delta\theta$ in the angular position of the source will result in a change in the radiance of $(d/d\theta)F(\theta)\Delta\theta$. If $\Delta\theta$ takes the form of an oscillatory function synchronous with the modulation in the channel under consideration, an additional signal proportional to $(d/d\theta)F(\theta)$ will be observed at the output of the channel. We call this effect motional chopping of the second kind, to distinguish it from amplitude modulation of a beam resulting from unwanted vibration of a nonuniform optical component near an aperture plane, long known to us as motional chopping.

It should be noted that in a pressure-modulated channel, the motionally chopped contribution is a wide band one derived from the whole channel bandwidth defined by the band pass filter, not just the pressure modulated fraction of that bandwidth. It is for this reason that the effect can be significant, even though the motions involved are very small. In SAMS an enhanced effect is also present in the wide band channels, since only a small part of the optical system aperture is modulated by the vibrating chopper, but the whole aperture contributes to the motionally chopped signal.

We describe the signals obtained as follows. In the absence of motional chopping the signal consists of a single term

$$S(\theta') = \alpha\left\{\int L_1(\theta)h_1(\theta - \theta')\, d\theta\right\}$$

where $L_1(\theta)$ describes the angular distribution of the source radiance which is selected spectrally by the channel, θ is an elevation angle referred to the instrument mountings, $h_1(\theta - \theta')$ is the field of view profile when the line of sight is directed at θ' in this coordinate system, and α is a constant. If the line of sight is now allowed to move at the modulation frequency,

$$\theta' = \theta'_0 + \Delta\theta' \sin(\omega t + \phi),$$

we obtain a second term, of the form

$$\alpha\Delta\theta' \cos\phi \cdot \frac{d}{d\theta'}\int L_2(\theta)h_2(\theta - \theta')\, d\theta$$

It should be noted that L_2 and h_2 are new functions which may differ from L_1 and h_1. For example, in the SAMS

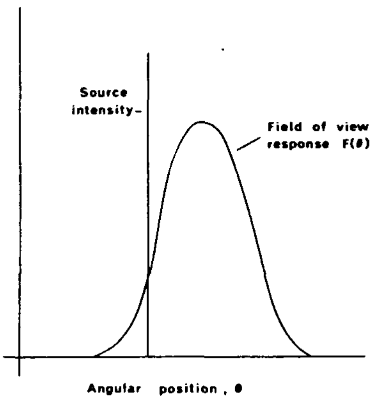

Fig. 3. Schematic illustration of field of view measurement.

pressure-modulated channels, L_1 is the pressure modulated (narrow band) radiance, while L_2 is a wide band radiance. We would, however, expect h_1 to be the same as h_2 in this case. In the wide band channels, h_1 is the field of view resulting from the modulation of the small part of the aperture occupied by the chopper blade, while h_2 is the field of view resulting from the use of the whole aperture. The main difference between h_1 and h_2 is a scaling factor, although there are minor differences in the shape of the profile caused by the off-axis siting of the chopper. L_1 and L_2 are in this case essentially the same function, but the off-axis nature of the wide band chopping has an effect on the spectral selection of the source radiance, owing to angle of incidence effects on dielectric interference filter coatings.

In the laboratory we approximate the shape of L_1 and L_2 by a delta function (the collimated beam); that is, $L_1 = k_1\delta(\theta)$ and $L_2 = k_2\delta(\theta)$, where k_1 and k_2 are constants. In this case the signal observed is

$$S_L(\theta') = \alpha k_1 \cdot h_1(\theta') + \alpha\Delta\theta' \cos\phi \cdot k_2 \frac{d}{d\theta'} h_2(\theta')$$

When observing the atmosphere, the signal obtained is

$$S_A(\theta') = \alpha \int L_1^A(\theta)h_1(\theta - \theta')\, d\theta + \alpha\Delta\theta' \cos\phi \int L_2^A(\theta) \frac{d}{d\theta'} h_2(\theta - \theta')\, d\theta$$

where we have used the fact that $L_2(\theta)$ does not depend on θ'.

Considering first the wide band channels and assuming that the differences between L_1 and L_2 (and, hence, between k_1 and k_2) can be neglected,

$$S_L(\theta') = \alpha k_1\{h_1(\theta') + \Delta\theta' \cos\phi \frac{d}{d\theta'} h_2(\theta')\}$$

and

$$S_A(\theta') = \alpha \int L_1^A(\theta)\left\{h_1(\theta - \theta') + \Delta\theta' \cos\phi \cdot \frac{d}{d\theta'} h_2(\theta - \theta')\right\} d\theta$$

Combining the two equations,

$$S_A(\theta') = \frac{1}{k_1}\int L_1^A(\theta)S_L(\theta - \theta')\, d\theta$$

We conclude that under the assumption that the effect is the same in zero-g, the motional chopping is taken into account simply by employing the field of view profile in the raw form measured in the laboratory (i.e., including the spikes). The consequences of this assumption being incorrect have been studied by *Barnett and Corney* [this issue].

The treatment of motional chopping in the pressure-modulated channels is not so straightforward. The reader will perhaps have realized that the conclusions in the wide band case do not in fact depend on the precise functional form of the additional term so long as it depends only on θ'. In the pressure-modulated case, however, we must establish the correctness of the model in order to proceed. The first step is to derive the underlying pressure-modulated field of view profile from the laboratory measurements. Equation (1) may be integrated numerically to obtain an estimate of $h_1(\theta)$ for trial values of the constant $\Delta\theta' \cos\phi \cdot k_2/k_1$. The result of such an integration using a value for $\Delta\theta \cos\phi \cdot k_2/k_1$ of $-0.01°$ is shown in Figure 4. It should be noted that the integration has had a useful smoothing effect, reducing the noise level. Also

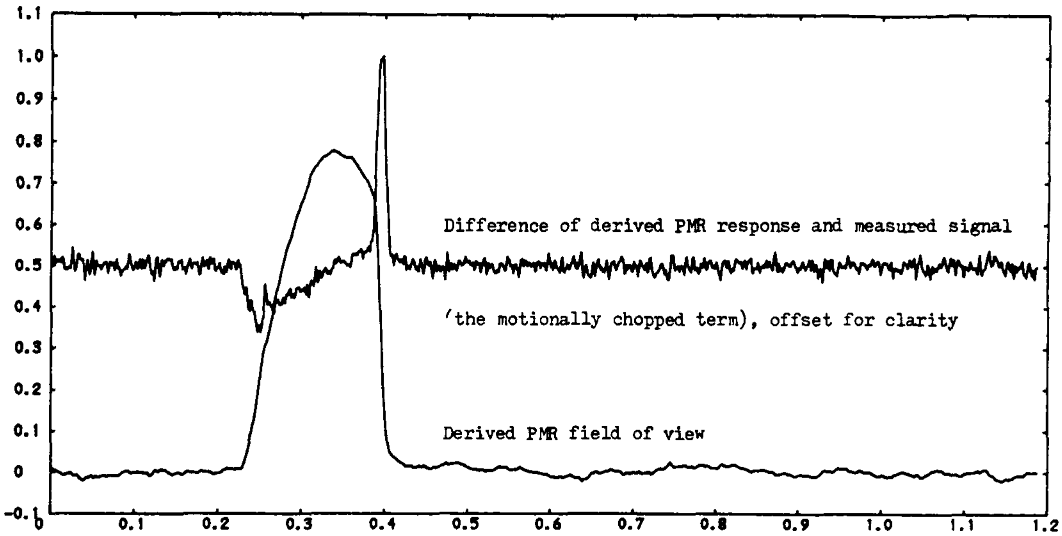

Fig. 4. Underlying pressure modulated field of view in channel C1 PMR, derived from the profile shown in Figure 2, using a value for the constant $\Delta\theta \cos k_2/k_1$ of $-0.01°$.

shown is the difference between the derived profile and the raw measurement.

Compelling evidence of the correctness of the model may be adduced by comparing the difference profile with the profile shown in Figure 5. The latter was obtained with an absorbing path of gas interposed between the collimator source and the sensor. The amount of gas in the path was sufficiently large for the pressure-modulated radiance L_1 to be strongly attenuated, but L_2 was scarcely affected.

When observing the atmosphere, the ratio of the magnitudes of L_1 and L_2 in the pressure-modulated channels is much smaller than the ratio of k_1 and k_2 in the laboratory.

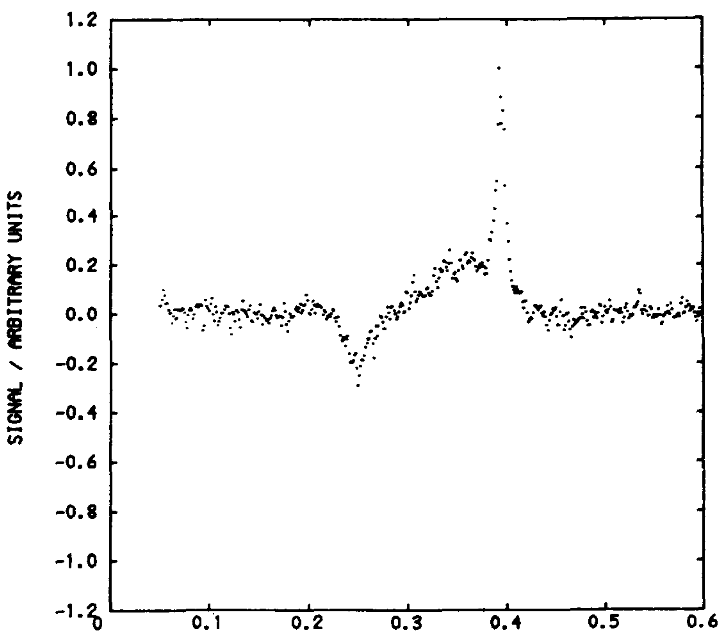

Fig. 5. Field of view profile observed in channel C1 PMR with a path of carbon dioxide interposed between the source and the SAMS instrument.

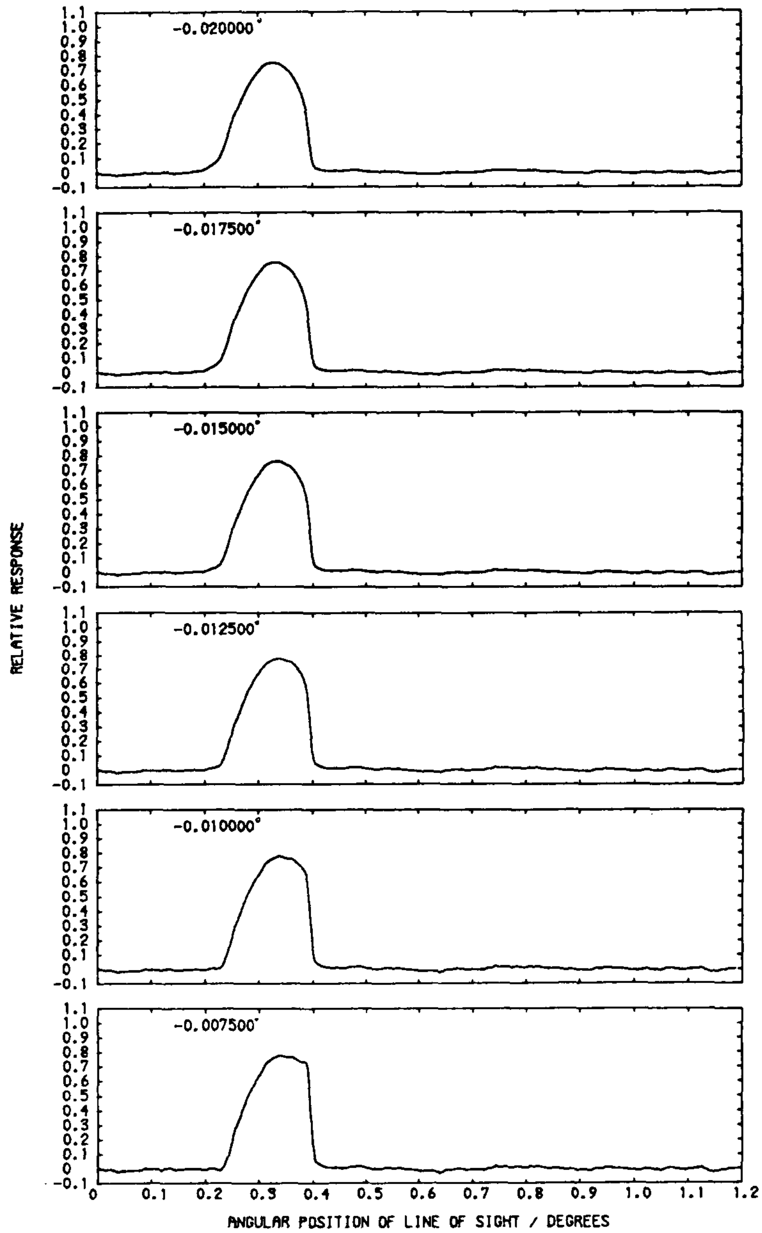

Fig. 6. Field of view profiles for channel C1 PMR derived by using different values of the constant $\Delta\theta \cos k_2/k_1$.

This is because a spectrally uniform source (a hot filament) was used in the latter case, and the motionally chopped term contains in consequence a large contribution from spectral regions between the absorption lines of the gas. In the atmospheric case, however, the emission lines are usually narrow and well separated, and the contribution from spectral regions between the wanted lines is much smaller than in the laboratory case. The best course in the pressure-modulated case is to ignore the motional chopping term and to use a derived field of view profile such as that shown in Figure 4.

The criteria for choosing the optimum value of the constant $\Delta\theta \cos \phi \cdot k_2/k_1$ are less clear than one might have hoped. A typical set of trial derivations is shown in Figure 6. The bottom profile may be rejected on the basis that spikes are still visible and the top two look suspiciously oversmoothed, but the remaining profiles are all plausible. The uncertainty in the value of the constant leads to an uncertainty of about $\pm 0.003°$ in the position of the center of the field of view in this case.

6. Concluding Remarks

We believe that the basic approaches employed in the design of SAMS were sound, but two changes of detail would be desirable if another instrument were to be built within the

APPENDIX G

same constraints. First, the linear momentum of the pressure-modulator pistons should be compensated in some way to eliminate the motional chopping (of the second kind) which results from vibrations excited in the instrument structure. Second, in the wide band channels, the use of a balanced rotating chopper instead of an unbalanced vibrating one would reduce the motional chopping effect to negligible levels and also eliminate the microphonic component of synchronous pickup. (This chopper should modulate the entire aperture, so that the spectral response profiles applicable to the pressure-modulated and wide band channels are identical.)

New spacecraft such as the Upper Atmospheric Research Satellite (UARS) offer a relaxation in the power and weight constraints, and closed cycle detector coolers suitable for use on long missions (e.g., 2 years) are now available. The much lower noise levels and absence of microphony offered by quantum detectors operating at medium temperatures (70–80 K) could improve the performance achieved in SAMS by 2 orders of magnitude. Such an enormous improvement, welcome though it is, will of course mean that all the effects mentioned in this paper and indeed all the design trade-offs will need to be re-examined very carefully if the additional signal to noise ratio is to be effectively utilized.

Acknowledgments. The authors gratefully acknowledge the work of all the members of the SAMS team. Financial support for the SAMS project was provided by the Science and Engineering Research Council. One of us (MJW) was supported during part of this work by a grant from the Natural Environment Research Council.

REFERENCES

Barnett, J. J., and M. Corney, Temperature comparisons between the NIMBUS 7 SAMS, rocket radio sondes, and the NOAA 6 SSU, *J. Geophys. Res.*, this issue.

Curtis, P. D., J. T. Houghton, G. D. Peskett, and C. D. Rodgers, Remote sounding of atmospheric temperature from satellites, 5, The pressure modulator radiometer for NIMBUS F, *Proc. R. Soc. London, Ser. A, 337*, 135–150, 1974.

Drummond, J. R., J. T. Houghton, G. D. Peskett, C. D. Rodgers, M. J. Wale, J. Whitney, and E. J. Williamson, The stratospheric and mesospheric sounder on NIMBUS 7, *Phil. Trans. R. Soc. London, Ser. A, 296*, 219–241, 1980.

Rodgers, C. D., R. L. Jones, and J. J. Barnett, Retrieval of temperature and composition from NIMBUS 7 SAMS measurements, *J. Geophys. Res.*, this issue.

Wale, M. J., Development of spectroscopic techniques for investigation of the stratosphere, D. Phil. Thesis, Univ. of Oxford, United Kingdom, 1981.

G. D. Peskett, Department of Atmospheric Physics, Clarendon Laboratory, University of Oxford, Parks Road, Oxford OX1 3PU, United Kingdom.

M. J. Wale, Plessey Research (Caswell) Ltd., Allen Clarke Research Centre, Caswell, Towcester, Northamptonshire NN12 8EQ, United Kingdom.

(Received May 6, 1983;
revised November 7, 1983;
accepted November 11, 1983.)

NASA
National Aeronautics and Space Administration

Report Documentation Page

1. Report No.	2. Government Accession No.	3. Recipient's Catalog No.
NASA RP-1221		

4. Title and Subtitle Nimbus-7 Stratospheric and Mesospheric Sounder (SAMS) Experiment Data User's Guide	5. Report Date May 1989
	6. Performing Organization Code 636
7. Author(s) F. W. Taylor, C. D. Rodgers, S. T. Nutter, and N. Oslik	8. Performing Organization Report No. 89B00074
	10. Work Unit No.
9. Performing Organization Name and Address Department of Atmospheric Physics University of Oxford, Oxford, England and ST Systems Corporation (STX) Lanham, Maryland	11. Contract or Grant No. NAS5-28063
12. Sponsoring Agency Name and Address Goddard Space Flight Center National Aeronautics and Space Administration Washington, DC 20546-0001	13. Type of Report and Period Covered Reference Publication
	14. Sponsoring Agency Code

15. Supplementary Notes

F. W. Taylor and C. D. Rodgers: Department of Atmospheric Physics, University of Oxford, Oxford, England.

S. T. Nutter and N. Oslik: ST Systems Corporation (STX), Lanham, Maryland.

16. Abstract

The Stratospheric and Mesospheric Sounder (SAMS) aboard Nimbus-7 observes infrared radiation from the atmospheric limb. Global upper atmosphere temperature profiles and vertical concentrations of H_2O, NO, N_2O, CH_4 and CO_2 are derived from these measurements. The status of all channels was carefully monitored. Temperature and composition were retrieved from the measurements by linearizing the direct equation about an a priori profile and using an optimum statistical estimator to find the most likely solution. The derived temperature and composition profiles are archived on two tape products whose file structure and record formats are described in detail. The Gridded Retrieved Temperature Tape (GRID-T) contains daily day and night average temperatures at 62 pressure levels in a 2.5° latitude by 10° longitude grid extending from 67.5°N to 50°S. The Zonal Mean Methane and Nitrous Oxide Composition Tape (ZMT-G) contains zonal mean day and night average CH_4 and N_2O mixing ratios at 31 pressure levels for 2.5° latitude zones extending from 67.5°N to 50°S.

17. Key Words (Suggested by Author(s))	18. Distribution Statement
Stratospheric and Mesospheric Sounder Temperature Methane Nitrous Oxide	Unclassified - Unlimited Subject Category 46

19. Security Classif. (of this report)	20. Security Classif. (of this page)	21. No. of pages	22. Price
Unclassified	Unclassified	164	A08